

Defining Key Molecules in a
Myeloma Cell Niche

Julia Paton-Hough

The Department of Human Metabolism

**Thesis submitted to The University of Sheffield for the degree
of Doctor of Philosophy**

August 2014

Presentations and publications

Presentations:

1. **J. Paton-Hough**, C. A. Eaton, P.I. Croucher and M. A. Lawson. *Identification of potential candidate molecules associated with myeloma cell engagement in a bone marrow niche*. Herbert Fleisch Workshop, Bruges, Belgium, 2014. **Oral and poster presentation.**
2. **J.Hough**, M.A.Lawson, C.A. Eaton & P. Croucher. *Identification of potential candidate molecules associated with myeloma cell engagement in a bone marrow niche*. Joint meeting of the Bone Research Society and the British Orthopaedic Research Society, Oxford, UK 2013. **Poster presentation.**
3. **J. Hough**, C. A. Eaton, P.I. Croucher and M. A. Lawson. *Identification of potential candidate molecules associated with myeloma cell engagement in a bone marrow niche*. International conference of Cancer-induced bone disease, Miami, Florida, USA, 2013. **Poster presentation.**
4. **J. Hough**, O.Al-Amer M.A. Lawson, C.A.Eaton and P.I. Croucher. *Identification of molecular determinants of myeloma cell engagement in the osteoblast niche in bone*. Mellanby Centre Annual Research Day, Sheffield, UK, 2012. **Poster presentation.**
5. **J. Hough**, O.Al-Amer M.A. Lawson, C.A.Eaton and P.I. Croucher. *Identification of molecular determinants of myeloma cell engagement in the osteoblast niche in bone*. Annual School Research Day, Sheffield, UK, 2012. **Poster presentation.**
6. **J. Hough**, O.Al-Amer M.A. Lawson, C.A.Eaton and P.I. Croucher. *Identification of molecular determinants of myeloma cell engagement in the osteoblast niche in*

bone. Mellanby Centre Annual Research Day, Sheffield, UK, 2012. **Oral and poster presentation.**

7. **J. Hough**, O.Al-Amer M.A. Lawson, C.A.Eaton and P.I. Croucher. *Identification of molecular determinants of myeloma cell engagement in the osteoblast niche in bone*. Mellanby Centre Annual Research Day, Sheffield, UK, 2011. **Oral and poster presentation.**
8. **J. Hough**, O.Al-Amer M.A. Lawson, C.A.Eaton and P.I. Croucher. *Identification of molecular determinants of myeloma cell engagement in the osteoblast niche in bone*. Annual School Research Day, Sheffield, UK, 2011. **Poster presentation.**

Publications:

1. ***NOD/SCID-GAMMA mice are an ideal strain to assess the efficacy of therapeutic agents used in the treatment of myeloma bone disease.*** M. A. Lawson, J. Paton-Hough, H. Evans, R.E. Walker, W. Harris, J. A. Snowden & A.D. Chantry. Submitted and under review at Plos One.
2. ***A Novel Method for Longitudinal Tracking of Dormant Cancer Cell Dynamics in the Skeleton as a Platform for Drug Discovery.*** Michelle A. Lawson, Michelle M. McDonald, Natasa Kovacic, Weng-Hua Khoo, Jenny Down, Warren Kaplan, **Julia Paton-Hough**, Clair Fellows, T. Neil Dear, Els Van Valckenborgh, Paul A. Baldock, Mike J. Rogers, Colby L. Eaton, Karin Vanderkerken, Tri Giang Phan, Peter I. Croucher. To be submitted to Cancer Discovery or similar.
3. ***A review of current murine models of myeloma used to assess the efficacy of therapeutic agents on tumour growth and bone disease.*** J. Paton-Hough, A.D. Chantry & M.A. Lawson: Invited review from The Journal of Laboratory Haematology, to be submitted, August 2014.

4. *N-cadherin is a key molecule for facilitating myeloma cell attachment to the osteoblastic niche and subsequent tumour development in bone.* J.Paton-Hough, O.Al-Amer, P.I. Croucher, C.A.Eaton, M.A.Lawson. Currently being written, to be submitted to Plos One or similar.

5. *Myeloma cells express haemopoietic stem cell markers of quiescence in vitro and in vivo.* J.Paton-Hough, P.I. Croucher, C.A.Eaton, M.A.Lawson. Currently being written, to be submitted to Leukaemia Research or similar.

Acknowledgements

I would like to firstly thank Prof. Peter Croucher for supporting my PhD application, which enabled me to conduct my PhD and to continue my technical role in the Bone Analysis Laboratory, and for this, I am extremely grateful. I would also like to thank him for his supervision and continual input despite leaving the University for warmer climates.

Thanks to Dr Colby Eaton who became my primary supervisor, replacing Peter in my second year. I am extremely grateful for all of the support and guidance he provided as well as boosting moral with anecdotes about pork pies and holidays.

I would especially like to thank Dr Shelly Lawson for her continued guidance and relentless support over the course of my PhD. I am particularly grateful for all of the help she provided (especially in the marathon field lab sessions) as well as her positive outlook in any situation, which helped me through some of the trying times in my PhD.

I would like to acknowledge everyone in the newly established SMaRT group; which includes Dr Andy Chantry, the usual source of entertainment (and by this I do not mean his punk band), Dr Clive Buckle, Holly Evans and Darren Lath, particularly for maintaining my sanity over the course of my PhD. I would also like to thank Orla Gallagher in the Bone Analysis Laboratory for her support, in addition to her histology training.

In addition, I would like to thank everybody in the Department of Human Metabolism for all of the help provided as well as making the department a pleasant environment to work in. This particularly includes Dr Gareth Richards for providing his expertise in molecular biology and Dr Suruchi Pacharne for all of her help with Western Blotting.

I would also like to thank people who are sorely missed at the University, which includes Dr Marco Baud'huin and Jay Gurubalan, for all of their help and guidance while they were here.

Finally, I would like to thank my (now) husband Tom Paton for all of his kindness, compassion, endless support, and motivational speeches which I could not have done without. I would also like to acknowledge my parents and new in-laws for their constant support and kindness.

Apologies if there is anyone that I have forgotten! Thank you to everyone that helped, guided, supported and offered a kind word to me over the course of my PhD.

Table of contents

Presentations and publications	
Acknowledgements	iv
Table of contents	vi
Abstract	xxi
Abbreviations	xxiii
Chapter I: Introduction	1
1.1 Multiple Myeloma	2
1.1.1 Epidemiology of multiple myeloma	2
1.1.2 Pathology of disease	2
1.1.3 Clinical features.....	4
1.1.4 Diagnosis	5
1.1.5 Pathology of tumour-induced lytic bone disease	7
1.1.6 Treatment options	10
1.1.7 Treatments to reduce tumour burden.....	10
1.1.8 Treatments to alleviate symptoms	11
1.1.9 Recurrence of disease	12
1.2 The HSC Niche	13
1.2.1 Evidence for a HSC niche.....	13
1.2.2 The osteoblastic HSC niche	15

1.2.3 The vascular HSC niche	17
1.3 Key molecules in the osteoblastic niche	18
1.3.1 CXCR4/CXCL12.....	18
1.3.2 Notch-1/Jag-1.....	21
1.3.3 Tie-2/Ang-1.....	25
1.3.4 N-cad	27
1.4 A potential myeloma cell niche.....	30
1.5 Preclinical multiple myeloma models.....	33
1.6 Summary.....	34
1.7 Aims, hypothesis and objectives	35
1.7.1 Aims and hypothesis	35
1.7.2 Objectives.....	35
Chapter II: Materials and methods	37
2.1 General cell culture methods.....	38
2.1.1 Cells	38
2.1.1.1 The 5T murine myeloma cell lines	38
2.1.1.2 MC3T3-E1 osteoblast cell line.....	38
2.1.1.3 Primary osteoblast lineage cells.....	38
2.1.2 Cell culture	39
2.1.2.1 5T murine myeloma cell line culture	39

2.1.2.2 MC3T3-E1 cell line culture	39
2.1.2.3 Primary osteoblast lineage cell culture.....	40
2.1.2.4 Cell counting.....	40
2.1.2.5 Cell thawing.....	40
2.1.2.6 Cell freezing.....	41
2.1.2.7 Primary osteoblast lineage cell differentiation.....	41
2.2 Primary animal cells and tissues	41
2.2.1 Animal cell isolation	41
2.2.1.1 Animals.....	42
2.2.1.2 Primary osteoblast lineage cell isolation	42
2.2.1.3 Bone marrow isolation for RNA extraction.....	43
2.2.1.4 Bone marrow, splenocyte and blood isolation for flow cytometry...	43
2.2.2 <i>In vivo</i> models of multiple myeloma.....	44
2.2.2.1 The 5T33-GFP and 5TGM1-GFP models of multiple myeloma for detection of HSC niche molecules and ligands	44
2.2.2.2 Gene knock-down experiments in the 5TGM1-GFP model.....	45
2.3 Molecular biology methods	45
2.3.1 RNA extraction	45
2.3.1.1 RNA methodology	45
2.3.1.2 Quantification of RNA	46
2.3.1.3 RNA fragment-length analysis	46

2.3.2 Reverse transcription	47
2.3.2.1 Reverse transcription methodology	47
2.3.3 Endpoint PCR.....	49
2.3.3.1 Principals of endpoint PCR.....	49
2.3.3.2 Endpoint PCR methodology	50
2.3.3.3 Primer design	51
2.3.4 Gel electrophoresis	52
2.3.4.1 Principals of gel electrophoresis	52
2.3.4.2 Gel electrophoresis methodology.....	52
2.3.4.3 Gene sequencing.....	53
2.3.5 Real-time PCR.....	53
2.3.5.1 Principals of real-time PCR.....	53
2.3.5.2 Real-time PCR methodology	54
2.3.5.3 Probe efficiency.....	56
2.4 Cell biology	56
2.4.1 Flow cytometry	56
2.4.1.1 General principles of flow cytometry	56
2.4.1.2 Flow cytometry methodology.....	58
2.4.2 Immunofluorescence staining	61
2.4.2.1 Principles of immunofluorescence staining.....	61

2.4.2.2 Immunofluorescence staining methodology	61
2.4.2.3 Fluorescent microscopy	63
2.4.3 IHC staining	65
2.4.3.1 Principles of IHC	65
2.4.3.2 Preparation of bones for IHC	66
2.4.3.3 IHC methodology for CD138	67
2.4.3.4 IHC methodology for N-cad	68
2.4.3.5 IHC methodology for CXCR4	69
2.4.3.6 CD138 staining quantification	69
2.4.4 Western blotting	70
2.4.4.1 Principals of Western blotting	71
2.4.4.2 Cell lysis	71
2.4.4.3 Protein quantification	72
2.4.4.4 Bicinchoninic acid assay methodology	72
2.4.4.5 Acrylamide gel methodology	74
2.4.4.6 Sodium dodecyl sulphate-polyacrylamide gel electrophoresis	75
2.4.4.7 Protein transfer	76
2.4.4.8 Immuno-blot	77
2.4.4.9 Immuno-blot development	77
2.4.4.10 Western blotting quantification	78

2.4.5 Myeloma cell growth curves	79
2.4.5.1 Growth curve methodology	79
2.5 Primary osteoblast lineage cell differentiation	80
2.5.1 Alkaline phosphatase production analysis.....	80
2.5.1.1 Principals of alkaline phosphatase analysis	80
2.5.1.2 Alkaline phosphatase assay methodology	81
2.5.1.3 DNA quantification methodology	82
2.5.1.4 Calculating alkaline phosphatase activity	83
2.5.2 Primary osteoblast lineage cell mineralisation analysis	84
2.5.2.1 Primary osteoblast lineage cell mineralisation assay methodology..	84
2.5.3 Myeloma and primary osteoblast lineage cell co-cultures.....	85
2.5.3.1 Myeloma and primary osteoblast lineage cell co-culture methodology	
.....	85
2.5.3.2 Co-culture analysis	85
2.6 Knock-down of key HSC niche molecules	88
2.6.1 Short hair-pin RNA gene knock-down technology.....	88
2.6.1.1 Principals of RNA interference technology	88
2.6.2 Puromycin killing curves.....	90
2.6.2.1 Principals of puromycin selection	90
2.6.2.2 Puromycin killing curve methodology	90
2.6.3. Polybrene optimisation.....	90

2.6.3.1 Polybrene optimisation methodology	91
2.6.4 Green fluorescent protein transduction in 5T33-WT cells and knock-down of CXCR4 and N-cad in 5TGM1-GFP cells	91
2.6.4.1 Green fluorescent protein transduction and knock-down of CXCR4 and N-cad in the 5TGM1-GFP cells methodology	91
2.6.4.2 PCR analysis.....	93
2.7. Bone parameter analysis	94
2.7.1 Micro-computed tomography	94
2.7.1.1 Principals of micro-computed tomography.....	94
2.7.1.2 Micro-computed tomography methodology.....	96
2.8. Statistics	97
Chapter III: The <i>in vitro</i> expression of HSC niche molecules and their complementary ligands by myeloma and osteoblastic cells	98
3.1 Introduction	99
3.2 Hypothesis, aims and objectives	101
3.2.1. Hypothesis and aims	101
3.2.2 Objectives.....	101
3.3 Methods	102
3.3.1 Gene expression analysis	102
3.3.1.1 Endpoint PCR.....	102
3.3.1.2 Real-time PCR.....	102

3.3.2 Protein quantification analysis.....	103
3.3.2.1 Flow cytometry	103
3.3.2.2 Immunofluorescence	103
3.3.3. Statistics	103
3.4 Results	104
3.4.1 Qualitative assessment of gene expression for the HSC niche molecules, ligands and CD138 by normal murine constituents and murine multiple myeloma cells, determined using endpoint PCR	104
3.4.2 Quantitative assessment of gene expression for the HSC niche molecules, ligands and CD138 by normal murine constituents and murine multiple myeloma cells, determined using real-time PCR	105
3.4.3 Protein quantification of HSC niche molecules, ligands and CD138 by normal murine constituents and murine multiple myeloma cells using flow cytometry	108
3.4.4 N-cad protein detection by 5T33-GFP and 5TGM1-GFP cells using Western blotting	113
3.4.5 Protein visualisation of HSC niche molecules, ligands and CD138 by 5T33- GFP and 5TGM1-GFP cells using immunofluorescence	115
3.4.6 Qualitative assessment of gene expression for the HSC niche molecules and ligands by MC3T3-E1 and primary osteoblast lineage cells using endpoint PCR	119

3.4.7 Quantitative assessment of gene expression for the HSC niche molecules and ligands by MC3T3-E1 and primary osteoblast lineage cells using real-time PCR	120
3.4.8 Protein quantification of the HSC niche molecules and ligands by MC3T3-E1 and primary osteoblast lineage cells using flow cytometry.....	122
3.5 Discussion	124
Chapter IV: The <i>ex vivo</i> and <i>in vivo</i> expression of HSC niche molecules and their ligands by murine myeloma cells	131
4.1 Introduction.....	132
4.2 Hypothesis, aims and objectives	135
4.2.1. Hypothesis and aims	135
4.2.2 Objectives.....	135
4.3 Methods	135
4.3.1 Murine models of multiple myeloma	135
4.3.2 Protein analysis of bone marrow and spleen derived myeloma cells, analysed <i>ex vivo</i>	136
4.3.2.1 Flow cytometry	136
4.3.3 Protein analysis of bone marrow derived myeloma cells, analysed <i>in vivo</i>	137
4.3.3.1 IHC	137
4.3.4 Statistics	138

4.4 Results	138
4.4.1 Quantification of tumour burden at the end-stage of disease in the bone marrow of mice injected with 5T33-GFP and 5TGM1-GFP cells.....	138
4.4.2 Protein quantification of the HSC niche molecules, ligands and CD138 by 5T33-GFP and 5TGM1-GFP cells <i>ex vivo</i> using flow cytometry	140
4.4.3 Protein quantification of the HSC niche molecules and ligands by the bone marrow and spleen-derived 5TGM1-GFP cells over-time analysed <i>ex vivo</i> using flow cytometry.....	146
4.4.4 Protein visualisation of the HSC niche molecules CXCR4 and N-cad, and CD138 by the 5TGM1-GFP cells in histological bone sections, over-time using IHC	148
4.5 Discussion	154
 Chapter V: Validating a model for primary osteoblast lineage cell differentiation <i>in vitro</i>, to determine the expression of HSC niche molecules and ligands, and to develop an osteoblastic and myeloma cell co-culture system	162
5.1 Introduction	163
5.2 Hypothesis, aims and objectives	168
5.2.1 Hypothesis and aims	168
5.2.2 Objectives.....	168
5.3 Methods	169
5.3.1 Assessment of primary osteoblast lineage cell differentiation	169
5.3.1.1 Primary osteoblast lineage cell differentiation assay	169

5.3.1.2 Alkaline phosphatase analysis	169
5.3.1.3 Mineralisation analysis.....	170
5.3.1.4 Gene expression analysis by real-time PCR	170
5.3.2 Assessment of 5TGM1-GFP adhesion to primary osteoblast lineage cells at different stages of differentiation.....	171
5.3.2.1 Co-culture assessment	171
5.3.3 Statistics	171
5.4 Results	171
5.4.1 Alkaline phosphatase production by primary osteoblast lineage cells cultured in standard or osteogenic media over-time	171
5.4.2 DNA content of primary osteoblast lineage cells cultured in standard or osteogenic media over-time	172
5.4.3 Mineralisation of primary osteoblast lineage cells cultured in osteogenic media over-time.....	174
5.4.4 Gene expression of osteoblast differentiation markers and HSC niche molecules and ligands by primary osteoblast lineage cells cultured in osteogenic media over-time.....	176
5.4.5 Adhesion of 5TGM1-GFP cells to primary osteoblast lineage cells cultured in osteogenic media	179
5.5 Discussion	181
 Chapter VI: The effect of knocking down HSC niche molecules in myeloma cells upon adhesion to osteoblast lineage cells <i>in vitro</i> and tumour burden <i>in vivo</i>...	 192

6.1 Introduction	193
6.2 Hypothesis, aims and objectives	195
6.2.1 Hypothesis and aims	195
6.2.2 Objectives.....	196
6.3 Methods	196
6.3.1 Short hair-pin RNA knock-down strategy	196
6.3.1.1 Puromycin killing curves	196
6.3.1.2 Polybrene optimisation.....	197
6.3.1.3 Lentiviral green fluorescent protein transduction.....	197
6.3.1.4 Lentiviral short hair-pin RNA transduction for CXCR4 and N-cad....	197
6.3.2 Assessment of gene knock-down.....	198
6.3.2.1 Real-time PCR.....	198
6.3.2.2 Western blotting	198
6.3.3 Assessment of the <i>in vitro</i> effects of HSC niche molecule gene knock-down in transduced myeloma cells	199
6.3.3.1 Growth curves	199
6.3.3.2 Adhesion experiments	199
6.3.4 Assessment of the <i>in vivo</i> effects of HSC niche molecule gene knock-down in transduced myeloma cells	199
6.3.4.1 Tumour burden analysis.....	200
6.3.4.2 Bone disease analysis.....	200

6.3.5 Statistics	201
6.4 Results	201
6.4.1 Killing curves to determine the optimum concentration of puromycin using flow cytometry	201
6.4.2 The effect of polybrene upon cell viability after 24 hours of treatment	204
6.4.3 Green fluorescent protein transduction in the 5T33-WT cells as a proof of principal.....	205
6.4.4 Real-time PCR to establish the success of knocking-down CXCR4 and N-cad using the lentiviral short hair-pin RNA transduction system.....	207
6.4.5 Real-time PCR to establish the stability of N-cad knock-down in cells cultured in puromycin free media	210
6.4.6 Western blotting to establish the success of knocking-down N-cad using the lentiviral short hair-pin RNA transduction system	211
6.4.7 Western blotting to establish the stability of N-cad knock-down in cells cultured in puromycin free media	212
6.4.8 The effect of N-cad knock-down upon cell proliferation.....	213
6.4.9 The effect of N-cad knock-down upon adhesion to primary osteoblast lineage cells <i>in vitro</i>	215
6.4.10 Flow cytometry to determine the effect of knocking-down N-cad in the 5TGM1-GFP cells upon myeloma cell growth <i>in vivo</i>	218
6.4.11 IHC to determine the effect of knocking-down N-cad in the 5TGM1-GFP cells upon myeloma cell growth <i>in vivo</i>	221

6.4.12 Micro-computed tomography to determine the effect of knocking-down N-cad in the 5TGM1-GFP cells upon bone parameters <i>in vivo</i>	223
6.5 Discussion	225
Chapter VII:	234
General discussion	234
7.1 General discussion.....	235
7.2 Future studies	244
Appendices.....	248
Appendix 1: Equipment, materials and reagents.....	248
1.1 Tissue culture	248
1.2 Animal cell isolation	249
1.3 RNA extraction	249
1.4 Reverse transcription	249
1.5 Endpoint PCR.....	250
1.6 Gel electrophoresis	250
1.7 Real-time PCR.....	250
1.8 Flow cytometry	251
1.9 Immunofluorescence	251
1.10 IHC.....	252
1.11 Western blotting	253
1.12 Primary osteoblast lineage cell differentiation.....	254

1.13 Gene knock-down using short hair-pin RNA.....	254
1.14 Micro-computed tomography	254
Appendix 2: Additional information for methodologies	255
2.1 RNA quantification and contamination analysis.....	255
2.2 RNA fragment length analysis.....	255
2.3 Endpoint PCR primer information.....	256
2.4 Endpoint PCR primer sequence information	256
2.5 Probes used for real-time PCR	257
2.6 Real-time PCR probe efficiencies	258
2.7 Optimisation experiments to determine the optimum amount of protein required to visualise N-cad using Western blotting	259
2.8 Alkaline phosphatase analysis.....	260
References	261

Abstract

Multiple myeloma is an incurable B cell malignancy characterised by the expansion of malignant plasma cells in the bone marrow. It has been suggested that during initial colonisation of bone and possibly during therapy, some myeloma cells may occupy a bone marrow niche similar to that inhabited by haemopoietic stem cells. Haemopoietic stem cells residing in BM niches adhere to osteoblastic cells via a series of molecules that promote haemopoietic stem cell quiescence. Therefore, we hypothesise that myeloma cells express the same molecules as haemopoietic stem cells, chemokine C-X-C-motif-receptor 4, notch-1, tyrosine kinase-2 and n-cadherin, which interact with their complementary ligands expressed by osteoblastic cells, chemokine C-X-C-motif-ligand 12, jagged-1, angiopoietin-1 and n-cadherin. These interactions may result in myeloma cell adhesion to an osteoblastic niche, resulting in myeloma cell dormancy. The aims of these studies were to determine the expression of haemopoietic stem cell niche molecules and ligands by murine myeloma cell lines and osteoblastic cells and to determine the role of one of the key molecules *in vitro* and *in vivo*.

5T33MMvt and 5TGM1 cells expressed the haemopoietic stem cell niche molecules; chemokine C-X-C-motif-receptor 4, notch-1, tyrosine kinase-2 and n-cadherin and the MC3T3-E1 cells and primary osteoblast lineage cells expressed the ligands chemokine C-X-C-ligand 12, jagged-1, angiopoietin-1 and n-cadherin. Knock-down of n-cadherin was achieved in the 5TGM1 cells, with 71% gene and 75% protein reduction. 5TGM1 n-cadherin knock-down cell attachment to primary osteoblast lineage cells was reduced *in vitro*, though this did not reach significance. Mice injected with 5TGM1 n-cadherin knock-down cells had significantly less tumour *in vivo* compared to controls.

In conclusion, murine myeloma cells expressed the same repertoire of molecules as haemopoietic stem cells and osteoblastic cells expressed their complementary ligands. Knock-down of one of these key molecules, n-cadherin, did not significantly

inhibit myeloma cell attachment to primary osteoblasts *in vitro* but potentially impaired tumour growth *in vivo*. Further experiments are required to confirm this.

Abbreviations

ADAM	A disintegrin and metalloproteinases
ADH-1	Adherin 1
AID	Activation-induced deaminase
Akt	Protein kinase B
Alp	Alkaline phosphatase
Ang	Angiopoietin
ANOVA	Analysis of variance
APC	Allophycocyanin
APS	Ammonium persulphate
Asc	Ascorbic acid
ATP	Adenosine triphosphate
ATCC	The American Type Culture Collection
BAD	B cell lymphoma-2 associated death promoter
BCA	Bicinchoninic acid
Bcl	B cell lymphoma
BCSH	British Committee for Standards in Haematology
BD	Becton Dickinson
BFU	Burst forming unit
BGP	Beta-glycerophosphate
BM	Bone marrow

BMP	Bone morphogenetic protein
BMPR	Bone morphogenetic protein receptor
BP	Base Pair
BSA	Bovine serum albumin
BV/TV	Bone volume/ tissue volume
CAR	Chemokine C-X-C motif ligand 12 abundant reticular
CBF1 α	Core binding factor 1 alpha
CD	Cluster of differentiation
cDNA	Complementary deoxyribonucleoside
CFU	Colony forming unit
CFU _b	Colony forming unit basophil
CFU _e	Colony forming unit erythrocyte
CFU _{Eo}	Colony forming unit eosinophil
CFU _G	Colony forming unit granulocyte
CFU _{GEMM}	Colony forming unit granulocyte erythroid monocyte and megakaryocyte
CFU _{GM}	Colony forming unit granulocyte monocyte
CFU _{GMEo}	Colony forming unit granulocyte monocyte eosinophil
CFU _M	Colony forming unit monocyte
CFU _{mega}	Colony forming unit megakaryocyte
Cm	Centimetre
COL1A1	Collagen type I alpha I

CSL	Core binding factor 1/ Recombination signal-binding protein 1 for J-kappa/ Su9H/Lag-1
Ct	Cycle threshold
CT	Computed tomography
CTRL	Control
Ct.th	Cortical thickness
Cu	Copper
CXCL	Chemokine C-X-C motif ligand
CXCR	Chemokine C-X-C motif receptor
DAB	3,3'-Diaminobenzidine
DAPI	4',6-Diamidino-2-phenylindole, dihydrochloride
DAPT	N-[(3,5-Difluorophenyl)acetyl]-L-alanyl-2-phenylglycine-1,1- dimethylethyl
DEPC	Diethylpyrocarbonate
Dex	Dexamethasone
dH ₂ O	Distilled water
DiD	1,1'-dioctadecyl-3,3,3',3' tetramethylindodicarbocyanine perchlorate
DKK	Dickkopf
dl	Decilitre
DMEM	Dulbecco's Modified Eagle Medium
DMSO	Dimethylsulphoxide
DNA	Deoxyribonucleic acid

dNTP	Deoxynucleotide triphosphate
DOS	Delta and oncostatin M
Dpi	Dots per inch
DPX	Di-N-butyl phthalate in xylene
Ds	Double stranded
DSL	Delta serrate lag-2 region
DTT	Dithiothreitol
dUTP	Deoxyuridine triphosphate
EC	Endothelial cell
E-cad	E-cadherin
ECL	Enhanced chemoluminescence substrate
EDTA	Ethylenediaminetetraacetic acid
EGF	Epithelial growth factor
ERK	Extracellular signal-related kinase
FACS	Fluorescence-Activation Cell Sorting
FAM	6-carboxyfluorescein
FBS	Foetal bovine serum
Fc	Fragment crystallisable
FISH	Fluorescent <i>in situ</i> hybridisation
FZ	Fungizone
G	Gram
G	Gravitational acceleration

GAPDH	Glyceraldehyde 3-phosphate dehydrogenase
GDP	Guanosine diphosphate
GFP	Green fluorescent protein
GOI	Gene of interest
GPCR	Guanosine nucleotide-binding protein-coupled receptor
GTP	Guanosine triphosphate
HBSS	Hank's balanced salt solution
HCl	Hydrogen chloride
HES	Hairy enhancer of split
Hey1	Hairy/ enhancer of split related with YRPW motif protein 1
HK	Housekeeping
HRP	Horseradish peroxidase
HPRT	Hypoxanthine-guanine phosphoribosyltransferase
HRT	Hairy-related
HSC	Haemopoietic stem cell
HUVEC	Human umbilical vein endothelial cell
H ₂ O	Water
H ₂ O ₂	Hydrogen peroxide
ICAM	Intercellular adhesion molecule
IF	Immunofluorescence

Ig	Immunoglobulin
IGF	Insulin-like growth factor
IgH	Immunoglobulin heavy
IHC	Immunohistochemistry
I κ B α	Nuclear factor of kappa light chain polypeptide gene enhancer in B-cells inhibitor alpha
IL	Interleukin
IMS	Industrial methylated spirits
IP	Intraperitoneal
IV	Intravenous
Jag-1	Jagged-1
kb	Kilo base
KCl	Potassium chloride
KD	Knock-down
KO	Knockout
KSL	C-kit ⁺ Sca-1 ⁺ Lineage ⁻
Kv	Kilo volt
LEPR	Leptin receptor
l	Litre
LT-HSC	Long-term haemopoietic stem cell
M	Molar
MAPK	Mitogen-activated protein kinase

MC	Myeloma cell
MEM α	Minimum essential medium alpha
MEM α -Nuc	Minimum essential medium alpha containing nucleosides
MFI	Mean fluorescent intensity
mg	Milligram
MGB	Minor groove binder
MgCl ₂	Magnesium chloride
MGUS	Monoclonal gammopathy of unknown significance
MHC	Major histocompatibility complex
Min	Minute
MIP	Macrophage inflammatory protein
miRNA	Micro ribonucleic acid
ml	Millilitre
mm	Millimetre
mM	Millimolar
MM	Multiple myeloma
MNNL	Module at the N-terminus of Notch ligands
MOI	Multiplicity of infection
MRI	Magnetic resonance imaging
mRNA	Messenger ribonucleic acid
ms	Millisecond

MSC	Mesenchymal stem cell
NaCl	Sodium chloride
NaOH	Sodium hydroxide
NaP	Sodium pyruvate
N-cad	Neural cadherin
NCKD	N-cadherin knock-down
NEAA	Non-essential amino acid
NF- κ B	Nuclear factor kappa B
ng	Nanogram
NK	Natural Killer
nm	Nanometre
nmol	Nanomolar
NOD/SCID	Non-obese diabetic/severe combined immunodeficiency
NP-40	Nonyl phenoxypolyethoxyethanol
Ocn	Osteocalcin
OD	Optical density
OGM	Osteogenic media
OLC	Osteoblast lineage cell
On	Osteonectin
OPG	Osteoprotegerin
Opn	Osteopontin

OSM	Oncostatin-M
Ostx	Osterix
PAC	Puromycin N-acetylc-transferase
PBS	Phosphate buffered saline
PBST	Phosphate buffered saline containing tween
PCR	Polymerase chain reaction
PE	Phycoerythrin
PEST	Proline, glutamic acid, serine and threonine
PET	Positron emission tomography
PET-CT	Positron emission tomography-computed tomography
PFA	Paraformaldehyde
PI	Propidium iodide
PIC	Protease inhibitor cocktail
PIK-3	Phosphatidylinositol 3-kinase
PK	Protein kinase
PKH	Paul Karl Horan
PLC	Phospholipase-c
PNPP	p-nitrophenyl phosphate
POI	Protein of interest
PPR	Parathyroid-related protein receptor
PS	Penicillin/ streptomycin
PTH	Parathyroid hormone

PTHrP	Parathyroid hormone- related protein
Q	Quencher
R	Reporter
RAG-1	Recombination activation gene-1
RAM	Recombination signal-binding protein 1 for J-kappa-associated molecule
RANK	Receptor activator of nuclear factor kappa beta
RANKL	Receptor activator of nuclear factor kappa beta ligand
RBC	Red blood cell
RBP-JK	Recombination signal-binding protein 1 for J-kappa
RISC	Ribonucleic acid induced silencing complex
RNA	Ribonucleic acid
RNAi	RNA interference
RNasin	Ribonucleic acidase inhibitor
RPM	Rotations per minute
RPMI	Roswell Park Memorial Institute medium
RT	Reverse transcription
RT-	Complementary deoxyribonucleic acid samples without reverse transcriptase enzyme
RT+	Complementary deoxyribonucleic acid samples with reverse transcriptase enzyme
RVD	Lenalidomide, bortezomib, dexamethasone
SA	Streptavidin

SA-HRP	Streptavidin horseradish peroxidase
SC	Subcutaneous
SCF	Stem cell factor
SCID	Severe combined immunodeficiency
SDF	Stromal-derived factor
SDS	Sodium dodecyl sulphate
SDS-PAGE	Sodium dodecyl sulphate-polyacrylamide gel electrophoresis
SEM	Standard error of the mean
SFRP	Secreted frizzled-related protein
shRNA	Short hair-pin RNA
siRNA	Silencing ribonucleic acid
SNP	Single nucleotide polymorphism
ST-HSCs	Short-term haemopoietic stem cell
TAD	Transcriptional activation domain
TAE	Trizma base, acetic acid and ethylenediaminetetraacetic acid
Tb.n	Trabecular number
Tb.pf	Trabecular pattern factor
Tb.th	Trabecular thickness
TEMED	Tetramethylethylenediamine
TGF	Transforming growth factor

Tie	Tyrosine kinase
TIFF	Tagged image file format file
Tm	Melting temperature
TNF	Tumour necrosis factor
TO-PRO-3	TO-PRO-3 iodide
TRAIL	Tumour necrosis factor-related apoptosis-inducing ligand
TU	Transducing units
UD	Undetermined
UV	Ultra violet
VCAM	Vascular cell adhesion molecule
V (D) J	Variable, diversity, joining
VEGF	Vascular endothelial growth factor
VLA-4	Very late antigen
WB	Western blotting
WBC	White blood cell
Wnt	Wingless
WT	Wild type
Zn	Zinc
5-FU	Fluorouracil
5'	Five prime end
5TGM1-GFP	5TGM1-green fluorescent protein

5TGM1vt	5TGM1 <i>in vitro</i>
5T33-GFP	5T33MM-green fluorescent protein
5T33MMvt	5T33 multiple myeloma <i>in vitro</i>
5T33-GFP	5T33MM-green fluorescent protein
3'	Three prime end
A	Alpha
B	Beta
β 2M	Beta 2 microglobulin
$^{\circ}$ C	Degrees Celsius
Δ	Delta
Δ Ct	Delta cycle threshold
γ	Gamma
κ	Kappa
Π	Pi
μ A	Microamperes
μ CT	Micro computed tomography
μ g	Microgram
μ l	Microlitre
μ m	Micrometre
μ mol	Micromolar

Chapter I: Introduction

1.1 Multiple Myeloma

1.1.1 Epidemiology of multiple myeloma

Multiple myeloma (MM) is a haematological malignancy predominantly characterised by the uncontrolled expansion of plasma cells in the bone marrow (BM), resulting in bone disease (1). It accounts for 1.5% of all cancers (2) and for at least 13% of all haematological malignancies worldwide (3). In the UK, the incidence of MM is 6-8 diagnoses per 100,000 people with over 4500 people diagnosed with MM per year (2).

MM is an age-dependent disorder where the mean age of diagnosis is 62 years for men (75% >70 years) and 61 years for women (79% >70 years) (4) and less than 15% are diagnosed before the age of 60 (5). It is the most common haematological cancer in African Caribbean ethnicities where twice as many are likely to develop myeloma compared to European Americans (6). There is also a higher incidence of MM in males rather than females (7). However, the genetic basis for any differences between specific ethnicities and sexes is unknown. When the frequency of immunoglobulin (Ig) heavy (IgH) translocations, translocation loci and genomic gain or loss were compared between European Americans and African Caribbeans, the only statistical difference observed was a greater frequency of IgH translocations in European Americans (6).

1.1.2 Pathology of disease

Myeloma cells (MCs) are classified as abnormal plasma cells. The primary role of a normal plasma cell is to provide a humoral immune response via the production of Igs when a foreign antigen is encountered. Plasma cells are typically un-dividing cells, which possess a distinct morphology, high endoplasmic reticulum and Golgi content, as well as the expression of specific molecules. Normal plasma cells express molecules such as syndecan-1 (also known as cluster of differentiation (CD) 138), very-late antigen (VLA)-4 and chemokine C-X-C motif receptor (CXCR) 4. Markers that

are down-regulated post plasma cell differentiation include B220, CD19, CD21, CD22, CXCR5 and the major histocompatibility complex (MHC) II (8).

Plasma cells originate from B lymphocytes which are produced from differentiated BM haemopoietic stem cells (HSCs), discussed in Chapter I Section 1.2. Throughout the stages of differentiation, several significant genetic modifications occur, which include; rearrangements of the variable, diversity and joining (V(D)J) regions of the IgH chain during somatic hypermutation (8, 9) and Ig class switching in the centrocyte and plasmablast (10). Both somatic hypermutation and class switching use activation-induced deaminase (AID), which produces double strand deoxyribonucleic acid (DNA) breaks. The DNA breaks are usually repaired locally however, they may lead to chromosomal translocations, which can occur in up to 1000 cells a day (11). Therefore, each DNA modification that occurs within a cell throughout the stages of B cell differentiation increases the risk of chromosomal abnormalities, which are a common feature in myeloma (12).

Several genetic mutations have been identified in myeloma patients and they are characterised into two cytogenetic categories, which include hyperdiploid or non-hyperdiploid. Hyperdiploid patients have more than the normal diploid number of chromosomes such as trisomies of chromosomes (this may include chromosomes 3, 5, 7, 9, 11, 15, 19), whereas non-hyperdiploid patients are hypodiploid, with fewer than the normal diploid number of chromosomes or may have chromosomal translocations, particularly of the IgH gene, which occurs in approximately 50% of monoclonal gammopathy of unknown significance (MGUS) patients (the pre-malignant condition before asymptomatic or symptomatic myeloma) and 60-65% of symptomatic myeloma patients (13, 14).

1.1.3 Clinical features

MM patients can present with several different clinical features, depending on the stage and severity of disease. Common features are haematological irregularities, renal disease and bone disease.

Haematological irregularities include a reduction in erythrocytes, platelets and white blood cells (WBCs) as well as normochromic and normocytic anaemia (iron <8.5 grams (g) per decilitre (dl)) which are exhibited as fatigue, abnormal bleeding and increased risk of infection. These signs are primarily caused by the rapid expansion of MCs in the BM (15).

Renal disease is also common in MM patients and is “one of the most common causes of death, second to infection” (16). Up to 50% of newly diagnosed patients can present with renal abnormalities and 20% of patients are diagnosed with severe renal impairments which require dialysis (17). Renal failure is caused by the presence of malignant plasma cells in the BM. Clonal plasma cells secrete monoclonal antibody, also known as paraprotein or M protein (50% of patient MCs secrete IgG, 20% IgA and 20% light chains) (17), which cause lesion formation in the kidneys, known as cast nephropathy. Lesions present in the kidneys have been associated with tubular rupture and nephritis, resulting in obstructions and poor filtration (16). In addition, amyloidosis caused by paraprotein or light chain secretion as well as hypercalcaemia, caused by the breakdown of bone (discussed in more detail in Chapter I section 1.1.5) also result in renal impairment (2).

Bone disease and the development of osteolytic lesions, as a result of MC infiltration of the BM, are also a major cause of morbidity and occur in 40-50% of MM patients (18). Patients suffering from lesions may experience bone pain and have increased risk of pathological fractures (2), discussed in greater detail in Chapter I, Section 1.1.5.

1.1.4 Diagnosis

Several tests are performed to reach a diagnosis of MM. These include analysis of the blood, urine, BM and skeleton.

Full blood counts, red blood cell (RBC) sedimentation rate and blood smears are used to assess abnormalities in the number of different cellular constituents in the peripheral blood, as well as to test iron and haemoglobin levels. Bone marrow aspirates or trephines may also be taken to determine the number of different cellular constituents, particularly the number of plasma cells, which is generally higher than 10% in MM patients (5). Plasma cell phenotyping can also be conducted using flow cytometry to characterise specific cell surface markers, as well as fluorescent *in situ* hybridisation (FISH) to determine cytogenetic abnormalities (19). Karyotyping can also be conducted to identify specific chromosomal abnormalities.

Renal defects are detected by urine biochemistry or urine electrophoresis, which detect the presence of paraprotein or Ig light chains, also known as Bence Jones protein, in the urine. In addition, serum electrophoresis, immuno-fixation and biochemical tests are also conducted to determine the presence of paraprotein present in the circulation as well as levels of creatinine, calcium, beta (β) 2 microglobulin (β 2M) and albumin, which indicate severity of renal dysfunction (5, 20).

Positron emission tomography (PET)-computed tomography (CT) (PET-CT), magnetic resonance imaging (MRI) and X-rays are used to visualise the extent of bone lesions and fractures in MM patients (20).

In early MM, it is often difficult to distinguish symptomatic MM from related disorders such as asymptomatic/smouldering MM and MGUS. Monoclonal gammopathy of unknown significance is the most common premalignant condition present in Western countries and is present in 3% of the general population over 50 years of age (21, 22). It is diagnosed by the presence of paraprotein however, levels are less than 30 g/l and patients do not show signs of bone disease or organ-related

disorders. The risk of developing MM or plasma cell related disorders increases at a rate of 1% every year following diagnosis, and it is uncertain whether all patients have the premalignant condition prior to MM diagnosis. However, Landgren *et al* (22) found that “virtually all” MM patients in their studies (N=71) had a form of MGUS (diagnosed by the presence of paraprotein < 30 g/dl) prior to MM, but the trigger which initiates progression to MM is unknown.

Smouldering/ asymptomatic MM is a precursor to MM, whereby approximately 3000 cases are diagnosed per year in the United States of America and patients have an average annual risk of progression to MM of 10% in the first 5 years after diagnosis, which decreases to 3% annually for the following 5 years and 1% thereafter (23). Smouldering MM patients are diagnosed due to paraprotein levels above 30 g/dl and more than 10% of plasma cells present in the BM, however they do not present with any organ related impairment (5).

An international diagnostic system to distinguish between MGUS, smouldering MM and symptomatic MM was developed by Smith *et al* (24), the International Myeloma Working Group (25) and the British Committee for Standards in Haematology (BCSH), as stated in the official Myeloma Guidelines (5), shown in Table 1.1.

Table 1.1: The diagnostic criteria to differentiate between MGUS, asymptomatic MM and symptomatic MM

Monoclonal gammopathy of unknown significance	Asymptomatic myeloma	Symptomatic myeloma
M protein in serum <30 g/l	M protein in serum >30 g/l	M protein present in serum and/or urine
BM clonal plasma cells <10%	And/or BM clonal plasma cells >10%	BM plasma cells and plasmacytoma
No myeloma related organ or tissue impairment	No myeloma related organ or tissue impairment, bone lesions or symptoms	Any myeloma related organ or tissue impairment including bone lesions

Adapted from the Bird et al (5), permission from The British Journal of Hematology 04.08.14. I: Litre.

In addition, a staging system was also designed by Durie and Salmon (26) and has been adapted by the BCSH in the MM guidelines (5), as shown in Table 1.2. This

staging system was designed to categorise patient stage and severity of disease in order to reach a prognosis and to decide upon suitable treatment options.

Table 1.2: The Durie and Salmon staging system of myeloma

Stage	Criteria	Median survival (months)
Stage I	Serum β 2M < 3.5 mg/l (296 nmol/l) Serum albumin \geq 3.5 g/dl (35g/l or 532 μ mol/l)	62
Stage II	Remainder fitting neither Stage I or III	45
Stage III	Serum β 2M \geq 5.5 mg/l (465 nmol/l)	29

Adapted from Durie and Salmon (26) by the BCSH (5), permission from The British Journal of Hematology 04.08.14. nmol: nanomole, μ mol: micromole, mg: milligram.

1.1.5 Pathology of tumour-induced lytic bone disease

The specific constituents of the BM and its microenvironment provide a suitable “soil” for the expansion and enhanced survival of MCs in MM, as explained by Paget (27) using the “seed and soil” hypothesis. Two specialised cells residing in the BM microenvironment, which are of importance with regards to the development of MM, are osteoblasts and osteoclasts. Osteoblasts are responsible for secreting the extracellular organic bone matrix known as osteoid, which is then mineralised to form new bone (28). Osteoclasts are able to secrete enzymes and proteins to digest the bone in the process of resorption (29). The mechanisms in which osteoblasts and osteoclasts work together to produce functioning bone is known as remodelling (30) and this balanced process is described in Figure 1.1.

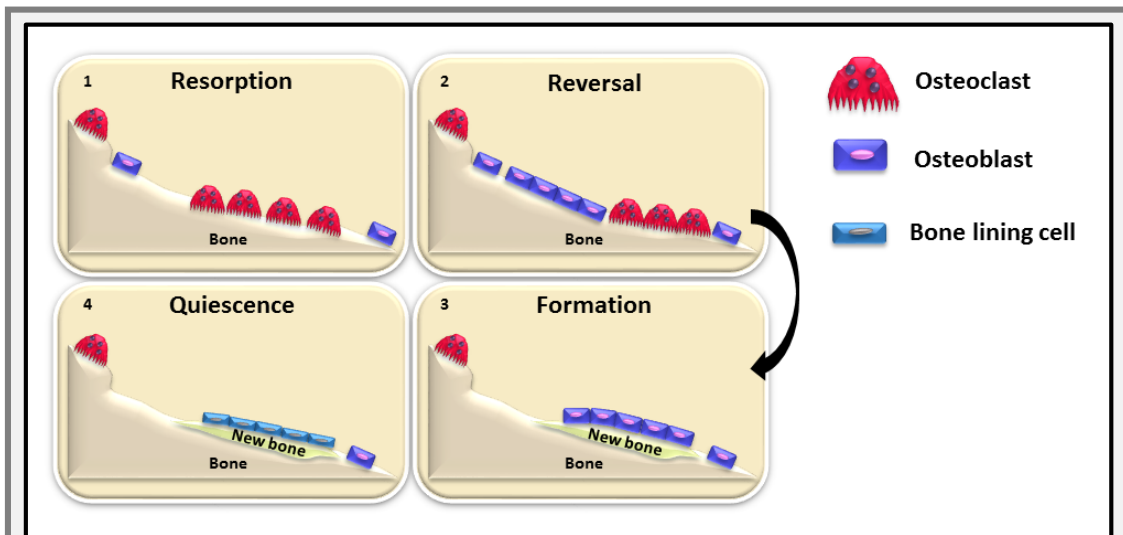
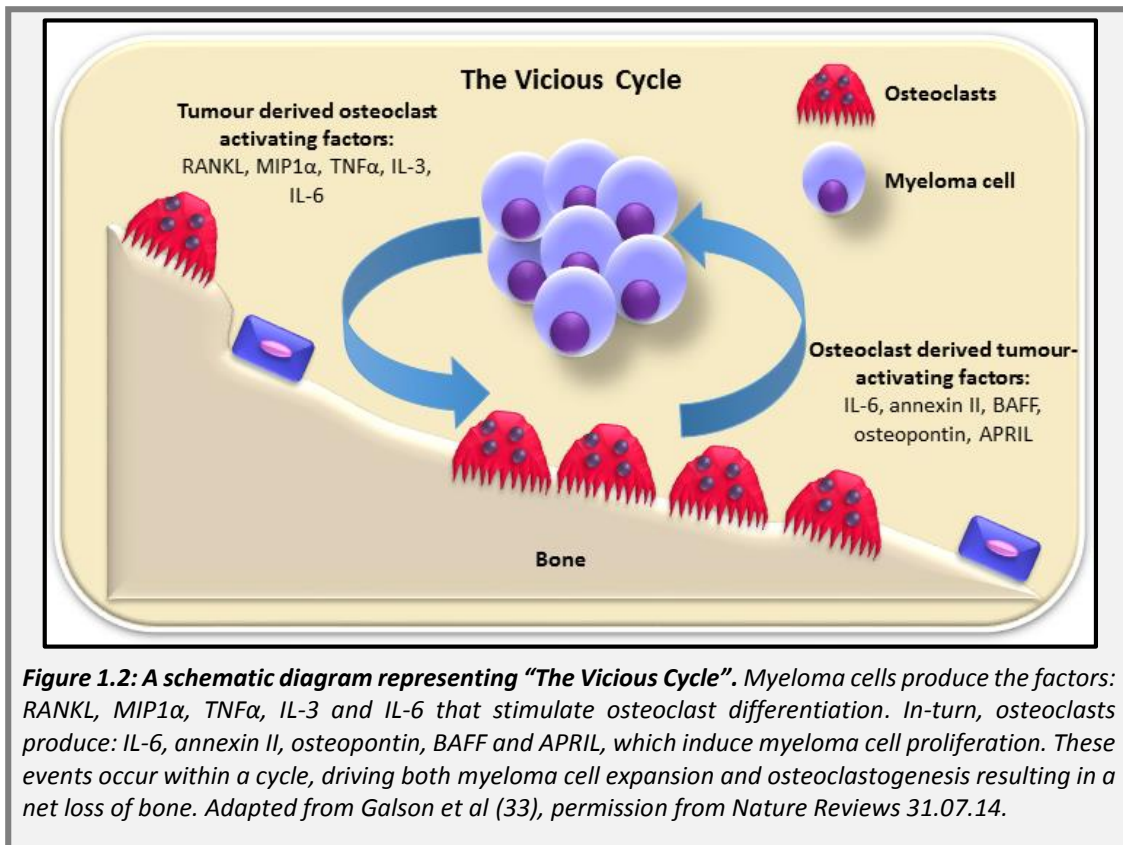


Figure 1.1: A schematic diagram representing the cycle of normal bone remodelling. The cycle consists of four phases: **1.** Bone resorption occurs by the activation of osteoclasts, which release acid phosphatases and collagenases, which degrade bone. **2.** The reversal phase in which apoptosis of osteoclasts occurs followed by recruitment of osteoblasts. **3.** Subsequent bone formation where osteoblasts secrete osteoid, which is mineralised with hydroxyapatite to form new bone. **4.** A resting phase in which neither resorption or formation occurs and osteoblastic cells become flattened bone lining cells (31).

In MM, the process of bone remodelling is “uncoupled” (32) and the osteoclast/osteoblast axis is disrupted, favouring osteoclastic bone resorption and suppressing osteoblastic bone formation, ultimately leading to lytic bone lesions and bone disease (18). This increase in bone loss is enhanced by what is known as “The Vicious Cycle” (33), where myeloma cells express or secrete factors such as nuclear factor kappa (κ) β ligand (RANKL) (32, 34), macrophage inflammatory protein 1 (MIP1 α) (35, 36), tumour necrosis factor α (TNF α) (37), interleukin 1 β (IL-1 β) (38), IL-3 (39) and IL-6 (40), which stimulate osteoclastic differentiation and activation. In turn, osteoclasts produce proteins including IL-6 (41), annexin II (42), osteopontin (43), B cell-activating factor belonging to the TNF family (BAFF) (44) and a proliferation-inducing ligand (APRIL) (44), which increase myeloma cell proliferation or prevent apoptosis. Overall, this cycle results in increased numbers of active osteoclasts and myeloma cells, leading to enhanced bone loss. This phenomenon is illustrated in Figure 1.2.



One of the main regulators of osteoclastogenesis in MM is the RANK/RANKL pathway. Receptor activator of nuclear factor κ β ligand is an essential cytokine for the differentiation of preosteoclasts to activated osteoclasts (45). Receptor activator of nuclear factor κ β ligand is expressed by stromal cells, osteoblasts and T cells and exists as a membrane bound form as well as soluble RANKL, when cleaved by metalloproteinases. Receptor activator of nuclear factor κ β ligand binds to its receptor RANK, expressed on preosteoclasts and activated osteoclasts. Receptor activator of nuclear factor κ β / RANKL interactions result in the differentiation of preosteoclasts, the fusion of polykaryons and the activation of resorption in mature osteoclasts. Osteoclastogenesis can however, be inhibited by a decoy receptor, known as osteoprotegerin (OPG), which is expressed by osteoblasts. Osteoprotegerin binds to RANKL, blocking the binding of RANK with RANKL, thus behaving as a paracrine inhibitor of osteoclast formation and activation (46). In MM, OPG is down regulated (47) therefore, osteoclastogenesis and thus bone resorption is not inhibited resulting in a disruption of normal bone remodelling.

As mentioned above, osteoblast number and bone formation are reduced in MM which may be due to inhibition of the wingless (Wnt) signalling pathway by MC secretion of soluble Wnt inhibitory factors including dickkopfs (DKKs) (48, 49) or secreted frizzled-related proteins (SFRPs) (50).

1.1.6 Treatment options

To date, MM remains an incurable disease and resulted in approximately 10,710 deaths in the USA in 2012 (51) and approximately 2600 in the UK in 2011 (<http://www.cancerresearchuk.org/cancer-info/cancerstats/keyfacts/myeloma/myeloma>). Survival rates post-diagnosis vary from several weeks to several decades. However, the 5 year or more survival rate in myeloma patients in the USA between 2002-2004 was 45-57% in patients less than 50 years of age, 39-48% in 51-59 year olds, 31-36% in 60-69 year olds and only 27-29% in those over the age of 70 (52). This was similar to UK statistics in 2010 where only 37% of patients survived 5 years post diagnosis (http://www.cancerresearchuk.org/cancerinfo/cancerstats/types/myeloma/survival/multiple-myeloma-survival-statistics#1_5_10_yr_survival).

There are a variety of treatments available for MM patients however, current treatments are not curative, but alleviate the symptoms to improve quality of life. Current treatments include radiotherapy, chemotherapy, bisphosphonates, surgery and BM and stem cell transplants. The type of treatment administered is dependent on the age of the patient and the severity of disease.

1.1.7 Treatments to reduce tumour burden

Radiotherapy is generally administered locally at the site of pain to reduce tumour burden which in-turn reduces osteoclastic bone resorption to help prevent further bone loss. Radiotherapy is also used to treat spinal cord compression and this may be given in combination with surgery or kyphoplasty (53).

Chemotherapeutic drugs are administered to reduce tumour burden. These include chemotherapies (lenalidomide, pomalidomide, thalidomide), corticosteroids (dexamethasone (dex) and prednisone), and proteasome inhibitors (bortezomib and carfilzomib). Treatments are given in combination such as lenalidomide, dex and bortezomib (RVD), lenalidomide cyclophosphamide and dex or RVD plus cyclophosphamide (54). Lenalidomide, thalidomide and pomalidomide are thought to work by inducing apoptosis in MCs via caspase 8 and tumour necrosis apoptosis-inducing ligand (TRAIL) signalling as well as down regulation of nuclear factor κ B (Nf- κ B), IL-6 and vascular endothelial growth factor (VEGF) (54-56). Proteasome inhibitors such as bortezomib and carfilzomib are thought to act by inhibiting the 26 S proteasome, resulting in the inhibition of the degradation of proteins involved in cell proliferation (57). In addition, bortezomib was found to inhibit angiogenesis by reducing the production of VEGF, IL-6, IGF-1, Angiopoietin (Ang)-1 and Ang-2 by endothelial cells *in vitro* (58), which could contribute to a reduction in tumour burden in patients.

1.1.8 Treatments to alleviate symptoms

Bisphosphonates are the most commonly administered drug to reduce bone resorption and to prevent further formation of osteolytic lesions or osteopenia. There are several different bisphosphonates available which include the nitrogen-containing bisphosphonates; zoledronic acid, pamidronate and ibandronate and non-nitrogen containing bisphosphonates; clodronate and etidronate. Bisphosphonates once administered, bind to hydroxyapatite in the bone and are released during bone resorption and internalised by osteoclasts. Once inside the cell they can either inhibit osteoclastic activity or induce osteoclast apoptosis (59). Non-nitrogen containing bisphosphonates are able to inhibit adenosine triphosphate (ATP)-dependent enzymes (60), whereas nitrogen containing bisphosphonates inhibit the enzyme farnesyl pyrophosphate synthase, required in the mevalonate pathway, an essential pathway for the post-translational modification of proteins (61). In the clinic, standard therapy usually uses zoledronic acid or pamidronate to

reduce bone pain (62). In addition, bisphosphonates have also been reported to exert an anti-tumour effect *in vitro* (63) and *in vivo* (64).

Autologous stem cell transplants may also act as standard therapy for newly diagnosed patients, however, transplants are usually only applied to younger patients and use also depends on the stage of disease. Other therapies that may be required to alleviate symptoms include dialysis, rehydration, blood transfusion, plasmaphoresis, antibiotics and Ig infusions (15).

1.1.9 Recurrence of disease

Despite continual development of novel therapies for MM, current treatments are unable to completely eradicate the disease and patient relapse is inevitable. Previous studies have proposed that residual MCs present in the BM following treatment are able to evade chemotherapy via (currently) unknown mechanisms; and some groups have categorised these cells as “cancer stem cells”(65). Several mechanisms have however been proposed. For example, previous studies have suggested that chemo-evasion is a result of MC mediated alterations in immune surveillance (suppression and dysfunction of T cells and natural killer (NK) cells) (66, 67); a lack of optimal microenvironment for growth, and some have also suggested that MC adhesion to specific niches in the BM microenvironment results in MC dormancy (65, 68). Concerning the latter, previous reports have speculated that dormant MCs may in fact hijack or reside in similar niches to those occupied by HSCs and they therefore utilise similar mechanisms as HSCs to acquire cell dormancy. The concept of the HSC niche has been explored for approximately the last thirty-five years and previous studies have found that HSCs were maintained in these niches by the expression and interactions of specific molecules on the HSCs and other cells in the BM microenvironment (69) (discussed in more detail below). In support of a MC niche, a recent study by Chen *et al* (70) found early MCs (identified by a lipophilic dye known as Paul Karl Horan dye (PKH26)) preferentially resided in osteoblastic niches and homed and survived to a lesser extent in vascular and splenic niches, using murine MM *in vivo* models. In addition, PKH26 positive cells demonstrated increased

chemoresistance compared to PKH26 negative cells. *in vitro* (70). However, current data is still inconclusive as to the specific molecule interactions responsible for the adhesion of MCs to these niches and mechanisms of MC dormancy and therefore, further research is required to explore this.

1.2 The HSC Niche

1.2.1 Evidence for a HSC niche

HSCs possess the ability for unlimited self-renewal and production of a variety of differentiated progeny by haematopoiesis (71), as illustrated in Figure 1.3. Schofield *et al* (72) proposed that HSCs reside in a specialised microenvironment or niche which is responsible for controlling self-renewal and differentiation of HSCs, required for maintenance of the different cell types within the BM. The HSC microenvironment is comprised of several supporting cells and components including stromal cells, extracellular matrix molecules and growth factors (73) all of which contribute to the maintenance of the stem cell pool size.

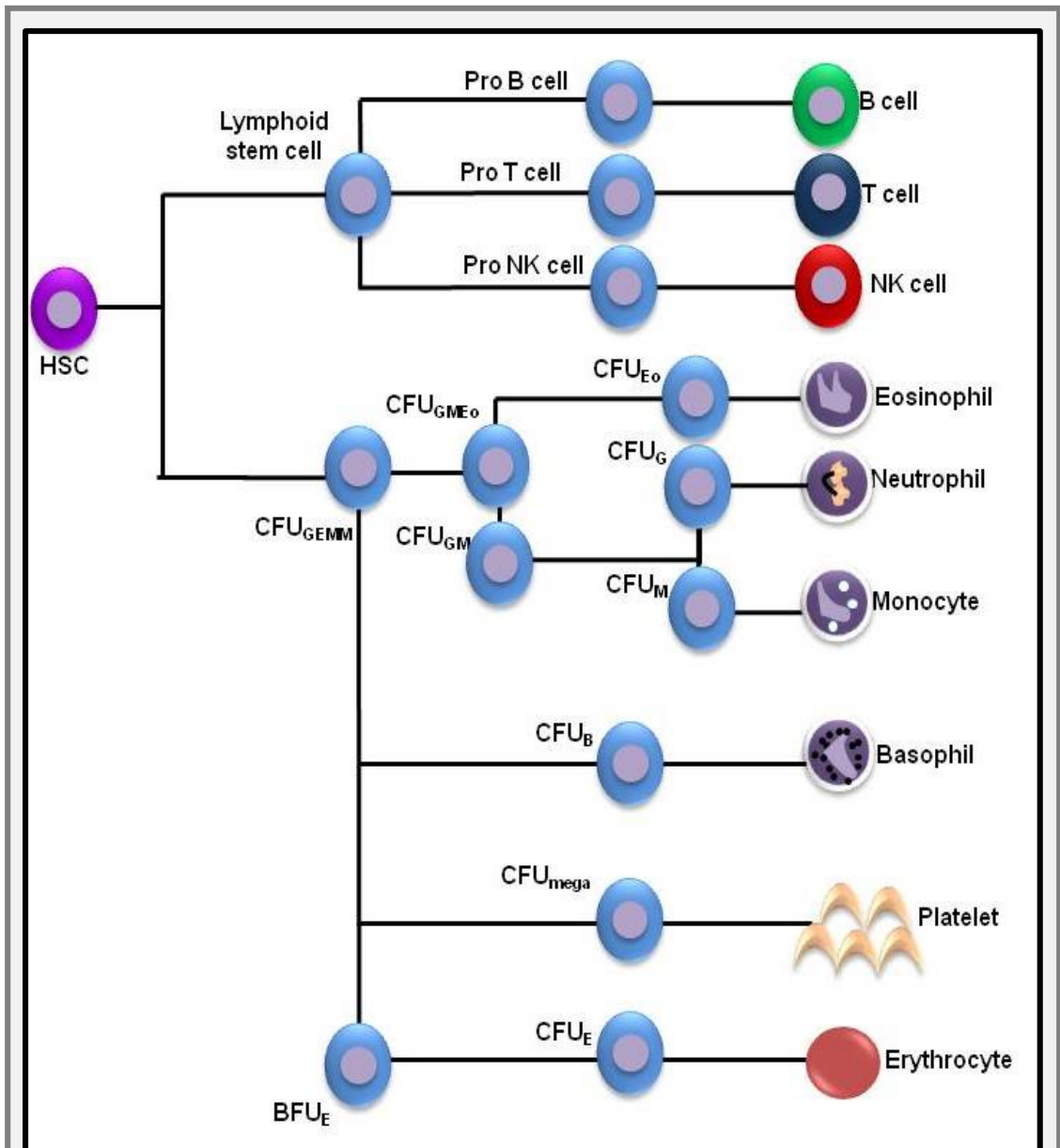
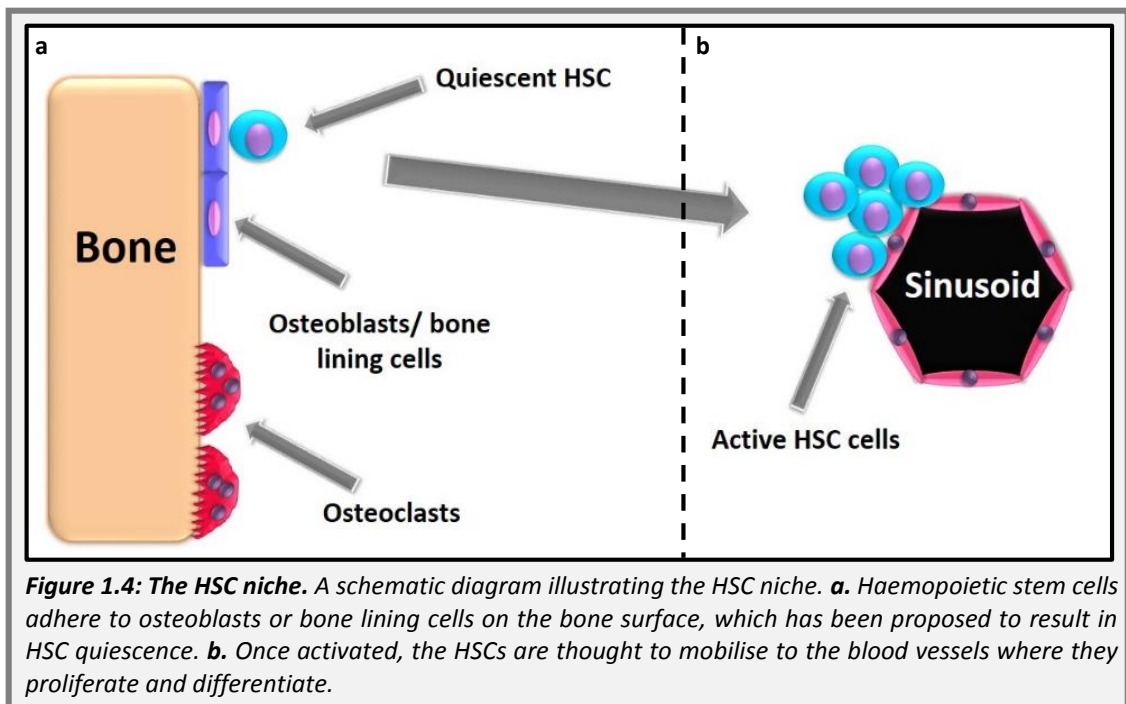


Figure 1.3: HSC differentiation into different cell lineages. A schematic diagram representing the process of haematopoiesis and the lineages in which each cell in the BM is derived. Haemopoietic stem cells differentiate into lymphoid and myeloid lineages. The lymphoid lineage produces B cells, T cells and NK cells. The myeloid lineage produces several progenitors which include colony forming unit (CFU), granulocyte erythroid monocyte and megakaryocyte (CFU_{GEMM}), CFU granulocyte monocyte eosinophil (CFU_{GMEo}), CFU eosinophil (CFU_{Eo}), CFU granulocyte monocyte (CFU_{GM}), CFU granulocyte (CFU_G), CFU monocyte (CFU_M), CFU basophil (CFU_B), CFU megakaryocyte (CFU_{Mega}), burst forming unit (BFU_E) and CFU erythrocyte (CFU_E). These progenitors then differentiate into their corresponding mature cell type. Adapted from Hoffbrand A.V (15) and Reya et al (74).

It has been proposed that HSCs may reside in two different niches entitled the “osteoblastic niche” and the “vascular niche” (75, 76) which are responsible for the maintenance of HSCs and their ability to survive and proliferate in the BM, as shown in Figure 1.4 . However, the existence of either niche remains controversial (77).

In addition to osteoblastic cells and ECs, several other cell types have been implicated in the HSC niche in the BM. These included the chemokine C-X-C motif ligand (CXCL) 12 abundant reticular (CAR) cells, mesenchymal stem cells (MSCs), osteoclasts and adipocytes (76). However, evidence is limited with regards to their roles in the HSC niche.



1.2.2 The osteoblastic HSC niche

The osteoblastic niche is composed of osteoblasts or “osteoblastic-like” cells possessing an osteoblastic phenotype, which includes expression of alkaline phosphatase (Alp). It has been hypothesised that HSCs adhere and interact with osteoblasts or their growth factors on trabecular and endocortical surfaces of bone (73), resulting in G_0 cycling quiescent HSCs and inhibition of their maturation.

Quiescent HSCs are often termed long term-HSCs (LT-HSCs) and possess a commonly recognised phenotype of c-kit positive, sca-1 positive and lineage negative (KSL) and possess the ability to self-renew unlike short-term HSCs (ST-HSCs) (69).

Several *in vivo* studies have identified the importance of osteoblastic cells for HSC survival and self-renewal in the BM, investigated by manipulating osteoblastic number using transgenic mice or administration of hormones in murine models. In core binding factor 1 α (CBF1 α) (an essential osteoblast differentiation transcription factor) knockout (KO) mice (a lethal mutation in homozygous mice), this resulted in a lack of BM cavity, little or no ossification of the skeleton and a decrease in osteoblast numbers. In addition, osteoblastic cells that were present seemed to be poorly differentiated with no osteocalcin (Ocn) expression and weak Alp expression (78). In CBF1 α KO embryos, loss of CBF1 α and therefore osteoblasts, correlated with a reduction in BM haemopoietic cells and also splenomegaly as a result of extramedullary haematopoiesis (79). These findings were also supported by Visnjic *et al* (71, 80) who noted a lack of BM cellularity and a reduction in KSL HSCs when osteoblast numbers were decreased using a thymidine kinase and 2.3 kilo base (kb) fragment of collagen type I α I (COL1A1) promotor, conditional KO mouse model.

Osteoblast stimulation using a constitutively active parathyroid hormone (PTH)/parathyroid hormone-related protein (PTHrP) receptor (PPR) mouse model (81) resulted in an increase in trabecular osteoblastic cells which correlated with a significant increase in HSCs in the long bones and increased HSC engraftment (82). In support of this, daily administration of PTH in C57Bl/6 mice, which increased osteoblast number, also resulted in an increase in HSC number in the BM and HSC engraftment *in vivo* (82). In addition, Zhang *et al* (83), also noted that when osteoblast number was increased using an inducible bone morphogenetic protein (BMP) receptor (BMPR) 1 α KO mouse model, LT-HSC number and HSC engraftment was also increased.

The location of HSCs in the BM microenvironment is also important when defining the HSC niche. Xie *et al* (84) and Zhang *et al* (83) both noted HSC localisation and/or

adhesion to osteoblasts on the endosteal and trabecular bone surfaces by immunohistochemistry (IHC) or immunofluorescence (IF). The osteoblasts that the HSCs adhered to seemed to be a distinct sub-population of mononuclear “spindle-shaped” osteoblasts, positive for neural cadherin (N-cad), a potentially important molecule for HSC proximity to osteoblasts and maintenance of HSC quiescence (83).

Several studies have also reported that LT-HSCs specifically adhering to bone are less sensitive to stresses such as treatment with the chemotherapeutic fluorouracil (5-FU) *in vivo*, which is potentially facilitated by their G₀ phase of cell cycle (85).

1.2.3 The vascular HSC niche

HSCs have also been reported to reside at peri-vascular surfaces in the BM, implicating a vascular niche may also be in existence. The vascular niche is composed of single layered ECs forming sinusoids, which lack connective tissue and therefore are highly permeable (86). It is hypothesised that active HSCs adhere to the ECs, establishing a site for proliferation, differentiation and mobilisation from the niche into the blood.

To illustrate the importance of ECs with regards to HSC maintenance, several *in vitro* studies have co-cultured tyrosine kinase (Tie)-2 positive murine ECs, (isolated from a variety of murine organs) with phenotypic HSCs (87). Co-culturing ECs with HSCs promoted HSC differentiation and cell expansion, compared to controls, illustrating the potential for ECs to provide an environment in which HSCs can survive and self-renew. Several *in vivo* mouse models have also demonstrated the importance of sinusoids for maintenance of haematopoiesis in the liver (88) and HSCs were found adjacent to stem cell factor (SCF) expressing vessels in the BM (89). Furthermore, KO of SCF in both Tie-2 positive ECs and leptin receptor (LEPR) positive peri-vascular stromal cells, significantly reduced HSC frequency in the BM and reduced BM cellularity in the SCF-LEPR KO animals (89), demonstrating the importance of the vasculature and peri-vasculature for the maintenance of HSC numbers.

1.3 Key molecules in the osteoblastic niche

Specific receptors expressed by HSCs and their complementary ligands expressed by either osteoblasts or ECs, may facilitate the adhesion of HSCs to the bone or vasculature. Adhesion to these two sites may also induce HSC dormancy or activation as well as influencing HSC homing to the BM or mobilisation into the circulation.

Several molecules of potential importance have been identified which include CXCR4 and CXCL12, Notch-1 and Jagged (Jag)-1, Tie-2 and Ang-1 and N-cad. Throughout this thesis CXCR4, Notch-1, Tie-2 and N-cad will be referred to as the HSC niche molecules, whereas CXCL12, Jag-1 and Ang-1 will be referred to as the complementary ligands to the HSC niche molecules.

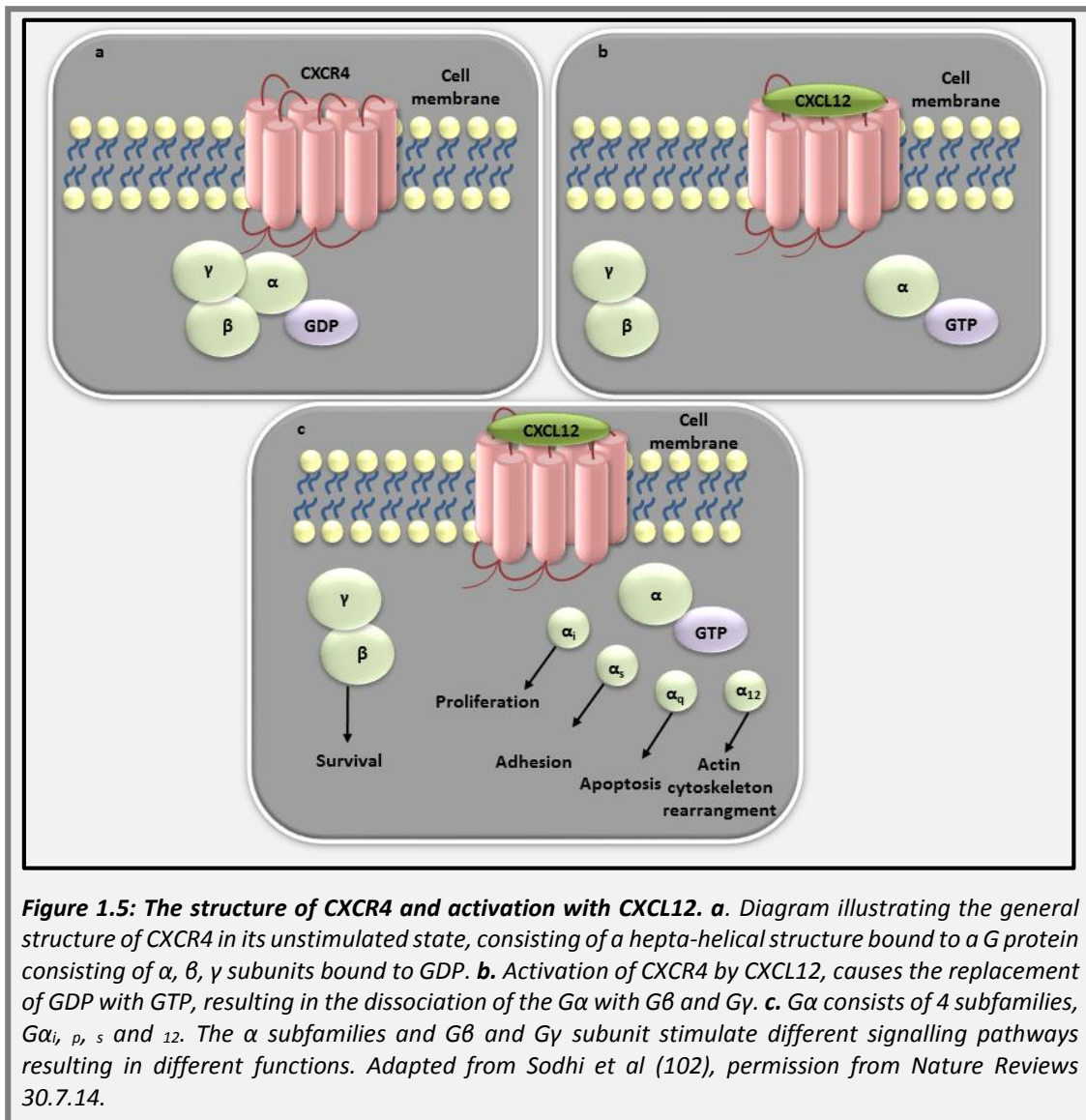
1.3.1 CXCR4/CXCL12

Chemokines are a large family of cytokines associated with many chemotactic responses, particularly inflammation. The family consists of over 50 structurally-related proteins which are 60-88 amino acids (AA) long and they are subdivided into four groups (90). They are classified upon their NH₂ terminal cysteine structure, which contain either adjacent cysteine AAs (CC), two cysteines separated by one different AA (CXC), two cysteines separated by three different AAs (CX3C) (91) or contain only one cysteine (XC) (91). The chemokine CXCL12 or stromal-cell derived factor (SDF)-1, has two splice variants, α and β . It is expressed by several cell types such as ECs, peri-vascular cells, (92) as well as stromal cells residing on endosteal bone surfaces (93). CXCL12 is also expressed on CAR cells residing near sinusoids in the BM (94).

CXCL12 binds to two receptors, CXCR4 and CXCR7 (95), which are known as heptahelical receptors as their chain of AAs “traverses” the membrane seven times (10) (Figure 1.5). They are also more commonly known as G-protein coupled receptors (GPCRs), which are the largest family of membrane proteins which “mediate cellular

responses to hormones, neurotransmitters and are also responsible for vision, olfaction and taste” (96). CXCR4, is one of nineteen known human chemokine receptors (97) and it is expressed in a variety of different tissues including neural, muscle, cord blood and stem cell populations (98), specifically HSCs (99).

As a GPCR, CXCR4 activation is mediated by an “intracellular heterotrimeric G protein” which is bound to the cell membrane (100). The G protein is comprised of three subunits, $G\alpha$, $G\beta$ and $G\gamma$, which bind to guanosine diphosphate (GDP) when the ligand CXCL12 is not bound. However, when CXCL12 is bound, GDP is replaced by guanosine triphosphate (GTP), resulting in the dissociation of the G protein into two separate subunits containing $G\alpha$ which is bound to the GTP and a second subunit containing $G\beta$ and $G\gamma$ (100). The $G\alpha$ subunit can also be classified into 4 separate families $G\alpha_s$, $G\alpha_i$, $G\alpha_q$, and $G\alpha_{12}$ (101, 102). Each $G\alpha$, and $G\beta$ and $G\gamma$ subunit, transmits the GPCR signal down different signalling pathways, which include phospholipase-c (PLC), phosphatidylinositol 3-kinase (PI3-K), extracellular signal-related kinase (ERK), protein kinase (PK) B (PKB/Akt), NF- κ B, mitogen-activated protein kinases (MAPK) and B cell lymphoma (bcl)-2 associated death promoter (BAD) pathways. This results in different downstream effects, which may include chemotaxis, gene transcription and cell survival, required for wound healing, angiogenesis, metastasis, cell recruitment and inflammation, to name but a few (94, 100, 103-107) (Figure 1.5). CXCR4 and CXCL12 signalling is also crucial for functioning tissues, as demonstrated by Nagasawa *et al*, who showed that KO of CXCL12 in a transgenic model resulted in foetal mortality and specifically defects in haemopoietic cells, cardiac tissue and brain tissue (108) .



The requirement for CXCR4/CXCL12 in HSC homing and mobilisation have been illustrated using CXCL12 (109) and CXCR4 KO (94) mouse models. Ara *et al* (109) showed that KO of CXCL12 in mouse embryos resulted in a reduction of HSCs in the liver, spleen and BM. In addition, Tzeng *et al* (110) demonstrated that conditional KO of CXCL12 resulted in a reduction in LT-HSCs, an increase in ST-HSCs and fewer G_0 cycling HSCs, therefore, demonstrating that the CXCR4/CXCL12 interactions may promote HSC quiescence.

These results were also consistent with the conditional KO of CXCR4, where fewer LT-HSCs and fewer G_0 cycling HSCs were present in the BM and there was also an

increase in HSCs in the peripheral blood (94). Therefore, in addition to the promoting quiescence, the CXCR4/CXCL12 axis is required for HSC homing to the BM, liver or spleen from the circulation.

CXCR4/CXCL12 signalling can be inhibited using antibodies or the antagonist AMD3100. *In vitro* migration assays demonstrated that HSCs migrate in response to CXCL12- α enriched media (99) and this was inhibited upon treatment with an anti-CXCR4 antibody (111). Pre-treatment of CD34 positive HSCs with anti-CXCR4 or anti-CXCL12 antibodies also severely reduced CD34 positive HSC engraftment in the BM when injected into non-obese diabetic/severe combined immunodeficiency (NOD/SCID) mice (112). This therefore again, reiterates the importance of CXCR4/CXCL12 signalling for the migration and homing of HSCs.

1.3.2 Notch-1/Jag-1

Notch-1 and Jag-1 have both been reported to possess several roles in stem cell fate, self-renewal and differentiation into specific progeny from HSCs (113, 114). Notch molecules exist as a family of transmembrane glycoprotein receptors, which occur as four homologues, 1-4 (115). Their basic structure consists of an intracellular and an extracellular domain, which contain several different motifs (116-118) as shown in Figure 1.6.

Notch-1 is expressed in a variety of different organs and tissues, such as the thymus, BM and foetal liver (119) as well as by various cell types which include BM precursors, lymphocytes, neutrophils (115) and CD34 positive HSCs (120).

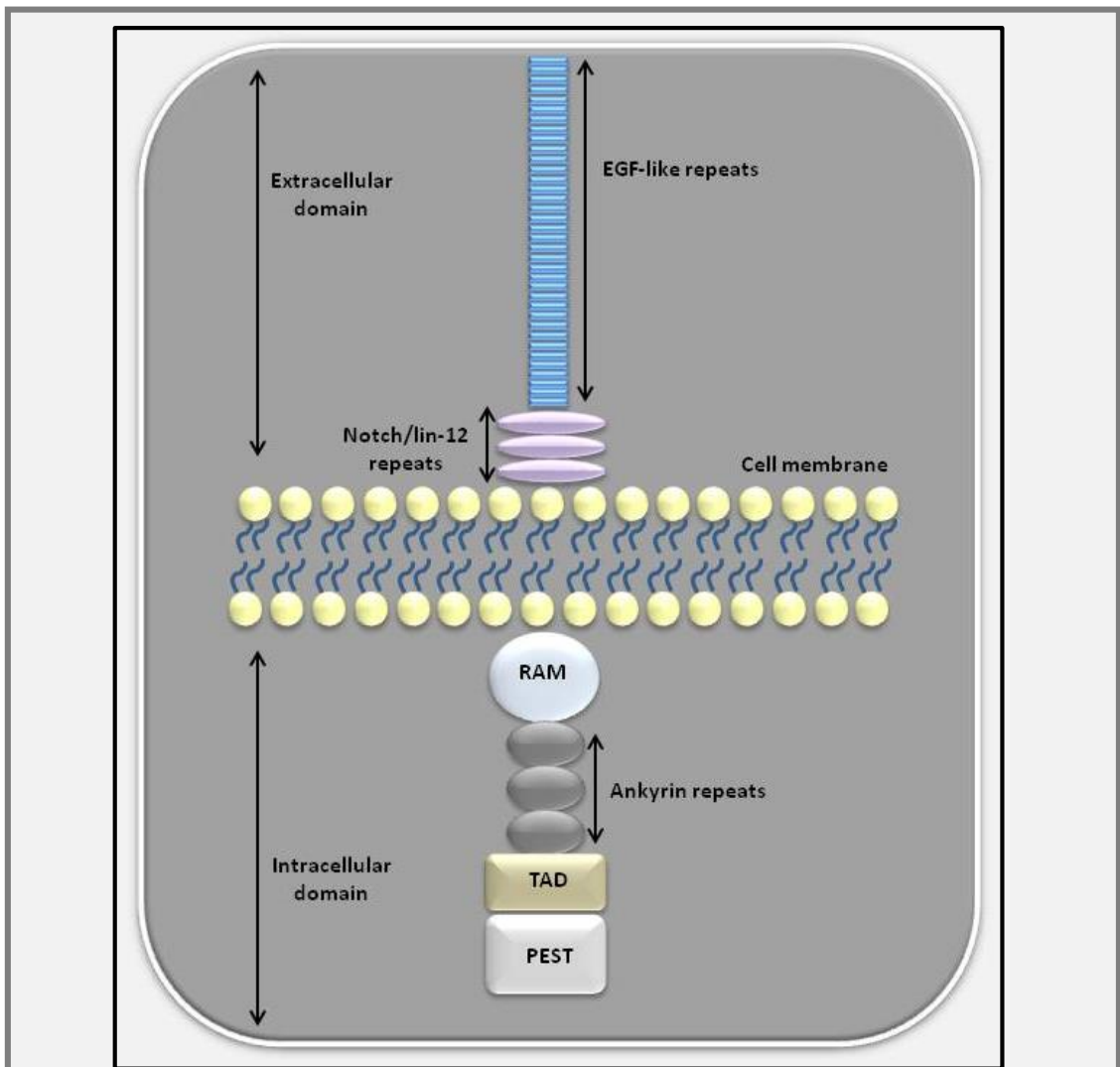
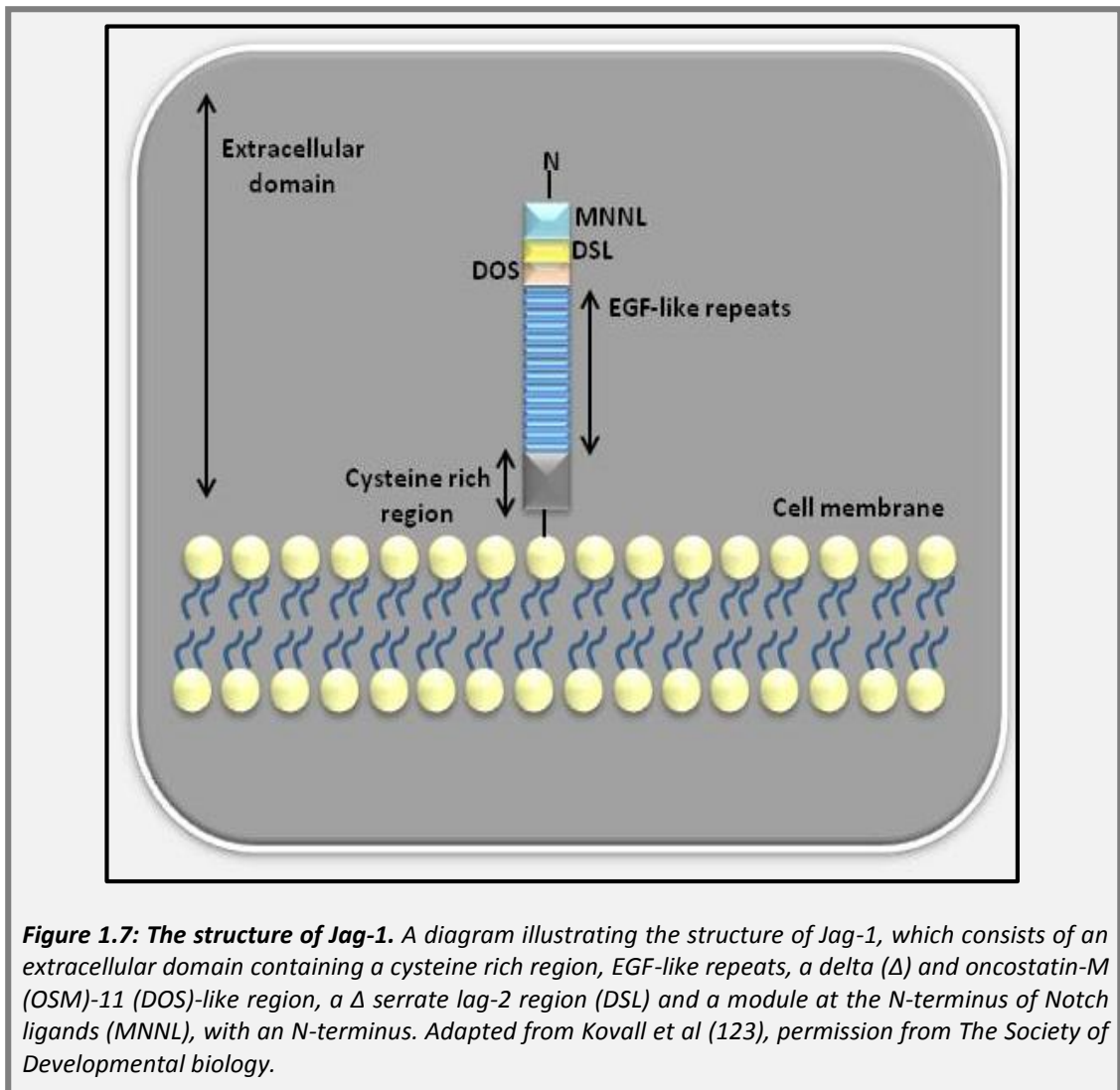


Figure 1.6: The structure of Notch-1. A diagram demonstrating the extracellular and intracellular structure of Notch-1. Its extracellular region consists of epidermal growth factor (EGF) like proteins and Notch-1/ Lin-1 repeats and its intracellular domain consist of a recombination signal-binding protein 1 for J- κ (RBP-JK)-associated molecule (RAM), ankyrin repeats and a transcriptional activation domain (TAD) and a proline, glutamic acid, serine and threonine (PEST) region. Adapted from Swiatek et al (121).

Notch-1 is activated by its complementary ligand Jag-1. The ligands were first characterised in *Drosophila*, which consist of two main groups of Notch ligands named Serrate and Delta. The mammalian homologues of each of these groups of ligands are Delta 1 and 2 and Jag-1 and 2 (113). Jag-1, illustrated in Figure 1.7, is expressed on several cell types, including primary BM stromal cells and human umbilical vein ECs (HUVECs) (114) as well as the murine preosteoblastic cell line MC3T3-E1 (122).



The activation of Notch-1 is initiated through the binding of its ligand Jag-1 (117, 124) as shown in Figure 1.8. Activation of Notch-1 has been achieved using a recombination activation gene-1 (RAG-1) mouse model (115). This model resulted in a 15-fold increase in KSL HSCs and inhibition of HSC differentiation towards the B cell lineage. Interestingly T cell differentiation was not impaired, providing evidence that Notch-1 is required for HSC and progenitor fate. Walker *et al* (113) also found that Jag-1 activation of Notch-1 resulted in reduced proliferation of HSCs and an increase in G_0/G_1 cycling cells *in vitro*, therefore, Notch signalling potentially facilitates HSC quiescence.

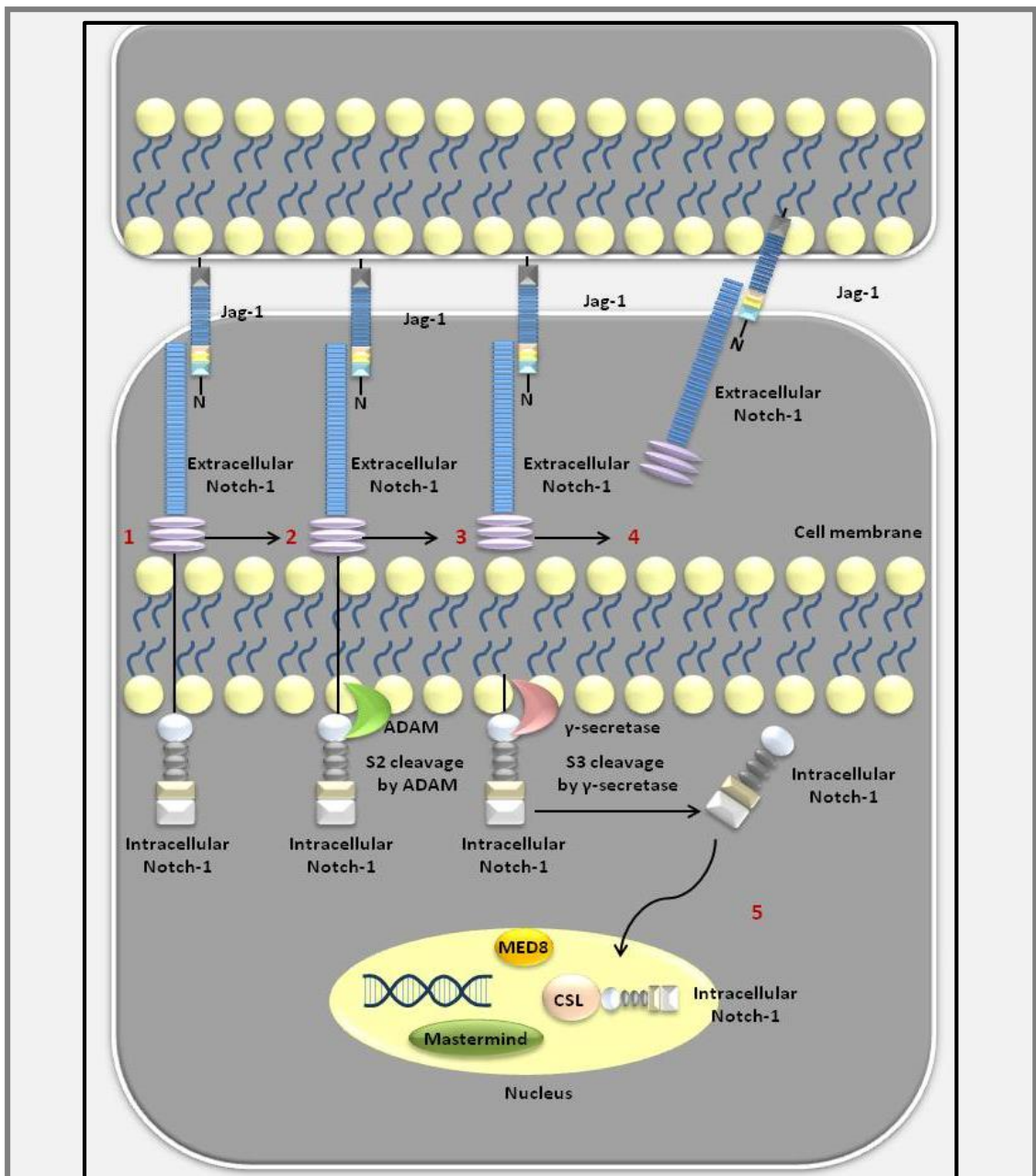


Figure 1.8: The activation of Notch-1 by Jag-1: A schematic diagram illustrating the activation of Notch-1 through the binding of Jag-1 in a neighbouring cell. **1.** Jag-1 binds to the EGF-like proteins in the extracellular region of Notch-1, causing a conformational change. **2.** A disintegrin and metalloproteinases (ADAMs) cleave sites at the intracellular Notch-1 domain resulting in a membrane tethered intracellular Notch-1. **3.** γ secretases cleave the membrane tethered intracellular Notch-1. **4.** Jag-1 and extracellular Notch-1 detach from the cell and intracellular Notch-1 is released. **5.** Intracellular Notch-1 translocates to the nucleus and binds to the DNA binding protein CBF1/RBPjk/Su9H) Lag-1 (CSL), resulting in the recruitment of mastermind and MED8, which induce up-stream target genes. These include hairy enhancer of split (HES), hairy-related (HRT) and hairy/enhancer of split related with YRPW motif protein 1 (Hey1). Adapted from Kopan et al (125), permission from Cell Press 30.07.14.

In addition, Karanu *et al* (114) reported an increase in stem cell self-renewal in the BM of mice that had received Jag-1 activated transplanted HSCs cells compared to

controls. This is further supported by Calvi *et al* (82) who demonstrated an increase in osteoblastogenesis using PPR, which resulted in an increase in Jag-1 expression as well as an increase in HSCs in the BM. In addition, Notch-1/ Jag-1 are essential molecules, as demonstrated using a Notch-1 KO mouse model (121). Embryos in this model died before birth suffering from necrotic tissue, cell death and developmental retardation from 8.5 days post-coitum (PC). Therefore, Notch-1 KO is a lethal mutation, potentially essential for long-term definitive haematopoiesis (119). To investigate the effects of Notch-1 in post embryonic development, a Notch-1 inducible KO model was developed which knocked-out Notch-1 after administration of polyI-polyC (126). This resulted in a decrease in mature thymocytes, mature T cells and an increase in cells of the B cell lineage in the thymus. This therefore, highlights that Notch-1 signalling is required for the differentiation of cells in the T cell lineage and when Notch-1 is deficient, this process is diminished. In addition to this, these data also imply that Notch-1 signalling may be responsible for inhibition of B cell differentiation.

1.3.3 Tie-2/Ang-1

Tie-2 is a cell surface receptor, which exists in the “Tie” family of receptors also containing Tie-1. Tie-2 is expressed by ECs (127), HSCs (85) neutrophils (128), dorsal root ganglion cells (129) as well as synovial lining cells and pericytes in patients with rheumatoid arthritis (127). Its structure consists of an extracellular binding domain and an intracellular kinase domain, as demonstrated in Figure 1.9.

Ang-1 is one of the primary ligands for Tie-2, which is expressed in several cell types such as BM stromal cells, MSCs (130), osteoblast and osteoblast progenitors (85), pericytes (131), neutrophils and monocytes (132). It belongs to a family of four of angiopoietins, known as Ang-1 to 4. Ang-1 and Ang-4 are both receptor agonists whilst, Ang-2 and Ang-3 are receptor antagonists and importantly, Ang-2 specifically blocks Tie-2 activation. The structure of Ang-1 consists of a small “super clustering region”, a coiled-coiled domain and a fibrinogen-like Tie-2 binding region (133) as illustrated in Figure 1.10.

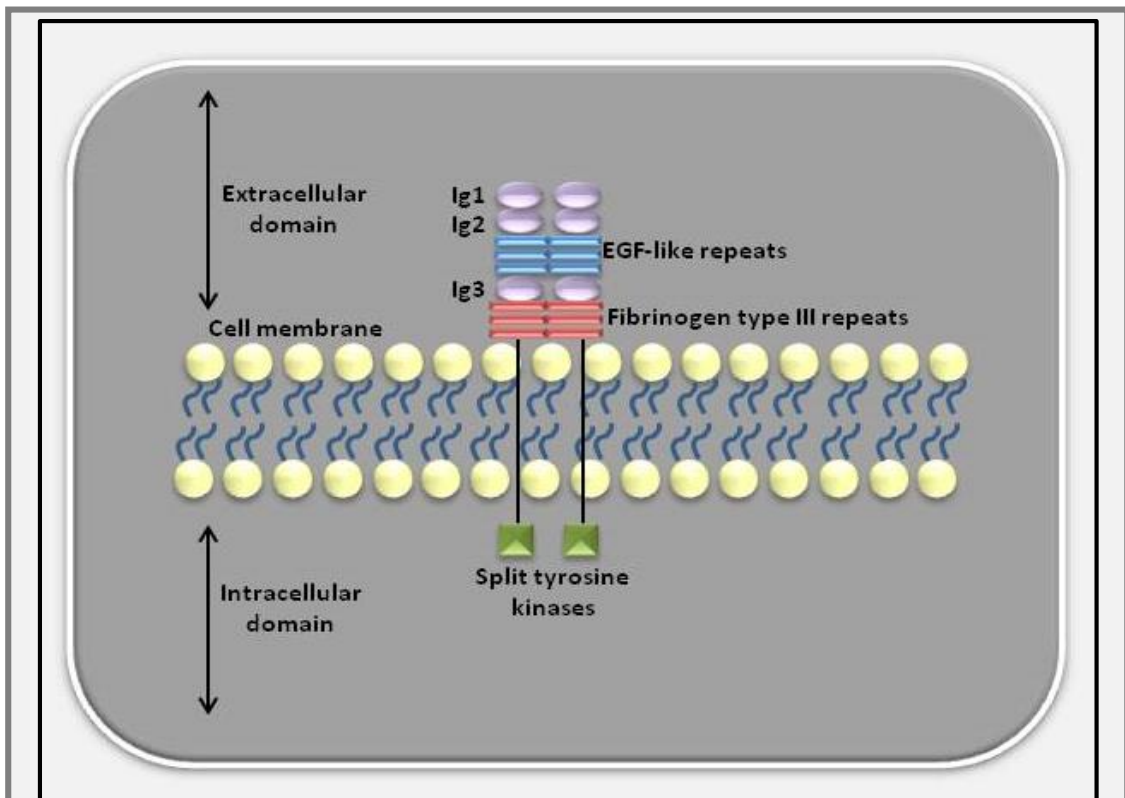


Figure 1.9: The structure of Tie-2. A diagram illustrating the structure of Tie-2, which consists of an extracellular region containing Ig 1-3 domains, EGF-like repeats and fibrinogen type III repeats. The intracellular domain comprises of split tyrosine kinases. Adapted from Huang et al (133), permission from Nature Reviews 30.07.14.

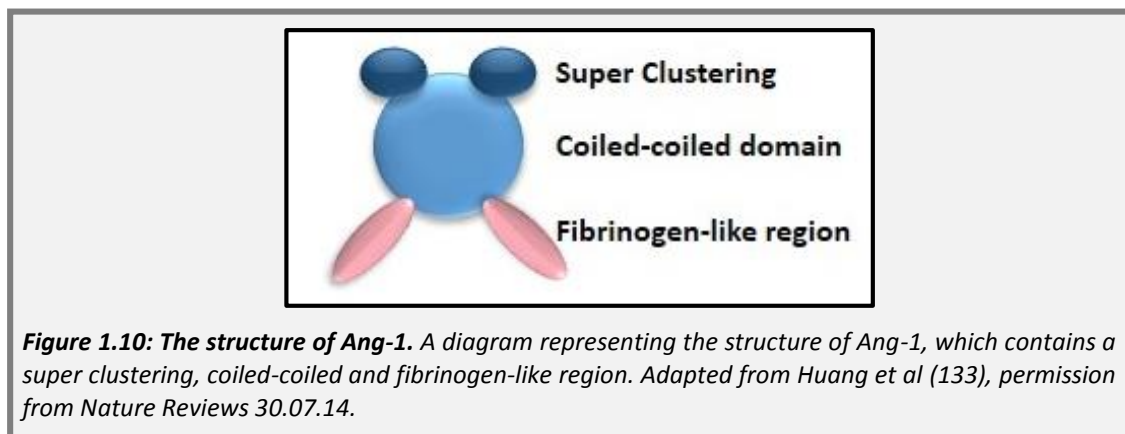


Figure 1.10: The structure of Ang-1. A diagram representing the structure of Ang-1, which contains a super clustering, coiled-coiled and fibrinogen-like region. Adapted from Huang et al (133), permission from Nature Reviews 30.07.14.

The binding of Tie-2 to its ligand results in dimerisation and activation of the kinase domain by phosphorylation (134). The activation of Tie-2 by Ang-1 is essential for several functions, which relate primarily to angiogenesis, but also to inflammation and haematopoiesis. For example activation of Tie-2 results in downstream signalling

of ERK, NF- κ B and PI3-K pathways which can result in cell survival, proliferation, migration, anti-inflammatory, anti-permeability and vessel sprouting/ reorganisation responses (85, 135-139). Tie-2/ Ang-1 signalling is also essential for the survival of functioning tissues. Knock-out of Tie-2 in murine models resulted in lethality before birth and specifically, embryos had impaired cardiac structures and underdeveloped vasculature (140). Similar defects were also noted in Ang-1 KO mouse embryos as well (141).

Tie-2 is also essential for haematopoiesis and is expressed in KSL HSCs (142). When Tie-2 was knocked-out in transgenic mouse models, adult mice experienced a dramatic reduction in haemopoietic cell lineages, therefore, demonstrating that Tie-2 is important for HSC differentiation and proliferation (143). In support of this, Arai *et al* (142) also showed that Tie-2 was important for cell cycling in HSCs. Tie-2 positive HSCs seemed to adhere to Ang-1 positive osteoblastic cells in an osteoblastic niche *in vivo*, resulting in HSC quiescence and evasion from chemotherapy (85).

1.3.4 N-cad

N-cad is a member of the cadherin superfamily. Typically, cadherins are single pass transmembrane, calcium dependent cell-cell adhesion glycoproteins (144). The cadherin superfamily can be categorised into four subfamilies, which are classical, desmosomal, proto-cadherin and cadherin-like proteins. N-cad is grouped into the category of classical Cadherins (145).

The standard structure of a Cadherin molecule consists of an extracellular region, transmembrane helix and a cytosolic domain, as shown in Figure 1.11. The extracellular domain, which acts as the binding domain, contains cadherin repeat proteins, the number of which are dependent on the subtype of classical cadherin, which are entitled I, II and III. Type I and II consist of five cadherin repeats whereas III contain a variable number. N-cad is a type I classical cadherin (146). The homotypic binding of N-cad between cell junctions results in several cleavages of N-cad and subsequent activation, as shown and described in Figure 1.12.

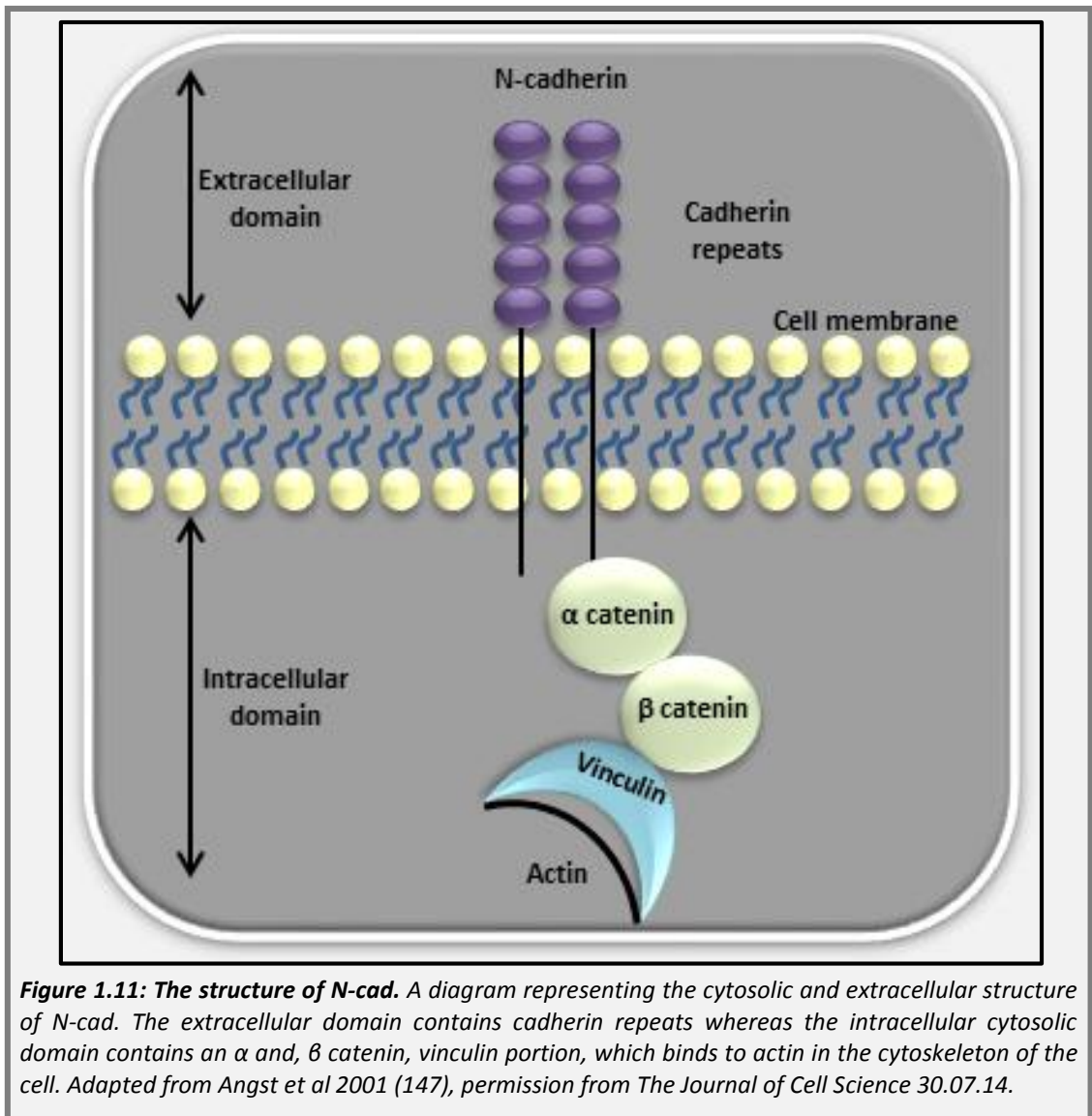


Figure 1.11: The structure of N-cad. A diagram representing the cytosolic and extracellular structure of N-cad. The extracellular domain contains cadherin repeats whereas the intracellular cytosolic domain contains an α and, β catenin, vinculin portion, which binds to actin in the cytoskeleton of the cell. Adapted from Angst et al 2001 (147), permission from The Journal of Cell Science 30.07.14.

N-cad possesses a number of roles throughout the body due to its expression in a variety of tissues including the heart, the nervous system and the BM. N-cad is an essential molecule in the body as demonstrated by N-cad KO mice which died before birth due to heart defects and malformed somites (148).

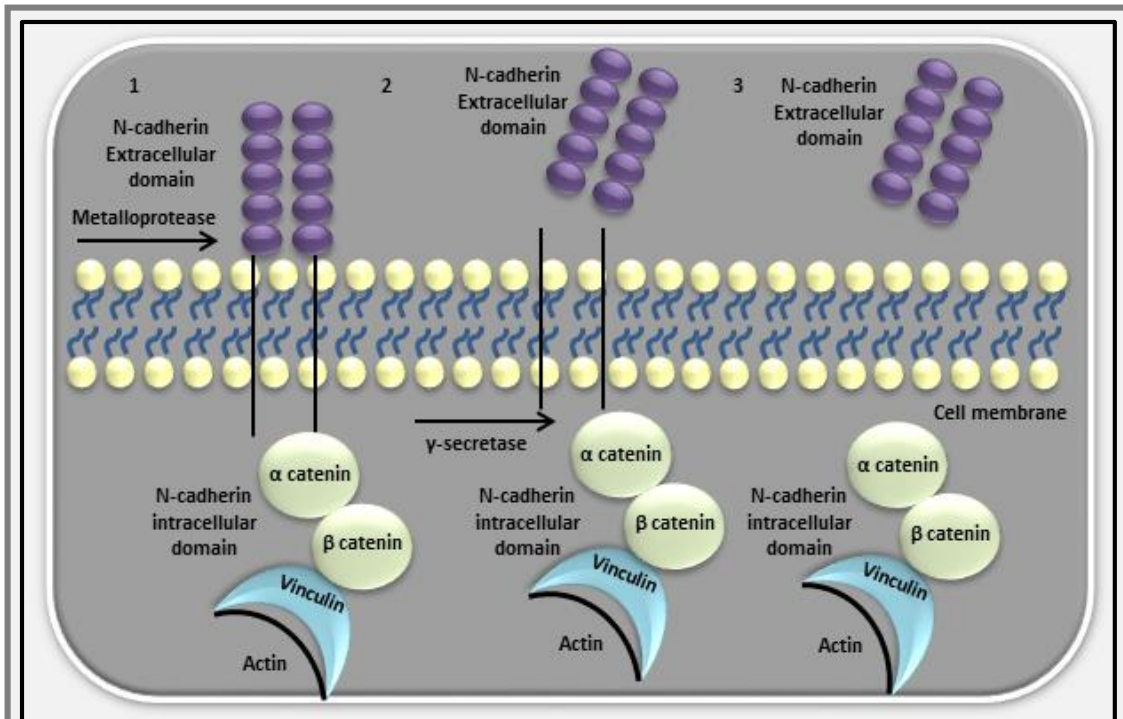


Figure 1.12: Cleavage of N-cad upon activation. 1. N-cad binds homotypically to another N-cad molecule, resulting in cleavage of the extracellular domain by metalloproteinases. 2. The extracellular domain dissociates from the cell membrane and the intracellular domain is subsequently cleaved by γ -secretase. 3. The intracellular domain dissociates from the cell membrane resulting in the release of a soluble α , β and zinc (zn) complex used in MAPK, ERK and β -catenin signalling pathways resulting in cellular invasion and migration. Adapted from Reiss *et al* 2005 (149).

One potential role for N-cad in the BM is its involvement in the HSC niche, where it may anchor HSCs to osteoblasts lining the surface of bone. However, whether N-cad is an essential molecule for HSC maintenance in an osteoblastic niche has been highly debated previously. Several studies reported that KO of N-cad had no effect upon haematopoiesis (77, 150, 151) and Kiel *et al* and Bromberg *et al* were also unable to detect N-cad in purified HSCs by polymerase chain reaction (PCR) and flow cytometry. In contrast, in support of the importance of N-cad in a HSC osteoblastic niche, N-cad was expressed in both human primary trabecular osteoblasts as well as the osteoblastic cell lines MG-63 and SAOS2 (152). N-cad was also found to be expressed in KSL HSCs (83, 84, 142), which specifically localised to N-cad positive osteoblasts with a distinct “spindle” shape. In addition, BMPR1A deficient mice demonstrated an increase in N-cad positive osteoblasts lining the cortical and trabecular bone surfaces, which correlated with an increase in HSCs. This therefore, implies that N-cad positive osteoblasts may be responsible for the self-renewal or

survival of LT-HSCs (83). In addition, knock-down (KD) of N-cad in HSCs reduced their localisation to the endosteum in the BM *in vivo* and significantly reduced HSC long-term repopulating ability in recipient mice in the BM but not in the spleen (153). Whereas, over-expression of N-cad in HSCs, resulted in slower cycling of HSCs, promoted HSC quiescence, and a higher number of HSCs were also found in close proximity to the bone *in vivo* (154).

1.4 A potential myeloma cell niche

As described in Chapter I Sections 1.2 and 1.3, there is a large amount of evidence in support of a HSC niche. The osteoblastic niche results in quiescence of the HSCs via the interactions of molecules expressed on the HSCs themselves and complementary molecules expressed by osteoblasts as shown in Figure 1.13a.

The concept of MCs existing within a niche and expressing the same molecules as those expressed by HSCs is a moderately new theory and as of yet little research has been conducted in order to support this hypothesis. As stated previously, Chen *et al* (70) found that MCs (identified by a PKH26 dye) seemed to home preferentially to osteoblastic niches compared to vascular or splenic niches *in vivo*. In addition, these cells had a higher capacity for chemoresistance compared to MCs that were PKH26 negative, when isolated and analysed *ex vivo*. Several reports have also demonstrated the importance of osteoblastic cells for prostate cancer metastasis to bone. Specifically, Shiozawa *et al* (155) found that using confocal microscopy, prostate cancer cells metastasised to osteoblastic niches in bone where they competed with existing HSCs. Upon, treatment with PTH to increase bone, or reduction of osteoblastic cells using the inducible Col 2.3 KO mouse model, there were increases and decreases respectively in prostate cancer metastasis to vossicles *in vivo*. In addition, treatment of naïve mice with the CXCR4 antagonist AMD3100 resulted in mobilisation of HSCs out of the BM, which increased metastatic potential upon injection of prostate cancer cells, due to reduced competition for the

osteoblastic niche. Similarly, when mice with prostate bone metastasis were treated with AMD3100, this caused mobilisation of prostate cancer cells from the niche. These results are also supported by Wang *et al* (156) who found that prostate cancer cells homed preferentially to the lateral surfaces of bone, which was potentially mediated by higher numbers of osteoblastic cells on that surface compared to the medial surface. As with Shiozawa *et al* (155), this interaction was also inhibited using the CXCR4 antagonist AMD3100.

A potential myeloma cell niche is illustrated in Figure 1.13b, which shows the expression of CXCR4, Notch-1, Tie-2 and N-cad by the MCs and the interaction of these molecules with their complementary ligands CXCL12, Jag-1, Ang-1 and N-cad, expressed by osteoblastic cells lining bone surfaces. These interactions may result in the adhesion of MCs to bone surfaces and may also propagate quiescence in these cells, providing a mechanism for MC survival in the BM.

Currently, there is some evidence, which demonstrates the expression of the HSC niche molecules CXCR4, Notch-1 and N-cad by MCs (which is discussed in the introductions of the individual results chapters). However, the expression of these molecules by MCs has not been reported in the context of an osteoblastic niche in the current literature. In order to determine the expression of these molecules in MCs, preclinical models are typically used. The most common existing preclinical myeloma models are described below in Section 1.5.

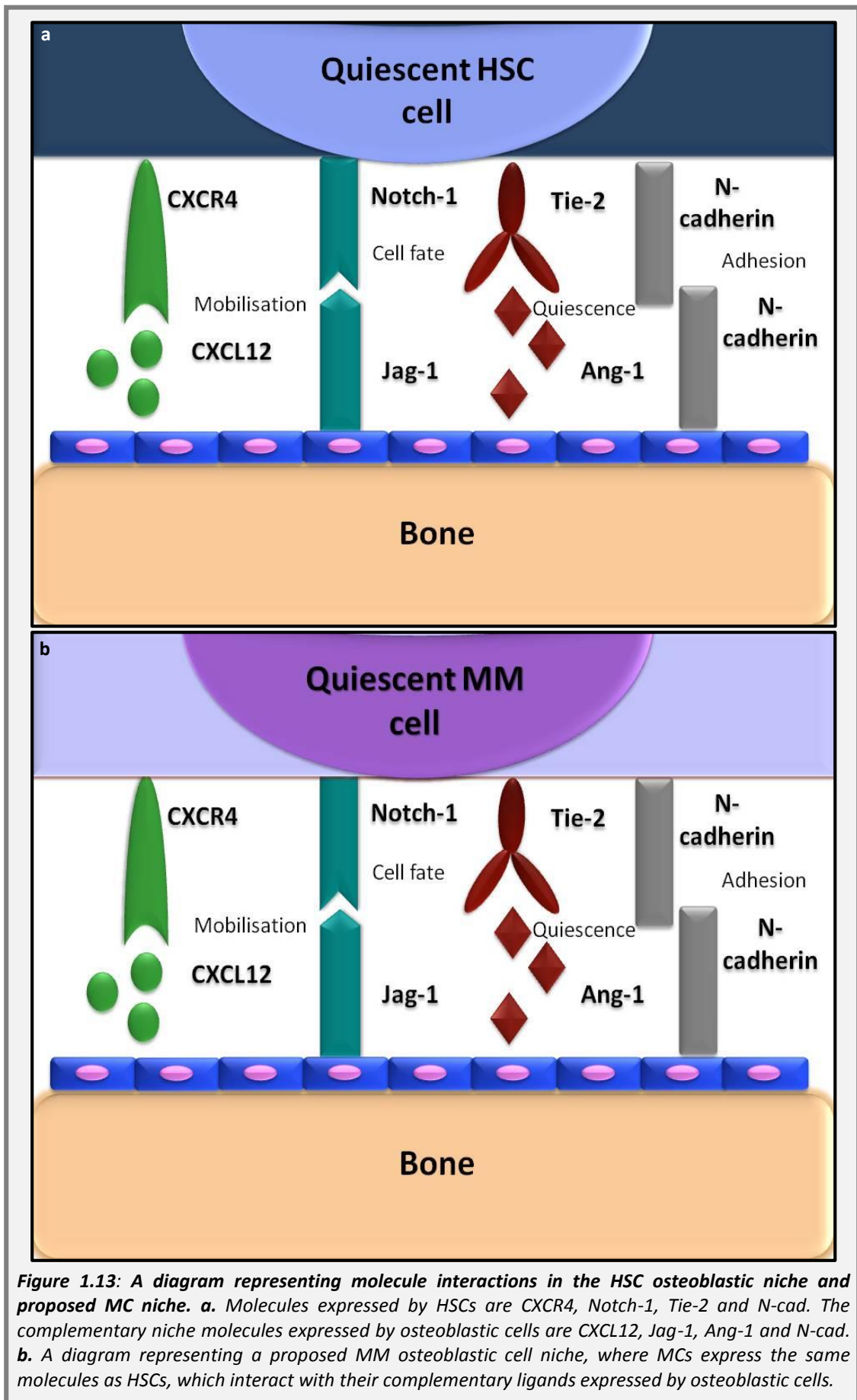


Figure 1.13: A diagram representing molecule interactions in the HSC osteoblastic niche and proposed MC niche. a. Molecules expressed by HSCs are CXCR4, Notch-1, Tie-2 and N-cad. The complementary niche molecules expressed by osteoblastic cells are CXCL12, Jag-1, Ang-1 and N-cad. **b.** A diagram representing a proposed MM osteoblastic cell niche, where MCs express the same molecules as HSCs, which interact with their complementary ligands expressed by osteoblastic cells.

1.5 Preclinical multiple myeloma models

Several models of myeloma have been developed over the past 40 years to assess the efficacy of drugs used in the treatment of MM. Common models previously used include immune-deficient xenograft models using human cell lines such as HS-Sultan (157), ARH-77 (158-160) and RPMI-8226 cells (161) injected intravenously (IV) or intraperitoneally (IP), or S6B45 cells injected subcutaneously (SC) (162) into Severe combined immunodeficiency (SCID) mice. Multiple myeloma disease is recapitulated in these animals (with the exception of the SC tumours), displaying characteristics of MM which include expansion of MCs in the BM, paralysis due to spinal cord compression and production of paraprotein. In addition, primary patient samples have previously been injected into human foetal long bone chips and implanted into immunocompromised mice resulting in MC growth in the human bone implant in the SCID-hu model of MM (163, 164). More recently MC cell lines including U266 and RPMI-8226 have also been injected into NOD.Cg-Prkdcscid Il2rgtm1Wjl/SzJ (NOD/SCID γ) mice intra-tibially and U266 cells have been injected IV (165). Also NOD.Cg-Rag1tm1Mom Il2rgtm1Wjl/SzJ mice, a radiation resistant alternative to NOD/SCID γ mice (166) have been used for recapitulation of MM by injection of U266 and H929 cell lines as well as primary MCs, injected IV.

Alternatively, immune-competent myeloma models are used. These include the 5T series of MM cells, where C57BL/KaLwRij mice are injected with murine “myeloma like cells” (167). The 5T series of murine MCs originated spontaneously in 0.5% of C57BL/KaLwRij mice older than two years, first reported by Radl *et al* (168). The 5T series of murine models of myeloma are maintained by the isolation of 5T cells from the BM of tumour bearing mice and re-injection into young syngeneic recipient mice, where cells typically home to the BM, which is the primary location of disease progression. The full list of 5T murine MCs and their characteristics are listed below in Table 1.3. Most commonly used are the 5T2MM (49, 169, 170) 5T33MM (171-173)

and 5TGM1 (a derivative of the 5T33MM model produced by continual *in vivo* passage of the 5T33MM cells (174)) models of myeloma (175-178).

Table: 1.3: The 5T series of murine models of MM

5TMM series	Isotype paraprotein	Osteolytic bone lesion	Growth pattern
5T2	IgG2a κ	Pronounced	Moderate
5T7	IgG2b κ	Sporadic	Slow, smouldering
5T13	IgG2b κ	Sporadic	Moderate
5T14	IgG1	Mainly osteolytic, some sub-lines osteosclerotic	Moderate, some sub-lines aggressive
5T21	IgD	Not studied	Aggressive
5T30	IgG2a κ	Not studied	Moderate
5T33	IgG2b κ	Diffuse	Aggressive
5TF	IgG3	Mainly peripheral	Moderate
5TGM1	IgG2b κ	Pronounced	Aggressive

Adapted from Asosign et al (179), permission from The Hematology Journal, 31.7.14.

In this thesis, the 5T33 and 5TGM1 murine myeloma models were used. These particular models are well characterised at The University of Sheffield and have the advantage of using immune competent animals. 5T33MM and 5TGM1 cells can be maintained *in vitro* (5T33MMvt and 5TGM1vt) and in addition to wild type (WT) cells; green fluorescent protein (GFP) transduced cells (5T33-GFP and 5TGM1-GFP), have been developed for visualisation by flow cytometry and fluorescent microscopy.

1.6 Summary

In conclusion, MM is a B cell malignancy that develops in a specialised microenvironment in the BM. The specific mechanisms as to how MCs home, colonise and survive in the BM are not fully understood and further research is required in order to understand these processes.

Haemopoietic stem cells exist in BM niches whereby their proliferation and differentiation is maintained by molecules expressed by the HSCs themselves and complementary niche molecules expressed by constituents of the BM microenvironment, which include osteoblastic cells. Myeloma cells may potentially

exist within a similar niche where they express a similar repertoire of molecules as the HSCs, which interact with their complementary ligands expressed by osteoblastic cells located on the surface of bone. These interactions may in-turn result in MC dormancy and subsequent survival in the BM. However, currently, little research has been conducted to identify whether these molecules are expressed by the MCs and whether they are important for the development of MM. Therefore, within my thesis I have conducted further research using the 5T series of murine myeloma models to explore whether MCs utilise the same molecular mechanisms as HSCs to acquire cell dormancy.

1.7 Aims, hypothesis and objectives

1.7.1 Aims and hypothesis

The aim of this project was to test the overall hypothesis that “Myeloma cells exist within an osteoblastic niche similar to that occupied by HSCs”.

Within this main hypothesis, further sub-hypotheses were explored:

1. Myeloma cells express the same repertoire of molecules as HSCs and their complementary ligands are expressed by osteoblastic cells *in vitro*.
2. Myeloma cells express the same repertoire of molecules as HSCs when analysed *ex vivo* and *in vivo*.
3. Treatment of murine primary osteoblast lineage cells (OLCs) with osteogenic media (OGM) will result in osteoblast differentiation and differences in MC adhesion to OLCs at different stages of differentiation.
4. The knock-down (KD) of HSC niche molecules in MCs will result in reduced MC adhesion to primary OLCs *in vitro* and a subsequent reduction in tumour burden *in vivo*.

1.7.2 Objectives

In order to test these hypotheses the following objectives were devised:

1. To determine the expression and presence of the HSC niche molecules CXCR4, Notch-1, Tie-2 and N-cad by the 5T33-WT, 5T33-GFP and 5TGM1-GFP cell lines using endpoint and real-time reverse transcription (RT)-PCR, flow cytometry and immunofluorescence (IF) *in vitro*. To also establish the expression and presence of the complementary ligands CXCL12, Jag-1, Ang-1 and N-cad by the MC3T3-E1 osteoblastic cell line and murine primary OLCs, using endpoint and real-time RT-PCR, flow cytometry and IF *in vitro*.
2. To identify the presence of protein for CXCR4, Notch-1, Tie-2 and N-cad and complementary ligands CXCL12 and Jag-1 by BM derived 5T33-GFP and 5TGM1-GFP cells and spleen derived 5TGM1-GFP cell lines *ex vivo* using flow cytometry. To also determine the presence of protein for CXCR4 and N-cad in 5TGM1-GFP infiltrated BM sections *in vivo* using IHC.
3. To examine the effect of differentiating primary OLCs with OGM on alkaline phosphatase (Alp) production, mineralisation, expression of differentiation markers and HSC niche molecules and ligands using real-time RT-PCR, and attachment to 5TGM1-GFP cells *in vitro*.
4. To Knock-down (KD) HSC niche molecules in 5TGM1-GFP cells using short hairpin ribonucleic acid (RNA) (shRNA), and to establish the effect of this on MC attachment to primary OLCs *in vitro* and tumour burden *in vivo*.

Chapter II: Materials and methods

2.1 General cell culture methods

All equipment, materials and reagents used in tissue culture are outlined in Appendix 1, Section 1.1, Table 1.1.

2.1.1 Cells

2.1.1.1 The 5T murine myeloma cell lines

The murine 5T33MM and 5TGM1 cell lines were kindly provided by Dr Karin Vanderkerken (Vrije Universiteit Brussel, Belgium) and Prof. Babatunde Olukayode Oyajobi (University of Texas Health Science Centre at San Antonio, USA) via Dr Claire Edwards (The University of Oxford, UK), respectively.

2.1.1.2 MC3T3-E1 osteoblast cell line

The MC3T3-E1 osteoblast cell line was originally purchased from The American Type Culture Collection (ATCC). Cells were previously isolated from the calvaria of C57BL/6 mice and sorted by Alp expression described by Kodama *et al* (180). The cell population exist primarily as preosteoblasts however, they are able to differentiate into mature osteoblasts using supplements such as β -glycerophosphate (BGP) and ascorbic acid (asc), described by Kitching *et al* (181).

2.1.1.3 Primary osteoblast lineage cells

Primary OLCs were isolated at The University of Sheffield from C57BL/6 mouse pups as described in Section 2.2.1.2, described previously by Bakker *et al* (182). Like MC3T3-E1 cells they are able to differentiate into mature osteoblasts using BGP and asc, explored thoroughly by Lian and Stein *et al* (183) using rat calvarial osteoblasts and described by Yang *et al* (184) using murine primary osteoblasts.

2.1.2 Cell culture

2.1.2.1 5T murine myeloma cell line culture

All 5T murine MC lines were grown in “complete” Roswell Park Memorial Institute medium (RPMI), containing 10% foetal bovine serum (FBS), 1% penicillin/streptomycin (100 units/100 micrograms (μg)/millilitre (ml) (PS), 1% non-essential amino acids (NEAA) (1X) and 1% (1 millimolar (mM)) sodium pyruvate (NaP), pre-warmed to 37 degrees Celcius ($^{\circ}\text{C}$). Cells were passaged every three days or when confluent to ensure viability. At passage, the cells were split at a 1:5 dilution by removing 3 ml of MCs in suspension and transferring them to a fresh T75 flask containing 12 ml complete RPMI media. Cells were not used experimentally beyond passage six. Cells were cultured at 37 $^{\circ}\text{C}$ in 5% CO_2 .

2.1.2.2 MC3T3-E1 cell line culture

MC3T3-E1 cells were cultured in “complete” Minimum essential medium alpha ($\text{MEM}\alpha$) medium in the absence of deoxyribonucleosides and ribonucleosides, with 10% FBS and 1% PS, pre-warmed to 37 $^{\circ}\text{C}$. Cells were passaged every three to four days or when confluent. At passage, the $\text{MEM}\alpha$ medium was removed and the cells were washed twice in 10 ml phosphate buffered saline (PBS). The cells were dissociated from the flask using 1.5 ml pre-warmed trypsin/ethylenediaminetetraacetic acid (EDTA) (0.25%) at 37 $^{\circ}\text{C}$ for 3 min (min). The trypsin/EDTA was neutralised using 8.5 ml complete $\text{MEM}\alpha$ medium and the cell suspension was transferred to a universal and centrifuged. All centrifugation was conducted at 300 x gravitational acceleration (G) for 5 min at room temperature unless stated otherwise. The cells were re-suspended in 10 ml complete $\text{MEM}\alpha$ media and 2 ml was transferred to a T75 flask containing 10 ml $\text{MEM}\alpha$ media. Cells were not used experimentally beyond passage six. Cells were cultured at 37 $^{\circ}\text{C}$ in 5% CO_2 .

2.1.2.3 Primary osteoblast lineage cell culture

All primary OLCs were cultured in “complete” MEM α , containing deoxyribonucleosides and ribonucleosides (MEM α -Nuc), 10% FBS, 1% PS and 1% fungizone anti-mycotic liquid (FZ), pre-warmed to 37°C. Primary OLCs not undergoing differentiation were not used beyond passage six, whereas cells for differentiation experiments were not used beyond passage two. Primary OLCs when passaged were split as described in Section 2.1.2.2 for the MC3T3-E1 cells. Cells were cultured at 37°C in 5% CO₂.

2.1.2.4 Cell counting

All cells were counted using a Neubauer haemocytometer, where 10 microlitres (μ l) of a cell suspension was combined with 10 μ l trypan blue. Ten μ l of the mixture was placed under a coverslip attached to the haemocytometer and the cells were counted as shown in Figure 2.1.

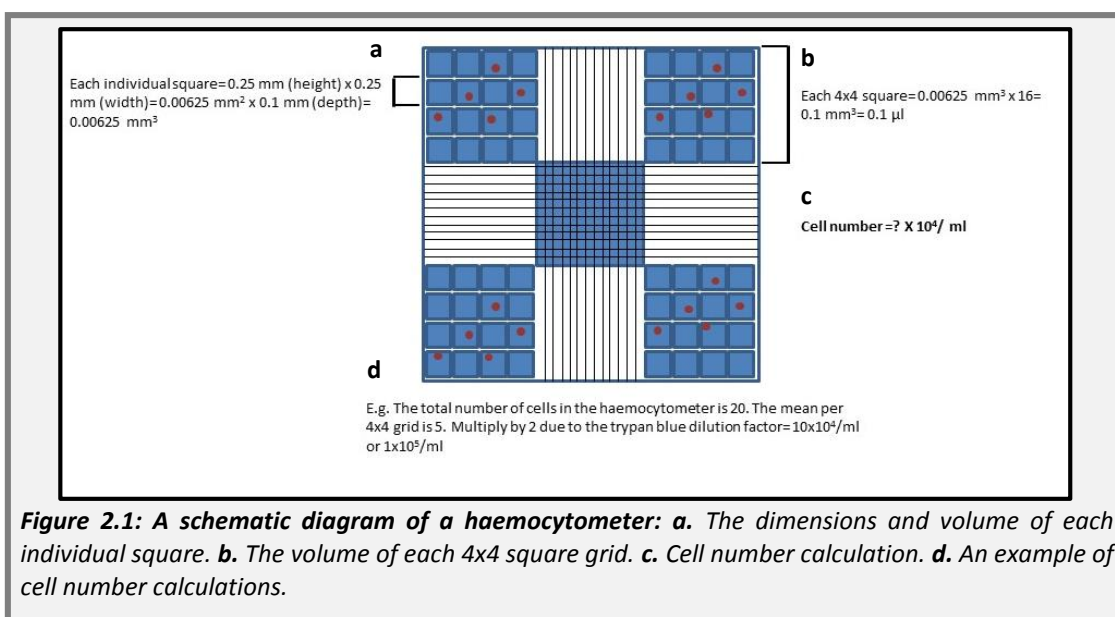


Figure 2.1: A schematic diagram of a haemocytometer: **a.** The dimensions and volume of each individual square. **b.** The volume of each 4x4 square grid. **c.** Cell number calculation. **d.** An example of cell number calculations.

2.1.2.5 Cell thawing

Each vial of cells was removed from liquid nitrogen and rapidly thawed by partial emersion in a 37°C water bath. The thawed cells were transferred to a universal containing 4 ml pre-warmed appropriate media, centrifuged and washed in 5 ml of

media. The wash step was repeated twice to ensure removal of dimethylsulphoxide (DMSO). After the final wash, the MCs were seeded at 1×10^6 cells per 12 ml of media into a T75 flask and the MC3T3-E1 and primary OLCs were seeded at 5×10^5 cells per 12 ml of media into a T75 flask.

2.1.2.6 Cell freezing

Cells were counted, centrifuged and resuspended in 1 ml 10% DMSO/90% FBS per 1×10^6 cells. Each ml was transferred to a cryovial and added to a freezing chamber containing 2-propanol. Cells were left over-night at -80°C , after which the vials were transferred to a liquid nitrogen dewar. This method allowed for uniform slow freezing of the cells and prevented ice crystal formation.

2.1.2.7 Primary osteoblast lineage cell differentiation

For all differentiation experiments, primary OLCs were seeded at a density of $6000/\text{cm}^2$, into a variety of different sized wells and flasks depending on the analysis. The design of the individual aspects of the differentiation experiments are described in the methods section in Chapter V. Three days after seeding, the cells were cultured with or without media containing fresh BGP (10 mM) and asc (50 $\mu\text{g}/\text{ml}$) (aliquoted at 100X and 1000X concentrations respectively and frozen at -20°C prior to use), referred to as OGM. When the cells were replenished, the old media was removed, the cells were washed twice in PBS and standard MEM α -nuc or OGM was then added. The cells were cultured in this manner every two-three days.

2.2 Primary animal cells and tissues

2.2.1 Animal cell isolation

All equipment, materials and reagents used for animal cell isolation are listed in Appendix 1, Section 1.2, Table 1.2.

2.2.1.1 Animals

C57BL/6 and C57BL/KaLwRij mice were purchased from Harlan (Leicester, UK) and the University of Leeds, respectively. All mice were housed in the University of Sheffield's Biological Services. All animal work was approved by the local ethical committee and carried out under Home Office project licence numbers 40/2901 and 40/3462.

2.2.1.2 Primary osteoblast lineage cell isolation

Two to four day old C57BL/6 pups were sacrificed by cervical dislocation per the Code of Practice for the Humane Killing of Animals under Schedule 1 (Scientific Procedures Act 1986). The calvaria from each pup was dissected free of soft tissue under sterile conditions and transferred into sterile PBS containing 1% PS. Each calvaria was washed three times in 5 ml of sterile Hank's balanced salt solution (HBSS), containing 1% FZ, by inversion. The calvariae were cut into small pieces and digested to release the osteoblastic cells. Firstly, 1 ml sterile collagenase II (1 mg/ml) per calvaria was added to the universal with the calvariae and incubated at 37°C for 15 min, inverting the tube every 5 min. The supernatant was removed and discarded (fraction 0). The calvariae were then digested in a further ml of collagenase II (1 ml per calvaria) for 30 min at 37°C, inverting every 10 min. The supernatant was removed, centrifuged at 300 x g for 10 min, and re-suspended in 1 ml complete MEM α -Nuc medium and stored at 4°C (fraction 1). The calvariae were washed twice in 1 ml PBS and further digested in 1 ml sterile EDTA in PBS (4 mM, pH 8.0) per calvaria and incubated at 37°C for 30 min, inverting the tube every 10 min. The supernatant was removed and treated as with fraction 1 (fraction 2). The calvariae were then washed twice in 1 ml HBSS followed by digestion using 1 ml collagenase II (per calvaria) and incubated at 37°C for 30 min, inverting the tubes every 10 min. The supernatant was removed and treated as with fraction 1 and 2 (fraction 3). All the fractions from each of the pups was pooled and divided between an equal number of T25 flasks to the number of pups. An additional 2 ml of media was added to each of the flasks to make a total volume of 5 ml. The cells were incubated until confluent (3-4 days), then pooled, counted and frozen down as described in Section 2.1.2.6.

2.2.1.3 Bone marrow isolation for RNA extraction

The BM from 9-10 week old C57BL/6 mice was isolated to act as a positive control in PCR and flow cytometry experiments for the detection of HSC niche molecules and ligands. Mice were sacrificed under the Schedule 1 Code of Practice for the Humane Killing of Animals (Scientific Procedures Act 1986) by IP injection of 100 μ l pentobarbitone (200 mg/ml) followed by cervical dislocation. The hind limbs were carefully dissected free of soft tissue and the femora and tibiae were separated at the knee joint. The proximal and distal ends of each bone were cut using a scalpel to expose the BM. To isolate the BM, each hind limb was flushed using a sterile needle (27 Gauge) containing 500 μ l PBS and the content of each bone was transferred to a 1.5 ml Eppendorf. The samples were centrifuged, the supernatant removed and the cell pellets were used for RNA extraction as described in Section 2.3.1 1.

2.2.1.4 Bone marrow, splenocyte and blood isolation for flow cytometry

Bone marrow, splenocytes and blood were isolated from 9-10 week old C57BLK/6 mice to act as a positive control for initial antibody optimisation experiments. In addition, the BM and spleen were isolated from 6-8-week-old C57BL/KaLwRij mice injected with 5T33-GFP or 5TGM1-GFP cells for the detection of HSC niche molecules and ligands in experimental flow cytometry experiments.

Bone marrow was isolated as described in Section 2.2.1.3. However, after the samples were centrifuged and the supernatant removed, 2 ml RBC lysis buffer (1X, diluted in distilled water (H₂O) (dH₂O)), was added to each cell pellet and incubated at room temperature for 10 min. Lysed RBCs were removed from the sample supernatant by centrifugation and the sample was subsequently washed twice in 1 ml wash buffer (1X diluted in dH₂O), provided in the RBC lysis kit. Bone marrow cells isolated from C57BL/6 mice were counted and 1×10^6 cells were used per flow cytometry sample for the detection of HSC niche molecules and ligands. Whereas, only 100,000 BM cells, isolated from C57BL/KaLwRij mice were used per flow cytometry sample, due to the large numbers of samples required.

To isolate the splenocytes, the spleen was carefully dissected and torn into 5 ml Dulbecco's Modified Eagle Medium (DMEM) into a petri dish. The suspension was filtered through a 70 μm cell strainer, to remove large pieces of tissue, followed by centrifugation. Red blood cells were lysed and 1×10^6 splenocytes, isolated from the C57BL/6 mice and 100,000 splenocytes isolated from the C57BL/KaLwRij mice were used per flow cytometry sample.

Blood was extracted from pentobarbitone-sedated mice via cardiac puncture using a sterile needle (27 Gauge). The blood was immediately transferred to a vacutainer coated in EDTA to prevent coagulation and 1 ml RBC lysis buffer was added per 100 μl of extracted blood for 10 min at room temperature. Red blood cells were removed from the supernatant following centrifugation at $600 \times g$ for 8 min at room temperature and the remaining cells were washed twice in RBC lysis wash buffer. Flow cytometry was then conducted using 100,000 blood cells per sample isolated from the C57BL/6 mice and 10,000 isolated from C57BL/KaLwRij mice.

2.2.2 *In vivo* models of multiple myeloma

2.2.2.1 The 5T33-GFP and 5TGM1-GFP models of multiple myeloma for detection of HSC niche molecules and ligands

Six to eight week old C57BL/KaLwRij mice were injected IV via the tail vein with either 1×10^6 5T33-GFP or 2×10^6 5TGM1-GFP cells. All mice were sacrificed upon presentation of hind limb paralysis (a clear indicator of tumour load). In the 5T33MM-GFP model this occurred within 4-6 weeks post-injection (P-I), whereas in the 5TGM1-GFP model this occurred at 21-23 days P-I. Tumour burden and the presence of protein for HSC niche molecules and ligands in the tibiae were assessed by flow cytometry as described in Sections 2.2.1.4 and 2.4.1.2. Further details of study design are outlined in the methods section in Chapter IV and Chapter VI.

2.2.2.2 Gene knock-down experiments in the 5TGM1-GFP model

For N-cad KD studies, a pilot experiment was firstly conducted where 11 week old female C57BL/KaLwRij mice were injected IV with either 2×10^6 un-transduced 5TGM1-GFP, scrambled control cells (CTRL 25) or N-cad KD (KD 25) cells. At the first signs of illness, the entire cohort of mice was sacrificed. Tumour burden was determined by flow cytometry and CD138 IHC, as described in Sections 2.4.1.2 and 2.4.3.3 respectively, and bone disease was analysed using micro CT (μ CT) as described in 2.7.1.1. Further details of the study design are outlined in the methods sections in Chapter VI.

2.3 Molecular biology methods

2.3.1 RNA extraction

All equipment, materials and reagents used for RNA extraction are outlined in Appendix 1, Section 1.3, Table 1.3.

2.3.1.1 RNA methodology

To detect the gene expression of each HSC niche molecule, ligand and the plasma cell marker CD138 from the desired tissue or cell type, the messenger RNA (mRNA) was firstly extracted using a phenol/chloroform method (Ultraspec reagent). Myeloma cells, MC3T3-E1 and primary OLCs were set-up in culture 24 hours prior to extraction, as described in the method sections in the individual results chapters. After 24 hours, the MC cells were centrifuged, washed once in 5 ml PBS and re-suspended in 1 ml Ultraspec RNA isolation solution. Whereas, for the MC3T3-E1 cells and primary OLCs, the media was removed, the cells were washed once in 5 ml PBS, and 1 ml Ultraspec was added directly to each flask. In addition, the cell pellets from the murine BM samples, following their isolation, as described in Section 2.2.1.3, were re-suspended directly into 1 ml of Ultraspec solution. All cells were then transferred to a 1.5 ml

RNase and DNase free tube and vigorously vortexed for homogenisation for 5 min at 4°C.

To each sample, 200 µl of chloroform was added and incubated at 4°C for 5 min. This was followed by centrifugation at 12,000 $\times g$ for 15 min at 4°C after which the content of each tube had separated into three phases; a lower organic phase, an inter-phase and an upper aqueous phase containing the RNA. The aqueous phase was transferred to a new 1.5 ml RNase and DNase free tube and an equal volume of isopropanol was added. The samples were then incubated for a further 20 min at 4°C and centrifuged again at 12,000 $\times g$ for 5 min at 4°C to precipitate the RNA. The samples were then washed twice in 70% ethanol diluted in diethylpyrocarbonate (DEPC) water and centrifuged at 7,500 $\times g$ for 5 min in between washes. The RNA pellet was air dried and solubilised in 30-50 µl of DEPC water. The samples were then stored at -80°C until required for RT.

2.3.1.2 Quantification of RNA

The purity and concentration of all RNA samples were determined using a NanoDrop 2000 and its dedicated software. The purity of each sample was determined using the 260/280 nanometre (nm) and 260/230 nm absorption ratios. Ribonucleic acids absent of protein contamination (260/280 nm) had a value above 1.8 and RNA which did not contain impurities such as phenol or ethanol (260/230 nm) had a value of between 2.0-2.2. An example of the curves generated using the NanoDrop 2000 software are shown in Appendix 2, Section 2.1. The concentration of the RNA, which was usually between 200-600 nanograms (ng)/µl, was also calculated using the NanoDrop 2000 software.

2.3.1.3 RNA fragment-length analysis

Fragment length analysis of each RNA sample was established using an Agilent Bioanalyser 2100 and analysed using 2100 Expert Software by Paul Heath at The

University of Sheffield. An RNA integrity number between 9.0 and 10 indicated suitable RNA fragment length. Examples of fragment length analysis are shown in Appendix 2, Section 2.2.

2.3.2 Reverse transcription

All equipment, materials and reagents used for RT are outlined in Appendix 1, Section 1.4, Table 1.4.

2.3.2.1 Reverse transcription methodology

Reverse transcription was conducted to convert mRNA into complementary DNA (cDNA), for subsequent PCR experiments. To remove any contamination before conducting RT, the required number of 0.5 ml RNase and DNase free tubes for the RT reaction were irradiated for 30 min in an ultra violet (UV) hood. Two micrograms of RNA was calculated and the required volume was transferred to an irradiated 0.5 ml tube and DEPC H₂O was added to make a final volume of 11 µl. For each RNA sample, a superscript positive (a sample with reverse transcriptase enzyme) (RT+) and superscript negative (a sample without reverse transcriptase enzyme) (RT-) replicate was prepared, to control for genomic contamination.

Reverse transcription was conducted by combining random primers, deoxynucleotide triphosphates dNTPs and DEPC H₂O together in a 0.5 ml tube. The volumes required of each reagent for one sample is shown in Table 2.1. Two microlitres of this mixed was added to each tube containing the RNA and DEPC H₂O to make a 13 µl solution. The samples were then placed in a MJ Research PTC 200 thermal cycler for 5 min at 65°C to allow for the binding of the random primers to the RNA template. After 5 min, the samples were removed from the thermal cycler and cooled at 4°C for at least 1 min.

Table 2.1: Reagents required for one sample in the first phase of reverse transcription

Reagent	Stock solution	Working solution	Volume (µL)
DEPC H ₂ O	n/a	n/a	0.5
Random primers	500 ng/ µl	250 ng	0.5
dNTPs	10 nM	5 nM	1

This was followed by combining first strand buffer, dithiothreitol (DTT), RNase inhibitor (RNasin) together and then adding either SuperScript RT enzyme (RT+) or DEPC H₂O (RT-). The volumes added are shown in Table 2.2.

Table 2.2: Reagents required to make one RT+ and RT- sample in the second phase of reverse transcription

Reagent	Stock solution	Working solution	RT- volume (µL)	RT+ Volume (µL)
First strand buffer	5X	1X	4	4
DTT	0.1 M	5 mM	1	1
RNasin	1 unit/ µl	1 unit	1	1
SuperScript III, Reverse transcriptase enzyme	200 units/ µl	200 units	0	1
DEPC H ₂ O	n/a	n/a	1	0

The entire 7 µl of the mix was then added to each RNA sample and placed in the thermal cycler. The RT samples were heated at 25 °C for 5 min, followed by 50 °C for 55 min, 70 °C for 15 min and 4 °C thereafter, as described in Table 2.3. The cDNA samples were then removed from the thermal cycler, diluted approximately to 20 ng/µl, using nuclease free water and stored at -20°C until required for PCR.

Table 2.3: Temperatures and times used for reverse transcription

Temperature (°C)	Time (Min)
25	5
50	55
70	15
4	Thereafter

2.3.3 Endpoint PCR

All equipment, materials and reagents used for endpoint PCR are outlined in Appendix 1, Section 1.5, Table 1.5.

2.3.3.1 Principals of endpoint PCR

Endpoint PCR is a tool used for the amplification of a sequence of DNA from a particular gene of interest (GOI). Once amplified, the gene product can be visualised by agarose gel electrophoresis. The basic principle of PCR, which is displayed in Figure 2.2, involves the use of a heat stable enzyme known as *Taq* polymerase, isolated from the bacterium *Thermus Aquaticus*. Within the PCR reaction, specific primers bind to their complementary nucleotides on the cDNA template, initiating the binding of *Taq* polymerase and subsequent transcription of a complementary strand of the template by the binding of dNTPs to their complementary nucleotides. After a number of cycles, the desired product is amplified sufficiently for visualisation in the agarose gel.

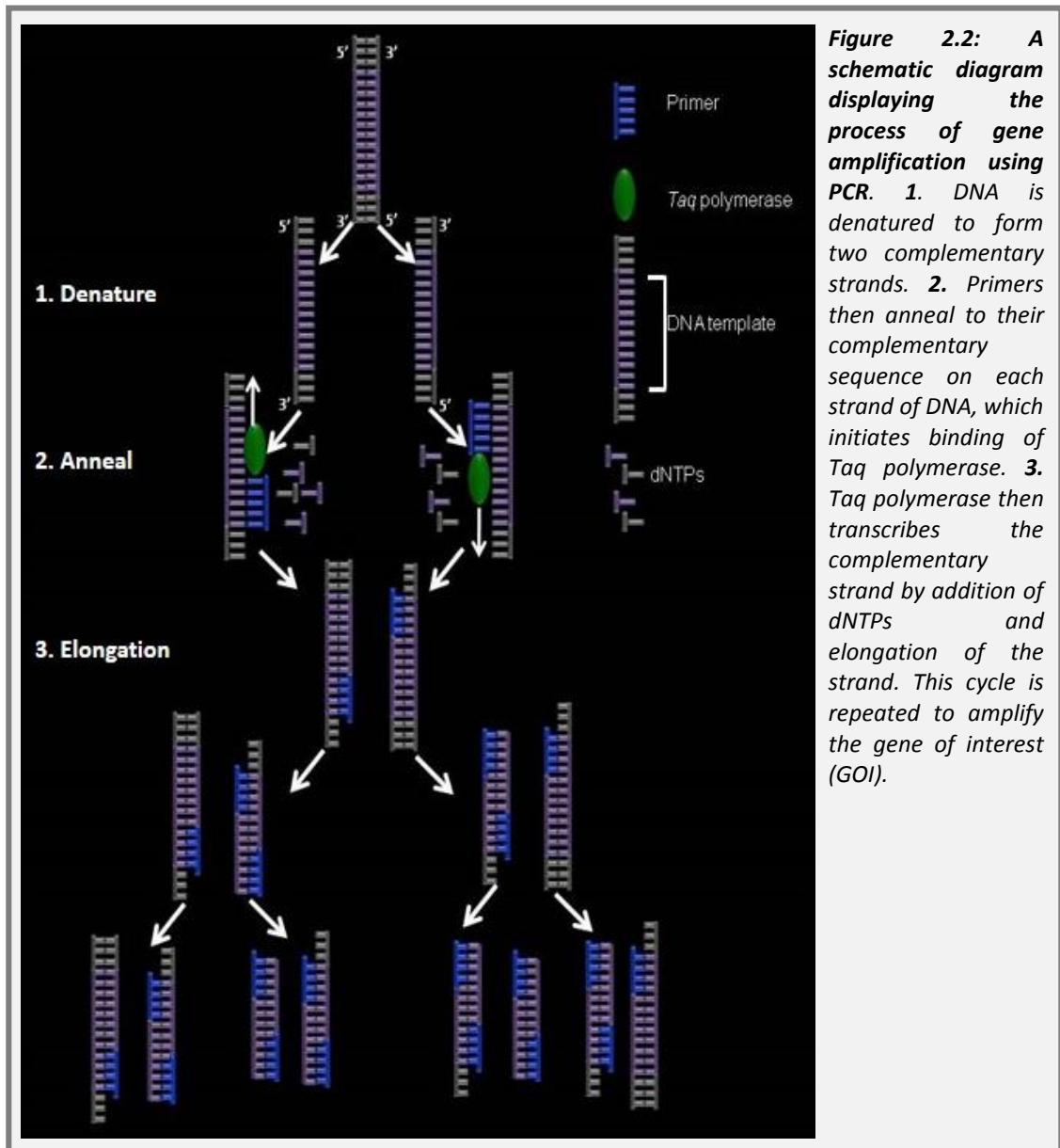


Figure 2.2: A schematic diagram displaying the process of gene amplification using PCR. 1. DNA is denatured to form two complementary strands. 2. Primers then anneal to their complementary sequence on each strand of DNA, which initiates binding of Taq polymerase. 3. Taq polymerase then transcribes the complementary strand by addition of dNTPs and elongation of the strand. This cycle is repeated to amplify the gene of interest (GOI).

2.3.3.2 Endpoint PCR methodology

An endpoint PCR mix was made by combining magnesium chloride ($MgCl_2$), ammonium buffer, dNTPs, sense and anti-sense primers, Taq polymerase and RT-PCR H_2O . Forty-eight microlitres of the PCR mix was added to 2 μl of cDNA (approximately 40 ng) to make a final volume of 50 μl . The volume required of each reagent for one sample is described in Table 2.4.

Table 2.4: Reagents required for one endpoint PCR sample

Reagent	Stock solution	Working solution	Volume (μL)
MgCl ₂	50 mM	3 mM	3
Ammonium buffer	10X	1X	5
dNTPS	10 nM	1 nM	5
Sense and anti-sense primers	5 μm	0.2 μm	2
<i>Taq</i> polymerase	5 units/ μ	2.5 units	0.5
RT-PCR H ₂ O	n/a	n/a	30.5

Samples were loaded into the thermal cycler. The standard settings for the PCR reactions were as follows; denaturation at 95°C for 5 min, annealing for 1 min (temperatures varied for each set of primers, see Appendix 2, Section 2.4, Table 2) and elongation at 72°C for 1 min. These steps were then repeated for the number of cycles required; see Appendix 2, Section 2.4, Table 2 for cycle numbers. This was followed by a final elongation step at 72°C for 10 min and the samples were then cooled to 4°C. The end PCR product was either stored at 4°C short-term or at -20°C long-term.

2.3.3.3 Primer design

Primers were designed using the following guidelines: 20 base pair (BP) in length, G+C content between 40%-60%, no repeated lengths greater than 3 BP, no repeat dinucleotides e.g. ATATATATA, primers must not be complementary to avoid primer dimer, must cross exon boundaries, the melting temperatures (T_m) must not differ by >5°C between the primers, the 3' end should contain a G or C (G/C Clamp).

The full sequence of each set of primers and their T_m s are shown in Appendix 2, Section 2.5, Table 2.2.

2.3.4 Gel electrophoresis

All equipment, materials and reagents used for gel electrophoresis are outlined in Appendix 1, Section 1.6, Table 1.6.

2.3.4.1 Principals of gel electrophoresis

Gel electrophoresis allows for the separation and subsequent visualisation of PCR products. The amplified DNA is loaded into an agarose gel and when a current is applied, the negatively charged DNA moves through the gel towards the anode. The larger the size of DNA product, the slower it moves through the gel due to the restriction of the agarose pore size. Therefore, larger products are visualised nearer to the top of the gel. A DNA ladder is also used to estimate the BP size of the DNA product. Ethidium bromide in the agarose binds to DNA present in the sample and subsequently fluoresces upon exposure to UV light. Therefore, gene expression of the sequences amplified by PCR are visualised as a white band.

2.3.4.2 Gel electrophoresis methodology

The agarose gel for the electrophoresis was made using trizma base, acetic acid, EDTA (TAE) buffer (pH 8.0) and agarose. The quantities of each reagent required to make one litre of 50X TAE buffer demonstrated in Table 2.5.

Table 2.5: Reagents and the quantities required to make 1 litre of 50X trizma base, acetic acid and EDTA buffer

Reagent	Stock solution	Working solution	Amount required
Trizma base	n/a	2 M	242 g
EDTA pH 8.0	0.5 M	50 mM	100 ml
Glacial acetic acid	Glacial	1 M	57.1 ml
dH ₂ O	n/a	n/a	842.9 ml

The 50X solution was then diluted 1:50 using dH₂O before use, to produce a solution containing 40 mM tris base, 20 mM glacial acetic acid and 1 mM EDTA, pH 8.0. To make the gel, agarose was added to the TAE buffer at a 1.6% concentration and then

dissolved by heating in a microwave. The agarose was then cooled to approximately 60°C and ethidium bromide was added at a final concentration of 0.5 µg/ ml. The agarose was then poured into a gel mould and electrophoresis combs were added to form wells. The gel was then left to cool to room temperature for 45 min. Once cooled the gel was transferred to an electrophoresis tank containing 1X TAE buffer, which covered the surface of the gel. The combs were removed to allow for the addition of PCR products into the wells. Twenty microlitres of PCR product and 5 µl of loading buffer (1X) were added to an irradiated 0.5 ml RNase and DNase free tube. Fifteen microlitres of RT+ and RT- samples were loaded into neighbouring wells preceded by 15 µl of RT-PCR H₂O and 15 µl of the hyperladder IV. The DNA was then separated at 120 Volts using a power pack for 40 min and visualised using a Bio-rad Gel Doc XR+ Imager system and Quantity One 4.6.8 software.

2.3.4.3 Gene sequencing

To confirm the specificity of the PCR products, each PCR sample was sequenced in-house by the University of Sheffield Medical School Genomics Facility. After sequencing, the exact homology was analysed by comparing the sequencing results with the expected template and GenBank archives.

2.3.5 Real-time PCR

All equipment, materials and reagents used for real-time PCR are outlined in Appendix 1, Section 1.7, Table 1.7.

2.3.5.1 Principals of real-time PCR

Real-time PCR uses the basic principles of PCR however, rather than displaying the results in an agarose gel the results are assessed quantitatively in “real-time”. In addition, rather than using primers, intercalating dyes or fluorescent hydrolysis probes are used. The intercalating dyes bind directly to the DNA whereas, the fluorescent probes, bind to complementary nucleotides on the cDNA template.

Fluorescent probes are made of DNA oligonucleotides with a 5 prime end (5') bound to a reporter molecule (such as 6-carboxyfluorescein (FAM)) and a 3 prime end (3') bound to a quencher molecule, such as minor groove binder (MGB). Their use in real-time PCR is shown in Figure 2.3.

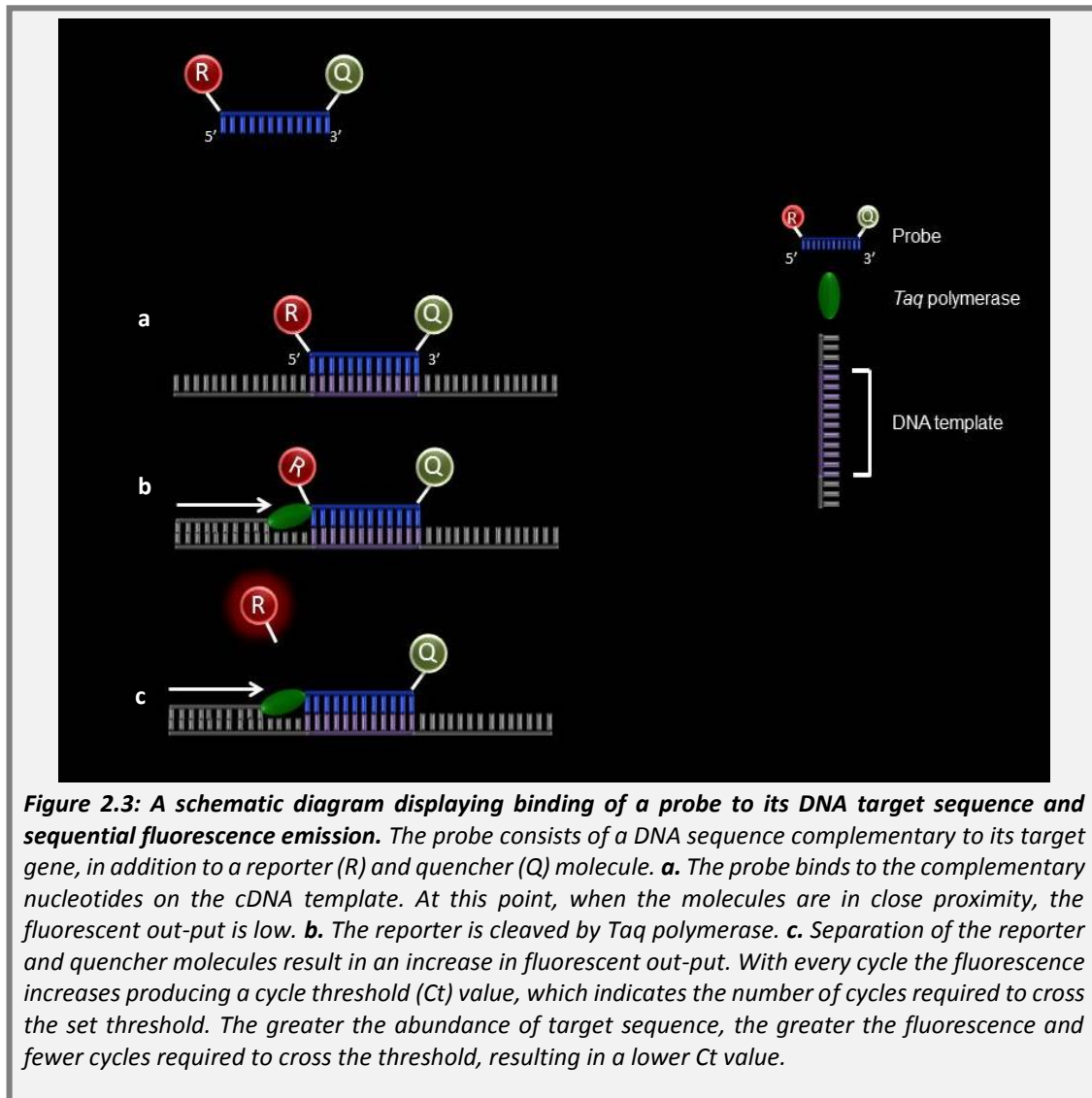


Figure 2.3: A schematic diagram displaying binding of a probe to its DNA target sequence and sequential fluorescence emission. The probe consists of a DNA sequence complementary to its target gene, in addition to a reporter (R) and quencher (Q) molecule. **a.** The probe binds to the complementary nucleotides on the cDNA template. At this point, when the molecules are in close proximity, the fluorescent out-put is low. **b.** The reporter is cleaved by Taq polymerase. **c.** Separation of the reporter and quencher molecules result in an increase in fluorescent out-put. With every cycle the fluorescence increases producing a cycle threshold (Ct) value, which indicates the number of cycles required to cross the set threshold. The greater the abundance of target sequence, the greater the fluorescence and fewer cycles required to cross the threshold, resulting in a lower Ct value.

2.3.5.2 Real-time PCR methodology

To remove any contamination, a 384 well plate, 0.5 ml RNase and DNase free tubes, RT-PCR H₂O, a microseal adhesive cover and tips were placed in the UV hood for 30 min. For each reaction, a mix containing RT-PCR H₂O, Master Mix and probes was made using the volumes for one sample demonstrated in Table 2.6.

Table 2.6: Reagents and the quantities required for one real-time PCR sample

Reagent	Stock solution	Working solution	Volume (μ l)
RT-PCR H ₂ O	n/a	n/a	2.5
Master Mix	5X	1X	5
Probe			0.5

The entire 8 μ l mix was transferred into a well of the 384 well plate and to this, 2 μ l of cDNA (approximately 40 ng) was added. The plate was covered using the microseal adhesive cover and centrifuged at 300 x g for 1 min at room temperature to ensure all liquid was combined at the bottom of the well. The probes used were designed to bind to complementary nucleotides on the cDNA template for the GOI and housekeeping (HK) genes, which included *β 2M*, *hypoxanthine-guanine phosphoribosyltransferase (HPRT)* or *transferrin receptor (TFRC)* designed by Life Technologies. The list of probes used and their reference numbers are in Appendix 2, Section 2.6, Table 2.4. The plate was analysed using the HT 7900 real-time PCR machine and SDS 2.3 software. Cycle conditions, which were standard for all real-time PCR machines per Applied Biosystems, are described in Figure 2.4.

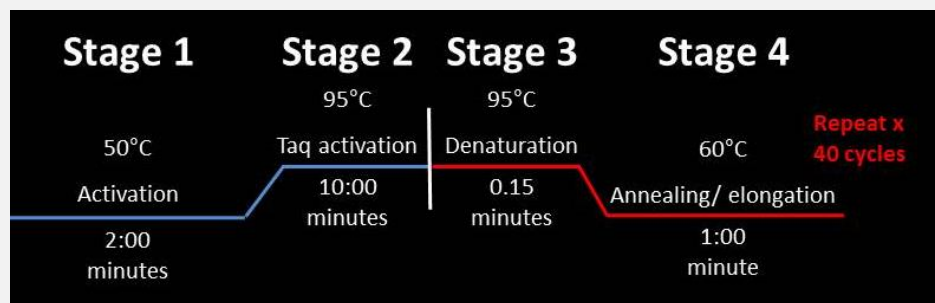


Figure 2.4: A diagram describing the conditions used for real-time PCR. At stage one the reaction mixture containing the probes, Master Mix and cDNA was heated to 50°C for 2 min to activate all reaction reagents, followed by specific Taq activation for 10 min at 95°C, at stage 2. Stage 3 and 4 conditions were repeated for 40 cycles whereby the cDNA and complementary strands were denatured at 95°C for 0.15 min followed by annealing of probes and elongation at 60°C for 1 min.

Gene expression of each molecule was either presented using their Ct values or $1/\Delta$ Ct value (calculated by normalisation to a HK gene), or using the fold change or percentage of gene expression using the $\Delta\Delta$ Ct method. The latter is shown in greater

detail in Table 2.19. Genes which were not expressed and had a Ct value of greater than 35 were referred to as undetermined (UD).

2.3.5.3 Probe efficiency

Probe efficiency experiments were conducted before use of the probes, the results for which are shown in Appendix 2, Section 2.6, Figure 2.3. Serial dilutions of control murine BM cDNA (10^1 - 10^4), were added as in the reactions described above. The data was presented graphically using the Ct values and trend lines were plotted. Primer efficiency was calculated using this formula: $\text{Efficiency}_x = 10^{(-1/\text{slope})} - 1 * 100$. The percentage efficiency values for each of the probes is shown in Appendix 2, Section 2.6, Table 2.6. All probes were within the acceptable range of efficiency of between 90-110% as advised by the manufacturer, with the exception of *TFRC*, which was not used in future experiments.

2.4 Cell biology

2.4.1 Flow cytometry

All equipment, materials and reagents used for flow cytometry are outlined in Appendix 1, Section 1.8, Table 1.8.

2.4.1.1 General principles of flow cytometry

Flow cytometry is a technique which allows for the quantification of protein on a per cell basis, as illustrated in Figure 2.5. In summary, a fluorescently labelled antibody binds to its antigen if present on the cell. The cell with the bound fluorescent antibody or a cell absent of fluorescent antibody moves through the pressurised system passing through beams of light and subsequent detectors, which detect the forward scatter (cell size) and side scatter (granularity) and therefore providing

information with regards to the general structure of the cell. In addition, a series of lasers excite the fluorochromes attached to the bound antibodies and the light reflected passes through dichroic mirrors to the detectors, which detect specific wavelengths dependent on the fluorochrome used. The results are then analysed using specialised computer software. If fluorescence is detected by the software, this implies that an antibody is bound, and the software expresses the results as a percentage of the cells with bound antibody. Therefore, this provides information about the percentage of the cell population, which are positive for the antigen of interest.

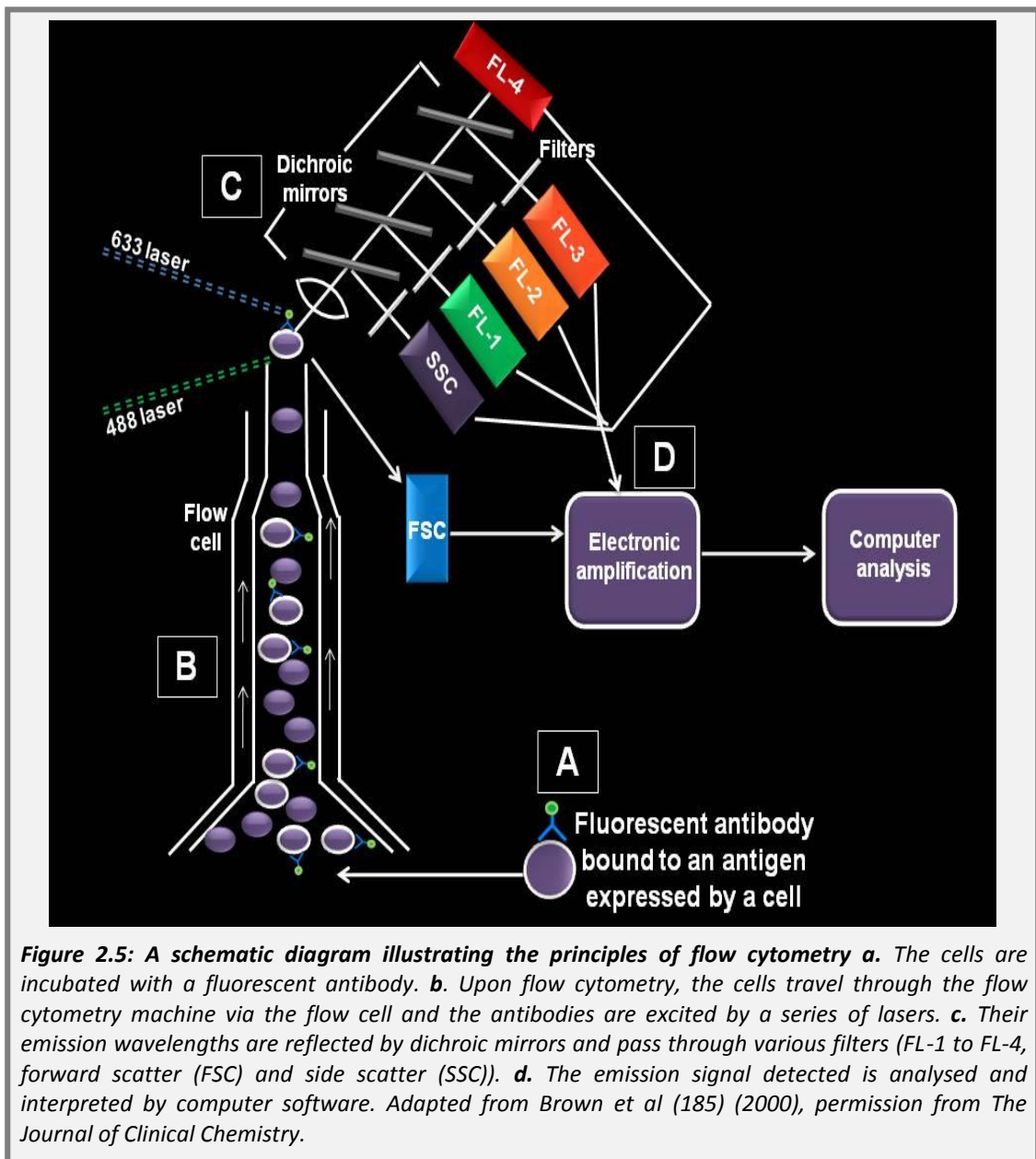


Figure 2.5: A schematic diagram illustrating the principles of flow cytometry a. The cells are incubated with a fluorescent antibody. **b.** Upon flow cytometry, the cells travel through the flow cytometry machine via the flow cell and the antibodies are excited by a series of lasers. **c.** Their emission wavelengths are reflected by dichroic mirrors and pass through various filters (FL-1 to FL-4, forward scatter (FSC) and side scatter (SSC)). **d.** The emission signal detected is analysed and interpreted by computer software. Adapted from Brown et al (185) (2000), permission from The Journal of Clinical Chemistry.

2.4.1.2 Flow cytometry methodology

The murine BM, splenocytes and blood samples were prepared for flow cytometry as described in Section 2.2.1.4. All cell lines were counted and set-up in tissue culture, 24 hours prior to flow cytometry as described for RNA extractions in Section 2.3.1 1.

On the day of flow cytometry, the MCs were harvested directly from the 6 well plate, transferred to a universal, centrifuged and washed twice in 10 ml PBS. The media from the MC3T3-E1 cells and primary OLC samples in the T75 flasks was removed and the cells were washed twice in 10 ml PBS before 5 ml cell dissociation solution was added. Flasks were then incubated at 37°C for 3 min to gently detach the cells from the surface of the flask without impairing surface protein expression. The remaining cells were gently scraped from the surface using a cell scraper and 10 ml of appropriate medium was added to the harvested cells. The cells were centrifuged and re-suspended in 10 ml of media, which was transferred to a T25 flask. This suspension of cells was then left standing upright in the incubator at 37°C for 3 hours to restore any receptor activity that may have been impaired. After the allocated time, the cells were harvested and washed twice in 10 ml PBS.

All cell types (which included the BM, splenocytes, blood cells, MCs and osteoblastic cells) were centrifuged and 200 µl 10% goat serum diluted in 0.5% bovine serum albumin (BSA) in PBS was added per sample, transferred to a well in a V-bottomed 96 well plate and incubated for 20 min at 4°C to block Fc receptors. After which, the cells were centrifuged as normal for the myeloma, osteoblastic, BM and spleen derived cells or 600 *x g* for 8 min at room temperature for the blood. They were then re-suspended in 100 µl 0.5% BSA and surface staining of CXCR4, Jag-1, Tie-2 and CD138 was conducted by adding an optimum concentration of antibody and matched dose of isotype control antibody (shown in Table 2.7) to each sample re-suspended in 100 µl 0.5% BSA. Samples were incubated at 4°C for 30 min in the dark. After incubation, the samples were washed three times in 200 µl 0.5% BSA, using the centrifugation settings described previously. After the final wash, the samples were

re-suspended in 300 µl 0.5% BSA, passed through a 70 µm cell strainer and transferred to flow cytometry tubes.

Notch-1 and CXCL12 protein detection required an intracellular staining technique, whereby the cells were centrifuged after blocking and fixed in 100 µl 4% paraformaldehyde (PFA) per sample, provided in the permeabilisation kit, for 10 min at room temperature. After fixation, the samples were centrifuged as before, washed once in 200 µl PBS and then washed twice in 200 µl permeabilisation buffer, provided in the permeabilisation kit (diluted to 1X using dH₂O). The cells were then re-suspended in 100 µl permeabilisation buffer, the optimum antibody concentration was added to the cells and the samples were incubated at 4°C for 30 min in the dark. After incubation, the cells were washed three times in 200 µl permeabilisation buffer, re-suspended in 300 µl 0.5% BSA and the cells were passed through a 70 µm strainer and transferred to flow cytometry tubes.

Table 2.7: Antibodies used in flow cytometry

Antibody specificity	Host	Isotype	Fluorochrome	Amount of antibody	Supplier
Anti-CXCR4	Rat	IgG2b κ	APC	0.5 µg	eBioscience
CXCR4 isotype	Rat	IgG2b κ	APC	0.5 µg	eBioscience
Anti-CXCL12	Mouse	IgG1	APC	0.25 µg	R&D Systems
CXCL12 isotype	Mouse	IgG1	APC	0.25 µg	R&D Systems
Anti-Notch-1	Mouse	IgG1 κ	PE	1.0 µg	eBioscience
Notch-1 isotype	Mouse	IgG1 κ	PE	1.0 µg	R&D Systems
Anti-Jag-1	Armenian hamster	IgG	PE	0.5 µg	eBioscience
Jag-1 isotype	Armenian hamster	IgG	PE	0.5 µg	Cambridge Bioscience
Anti-Tie-2	Rat	IgG1 κ	PE	0.5 µg	eBioscience
Tie-2 isotype	Rat	IgG1 κ	PE	0.5 µg	Cambridge Bioscience
Anti-N-cad	Mouse	IgG1	Dylight 650	0.25-1.0 µg	Novus Biologicals
N-cad isotype	Mouse	IgG1	APC	0.25-1.0 µg	R&D Systems
Anti-CD138	Rat	IgG2a κ	APC	0.5 µg	BD Pharmingen
CD138 isotype	Rat	IgG2a κ	APC	0.5 µg	eBioscience

To detect the viability of cells, where possible, cells were stained with 2 μ l of either TO-PRO 3 iodide (TO-PRO-3) (final concentration of 2 nM) or propidium iodide (PI) (final concentration of 50 μ g/ml). The samples were analysed using a Fluorescence-Activated Cell Sorting (FACS) Calibur machine (Becton Dickinson) (BD). The laser and detectors used for analysis were dependent on the absorbance and emission spectra of each fluorochrome. The lasers used to excite each fluorochrome and the detector used to analyse their emissions are displayed in Table 2.8. In order to prevent spectral overlap between the GFP in FL-1 and the PI or PE in FL-2, compensation was applied. Compensation used to prevent FL-1/FL-2 overlap was 20%, established using naïve BM or WT myeloma cell samples by comparing it to GFP positive samples. Compensation to prevent FL-2/FL-1 overlap was 4.5%, established using PI and PE negative BM or cell samples, which were compared to PI and PE positive samples. These settings were consistently used throughout all experiments with GFP expressing cells and PE and PI fluorochromes.

The percentage of cells which were positive for each fluorochrome and therefore, positive for tumour burden or each molecule in 10,000-100,000 events was then calculated using the Cell Quest software. These were calculated by drawing a gate around the GFP or fluorochrome positive population based on naïve BM or isotype control samples, to ensure that less than one percent of staining was evident in the gated region. The settings for the gates then remained the same throughout each experiment.

The Cell Quest software can also analyse mean fluorescent intensity (MFI), however, the main focus within these experiments was the number of positive cells in the population rather than intensity on a per cell basis, therefore, MFI was not calculated.

Table 2.8: Laser, absorbance, emission and detector information for each fluorochrome used in flow cytometry

	Laser excitation (nm)	Absorbance Max (nm)	Emission Max (nm)	Detector
GFP	488	490	515	FL-1
Phycoerythrin (PE)	488	496	578	FL-2
Allophycocyanin (APC)	633	650	660	FL-4
PI	488	540	620	FL-2
TO-PRO-3	633	640	657	FL-4

2.4.2 Immunofluorescence staining

All equipment, materials and reagents used for IF are outlined in Appendix 1, Section 1.9, Table 1.9.

2.4.2.1 Principles of immunofluorescence staining

Immunofluorescence was used for the visualisation and quantification of the presence of protein by the 5T33-GFP and 5TGM1-GFP MCs. The general principals are similar to flow cytometry whereby a fluorescent antibody binds to the antigen of interest on cells however; the cells are bound to a fixed surface rather than in suspension. When the cells are placed under a fluorescent microscope, bound fluorescent antibodies attached to the cells, are excited by a light source, and light emitted passes through a series of filters and detectors to produce an image using the computer software.

2.4.2.2 Immunofluorescence staining methodology

The 5T33-GFP and 5TGM1-GFP cells were grown in culture as described in 2.1.2.1 and subsequently stained for the HSC niche molecules, ligands and CD138 by IF. On the day of IF staining, 1×10^5 cells per sample were transferred to a universal and washed once in 5 ml PBS before fixation in 500 μ l 4% PFA for 10 min at room temperature. After fixation, the cells were washed twice in 5 ml PBS and re-suspended in 200 μ l

PBS. The cells (1×10^5) were then cytospun at 500 rotations per min (RPM) for 5 min on a medium acceleration on to a super-frost slide and then left to dry for 5 min at room temperature before beginning the staining the procedure.

The cells were isolated using a hydrophobic barrier pen to contain staining solutions and the slides were placed in PBS. They were then added to a humidified immunotray where they were blocked in approximately 200 μ l 10% goat serum in PBS for 20 min at room temperature. For cell surface staining of CXCR4, Notch-1 and CD138, the block was “tapped” off and approximately 200 μ l primary fluorescent antibody or matched dose isotype antibody diluted in PBS was added. The dilution of each antibody is displayed in Table 2.9. The antibodies were incubated for 45 min at room temperature in the dark, followed by washing in PBS three times for 5 min.

For intracellular staining of CXCL12, the cells were permeabilised after blocking by washing the slides twice in a bath containing 0.5% tween diluted in PBS (PBST) for 5 min per wash. After which the slides were stained with the appropriate dilution of antibody in 0.5% PBST for 45 min at room temperature in the dark. The slides were then washed three times in a bath containing 0.5% in PBST, 5 min per wash.

Table 2.9: Antibodies used for immunofluorescence staining

Antibody specificity	Host	Isotype	Fluorochrome	Concentration	Dilution	Supplier
Anti-CXCR4 CXCR4 isotype	Rat	IgG2b κ	APC	0.2 mg/ml	1:300	eBioscience
	Rat	IgG2b κ	APC	0.2 mg/ml	1:300	eBioscience
Anti-CXCL12 CXCL12 isotype	Mouse	IgG1	APC	20 μ g/ml	1:5	R&D Systems
	Mouse	IgG1	APC	10 μ g/ml	1:2.5	R&D Systems
Anti-Notch-1 Notch-1 isotype	Mouse	IgG2a κ	APC	0.2 mg/ml	1:20	eBioscience
	Mouse	IgG2a κ	APC	0.2 mg/ml	1:20	eBioscience
Anti-CD138 CD138 isotype	Rat	IgG2a κ	APC	0.2 mg/ml	1:300	BD Pharmingen
	Rat	IgG2a κ	APC	0.2 mg/ml	1:300	eBioscience

After extracellular and intracellular staining and subsequent washing, the slides were cover-slipped using the aqueous Prolong Gold mount containing 4',6-Diamidino-2-phenylindole, dihydrochloride (DAPI) and 22 x 22 millimetre (mm) cover slips. The edges were then sealed with nail varnish and the slides were left to dry for an hour before examining by fluorescent microscopy.

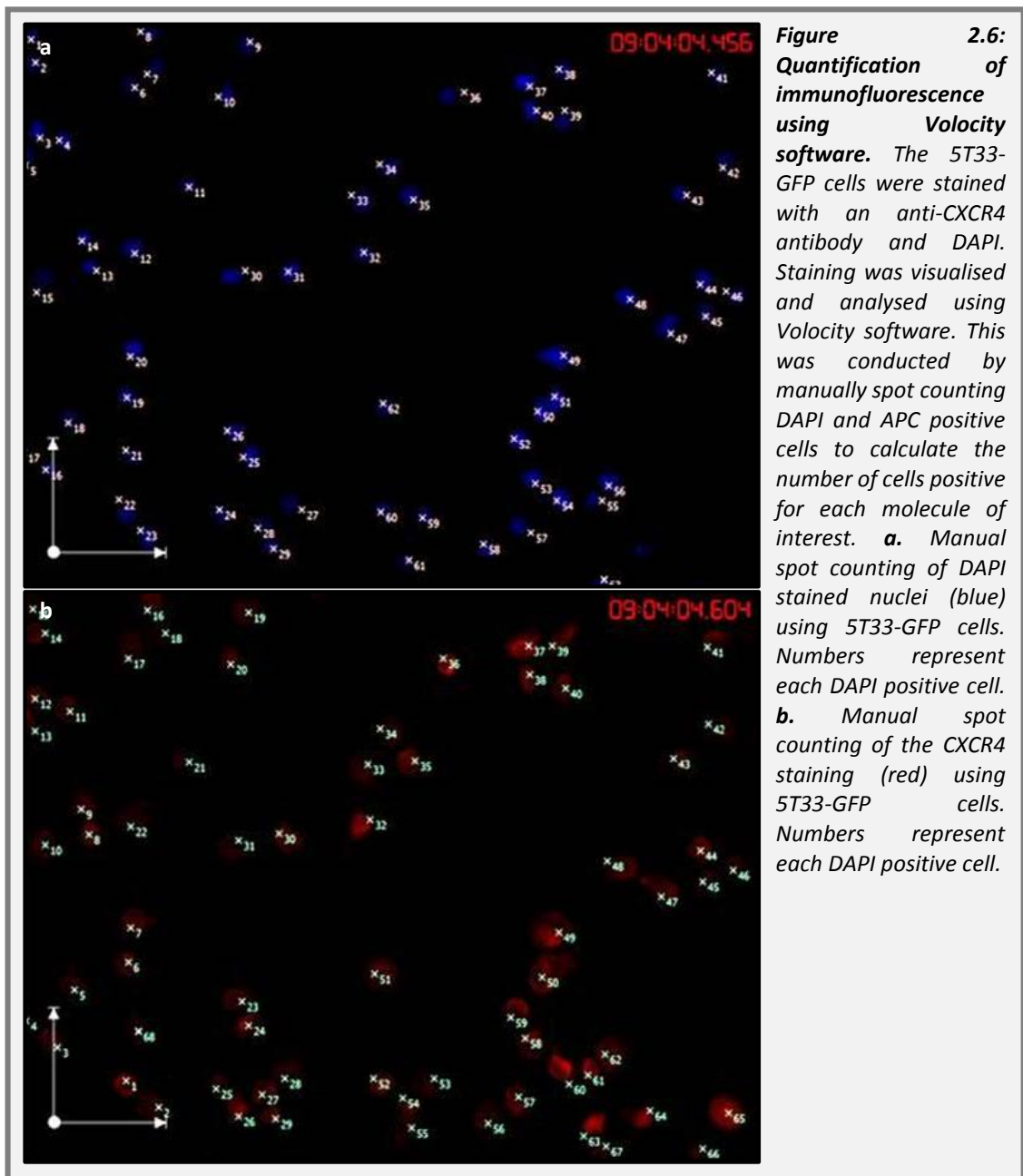
2.4.2.3 Fluorescent microscopy

Immunofluorescence staining was visualised using a Leica AF6000 microscope and LAS-AF software. The settings for visualising both the DAPI and APC are displayed in Table 2.10. The settings differed slightly depending on the molecule being analysed.

Table 2.10: Leica AF6000 microscope and LAS-AF settings used to visualise immunofluorescence staining of the HSC niche molecules, ligands and CD138 in the 5T33-GFP and 5TGM1-GFP cells

Molecule	Fluorochrome	Filter cube	Exposure time millisecond (ms)	Gain	Intensity	Binning
CXCR4	DAPI	A4	250	3.1	4	1x1
	APC	Y5	590	10	5	1x1
CXCL12	DAPI	A4	300	3.1	4	1x1
	APC	Y5	590	10	5	1x1
Notch-1	DAPI	A4	220	3.1	4	2x2
	APC	Y5	480	10	5	2x2
CD138	DAPI	A4	220	3.1	4	2x2
	APC	Y5	480	10	5	2x2

After visualisation, the pictures were exported as tagged image file format files (TIFFs) and imported into Velocity software (Perkin Elmer) for image analysis. Velocity software was used to manually spot count the number of DAPI stained nuclei and APC labelled cells to calculate the percentage of cells positive for each molecule of interest. An example of this is shown in Figure 2.6.



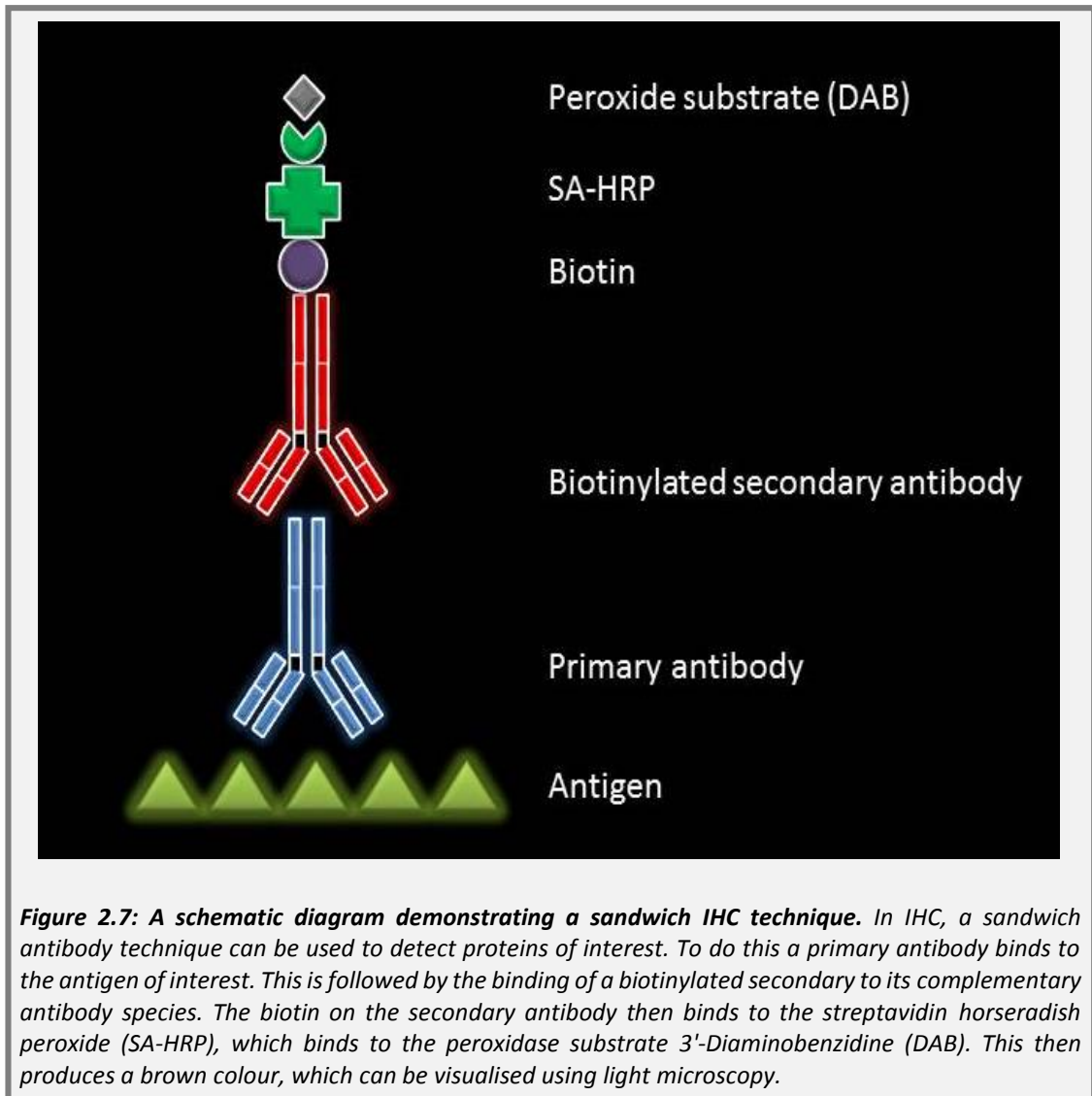
2.4.3 IHC staining

All equipment, materials and reagents used for IHC are outlined in Appendix 1, Section 1.10, Table 1.10.

2.4.3.1 Principles of IHC

Immunohistochemical techniques were developed to visualise the expression of the HSC molecules of interest *ex vivo*. A “sandwich” IHC system was optimised to visualise the presence of protein for N-cad, CXCR4 and CD138 in BM histological

sections taken from mice injected with 5TGM1-GFP cells. The basic IHC method used is displayed in Figure 2.7.



2.4.3.2 Preparation of bones for IHC

Tibiae were dissected free of soft tissue from C57BL/KaLwRij mice which had been injected with 5TGM1-GFP cells after 10, 14, 17 and 21 days P-I. The bones were fixed in 4% PFA for 24 hours and then decalcified in 0.4 M EDTA pH 8.0 containing 0.5% PFA for 2 weeks, changing the solution every other day. The bones were placed into tissue processor cassettes and washed three times, an hour per wash, in PBS to rinse away residual EDTA. The bones were placed into the Leica TP2010 processor to dehydrate the tissues and infiltrate them with wax using the programme as described in Table 2.11.

Table 2.11: Processing schedule for bones using the Leica TP2010 processor

STATION	SOLUTION	TIME	VACUUM
1	70% Ethanol	2 hours	No
2	70% Ethanol	2 hours	No
3	70% Ethanol	2 hours	No
4	95% Ethanol	2 hours	No
5	95% Ethanol	2 hours	No
6	100% Ethanol	2 hours	No
7	100% Ethanol	2 hours	No
8	Xylene	2 hours	No
9	Xylene	2 hours	No
10	Wax	2 hours	Yes
11	Wax	2 hours	Yes

After processing, the bones were embedded into wax in a specific orientation, which was the same for each tibia. The wax blocks were trimmed using a Leica microtome to expose the length of the BM (approximately 900 μm) and 3 μm sections were cut in serial, and put on to a 45°C water bath to “float-out” for 30 min. They were then attached to super-frost positively charged slides and placed onto a hot plate at 45°C to remove residual creases. Finally, they were placed in an oven at 37°C to fully adhere to the slides over-night before they were used for IHC.

2.4.3.3 IHC methodology for CD138

On the day of staining, sections were deparaffinised twice in xylene for 4 min followed by rehydration through a series of alcohols (99%, 99%, 95% and 70% industrial methylated spirits (IMS)) for 4 min each. The sections were then washed in tap water for 5 min and transferred to PBS for a further 5 min. Antigen retrieval (A. Menarini kit) was performed by diluting trypsin 1:4 in the buffer provided. The trypsin was pre-warmed for 45 min at 37°C before adding approximately 200 μl of solution

to each slide and incubating for 10 min at room temperature. The sections were then washed twice in PBS, with agitation for 4 min per wash. To reduce non-specific staining, the sections were blocked by adding 200 µl 10% goat serum in PBS to each slide for 1 hour at room temperature. The block was tapped off and the slides were then incubated with 200 µl primary or concentration matched isotype control antibody diluted in PBS, for 1 hour at room temperature (as shown in Table 2.12). The sections were then washed twice in PBS for 4 min with gentle agitation. To block endogenous hydrogen peroxidase, 200 µl 3% hydrogen peroxide (H₂O₂) (1:10) in PBS was added to each slide for 30 min at room temperature, followed by washing twice in PBS with gentle agitation. Two hundred microlitres of goat anti-rat secondary antibody, diluted 1:300, was added to the slides for 30 min at room temperature and slides were subsequently washed twice in PBS. This was followed by incubation with 200 µl SA-HRP at a dilution of 1:300 for 30 min at room temperature followed by washing twice in PBS. Finally, the peroxide substrate reagent was prepared by adding 1 ml of diluent to 1 drop of DAB in the Impact DAB kit. Two hundred microlitres of this solution was then added to the slides for 10 min at room temperature. The slides were washed in tap water to remove excess DAB, followed by counter staining in Gill's haematoxylin for 20 seconds to visualise the nuclei. The slides were then left to "blue" in running tap water for 3 min after which they were dehydrated through a series of alcohols (70%, 95% and 99% IMS) for 10 seconds each and a final 99% IMS for 30 seconds. This was followed by two xylene washes, the first for 1 min and the second for a further 3 min. The slides were then cover-slipped using 22 x 22 (mm) coverslips with Di-N-Butyl Phthalate in Xylene (DPX). Staining was visualised by scanning the slides using an Aperio Scan Scope scanner and images were captured at a 2X and 40X magnification using Image Scope Software.

2.4.3.4 IHC methodology for N-cad

The method for staining N-cad in the 5TGM1-GFP infiltrated bone sections by IHC was similar to the protocol used for CD138 (Section 2.4.3.3). However, there were some differences with regards to buffers, antigen retrieval and the antibodies used. The wash buffer and diluent throughout the protocol was 0.1% PBST. For antigen

retrieval, the trypsin was diluted 1:1 and was used at room temperature immediately without pre-heating, for 15 min. In addition, an anti-N-cad antibody and dose matched isotype control antibody was used at a 1:100 dilution (as shown in Table 2.12) and incubated for 1 hour at room temperature. The secondary antibody used was a goat anti-rabbit, at a 1:200 dilution, incubated for 30 min at room temperature. All other details were the same as in the CD138 protocol.

2.4.3.5 IHC methodology for CXCR4

The method for staining CXCR4 in the 5TGM1-GFP infiltrated bone sections by IHC was similar to the protocol used for CD138 IHC. However, antigen retrieval was not required and an anti-CXCR4 and dose matched isotype control antibody was used at a 1:50 dilution (Table 2.12). The slides were then treated in the exact same manner as in the CD138 protocol.

Table 2.12: Antibodies used for IHC

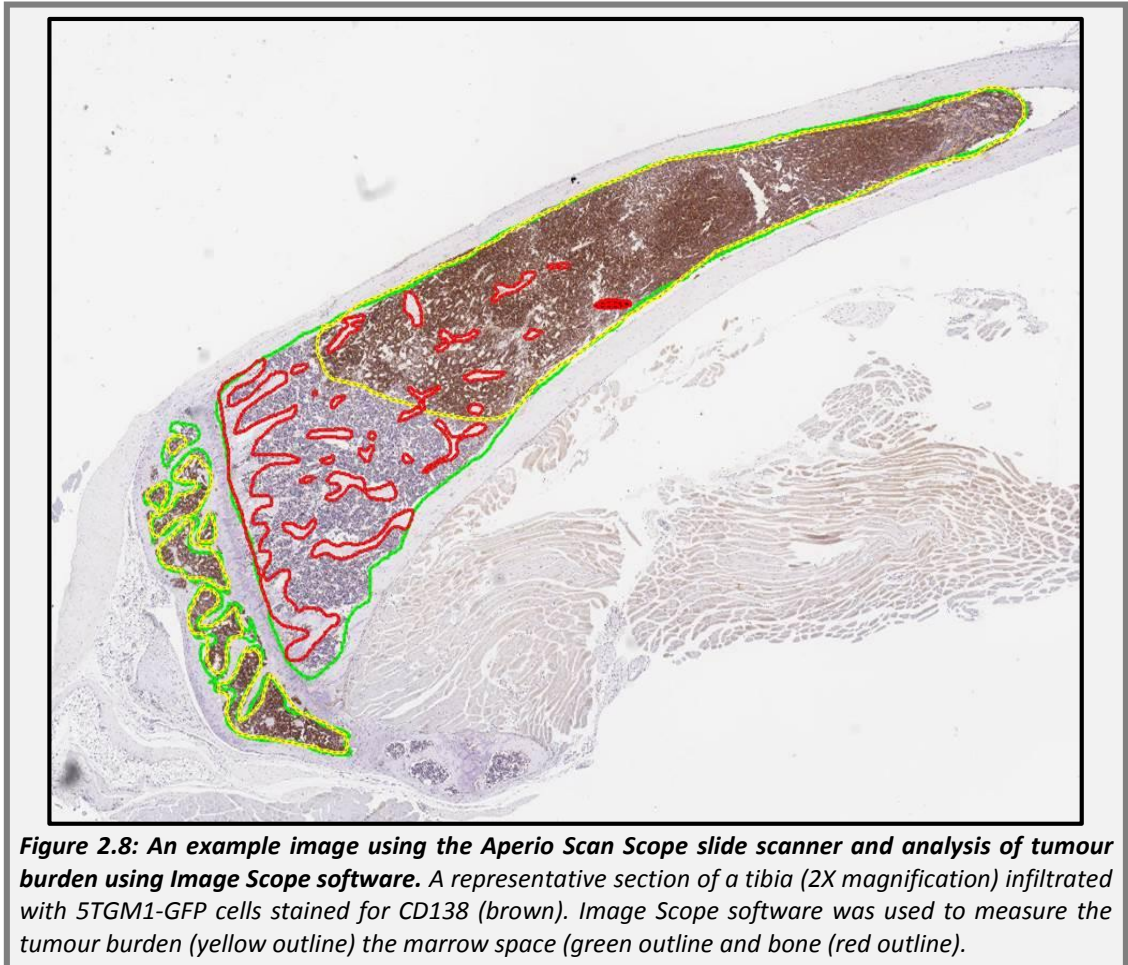
Antibody specificity	Host	Isotype	Concentration	Dilution	Supplier
Anti-CD138 primary	Rat	IgG2a	0.5 mg/ml	1:300	BD Pharmingen
CD138 isotype	Rat	IgG2a	0.5 mg/ml	1:300	BD Pharmingen
Anti-N-cad primary	Rabbit	IgG	1.0 mg/ml	1:100	Pierce Antibodies
N-cad isotype	Rabbit	IgG	*1.0 mg/ml	1:100	Dako cytotation
Anti-CXCR4 primary	Rat	IgG2b	0.5 mg/ml	1:50	BD Pharmingen
CXCR4 isotype	Rat	IgG2b	0.5 mg/ml	1:50	BD Pharmingen

*This was initially at a 15 mg/ml concentration, which was subsequently diluted to 1mg/ml to match the primary antibody and then further diluted 1.100 as indicated in the table.

2.4.3.6 CD138 staining quantification

To quantify CD138 staining in tumour bearing 5TGM1-GFP infiltrated bone sections, an Aperio Scan Scope slider scanner and Image Scope software were used. An image of an example bone section, which has been analysed, is shown in Figure 2.8. To analyse the bones, the total area of BM space, trabecular bone and CD138 stained

tumour colonies were calculated (mm^2). As only the cellular BM space was required, the area of trabecular bone was subtracted from the total BM area. To calculate the percentage of tumour burden, the total area of tumour was then divided by the cellular BM area and multiplied by 100. This technique has also been successfully used by others at the University of Sheffield (Dr S. Lawson personal communication).



2.4.4 Western blotting

All equipment, materials and reagents used for Western blotting (WB) are outlined in Appendix 1, Section 1.11, Table 1.11.

2.4.4.1 Principals of Western blotting

Western blotting was used to determine the protein levels of N-cad in 5T33-GFP and 5TGM1-GFP cells, which had been knocked-down for N-cad (method described in 2.6.4). Western blotting is a technique whereby proteins are separated through an acrylamide gel, transferred on to a nitrocellulose membrane and visualised using a sandwich antibody reaction similar to IHC. However, rather than using a biotinylated secondary antibody, a HRP conjugated secondary antibody and enhanced chemoluminescence substrate (ECL) is used. Enhanced chemoluminescence substrate consists of H₂O₂ and luminol, which binds to HRP on the secondary antibody, resulting in oxidation of the luminol and emission of iridescent light. Chemo-luminescence is visualised by standard x-ray development and the protein appears as a band on an x-ray film.

2.4.4.2 Cell lysis

For whole cell lysis, a nonyl phenoxy polyethoxy ethanol (NP-40) substitute buffer containing tris buffer, sodium chloride (NaCl) and NP-40 was used. This was made using the quantities in Table 2.13. The buffer was then stored at 4°C until required.

Table 2.13: Reagents and the quantities required to make 10 ml NP-40 buffer

Reagent	Stock solution	Working solution	Amount required
Tris hydrochloride (pH 8.0)	1 M	50 mM	500 µl
NaCl	3 M	150 mM	500 µl
NP-40	n/a	n/	100 µl
dH ₂ O	n/a	n/a	8.9 ml

The 5T33-GFP or 5TGM1-GFP cells were lysed by transferring 1×10^7 cells per sample into a universal, followed by centrifugation and washing once in 10 ml PBS. A protease inhibitor cocktail (PIC) (1X) was added to the NP-40 buffer at a 1:100 dilution and the cell pellet was re-suspended in 200 µl of NP-40/PIC solution. The samples were then water sonicated to produce ultrasound waves that mechanically disrupt

cells to further release proteins in addition to breaking down interfering cellular DNA. The lysates were then frozen at -20°C and stored until required.

2.4.4.3 Protein quantification

Protein quantification was conducted using a bicinchoninic acid (BCA) assay. The assay produces a purple colour in the presence of protein, which is analysed by spectrophotometry. The colour reaction is produced by the reduction of copper (Cu^{2+}) ions to Cu^{+} ions by peptide bonds present in proteins. The Cu^{+} ions interact with the BCA, which produces a purple by-product. The intensity of the purple is measured by the absorbance at 562 nm using a spectrophotometer and the optical density (OD) readings of the samples are then extrapolated from the OD readings of a set of protein standards to calculate the quantity of protein present.

2.4.4.4 Bicinchoninic acid assay methodology

Firstly, a 100 mg/ml BSA stock was made in NP-40 buffer and this was subsequently diluted at a 1:100 dilution to 1 mg/ml using NP-40 buffer. The concentrations used for the standards and the volume of BSA and NP-40 diluent required are shown in Table 2.14 and those volumes were loaded into a 96 well plate.

Table 2.14: Volumes of bovine serum albumin and NP-40 required for the bovine serum albumin standards

Standard Concentration ($\mu\text{g/ml}$)	Volume of BSA (μl)	Volume of NP-40 (μl)
1000	10	0
800	8	2
600	6	4
400	4	6
200	2	8
100	1	9
0	0	10

Protein from the 5T33-GFP and 5TGM1-GFP cells was loaded into the wells at either a 1:5 or 1:10 dilution with NP-40 buffer, making a total volume of 10 μl , as with the

protein standards. Bicinchoninic acid and copper II sulphate were combined at a 50:1 ratio respectively and 200 µl of this solution was added to the wells containing either 10 µl of BSA standard or 5T33-GFP or 5TGM1-GFP lysates. The plate was then incubated at 37°C for 30 min to catalyse the colour change reaction and read using the SpectraMax plate reader at 562 nm. A standard curve was plotted, as shown in Figure 2.9.

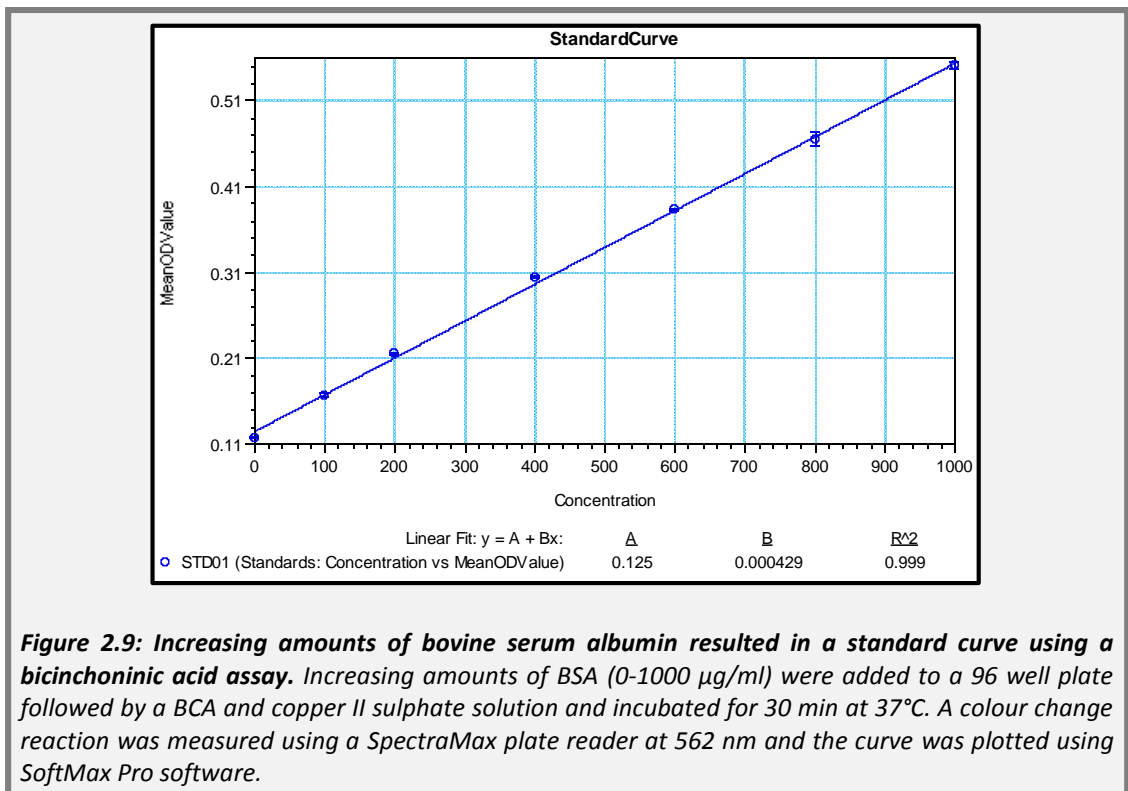


Figure 2.9: Increasing amounts of bovine serum albumin resulted in a standard curve using a bicinchoninic acid assay. Increasing amounts of BSA (0-1000 µg/ml) were added to a 96 well plate followed by a BCA and copper II sulphate solution and incubated for 30 min at 37°C. A colour change reaction was measured using a SpectraMax plate reader at 562 nm and the curve was plotted using SoftMax Pro software.

The concentrations of the unknown sample proteins were calculated by extrapolation of their ODs from OD and concentration values in the BSA standard curve using the following formula:

$$y = a + bx$$

a= The intercept

b= Slope

x= Unknown concentration

y= Known OD

Rearrangement of formula= $x=(y-a)/b$

Using this equation the concentration of the unknown protein was calculated, as shown in the example below using the slope and intercept values calculated from the standard curve in Figure 2.9.

$$0.396 \text{ (OD)} - 0.125 \text{ (Intercept)} / 0.000429 \text{ (Slope)} = 631$$

This concentration was then multiplied by 5 or 10 to account for the dilution factors and to provide a concentration in $\mu\text{g/ml}$.

2.4.4.5 Acrylamide gel methodology

To make the acrylamide gel, firstly, the separator and cover plates were placed in the casting frames and added to the casting stand. The plates were then tested for leakages before loading the gel into them.

A 7% resolving gel was made using tris buffer, acrylamide, sodium dodecyl sulphate (SDS), ammonium persulphate (APS) and tetramethylethylenediamine (TEMED). The gel was made using the volumes shown in Table 2.15. The resolving gel was added to casting plates and left to set for 45 min, at room temperature.

Table 2.15: Reagents and volumes required to make one 7% resolving acrylamide gel.

Reagent	Volume
dH ₂ O	4 ml
30% Acrylamide	1.87 ml
1.5 M tris pH 8.0	2 ml
10% SDS	80 μl
10% APS	80 μl
(TEMED)	8 μl

A 4% stacking gel was then made using the same reagents as for the resolving gel however; 0.5 M tris buffer pH 6.8 was used rather than 1.5 M tris buffer pH 8.0. The gel was made using the volumes shown in Table 2.16. The stacking gel was then

added to the top of the resolving gel, ensuring there were no bubbles and was left to set for approximately 45 min.

Table 2.16: Reagents and volumes required to make one 4% stacking acrylamide gel

Reagent	Volume
dH ₂ O	3 ml
30% Acrylamide	0.67 ml
0.5 M tris pH 6.8	1.25 ml
10% SDS	50 μ l
10% APS	50 μ l
TEMED	5 μ l

2.4.4.6 Sodium dodecyl sulphate-polyacrylamide gel electrophoresis

In initial experiments, different amounts of protein were loaded and run using sodium dodecyl sulphate-polyacrylamide gel electrophoresis (SDS-PAGE) to determine which protein amount was sufficient to visualise a band for N-cad in the 5TGM1-GFP cells as shown in Appendix 2, Section 2.7, Figure 2.4. The optimum amount of protein used was 20 μ g and this was used in subsequent experiments.

The desired quantity of protein (20 μ g) per sample was calculated using the concentrations determined using the BCA assay in Section 2.4.4.4. Prior to use, laemmli buffer (4X) was added to β -mercaptoethanol at a 1:20 dilution and the laemmli buffer was then added to the protein samples to make a total volume of 20 μ l. The biotinylated protein ladder was also diluted 1:10 using the laemmli buffer. The samples and biotinylated marker were then denatured by heating in a hot block at 90°C for 10 min after which they were cooled at 4°C. Before loading, the gel (in the glass plates) was added to the electrophoresis assembly kit and inserted into an electrophoresis tank containing 1X running buffer. The running buffer was initially made as a 10X solution containing tris base, glycine and SDS and diluted 1:10 in dH₂O upon use. The amounts and volumes of reagents required to make 10X running buffer and the final working 1X solution are displayed in Table 2.17.

Table 2.17: Amounts and volumes of reagents required to make a litre of 10X running buffer and final amounts of reagent present in 1 litre of 1X running buffer

Reagent	10X running buffer stock solution	Amounts required for 10X running buffer	1X running buffer working solution
Tris base	250 mM	30.3 g	25 mM
Glycine	1920 mM	144 g	192 mM
SDS (20%)	1%	50 ml	0.1%
dH ₂ O	n/a	950 ml	n/a

The biotinylated protein ladder (10 µl), a pre-stained protein ladder (5 µl) and the samples (20 µl) were then loaded in the gel. Using the Biorad power pack, a current was applied at 80 Volts to allow for the separation of the pre-stained marker through the stacking layer followed by 150 V for approximately 1 hour and 30 min for separation of the proteins through the resolving gel.

2.4.4.7 Protein transfer

Following loading and separation of the proteins through the acrylamide gel, the proteins in the gel were transferred to a hybond nitrocellulose membrane. Firstly, the nitrocellulose membrane, which was cut to the same size as the gel, was soaked in methanol for 5 min followed by 1X transfer buffer. Ten times transfer buffer was made using tris base, glycine and dH₂O, which was diluted 1:10 to 1X using d H₂O and methanol. The amounts required for the 10X transfer buffer stock solution and final amounts present in working 1X solution are shown in Table 2.18.

Table 2.18: Amounts and volumes of reagents required to make a litre of 10X transfer buffer and final amounts of reagent present in 1 litre of 1X transfer buffer

Reagent	10X transfer buffer stock solution	Amounts required for 10X transfer buffer	1X transfer buffer working solution
Tris base	250 mM	30.3 g	25 mM
Glycine	1920 mM	144 g	192 mM
Methanol	n/a	n/a	20%
dH ₂ O	n/a	1000 ml	n/a

Per gel, two teflon pads and four pieces of filter paper cut to the same size as the gel were soaked in 1X transfer buffer and were then used to form a sandwich between the gel and nitrocellulose membrane which was placed onto a transfer cassette in the correct orientation so that the proteins would transfer on to the membrane. The gel and membrane sandwich was placed in a transfer cassette facing towards the anode. The cassette was placed in a tank containing transfer buffer and the tank was surrounded by ice. The proteins were transferred onto the membrane at 50 Volts for 7 hours.

2.4.4.8 Immuno-blot

After transfer, the membrane was removed from the transfer cassette for immuno-blotting. Firstly, the membrane was blocked in 5% skimmed milk diluted in 0.25% PBST for 45 min at room temperature with agitation. After blocking, the membrane was cut to separate the biotinylated protein ladder, β -actin (42 kDa) and N-cad (135 kDa) areas, using the pre-stained marker as a guide. The pieces of membrane were placed in separate universals containing either PBST for the biotinylated marker, β -actin antibody in PBST at a 1:3000 dilution or N-cad antibody (used previously for the IHC staining in Section 2.4.3.5) at a dilution of 1:1000 in PBST for 1 hour, room temperature with agitation. The membranes were then washed three times in PBST for 5 min per wash with agitation, followed by an incubation with an anti-rabbit HRP secondary at a dilution of 1:10000 in PBST for the β -actin and N-cad or the anti-biotin HRP secondary antibody at 1:1000 in PBST for the biotinylated ladder for 45 min at room temperature with agitation. The membranes were then washed three times in PBST for 5 min per wash on a tube roller.

2.4.4.9 Immuno-blot development

After the final wash, the membranes were pieced back together onto a sheet of plastic. Using the ECL kit, solution A was combined with an equal quantity of solution B and this was then added to the membrane, which was then covered in plastic and smoothed down to remove air bubbles. Chemo-luminescence was then visualised in

a dark room. The membrane in the plastic was placed inside a developing cassette with the film. The membrane was exposed for a series of different times to optimise the exposure. Two different ECL kits were used, a Thermo Scientific kit (30 seconds of exposure) and a Santa Cruz kit (5 min of exposure). The film was then placed into a developing solution until bands began to appear (approximately 30 seconds), followed by washing in running tap water for 1 min after which the film was fixed (fixer solution) for 2 min and washed in running tap water for 5 min. The film was then left to air-dry over-night.

2.4.4.10 Western blotting quantification

After immuno-blotting and developing, the bands were quantified. This was conducted by scanning the film using the Epson 4990 scanner and software using a 16-bit grey-scale. Once scanned, the bands were measured by densitometry using ImageJ software, which provided a density value for each band present on the film. Data was displayed as a fold change and percentage of protein KD. This was calculated by normalising the band density of N-cad protein to the HK (β -actin) band density, followed by comparing this value between the CTRL and N-cad known-down samples to provide a fold change and percentage of protein KD. An example of these calculations are shown in Table 2.19.

Table 2.19: Calculations to determine the percentage of protein knock-down between the CTRL and KD transduced cells

Treatment	β -actin	N-cad	Normalisation	Mean of normalisation	Fold change	%
	HK	Protein of interest (POI)	POI/HK	Mean of all replicates	KD/CTRL	1-KD/CTRL*100
CTRL	17.21	19.34	1.12377964			
CTRL	17.50	24.13	1.37873507			
CTRL	15.12	28.65	1.89420087			
CTRL Mean				1.46557187		100
KD	20.03	8.19	0.40905687			
KD	16.77	9.54	0.56843925			
KD	13.36	10.16	0.75999102			
KD mean				0.57916238	0.40	40

2.4.5 Myeloma cell growth curves

2.4.5.1 Growth curve methodology

To assess the effect of the N-cad KD upon cell proliferation *in vitro*, growth curve experiments were conducted. The untreated, CTRL and KD 5TGM1-GFP cells were seeded at a density of 5×10^3 cells into a 96 well plate in 200 μ l complete RPMI media. Cells were counted every 2 days and media was replenished on days 0, 2, 4, 6, 8 and 10. Cell proliferation was presented in a graphical format to visualise each phase of growth, which included the lag, exponential, stationary and death phase as demonstrated in Figure 2.10. The doubling-time in the exponential phase was calculated using the following formula:

$$1 / ((\log \text{ cell number at the end of the exponential phase} - \log \text{ cell number at the beginning of the exponential phase}) 3.32 / \text{time})$$

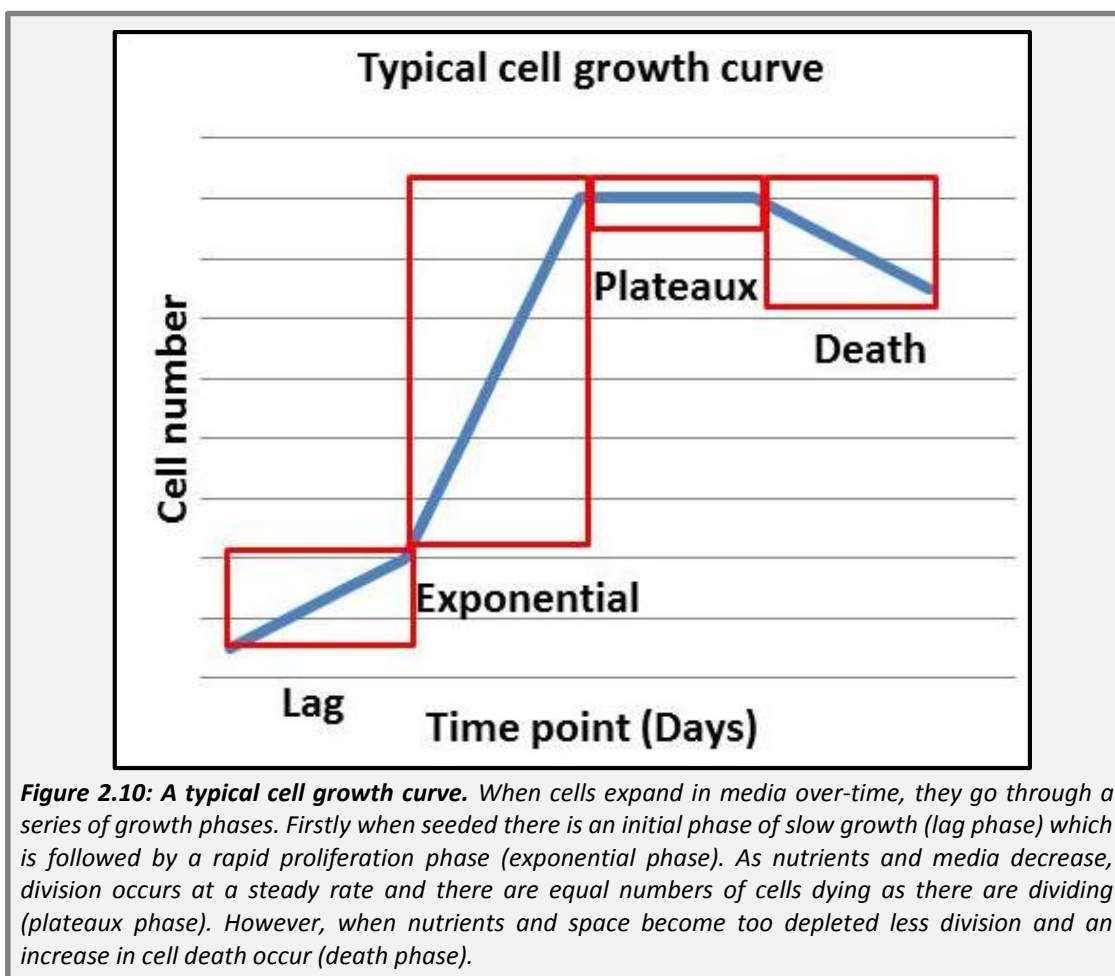


Figure 2.10: A typical cell growth curve. When cells expand in media over-time, they go through a series of growth phases. Firstly when seeded there is an initial phase of slow growth (lag phase) which is followed by a rapid proliferation phase (exponential phase). As nutrients and media decrease, division occurs at a steady rate and there are equal numbers of cells dying as there are dividing (plateaux phase). However, when nutrients and space become too depleted less division and an increase in cell death occur (death phase).

2.5 Primary osteoblast lineage cell differentiation

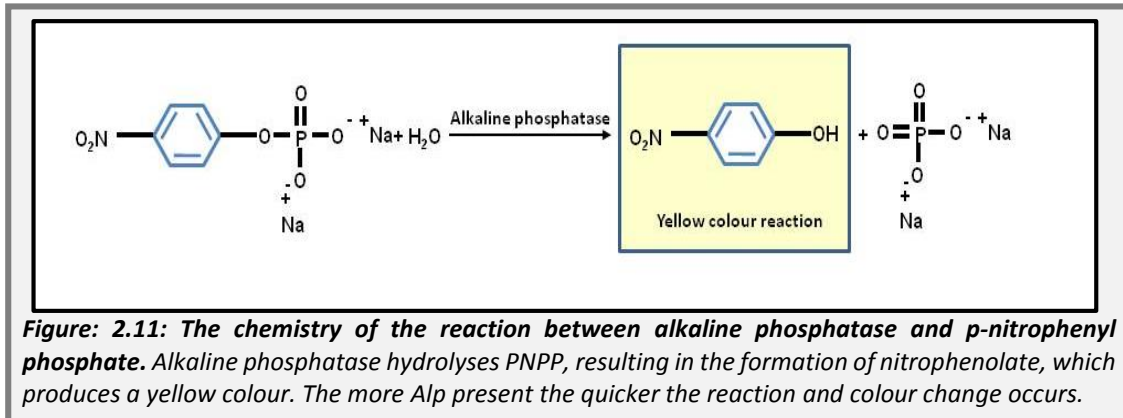
All equipment, materials and reagents used for all primary OLC differentiation experiments are outlined in Appendix 1, Section 1.12, Table 1.12.

2.5.1 Alkaline phosphatase production analysis

2.5.1.1 Principals of alkaline phosphatase analysis

Alkaline phosphatase is a well-known marker of osteoblast differentiation and is up regulated in the early differentiation of preosteoblasts to mature osteoblasts. Alkaline phosphatase production by a cell can be determined using a p-nitrophenyl phosphate (PNPP) reaction based on a colour change described by Sabakbar *et al*

(186). This reaction can be detected using a plate reader by spectrophotometry (Figure 2.11).



2.5.1.2 Alkaline phosphatase assay methodology

Alkaline phosphatase assays were conducted on days 0, 3, 7, 10, 14, 21 and 28 post-OGM treatment. On the day of the assay, the media was removed and the cells were washed twice in 150 μ l of ice cold PBS. The cells were lysed in 0.1% triton in PBS and shaken on a rotating platform for 20 min. Whilst the cells were lysing, one PNPP tablet and one tris buffer tablet were dissolved in 20 ml of dH₂O, forming a final solution containing 1 mg/ml PNPP and 0.2 M tris buffer. Two hundred microlitre of this solution was then added to the lysed cells, avoiding production of air bubbles and the plate was immediately read using the SpectraMax plate reader. The plate was read using the kinetic settings, every 5 min for 90 min, to provide a read out of OD readings. The higher the intensity of the colour reaction, the higher the OD, as shown in the example in Figure 2.12.

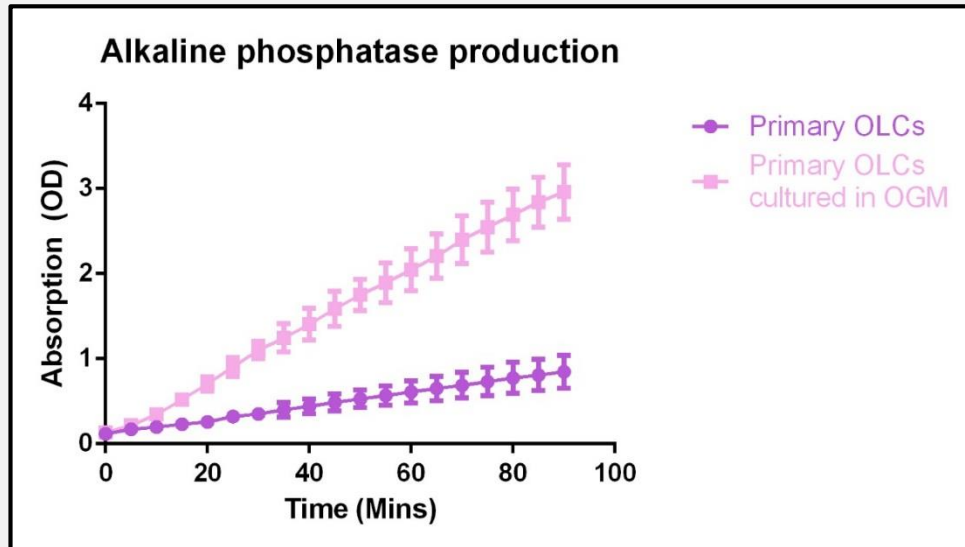


Figure: 2.12: Alkaline phosphatase production in primary osteoblast lineage cells cultured in standard MEM α -nuc media compared to those in osteogenic media. Primary osteoblast lineage cells were cultured with standard MEM α -nuc or OGM. After 14 days, the cells were lysed using 0.1% triton and incubated with PNPP. This resulted in a colour reaction when in the presence of Alp. Results were analysed by spectrometry using a SpectraMax plate reader, which provided OD readings over the course of 90 min. Cells that were cultured in OGM had higher OD readings, which plateaued before those cultured with the standard MEM α -nuc media.

2.5.1.3 DNA quantification methodology

After conducting the Alp experiments, the DNA of the same cells was quantified using a PicoGreen[®] assay. This was conducted to enable normalisation of the Alp production to DNA concentration. The DNA standard (100 μ g/ml) in the Quant-it PicoGreen[®] kit was diluted 1:50 (2.0 μ g/ml) with tris/EDTA buffer. The DNA standards were then set up in duplicate at 0, 50, 100, 200, 400, 600, 800 and 1000 ng/ml of DNA in a 100 μ l volume and transferred into a 96 well plate. Fifty microlitres of each sample used for Alp detection was then transferred into the 96 plate and to this, 50 μ l of tris/EDTA buffer was added. The PicoGreen[®] reagent was prepared by thawing a 25 μ l aliquot and diluting it with 9975 μ l of tris/EDTA buffer. One hundred microlitres of this solution was then added to each well. The plate was wrapped in foil to avoid bleaching and mixed gently on a rocker for 5 min before reading on a SpectraMax plate reader with an excitation at 488 nm and emission at 535 nm.

A standard curve was generated and the unknown DNA concentrations were calculated as with the BCA assay described in Section 2.4.4.4. The DNA concentration of each sample was multiplied by 4 to take into account the dilution factor and the final concentration was expressed as ng/ml.

2.5.1.4 Calculating alkaline phosphatase activity

To calculate Alp activity, Beer-Lambert Law was used:

$$U = \frac{(OD_{t_1} - OD_{t_0}) \times V}{t \times \epsilon \times l}$$

- OD t_1 : The OD at the end of the reaction where the reaction reaches a plateau
- OD t_0 : The OD at the beginning of the linear part of the reaction
- V: Volume of reaction (220 μ l)
- t: Reaction time (min)
- ϵ : Molar coefficient of the PNPP ($18.5 \text{ M}^{-1} \text{ centimetre (cm)}^{-1}$)
- l: Light path (0.635 cm)

The light path, which is the length in cm in which light travels in the plate reader to reach the reaction, was calculated as follows:

$$V = \pi R^2 h$$

Or: $H = V / \pi R^2$

- V= the volume= 0.2 cm^3
- H= Height of the well or light path
- R^2 = Radius of the well $0.3175 \text{ cm}^2 = 0.1008 \text{ cm}$

- $\pi = \text{Pi} = 3.142$

Therefore, light path = 0.63 cm

This calculation was then normalised to the amount of DNA in μg by dividing the Alp calculation by the amount of DNA present in the sample. This was then presented as U/ μg of DNA, a common way to present the data in recent literature (187). An example of the full calculations for this are shown in Appendix 2, Section 2.9, Table 2.6.

2.5.2 Primary osteoblast lineage cell mineralisation analysis

2.5.2.1 Primary osteoblast lineage cell mineralisation assay methodology

Osteoblast mineralisation assays were conducted on days 7, 14, 21 and 28 post-differentiation. Media was removed from the 24 well plates and washed twice in 1 ml PBS. The cells were fixed in 100% IMS over-night at 4°C and then washed twice in PBS. The wells were stained with 1 ml 40 mM pH 4.2 alizarin red (a calcium binding dye) in dH₂O per well for 90 min at room temperature. Following this, the cells were washed in 95% IMS, approximately four times to remove excess alizarin red. All of the liquid was then removed and the cells were air-dried over-night. Plastic discs were then added to each well and the intersections of the wells were filled with cotton wool to allow for contrast when scanned using an Epson 4990 scanner using the settings of: reflective, 24-bit colour and 2400 dots per inch (dpi). Mineralisation was analysed using ImageJ software. This was conducted by opening the mineralisation image file (TIFF) and setting it as a grey scale image. The threshold was then adjusted so that no mineralisation nodules were excluded or over-exposed and the threshold was then the same for each well within that plate. The software then calculated the percentage of nodules in the well area.

2.5.3 Myeloma and primary osteoblast lineage cell co-cultures

2.5.3.1 Myeloma and primary osteoblast lineage cell co-culture methodology

To establish whether MCs adhere to primary OLCs in culture and whether the stage of differentiation affects this adhesion, co-culture experiments were conducted. Primary OLCs were set up and cultured with OGM as described previously in Section 2.1.2.7. On days, 3, 14 and 28 post-differentiation the media was removed and the cells were washed twice in 150 μ l PBS. Un-transduced, CTRL and KD 5TGM1-GFP cells were seeded at a density of 5×10^4 into wells with or without primary OLCs, in a total volume of 200 μ l complete RPMI media per well. The plates were incubated for 1 hour and 6 hours after which, the media was removed and the wells were washed four times in 200 μ l PBS. This number of washes was sufficient to remove the majority of cells from the wells, which did not contain primary OLCs. After the fourth wash a final 200 μ l of PBS was added to the wells and the adhesion of the 5TGM1-GFP cells to the primary OLCs was visualised using fluorescent microscopy to quantify the number of GFP positive cells present.

2.5.3.2 Co-culture analysis

The GFP positive MCs were visualised using the Leica AF6000 microscope and the settings are demonstrated in Table 2.20.

Table 2.20: Settings used for the Leica AF6000 microscope

Contrast/ fluorochrome	Filter cube	Exposure time millisecond (ms)	Gain	Intensity	Binning
*Phase	EMP (phase)	11	2.9	32	1x1
**GFP	L5	262	7.9	4	1x1

*To detect primary osteoblast lineage cells. **To detect 5TGM1-GFP cells.

Five pictures were taken over the entire area of the well as shown in Figure 2.13 and each image was exported as a TIFF and analysed using automated Volocity software, which calculated the number of GFP positive cells in each image, as shown in Figure 2.14.

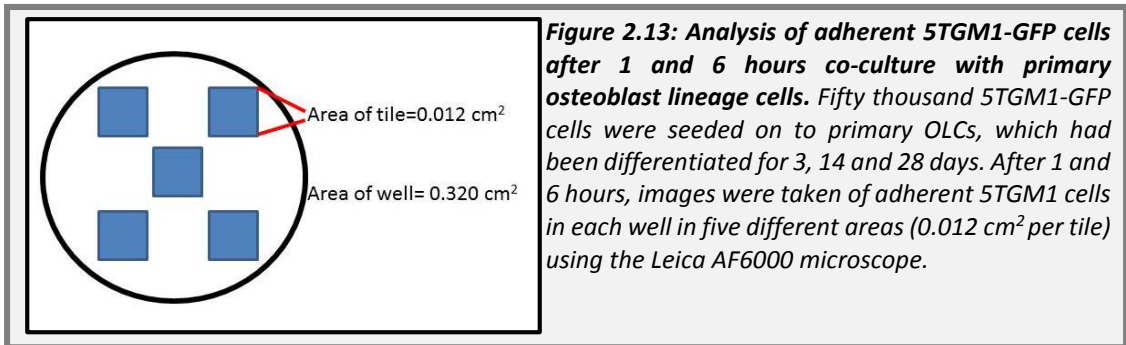
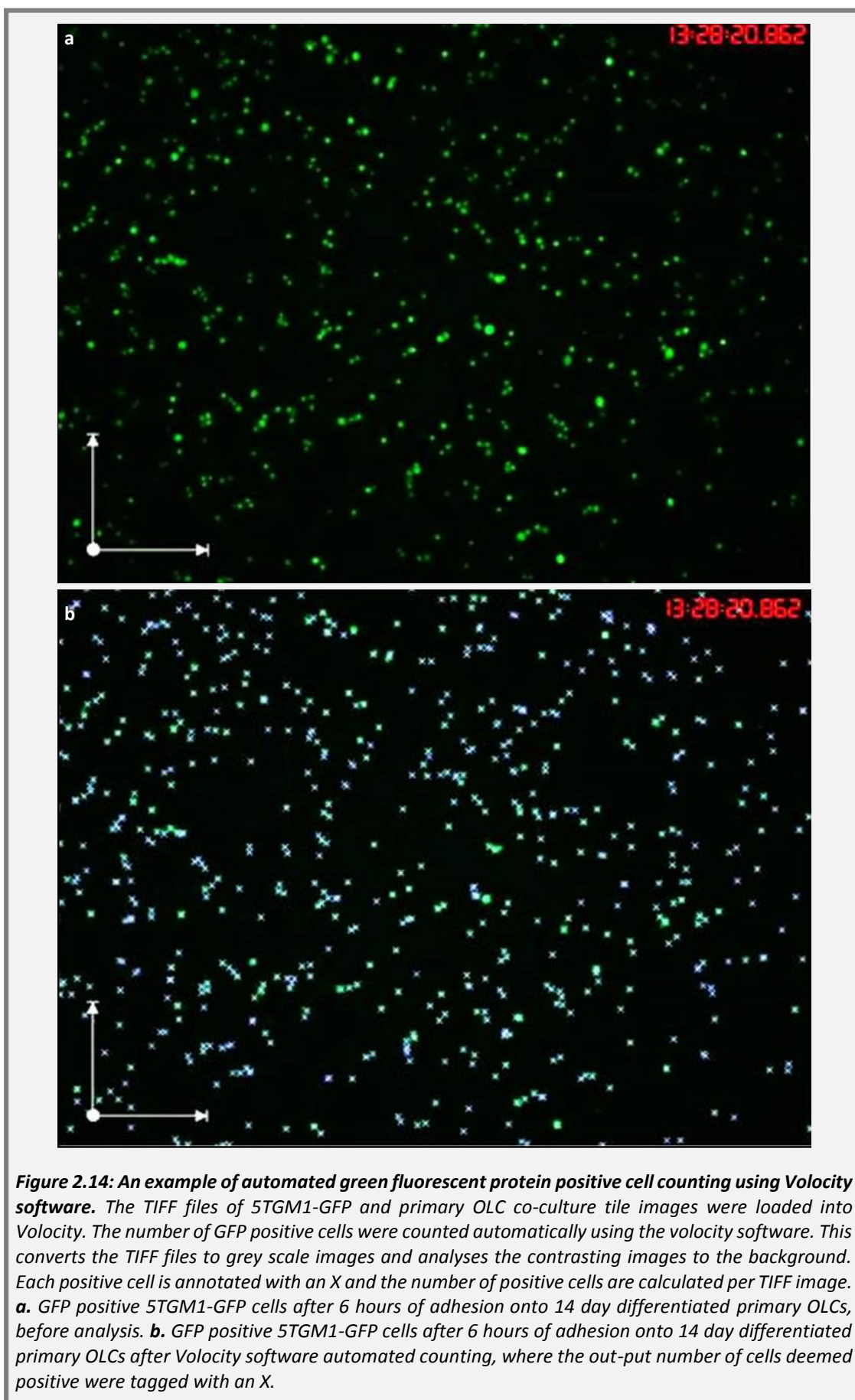


Figure 2.13: Analysis of adherent 5TGM1-GFP cells after 1 and 6 hours co-culture with primary osteoblast lineage cells. Fifty thousand 5TGM1-GFP cells were seeded on to primary OLCs, which had been differentiated for 3, 14 and 28 days. After 1 and 6 hours, images were taken of adherent 5TGM1 cells in each well in five different areas (0.012 cm² per tile) using the Leica AF6000 microscope.



2.6 Knock-down of key HSC niche molecules

All equipment, materials and reagents used for all KD experiments are outlined in Appendix 1, Section 1.13, Table 1.13.

2.6.1 Short hair-pin RNA gene knock-down technology

2.6.1.1 Principals of RNA interference technology

Ribonucleic acid interference (RNAi) technology was used to KD key HSC niche molecules in the MCs. Different forms of RNAi technology are available for silencing genes, which include silencing RNA (siRNA), shRNA and micro RNA (miRNA). Specific sequences for siRNAs, shRNAs and miRNAs can be packaged into lentiviral particles for effective delivery into cells. Short hair-pin RNAs are usually designed to be between 19 and 23 nucleotide BPs long on both the sense and anti-sense strands with a 9 BP loop and are identical to the target mRNA sequence (188).

Lentiviral particles are commonly produced in HEK293T cells, a type of renal epithelial cell line, which are notably easy to transfect. In third generation shRNA containing lentiviral particles, these cells are transfected with 3-4 vectors, which contain:

1. A transgene expression cassette vector, which contains packaging genes as well as the shRNA sequence and resistance genes e.g. pLu-green
2. A packaging vector, which encodes packaging genes such as *pol*, *gag*, *rev*, *tat*
3. An envelope expression vector, required for the formation of the viral envelope encoding for the G-protein vesicular stomatitis virus envelope gene

The viral particles are then produced by the HEK293T cells and collected in the cell supernatants (189), as shown in Figure 2.15. The lentiviral particles are transduced into the host cells where the shRNA is integrated into the hosts DNA. The shRNA is

then transcribed by Polymerase II or III and translocated from the nucleus to the cytoplasm where the hairpin loop is cleaved by an enzyme known as dicer to form siRNA. The siRNA is then incorporated into the RNA induced silencing complex (RISC), which cleaves the double stranded (Ds) shRNA to single stranded siRNA and guides the single strand towards the target mRNA (190). The binding of siRNAs to their complementary mRNA results in degradation of the complementary mRNA strand by the enzyme argonaute-2, as shown in Figure 2.15. This therefore, removes any mRNA for the GOI and stops subsequent translation to protein (191). As the shRNA is directly integrated into the genome, there is permanent silencing of the gene compared to siRNA, which has a short half-life, is also easily degraded and less than 1% of the siRNA duplex is usually present 48 hours after transduction (191).

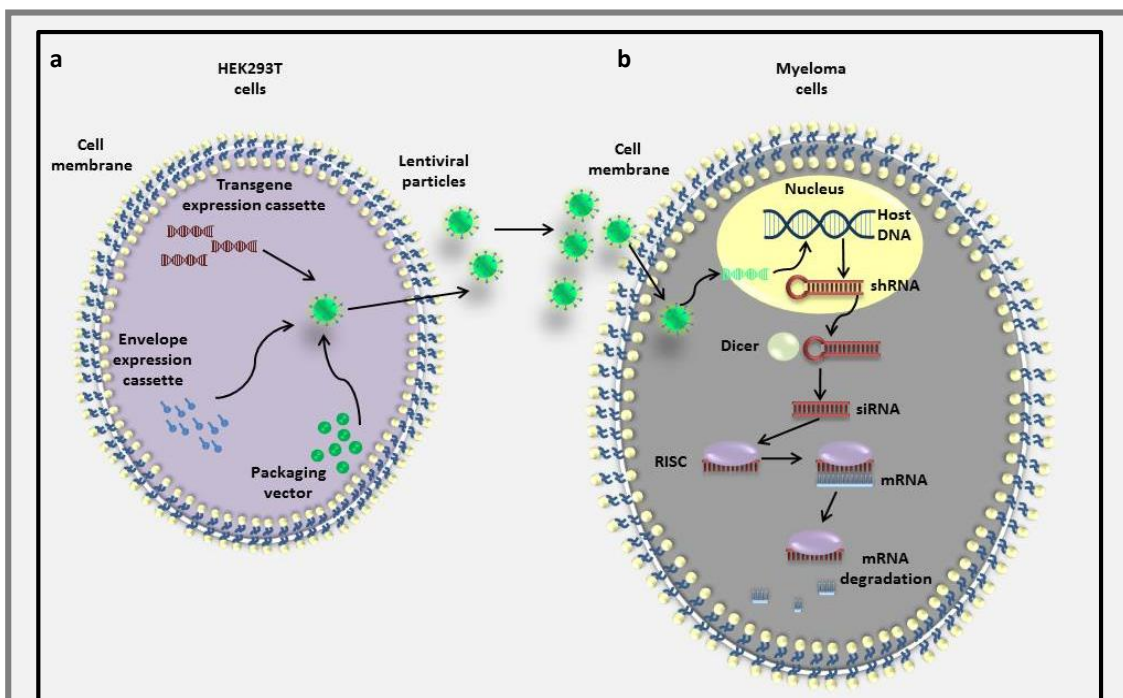


Figure 2.15: The principals of lentiviral short hair-pin RNA, to knock-down N-cad and CXCR4 in the 5TGM1-GFP cells. **a.** The production of lentiviral particles from HEK293T cells. HEK293T cells can be transfected with plasmids for the transgene, which contains the shRNA and resistance sequences, a packaging vector and the enveloped cassette. The particles produced are then collected for use from the cell supernatant. **b.** The transduction of the lentiviral shRNA particles into the MCs to KD the GOI. The lentiviral particles are transduced into the MC and the transgene is incorporated into the hosts DNA. The shRNA is transcribed and transported from the nucleus to the cytoplasm. The hairpin is then removed by the enzyme dicer to produce siRNA. The siRNA then enters the RISC complex where the double stranded (ds) RNA is cleaved to form a single strand, which binds to the complementary mRNA, resulting in degradation by argonaute-2. This removes the mRNA and prevents protein translation. Adapted from Manjunath et al (189), permission from *The Journal of Advanced Drug Delivery Reviews* 30.07.14.

2.6.2 Puromycin killing curves

2.6.2.1 Principals of puromycin selection

Puromycin is an aminonucleoside antibiotic, derived from the bacterium *Streptomyces alboniger* which is able to kill cells via disruption of protein synthesis. However, if the cells possess a puromycin n-acetylate-transferase (*PAC*) gene, they are able to produce *PAC*, which is able to inactivate puromycin; resulting in viable cells.

Prior to conducting GFP transduction or KD experiments, puromycin killing curves were conducted to establish the lowest dose of puromycin required to kill 100% of cells within four days of treatment. The optimum dose was then used to select for cells containing the transduced *PAC* gene, acquired from the control or shRNA vector.

2.6.2.2 Puromycin killing curve methodology

5T33-WT or 5TGM1-GFP cells were seeded at a density of 1×10^5 cells into a 12 well plate in 2 ml complete RPMI media and incubated for 24 hours. The following day, the cells were centrifuged and re-suspended in 2 ml of fresh complete RPMI media followed by treatment with 0 (PBS), 0.5, 1.0, 2.5, 5.0, 7.5 and 10 $\mu\text{g}/\text{ml}$ of puromycin. After 2 and 4 days following treatment, the viability of the cells were tested by centrifuging the cells and re-suspending them in 300 μl of PBS before staining the dead cells with TO-PRO-3 as described in Section 2.4.1.2. The lowest dose required for 100% cell death over a 4-day period was then established by analysing the number of viable cells remaining at the different concentrations of puromycin at the 2 and 4 day time points.

2.6.3. Polybrene optimisation

The reagent polybrene was used to aid the binding of the viral capsid to the cells being transduced by neutralising the charge on the sialic acid present on the cell membrane. The optimum concentration of polybrene per the data sheet was 5

µg/ml, however, as some concentrations of polybrene can be toxic in certain cells optimisation was required.

2.6.3.1 Polybrene optimisation methodology

The effect of polybrene upon cell viability after 24 hours was established before use in the GFP transduction or KD experiments. Before use, polybrene was immediately diluted to 1 mg/ml in sterile H₂O and frozen in 1 ml aliquots, which were thawed as required. For polybrene optimisation, the 5T33-WT and 5TGM1-GFP cells were counted and seeded into a 48 well plate at a density of 5×10^4 in 500 µl complete RPMI media containing 0, 2.5, 5.0, 7.5 and 10 µg/ml polybrene and incubated for 24 hours. After 24 hours, the number of cells present in each well were counted to establish whether the polybrene had prevented proliferation or caused cell death after 24 hours. Viability staining could not be used in this instance as polybrene treatment resulted in false positives by allowing the DNA binding dye to enter viable cells.

2.6.4 Green fluorescent protein transduction in 5T33-WT cells and knock-down of CXCR4 and N-cad in 5TGM1-GFP cells

2.6.4.1 Green fluorescent protein transduction and knock-down of CXCR4 and N-cad in the 5TGM1-GFP cells methodology

To transduce GFP and to KD CXCR4 and N-cad in the MCs, a lentiviral particle transduction system was used which contained replication incompetent viral particles. The particles contained the shRNA sequences for CXCR4 and N-cad or scrambled sequence for the CTRL particles or GFP sequence. In addition, they also contained the PAC gene to enable puromycin resistance. The sequences of the hairpin loop and subsequent siRNA are shown in Table 2.21.

Table 2.21: The hairpin loop sequences and subsequent siRNA sequences provided in the lentiviral particles, for CXCR4 and N-cad knock-down

Gene	shRNA	SiRNA Sense	siRNA anti-sense
CXCR4 A	5'GATCCCCACGCCACCAA CAGTCAATTCAAGAGATT GACTGTTGGTGGCGTGGT TTTT	5'CCACGCCACCAACAGUC AAtt	5'UUGACUGUUGGUGGC GUGGtt
CXCR4 B	5'GATCCCCTCAAGATCCT TTCCAAATCAAGAGATT GGAAAGGATCTTGAGGTT TTT	5'CCUCAAGAUCUUUCC AAAtt	5'UUUGGAAAGGAUCUUG AGGtt
CXCR4 C	5'GATCCGAGACTGACCA GTCTTGATTCAAGAGAT ACAAGACTGGTCAGTCTC TTTTT	5'GAGACUGACCAGUCUU GUAtt	5'UACAAGACUGGUCAGU CUCtt
N-cad A	5'GATCCGGAACCACATGA AATTGAATTCAAGAGATT CAATTCATGTGGTTCCTT TTT	5'GGAACCACAUGAAUU GAAtt	5'UUCAAUUUCAUGUGGU UCctt
N-cad B	5'GATCCGAACCCAACTCA ATTAACATTCAAGAGATG TTAATTGAGTTGGTTCCTT TTT	5'GAACCCAACUCAUUUA ACAtt	5'UGUUAAUUGAGUUGG GUUctt
N-cad C	5'GATCCGGAAGCTGGTAT CTATGAATTCAAGAGATT CATAGATACCAGCTTCCTT TTT	5'GGAAGCUGGUAUCUA UGAAtt	5'UUCAUAGAUACCAGCU UCctt

The 5T33-WT and 5TGM1-GFP cells were seeded at a density of 2×10^4 cells in 100 μ l complete RPMI media containing 5 μ g/ml polybrene (optimised using the method in Section 2.6.3.1) and the cells were transferred to a 96 well plate. To this, lentiviral particles were added at a range of multiplicity of infections (MOIs), which is defined as the number of transducing lentiviral particles per cell. The formula calculating the MOI is shown below:

MOI calculations:

Total number of cells per well X desired MOI= total transducing units (TU) required
 Total TU required / TU/ml in vial of lentiviral particles = volume of lentiviral particles required.

E.g. MOI=20,000 cells x MOI 5.0= 100,000

$100,000/5 \times 10^6 = 0.02 \text{ ml} = 20 \mu\text{l}$

MOIs of 5, 15 and 25 were used and the correct volume of lentiviral particles was added to each well. The cells were incubated for 20 hours after which they were centrifuged and washed twice in 1 ml complete RPMI, re-suspended in 200 μ l complete RPMI and incubated. After three further days of incubation, the cells were centrifuged and re-suspended in 500 μ l complete RPMI media containing 7.5 μ g/ml puromycin for the 5T33-WT cells and 5 μ g/ml puromycin for the 5TGM1-GFP cells. The cells were then incubated until resistant colonies were visualised, approximately 5 days after selection. The 5T33-WT resistant colonies were expanded and analysed to detect GFP expression using flow cytometry. The method for this was the same for GFP detection in the cell lines using flow cytometry in Section 2.4.1.2. The 5TGM1-GFP cells transduced with shRNA, were set-up for RNA extraction as described in Section 2.3.1 1 to confirm KD of the genes. Cells were also frozen down for future experiments as described in 2.1.2.6 or they were also isolated for WB to confirm KD of protein, as described in Section 2.4.4.2.

The cells which had been successfully knocked-down for CXCR4 and N-cad were also cultured in the absence of puromycin for 4 weeks to mimic the time in which they would not be under selection when *in vivo*. Real-time PCR and WB were conducted in these cells to confirm the stability of the KD.

2.6.4.2 PCR analysis

PCR analysis of the KD of CXCR4 and N-cad was performed by conducting RNA extraction (Section 2.3.1 1), RT (Section 2.3.2.1) and real-time PCR (Section 2.3.5.2) using the CTRL and KD cells at the various MOIs. The fold change and percentage of KD was calculated by normalising the GOI Ct values to the HK gene β 2M and the KD was then calculated using the comparative $\Delta\Delta$ Ct method as shown in Table 2.22.

Table 2.22: An example of calculations used to quantify the knock-down of CXCR4 and N-cad compared to CTRLs using real-time PCR

Treatment	$\beta 2M$	N-cad	Δct	$\Delta \Delta Ct$	SD	Fold change	SD	%
	HK	GOI	GOI-HK	$2^{-\Delta \Delta Ct}$	SD	KD/CTRL	SD control/control average amount	
CTRL 15	15.38	23.10	7.71	0.00476492	0.00112332	1.00	0.195709 40	100
CTRL 15	15.37	22.88	7.51	0.00548611				
CTRL 15	15.62	22.78	7.17	0.00696819				
Mean	15.46	22.92	7.46	0.00573974				
							SD treatment / control amount	
KD 15	16.01	24.61	8.60	0.00257122	0.00073240	0.30	0.127601 74	30
KD 15	15.60	25.42	9.81	0.00111210				
KD 15	15.50	24.68	9.18	0.00173001				
Mean	15.70	24.90	9.20	0.00170390				

2.7. Bone parameter analysis

All equipment, materials and reagents used for bone parameter analysis are outlined in Appendix 1, Section 1.14, Table 1.14.

2.7.1 Micro-computed tomography

2.7.1.1 Principals of micro-computed tomography

To determine any differences between the bone parameters in the mice injected with 5TGM1-GFP cells, CTRL or KD cells, micro-computed tomography (μ CT) was used. Micro-computed tomography was introduced in the 1980s by Feldcamp *et al* for the evaluation of the bone micro-architecture in mice and small rodents (192). However, the concept of producing three-dimensional images of bone originated in

1917 and was proposed by John Radon. Micro-computed tomography is a non-invasive and non-destructive technique using X-rays. X-ray photons are generated by accelerated electrons in the source (usually an X-ray tube) which strike the tungsten within the tube. X-rays are emitted as a polychromatic beam, which pass through a rotating sample within the sample holder. X-rays are then absorbed or scattered depending on the density of the sample, dense samples such as bone which contain calcium cause x-ray absorption whereas soft tissues result in x-ray scattering. The images are detected and projected as two-dimensional image slices, which are reassembled to produce three-dimensional images. The main advantage of μ CT is the spatial resolution of the machine, which can be as low as 4 μm producing highly accurate and detailed images. The main constituents of a CT machine are shown in Figure 2.16. A number of parameters can be analysed using μ CT and the most informative are trabecular bone volume normalised to tissue volume (BV/TV), trabecular thickness (tb.th), trabecular number (tb.n), trabecular pattern factor (tb.pf) and cortical thickness (ct.th). In addition, lesion number and lesion area can be calculated.

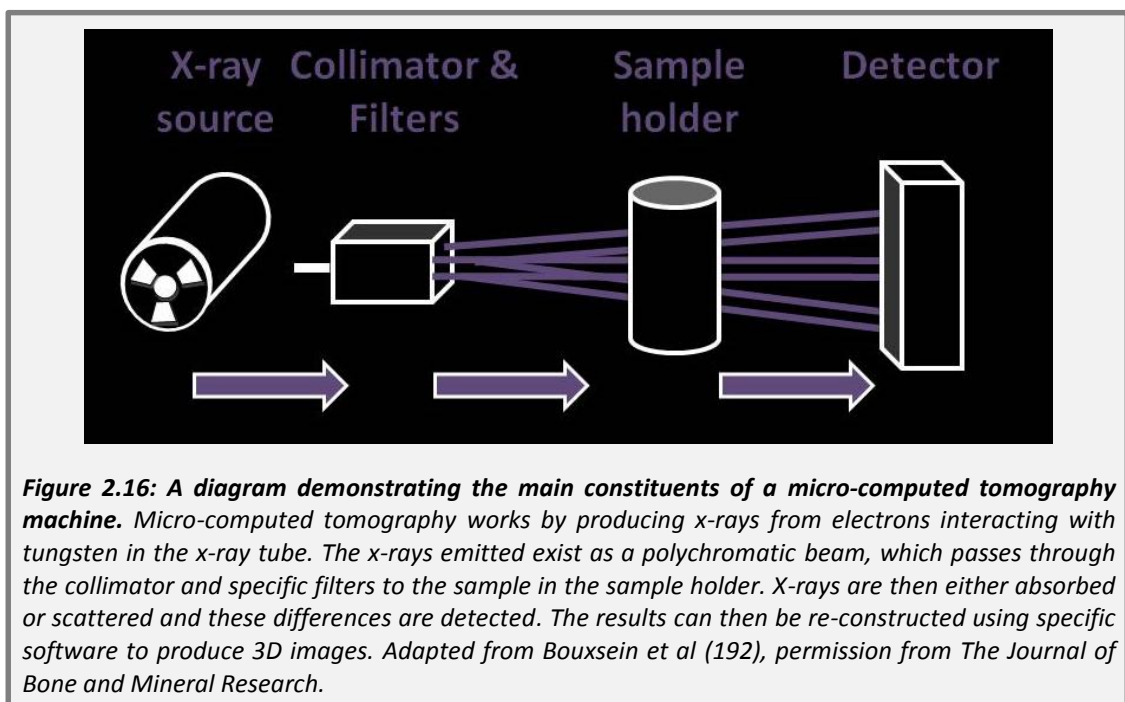


Figure 2.16: A diagram demonstrating the main constituents of a micro-computed tomography machine. Micro-computed tomography works by producing x-rays from electrons interacting with tungsten in the x-ray tube. The x-rays emitted exist as a polychromatic beam, which passes through the collimator and specific filters to the sample in the sample holder. X-rays are then either absorbed or scattered and these differences are detected. The results can then be re-constructed using specific software to produce 3D images. Adapted from Bouxsein et al (192), permission from *The Journal of Bone and Mineral Research*.

2.7.1.2 Micro-computed tomography methodology

The right tibia from each mouse was fixed in 10% formalin prior to scanning. Formalin was made using the reagents and volumes shown in Table 2.23. Bones were then scanned using a SkyScan 1172 at 50 kilo volts (Kv), 200 microamperes (μA), using an aluminium filter of 0.5 mm and pixel size of $4.3 \mu\text{m}^2$ and images were then reconstructed using N-Recon software. Trabecular bone, 0.2 mm below the growth plate, was analysed using Ct-an and Batman software to provide data for bone parameters including BV/TV, tb.n and tb.th. All bones were scanned in-house by Holly Evans, a trained $\mu\text{-CT}$ technician.

Table 2.23: Reagents and quantities required to make 10% formalin

Item	Supplier
Sodium dihydrogen orthophosphate dihydrate	8 g
Disodium hydrogen orthophosphate dihydrate	13 g
Concentrated formaldehyde (i.e. 37-41%)	200 ml
dH ₂ O	1800

2.7.1.2 Lesion counting

To count the number of lesions and lesion area, data sets for each bone were resized from a $4.3 \mu\text{m}^2$ pixel size to $12.9 \mu\text{m}^2$. The cortical bone was hollowed out and files were imported into Drishti I, rendering software. Using this software, a 3D model of each bone was produced and each plane of bone (3 in total) was imaged and saved as a separate file. These files were resized using Picassa 3 software and the files were imported into ImageJ software. Lesions were then counted using the grey scale automated analysis function to count the number and the area of each hole (pixels²).

2.8. Statistics

All data throughout are presented as the mean using the standard error of the mean (SEM) unless stated otherwise in the figure legend. All data were analysed statistically using GraphPad Prism Version 6. Where relevant, statistical analysis was conducted with guidance from the University of Sheffield Maths and Statistics Help group and advice from a senior clinical scientist with expertise in statistics. Throughout all experiments, non-parametric tests were used, as Gaussian distribution could not be assessed, as N numbers were not above the required number of eight. Mann-Whitney U tests were used to compare values between two groups of unpaired data and a Wilcoxon matched pairs signed rank test was used to compare two groups of paired data. In addition, a Kruskal-Wallis test followed by Dunn's post test was used to compare more than two groups of unpaired data and a Friedman test followed by Dunn's post test was used to compare more than two groups of paired data.

Chapter III: The *in vitro* expression of HSC niche molecules and their complementary ligands by myeloma and osteoblastic cells

3.1 Introduction

HSCs reside in BM microenvironmental niches in which their proximity to certain BM constituents influences their behaviour. Their proximity to osteoblasts is thought to inhibit HSC proliferation and promote entry into the G₀ phase of cell cycle, whereas, their proximity to the vasculature stimulates proliferation and differentiation into a variety of cell lineages (82, 83, 85). Molecules which have been implicated in the physical interaction between HSCs and osteoblastic cells, are the receptors CXCR4, Notch-1, Tie-2 and the adherin molecule N-cad, expressed by the HSCs, and their complementary ligands, CXCL12, Jag-1, Ang-1 and N-cad, expressed or secreted by the osteoblastic cells. The BM and its cellular constituents also play an important role in MC homing, growth and survival. Previous studies have largely focussed upon the influence of the BM microenvironment in the later stages of disease and current research is particularly limited with regards to early myeloma development as well as MC survival following chemotherapy. It has been suggested that MCs may exist within a BM microenvironmental niche, distinct but similar to that occupied by HSCs, or, MCs may in fact “hijack” the HSC niche. As with HSCs, occupancy of the niche may result in MC quiescence if located in close proximity to osteoblasts. Currently, little research has been conducted to test this hypothesis. However, previous papers have identified the expression of some of the HSC niche molecules by MCs *in vitro*.

There is substantial evidence in support of the CXCR4/ CXCL12 axis as part of the mechanism for MC homing and mobilisation to the BM. Previous data have described the *in vitro* expression of CXCR4 by various patient cells and human myeloma cell lines including MM.1S, U266, OPM-2, Kas/61, RPMI-8226, KMS-12BM, KMS-12PE and KHM-1B cells (193-195) and murine cell lines such as the 5T2MM and 5T33MMvt (170). In addition, its ligand CXCL12 is widely known to be expressed by human osteoblast cell lines including MBA-15, MG63 (111) and MC3T3-E1 (196) as well as primary human osteoblasts (111) *in vitro*.

The interactions of Notch-1 and Jag-1 have also been investigated in MM. Notch-1 was expressed by several human MC lines *in vitro* including; NCI H929, RPMI-8226, HS-Sultan, ARH-77, IM-9, MC/CAR and MM.1S (197) as well as primary human MCs (198). The ligand Jag-1 was also expressed by human primary BM stromal cells (199) and MC3T3-E1 osteoblastic cells (200) *in vitro*.

Currently there is limited data available in support of the expression of Tie-2 by MCs compared to that published for CXCR4 and Notch-1. However, Tie-2 expression was determined in the human cell line XG-1 and in 4 out of 23 MM patient plasma cell samples by RT-PCR. Ang-1 expression was identified in numerous myeloma cell lines *in vitro*, including RPMI-8226, U266, OPM-2, XG-1, and XG-6 as well as 11 out of 22 patient samples (201). Ang-1 was also expressed by murine primary osteoblastic cells, ST-2 cells and C2C12 myoblastic cells (202) *in vitro*.

A role for N-cad in metastasis has been explored in several cancers including prostate and breast cancer. Prostate cell lines PC-3 and LAPC4 and LAPC9 cells (203) and breast carcinoma cell lines BT549, Hs578t, SUM159PT, MDA-MB-435 and MDA-MB-436 expressed N-cad (204). N-cad expression has also been determined in human patient MM cells (205) and in human MC lines; LME-1, UM-1, OPM-1, NCI-H929 (206), U266 and RPMI (207) *in vitro*. N-cad was also expressed by C2C12 myoblasts and the MSC progenitor cell line C3H10T1/2 (which undergo osteoblast differentiation once treated with BMP-2 and 7), KS483 osteoblastic cells (206) as well as murine MC3T3-E1 cells (208) *in vitro*.

Taken together the studies above provide evidence for a myeloma and osteoblastic cell axis in which the MCs express the HSC niche molecules CXCR4, Notch-1, Tie-2 and N-cad and the osteoblastic cells express the ligands CXCL12, Jag-1, Ang-1 and N-cad.

Currently there is no data, which systematically determines the expression of these molecules in the 5TGM1-GFP cell line and limited data for the 5T33MMvt model. In my studies, I have determined the *in vitro* expression profile of CXCR4, Notch-1, Tie-2 and N-cad by the 5T33-WT, 5T33-GFP and the 5TGM1-GFP cells and the expression of the complementary ligands CXCL12, Jag-1, Ang-1 and N-cad by murine osteoblastic cells, cultured *in vitro*.

3.2 Hypothesis, aims and objectives

3.2.1. Hypothesis and aims

The aim of these studies was to test the hypothesis that “Myeloma cells express the same repertoire of molecules as HSCs, and their complementary ligands are expressed by osteoblastic cells *in vitro*”.

3.2.2 Objectives

The hypothesis will be tested by the following objectives:

1. To determine the expression of CXCR4, Notch-1, Tie-2 and N-cad by the 5T33-WT, 5T33-GFP and 5TGM1-GFP cell lines using endpoint and real-time PCR and to evaluate the presence of each protein by flow cytometry, immunofluorescence (IF) and Western blotting (WB).
2. To determine the expression of CXCL12, Jag-1, Ang-1 and N-cad by the MC3T3-E1 cells and murine primary osteoblast lineage cells (OLCs) using endpoint and real-time PCR and to evaluate the presence of each protein by flow cytometry.

3.3 Methods

3.3.1 Gene expression analysis

3.3.1.1 Endpoint PCR

Murine BM was isolated from C57BL/6 mice (N=3) as described in Chapter II, Section 2.2.1. The 5T33-WT, 5T33-GFP, 5TGM1-GFP, MC3T3-E1 cells and primary OLCs were prepared 24 hours prior to RNA extraction to ensure experimental consistency. One million MCs were seeded in triplicate into a 6 well plate with 3 ml complete RPMI media. The MC3T3-E1 cells and primary OLCs were seeded in triplicate at a density of 1×10^6 into a T75 flask in 12 ml of complete media, appropriate for the cell type. Each cell type was incubated for 24 hours before RNA extraction, followed by cDNA synthesis and PCR as described in sections 2.3.1, 2.3.2, 2.3.3 and 2.3.4. The process from seeding the cells to PCR was repeated three times to produce three biological replicates. The Genomics Facility at The University of Sheffield then sequenced all PCR products and the homology was analysed by comparing the sequencing results with the expected template and GenBank archives.

3.3.1.2 Real-time PCR

The cDNA from each cell type, generated as described above was also used for real-time PCR analysis as described in section 2.3.5. Expression was analysed using an Applied Biosystems 7900HT real-time PCR machine to produce a Ct value, which was normalised to the HK gene *β2M* to produce the Δ Ct value. As with endpoint PCR, the process from RNA extraction to PCR was repeated three times to produce three biological replicates (N=3).

3.3.2 Protein quantification analysis

3.3.2.1 Flow cytometry

The murine BM, splenocytes and blood were isolated and processed for flow cytometry as described in section 2.2.1 and the MCs and murine osteoblastic cells were set-up as described above for RNA extraction (N=3-6). Cells were then processed for flow cytometry as described in section 2.4.1. The percentage of positive viable cells (using PI or TO-PRO-3 staining) was measured using a FACS Calibur and analysed using Cell Quest software by gating against the negative isotype control, which demonstrated less than 1% positive staining. Each cell type was set-up in triplicate and repeated three times (N=3) to produce a mean percentage of cells positive for each molecule.

3.3.2.2 Immunofluorescence

Immunofluorescence was used to quantify and visualise the protein for the HSC niche molecules, ligands and CD138 by the 5T33-GFP and 5TGM1-GFP cells as described in section 2.4.2. Positive cells were visualised using a Leica AF6000LX microscope, a 40X magnification and LAS LF software. Analysis was conducted using Volocity software to calculate the percentage of cells, which were positive for each molecule. Each experiment was set-up in triplicate (using three slides) and repeated three times (N=3) to calculate a mean percentage of cells which were positive for each molecule.

3.3.3. Statistics

Where relevant non-parametric statistical tests were used. A Kruskal-Wallis test followed by a Dunn's post test ($P < 0.05$) was used to determine any differences in gene expression between the MCs and the presence of protein for the HSC niche molecules and ligands between the murine constituents and MCs. Where relevant, error bars were displayed on all graphs using the SEM unless stated otherwise in the legend.

3.4 Results

3.4.1 Qualitative assessment of gene expression for the HSC niche molecules, ligands and CD138 by normal murine constituents and murine multiple myeloma cells, determined using endpoint PCR

Endpoint PCR was used to determine the qualitative gene expression of the HSC niche molecules, their ligands and the plasma cell marker CD138 by murine BM (to act as a positive control for the primers), 5T33-WT, 5T33-GFP and 5TGM1-GFP cells. As demonstrated in Figure 3.1, endpoint PCR of the murine BM generated products of expected size for the HK gene *GAPDH* (354 BP) and the HSC niche molecules; *CXCR4* (711 BP), *Notch-1* (348 BP), *Tie-2* (648 BP) and *N-cad* (560 BP) and ligands; *CXCL12* (205 BP), *Jag-1* (370 BP), *Ang-1* (401 BP) and *CD138* (559 BP). These results therefore, confirmed that endpoint PCR primers were working effectively.

Endpoint PCR was also used to determine the qualitative gene expression of the HSC niche molecules, ligands and CD138 by the MCs. Endpoint PCR of the 5T33-WT, 5T33-GFP and 5TGM1-GFP cells generated products of expected size for the HK gene *GAPDH* and the HSC niche molecules *CXCR4* and *Notch-1*. In addition, the 5T33-WT and 5TGM1-GFP samples also generated a band for *N-cad* but the 5T33-GFP cells did not (Figure 3.1). A band for *CD138* was visualised in each MC type. Endpoint PCR analysis of MC lines did not generate products for the ligands *CXCL12*, *Jag-1*, *Ang-1* or the receptor *Tie-2*. Therefore, the MCs expressed some HSC niche molecules and no ligands by endpoint PCR.

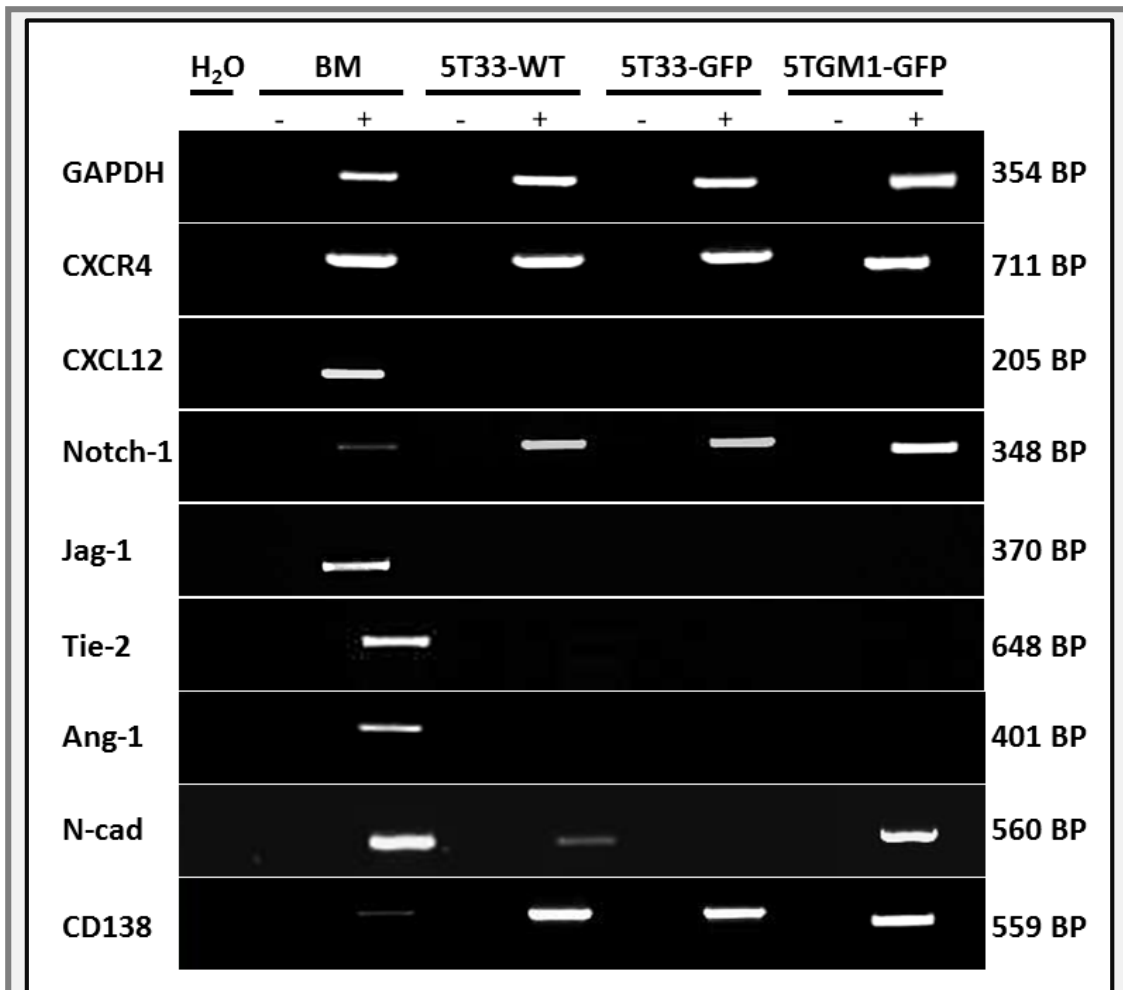


Figure 3.1: Murine bone marrow and myeloma cells expressed HSC niche molecules, ligands and CD138 by endpoint PCR. Endpoint PCR reactions were run using approximately 40 ng of RT+ cDNA samples. An equal volume of RT- and H₂O control samples were used to assess genomic and reagent contamination. The PCR reactions were run for 25 cycles for GAPDH and 35 cycles for the HSC niche molecules, ligands and CD138. The PCR products were separated by electrophoresis in a 1.6% agarose gel and visualised using a Bio-rad Gel Doc XR+ Imager system and Quantity One 4.6.8 software. Each row depicts an individual gel electrophoresis for GAPDH and each HSC molecule and ligand. The base pair (BP) number on the right corresponds to the size of bands visualised and band products were confirmed by in-house sequencing. Results are representative of three independent experiments.

3.4.2 Quantitative assessment of gene expression for the HSC niche molecules, ligands and CD138 by normal murine constituents and murine multiple myeloma cells, determined using real-time PCR

Real-time PCR was used to determine the quantitative expression of the HSC niche molecules, their ligands and CD138 by the murine BM, 5T33-WT, 5T33-GFP and 5TGM1-GFP cells. Table 3.1 demonstrates a summary of the absolute gene expression values (Ct values) generated using real-time PCR. The BM expressed the

HK genes *β2M* and *HPRT*, HSC niche molecules *CXCR4*, *Notch-1*, *Tie-2* and *N-cad* and ligands *CXCL12*, *Jag-1* and *Ang-1*. In addition, they also expressed *CD138*. This confirmed that all probes were effective.

Table 3.1 also shows the absolute gene expression of the HK, HSC niche molecules and ligands by the 5T33-WT, 5T33-GFP and 5TGM1-GFP cells and in addition, Figure 3.2 shows the $1/\Delta\text{Ct}$ values relative to the HK gene *β2M*. The 5T33-WT, 5T33-GFP and 5TGM1-GFP samples highly expressed the HK genes *β2M* and *HPRT*, the HSC niche molecules *CXCR4* and *Notch-1* and plasma cell marker *CD138* but demonstrated low expression of the ligand *CXCL12*. The 5T33-WT expressed *N-cad*, as did the 5TGM1-GFP, though at a higher level, whereas, *N-cad* was undetermined (UD) in the 5T33-GFP samples. The 5TGM1-GFP samples also had marginal expression of *Tie-2* and *Ang-1*, which were absent in both the 5T33-WT and 5T33-GFP samples. Each cell type did not express the ligand *Jag-1*. When the data was analysed statistically to compare the expression between the MCS, there were no significant differences. However, it was clear from the data that *N-cad* expression was higher in the 5TGM1-GFP cells compared to both the 5T33-WT and 5T33-GFP cells but because some of the values were UD this was unable to be analysed statistically.

In summary, as with the endpoint PCR analysis, the MCs expressed only some of the HSC niche molecules and ligands using real-time PCR and the pattern of expression was broadly similar to the endpoint PCR analysis where absent expression corresponded with high or UD Ct values.

Table 3.1: A summary of the absolute gene expression of the HSC niche molecules, ligands and CD138 by murine bone marrow and myeloma cells using real-time PCR

Gene	BM	5T33-WT	5T33-GFP	5TGM1-GFP
<i>β2M</i>	17 ± 0.16	15 ± 0.11	15 ± 0.06	12 ± 0.22
<i>HPRT</i>	22 ± 0.17	20 ± 0.24	20 ± 0.04	17 ± 0.17
<i>CXCR4</i>	21 ± 0.08	21 ± 0.05	21 ± 0.25	19 ± 0.08
<i>Notch-1</i>	23 ± 0.23	24 ± 0.09	25 ± 1.38	22 ± 0.34
<i>Tie-2</i>	29 ± 0.07	UD	UD	34 ± 0.56
<i>N-cad</i>	27 ± 0.44	33 ± 0.33	UD	20 ± 0.06
<i>CXCL12</i>	21 ± 0.55	31 ± 0.99	33 ± 1.38	30 ± 0.51
<i>Jag-1</i>	28 ± 0.51	UD	UD	UD
<i>Ang-1</i>	27 ± 0.17	UD	UD	34 ± 0.75
<i>CD138</i>	28 ± 0.81	21 ± 0.06	21 ± 0.10	18 ± 0.20

Mean Ct values ± SEM UD= Undetermined, Ct value > 35.

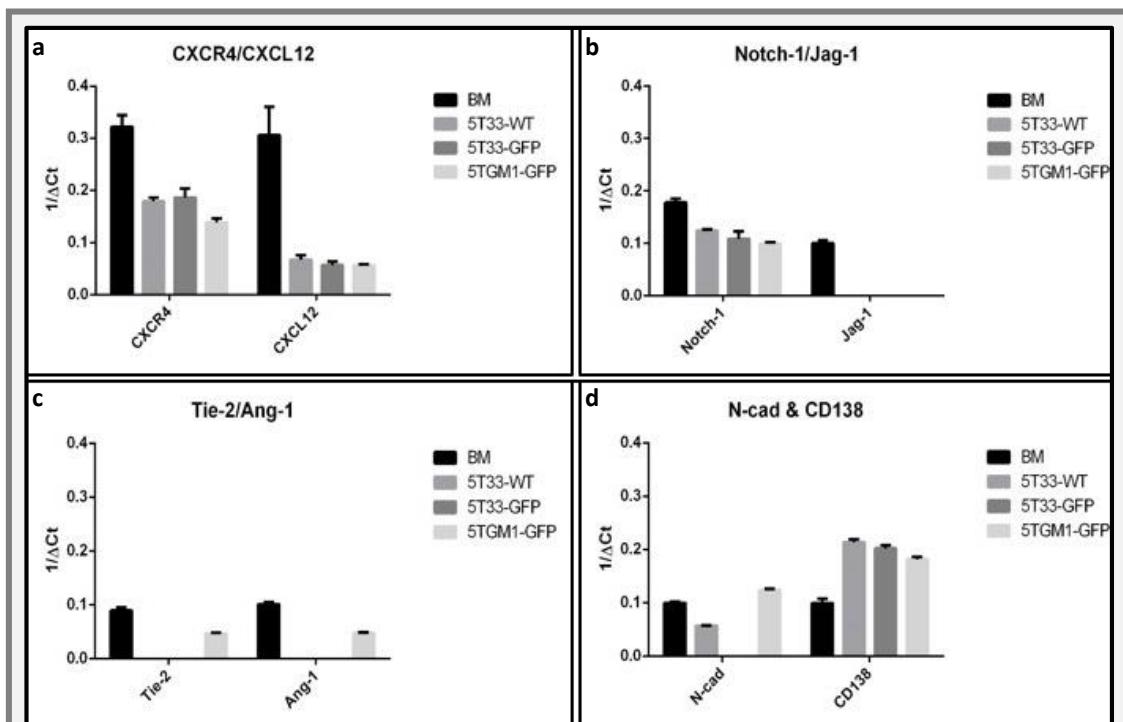


Figure 3.2: The murine bone marrow and myeloma cells expressed the HSC niche molecules and complementary ligands at varying levels using real-time PCR analysis. Gene expression was assessed by normalising the Ct values produced in real-time PCR for CXCR4 & CXCL12 (a), Notch-1 & Jag-1 (b), Tie-2 & Ang-1 (c) and N-cad & CD138 (d) to the HK gene *β2M* to produce the $1/\Delta Ct$ (y-axis) value. Data was analysed statistically using a Kruskal-Wallis test followed by Dunn's post test ($P < 0.05$) to compare expression between the MCs. Results were determined from three independent experiments ($N=3$) using the SEM.

3.4.3 Protein quantification of HSC niche molecules, ligands and CD138 by normal murine constituents and murine multiple myeloma cells using flow cytometry

Flow cytometry was used to determine the number of murine BM, splenocytes, blood cells and MCs, which were positive for the HSC niche molecules, ligands and CD138. Figure 3.3a demonstrates an example of the flow cytometry plots produced for the staining of CD138 and the viability dye PI in samples of control BM, splenocytes and peripheral blood. The mean percentage of cells which were positive for each HSC niche molecule and ligand (excluding Ang-1 and N-cad) are shown in Figure 3.3.b and summarised in Table 3.2. The BM, splenocytes and blood were positive for the HSC niche molecules; CXCR4, Notch-1 and Tie-2 and the ligands; CXCL12 and Jag-1. CD138 positive staining was also detected in the BM, splenocytes and blood. When the results were compared statistically, a significantly greater number of BM cells were positive for CXCR4 compared to the splenocytes ($P < 0.05$) and there were no other statistically significant differences between the remaining HSC niche molecules and ligands when comparing the different cell types.

Ang-1 was not analysed by flow cytometry due a lack of directly conjugated antibody and unsuccessful use of an indirect antibody method using the murine constituents (data not shown). In addition, when the work was originally conducted there were no directly conjugated N-cad antibodies available and indirect methods failed to stain the murine positive controls (data not shown). However, more recently a directly conjugated N-cad antibody became available and this was tested using the 5TGM1-GFP cells and the 5T33-GFP cells as a negative control as shown later in Figure 3.5.

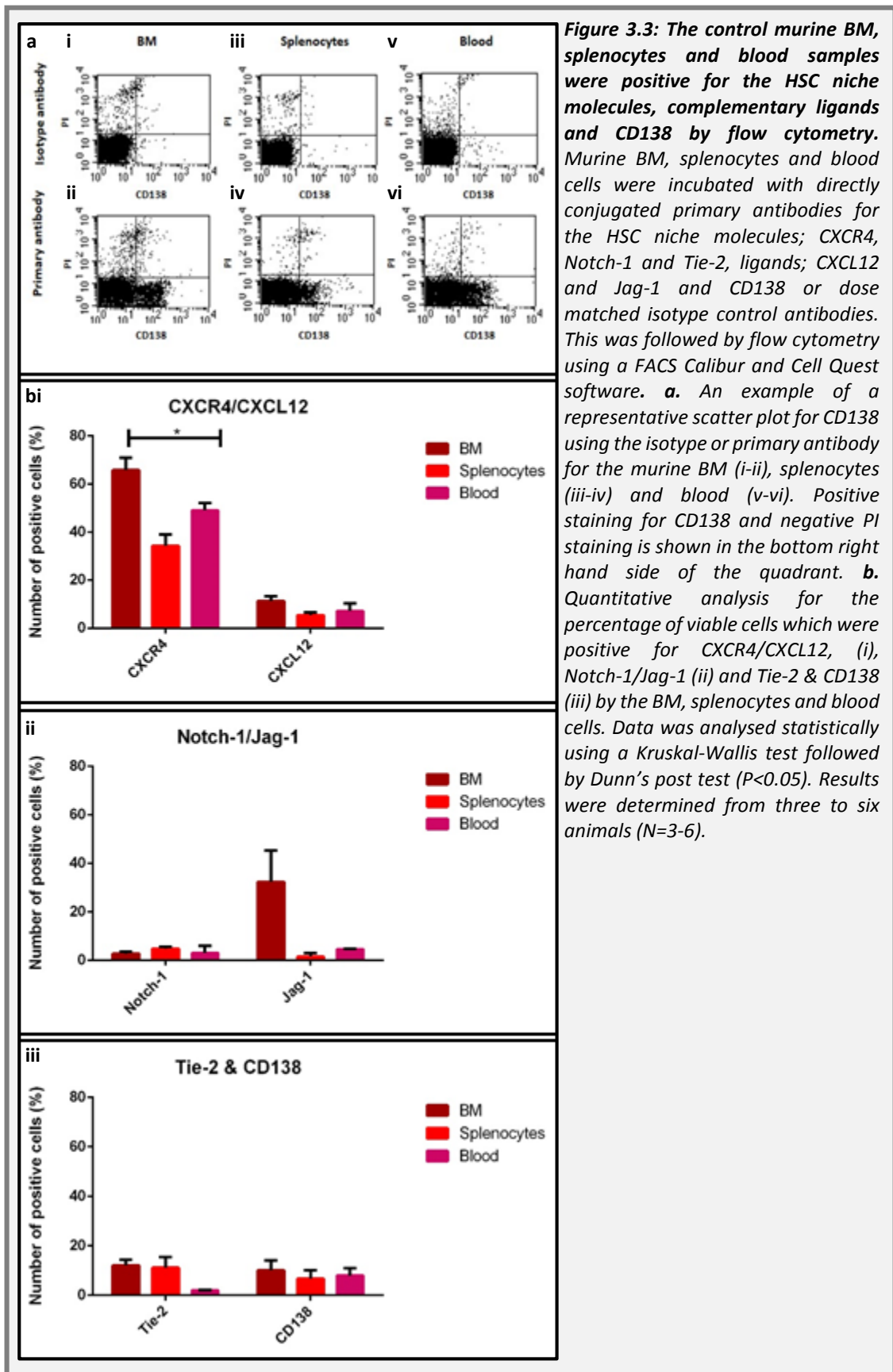


Table 3.2: A summary of the quantitative analysis for the percentage of control murine constituents, which were positive for the HSC niche molecules, ligands and CD138 using flow cytometry

Protein	BM	Splenocytes	Blood
CXCR4	65.75 ± 5.08	37.24 ± 4.70	49.06 ± 3.04
Notch-1	2.79 ± 0.81	4.87 ± 0.69	3.00 ± 2.98
Tie-2	11.95 ± 2.37	11.09 ± 4.34	1.89 ± 0.16
CXCL12	11.29 ± 2.39	5.44 ± 1.12	7.19 ± 3.09
Jag-1	13.18 ± 13.18	1.48 ± 1.48	4.57 ± 0.20
CD138	10.01 ± 4.03	6.68 ± 3.36	7.87 ± 3.06

Mean percentage of positive cells ± SEM

Figure 3.4.a. shows an example of the flow cytometry plots produced for the staining of CD138 and the viability dye PI in the 5T33-WT, 5T33-GFP and 5TGM1-GFP cells. The mean percentage of cells which were positive for each HSC niche molecule and ligand are shown in Figure 3.4.b. Table 3.3 also summaries the percentages and SEM values for the mean number of 5T33-WT and GFP and 5TGM1-GFP cells which were positive for the HSC niche molecules, ligands and CD138. Each MC was positive for the HSC niche molecules CXCR4, CXCL12, Notch-1, Tie-2 and CD138. In addition, the 5TGM1-GFP cells were positive for the ligand Jag-1. When the proportion of positive cells were compared between the MCs statistically, a greater number of 5T33-WT cells were positive for CXCR4 ($P < 0.05$) and Notch-1 ($P < 0.05$) compared to the 5T33-GFP cells. In addition a greater number of 5TGM1-GFP cells were positive for CXCL12 ($P < 0.05$), Notch-1 ($P < 0.05$) and Jag-1 ($P < 0.05$) compared to the 5T33-GFP cells.

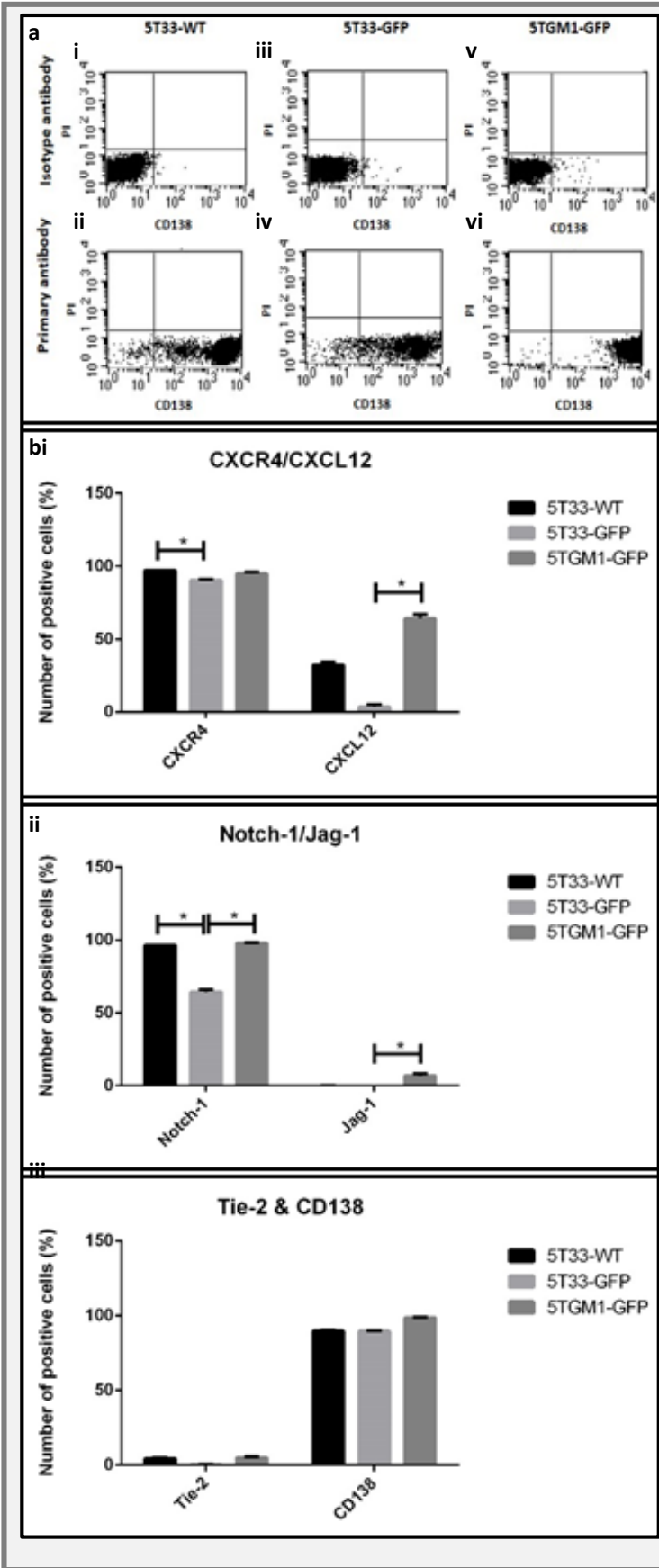


Figure 3.4: The MM cells were positive for the HSC niche molecules, some of the complementary ligands and CD138 at varying degrees using flow cytometry. 5T33-WT, 5T33-GFP and 5TGM1-GFP cells were incubated with directly conjugated primary antibodies for the HSC niche molecules CXCR4, Notch-1 and Tie-2, ligands CXCL12 and Jag-1 and, CD138 or dose matched isotype control antibodies. This was followed by flow cytometry using a FACS Calibur and Cell Quest software. **a.** An example of a representative scatter plot for CD138 using the isotype control and primary antibody by the 5T33-WT (i-ii), 5T33-GFP (iii-iv) and 5TGM1-GFP cells (v-vi). Positive staining for CD138 and negative PI staining is shown in the bottom right hand side of the quadrant. **b.** Quantitative analysis for the percentage of viable cells which were positive for CXCR4/ CXCL12 (i), Notch-1/Jag-1 (ii) and Tie-2 & CD138 (iii) by the 5T33-WT, 5T33-GFP and 5TGM1-GFP cells. Data was analysed statistically using a Kruskal-Wallis test followed by Dunn's post test ($P < 0.05$) Results were determined from three independent experiments ($N = 3$).

Table 3.3: A summary of the quantitative analysis for the percentage of myeloma cells, which were positive for the HSC niche molecules, ligands and CD138 using flow cytometry

Protein	5T33-WT	5T33-GFP	5TGM1-GFP
CXCR4	97.19 ± 0.06	90.59 ± 0.32	94.79 ± 1.41
Notch-1	96.45 ± 0.10	64.43 ± 1.68	97.91 ± 0.26
Tie-2	4.15 ± 0.67	0.34 ± 0.07	4.97 ± 0.78
CXCL12	32.19 ± 4.15	3.76 ± 1.40	64.20 ± 3.00
Jag-1	0.10 ± 0.03	0.03 ± 0.01	6.99 ± 1.18
CD138	89.56 ± 0.93	89.59 ± 0.38	98.65 ± 0.20

Mean percentage of positive cells ± SEM

As stated previously, in more recent experiments a directly conjugated N-cad antibody was used to stain the 5T33-GFP (used as a negative control due to the endpoint and real-time PCR data) and 5TGM1-GFP cells for N-cad. A dose matched isotype control was also used however; the isotype control did not have the same conjugate as the primary antibody (Dylight 650) as this was unavailable. Therefore, the results between the isotype and primary antibody are not completely comparable. Figure 3.5 demonstrates the percentages of 5T33-GFP and 5TGM1-GFP cells, which were positively stained for N-cad using increasing amounts of primary antibody. As demonstrated in the graph, there was an increase in the number of positive 5T33-GFP and 5TGM1-GFP cells as the amount of primary antibody increased and using 1.0 µg of antibody, nearly all of the 5T33-GFP and the 5TGM1-GFP cells were positively stained (98% and 96% respectively). In addition, there were no differences between the number of 5T33-GFP or 5TGM1-GFP cells, which were positive for N-cad, when the percentages were examined. As these data were contradictory to the endpoint and real-time PCR data, where 5T33-GFP cells did not show any expression of N-cad, the reliability of the antibody is questionable.

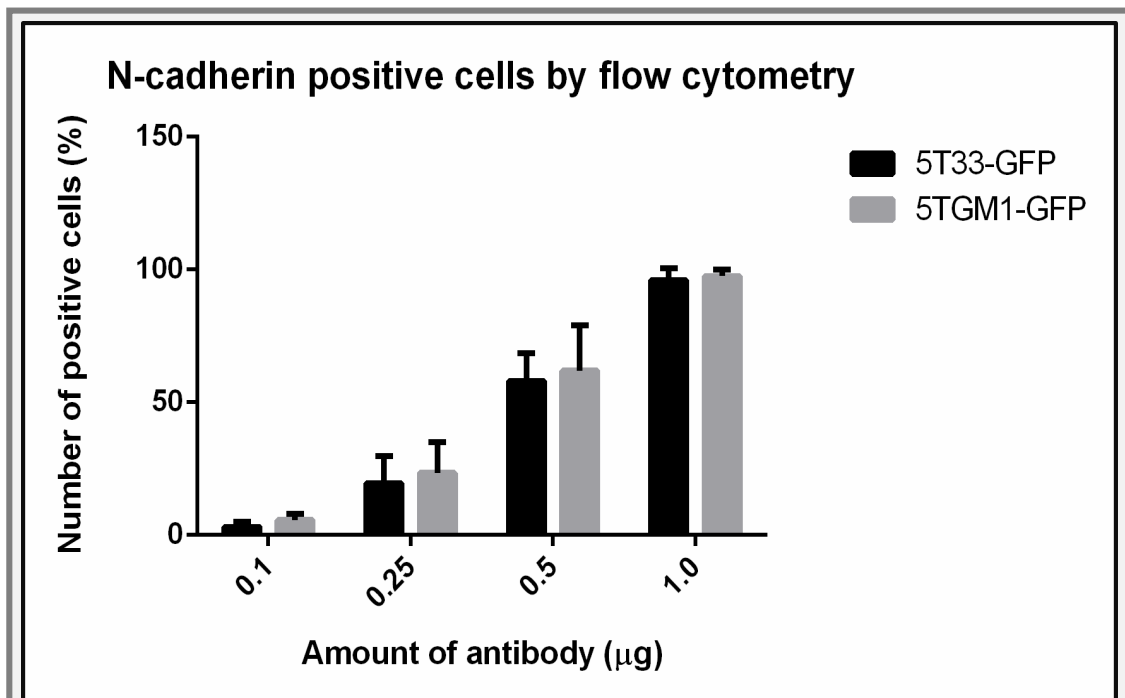


Figure 3.5: An increase in the concentration of N-cad antibody correlated with an increase in positive staining in both the 5T33-GFP and 5TGM1-GFP cells using flow cytometry. 5T33-GFP and 5TGM1-GFP cells were incubated with increasing doses of primary conjugated antibodies for N-cad or dose matched isotype control antibodies. This was followed by flow cytometry using a FACS Calibur and Cell Quest software. Quantitative analysis for the percentage of positive viable cells for N-cad by the 5T33-GFP and 5TGM1-GFP was conducted. No statistical analysis was conducted. Results were determined from three independent experiments (N=3).

3.4.4 N-cad protein detection by 5T33-GFP and 5TGM1-GFP cells using Western blotting

As the flow cytometry data for N-cad did not seem reliable due to the linear increase in positive staining as the amount of antibody increased using the 5T33-GFP and 5TGM1-GFP cells, WB was used as an alternative. This was conducted using a different unconjugated primary antibody, described in Section 2.4.4.

Figure 3.6 demonstrates the WB produced to detect N-cad in the 5T33-GFP and 5TGM1-GFP lysates. Two different ECL solutions were used, one was purchased from Thermo Scientific, as shown in Figure 3.6a and b respectively and the other was purchased from Santa Cruz Biotechnology as shown in Figure 3.6c and d. The ECL purchased from Thermo Scientific, despite a significantly shorter exposure time than the Santa Cruz Biotechnology ECL (30 seconds), over-exposed the protein bands,

particularly in the protein ladder, which made the ladder difficult to interpret. Whereas, the Santa Cruz Biotechnology ECL which needed a longer exposure time (5 min), produced clearer WBs with a distinguishable protein ladder and clear bands for β -actin and N-cad. Therefore, this ECL was the most desirable to use in future experiments.

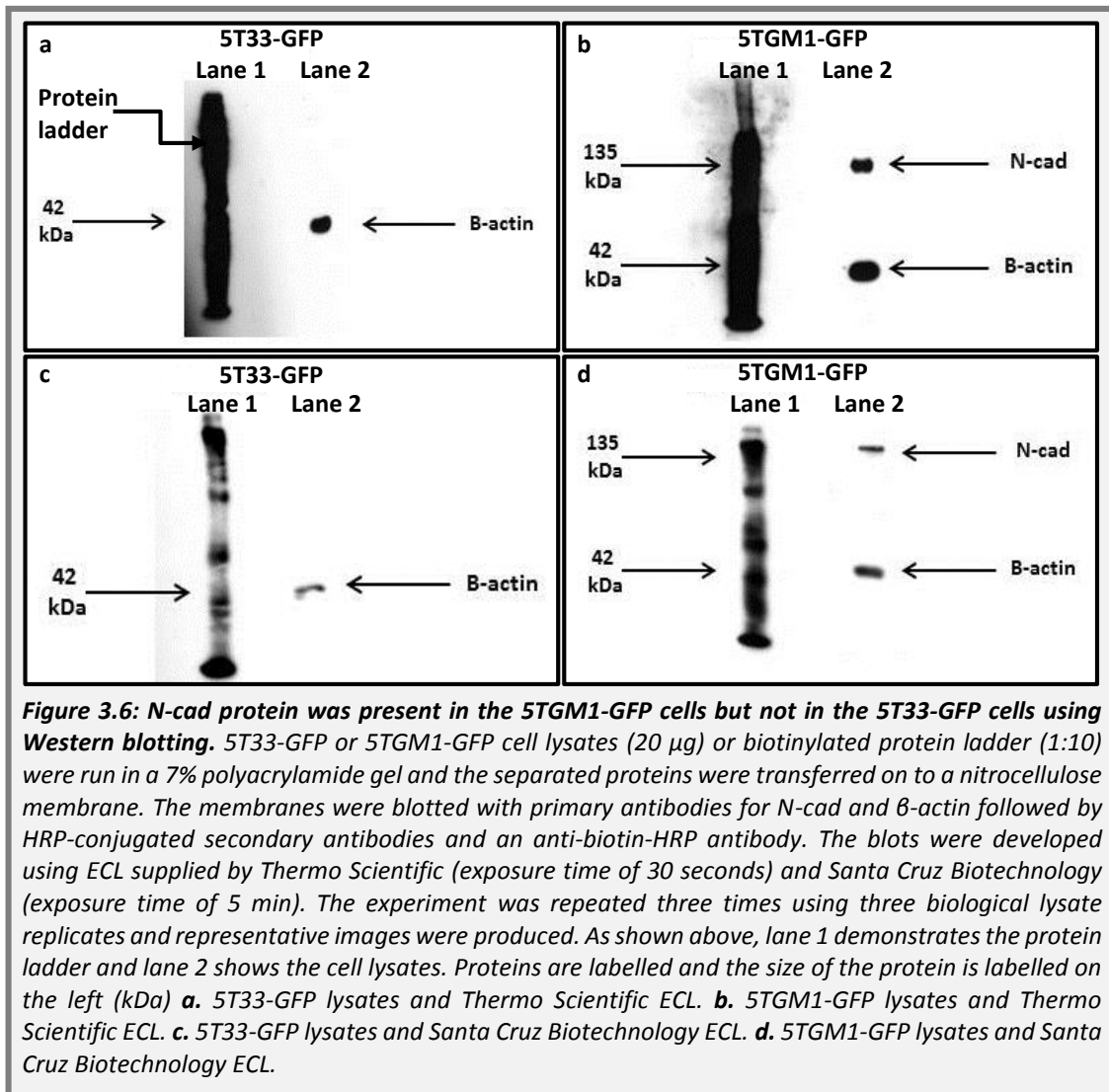
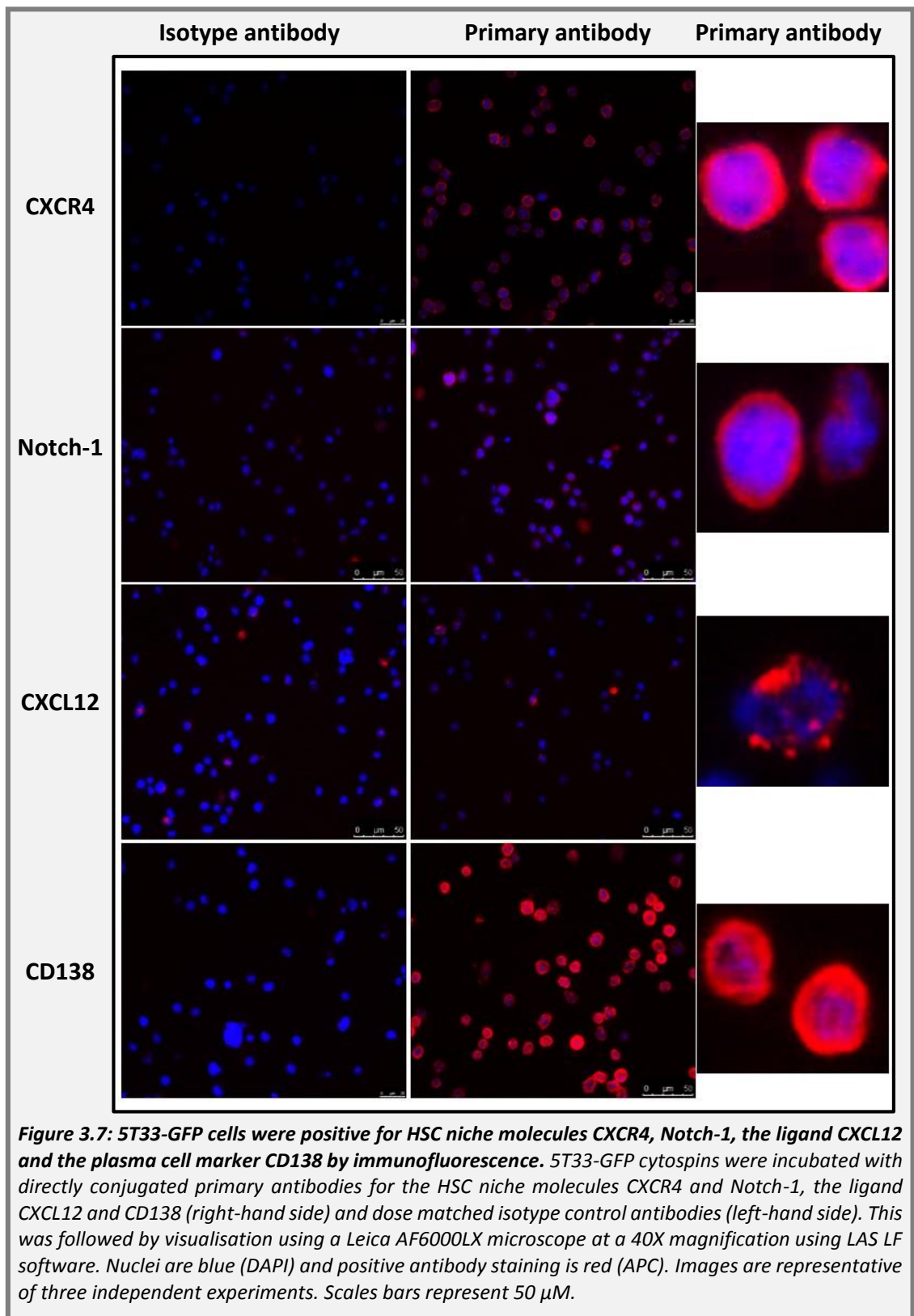


Figure 3.6 also demonstrates differences in the presence of N-cad between the 5T33-GFP (Figure 3.6a and c) and 5TGM1-GFP cells (Figure 3.6b and d). Using both the Thermo Scientific ECL and Santa Cruz ECL, clear β -actin bands were produced of the correct size for both the 5T33-GFP and 5TGM1-GFP lysates. However, there was no band for N-cad using the 5T33-GFP lysates whereas, clear bands of the correct size

were detected using the 5TGM1-GFP lysates. Therefore, this implies that N-cad protein is not present in the 5T33-GFP cells but is present in the 5TGM1-GFP cells.

3.4.5 Protein visualisation of HSC niche molecules, ligands and CD138 by 5T33-GFP and 5TGM1-GFP cells using immunofluorescence

Immunofluorescence was used to confirm the presence of protein for the HSC niche molecules, ligands and CD138 by the 5T33-GFP and 5TGM1-GFP cells as well as to visualise the protein within the cells. Figures 3.7 and 3.8 demonstrate the images taken of 5T33-GFP and 5TGM1-GFP cells respectively, stained for CXCR4, Notch-1, CXCL12 and CD138. Images of Tie-2 and Jag-1 were not shown, as primary antibody staining was not apparent in either cell type compared to the isotype control. From the images, it was clear that both cell types were positive for CXCR4, CXCL12, Notch-1 and CD138 and the positive staining appeared to locate to specific regions of the cells depending on the molecule. CXCR4 and CD138 staining was visualised on the membrane of the cells whereas Notch-1 seemed to be stained within membranous and cytoplasmic regions and CXCL12 was present inside the cell cytoplasm as discrete foci.



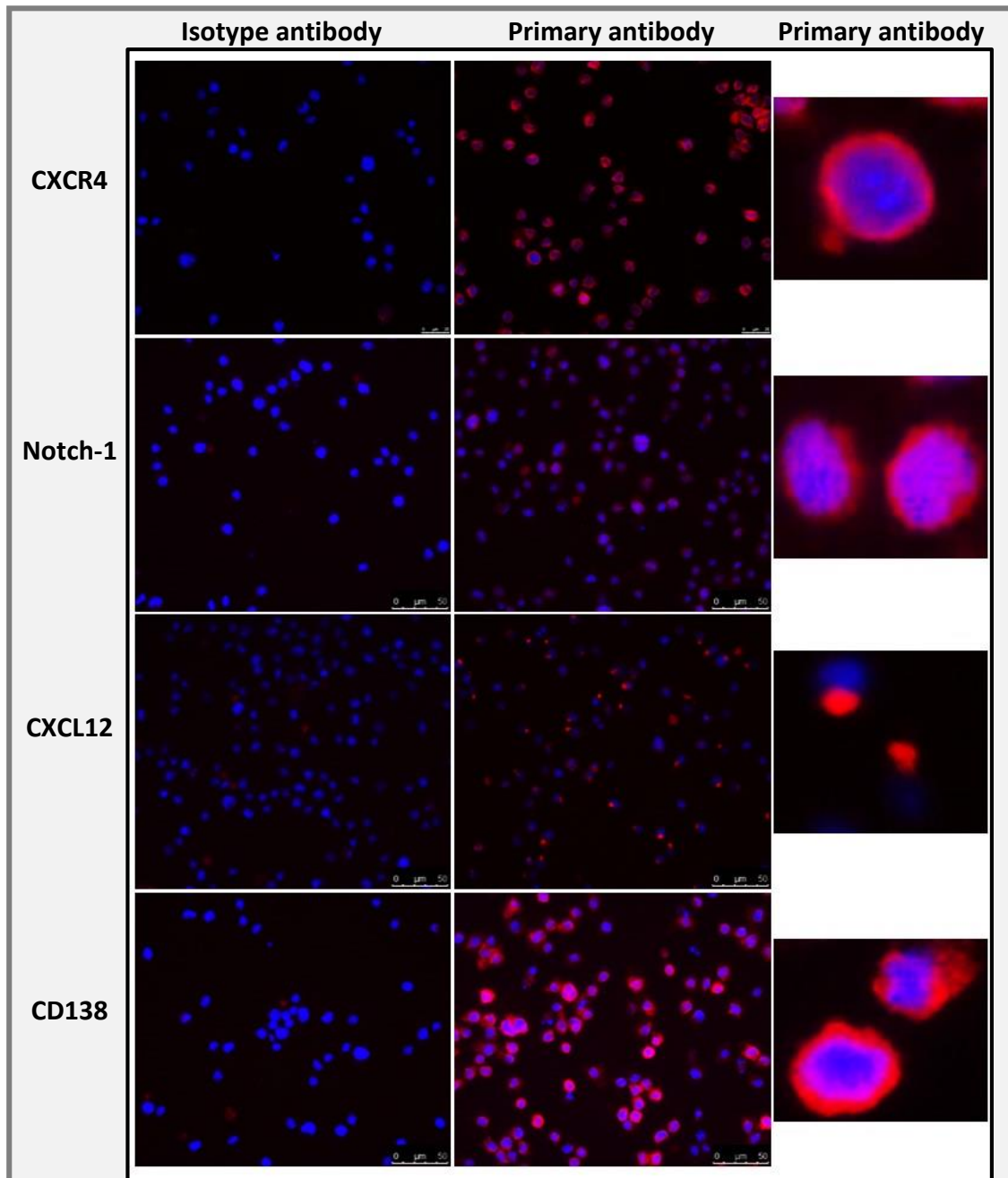


Figure 3.8: 5TGM1-GFP cells were positive for HSC niche molecules CXCR4, Notch-1, the ligand CXCL12 and the plasma cell marker CD138 by immunofluorescence. 5TGM1-GFP cytopspins were incubated with directly conjugated primary antibodies for the HSC niche molecules CXCR4 and Notch-1, the ligand CXCL12 and CD138 (right-hand side) and dose matched isotype control antibodies (left-hand side). This was followed by visualisation using a Leica AF6000LX microscope at a 40X magnification using LAS LF software. Nuclei are blue (DAPI) and positive antibody staining is red (APC). Images are representative of three independent experiments. Scales bars represent 50 μ M.

Using the images generated from IF, the percentage of 5T33-GFP and 5TGM1-GFP cells, which were positive for each molecule, was calculated, shown graphically in Figure 3.9 and summarised in Table 3.4. From the data, there were no differences between the number of cells 5T33-GFP and 5TGM1-GFP cells, which were positive

for CXCR4, Notch-1 or CD138, but a greater number of 5TGM1-GFP cells, were positive for CXCL12 compared to the 5T33-GFP cells.

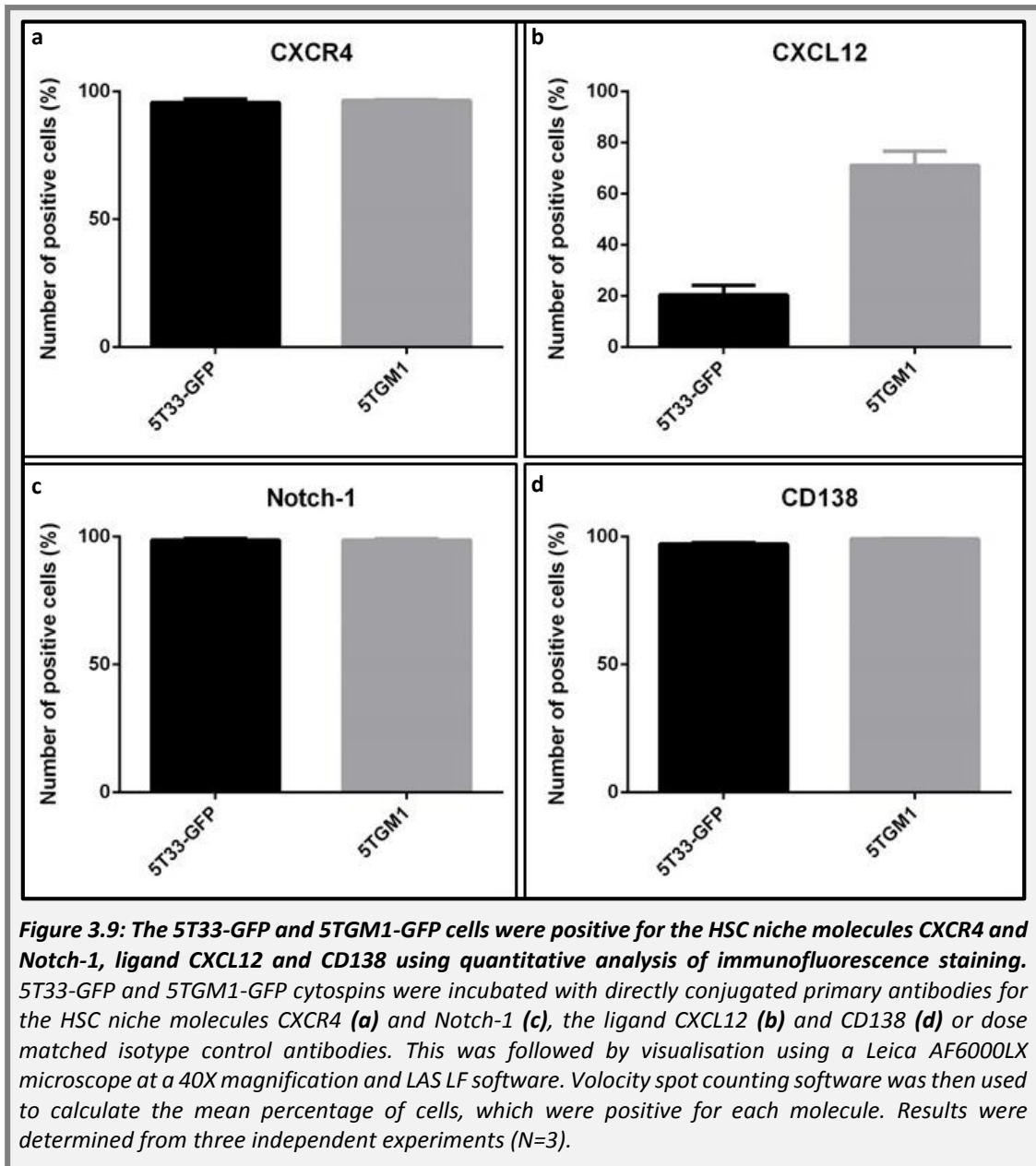


Table 3.4: A summary of the quantitative analysis for the percentage of 5T33-GFP and 5TGM1-GFP cells, which were positive for the HSC niche molecules; CXCR4 and Notch-1, ligand CXCL12, and CD138 using immunofluorescence

Protein	5T33-GFP	5TGM1-GFP
CXCR4	95.70 ± 1.21	96.33 ± 0.34
Notch-1	98.70 ± 0.89	98.67 ± 0.34
CXCL12	20.30 ± 3.78	71.00 ± 5.55
CD138	97.00 ± 0.58	99.90 ± 1.01

Mean percentage of positive cells ± SEM

3.4.6 Qualitative assessment of gene expression for the HSC niche molecules and ligands by MC3T3-E1 and primary osteoblast lineage cells using endpoint PCR

Endpoint PCR was used to determine the qualitative gene expression of the HSC niche molecules and their ligands by the murine MC3T3-E1 cells and murine primary osteoblast lineage cells (OLCs). As demonstrated in Figure 3.10, both the MC3T3-E1 cells and primary OLC samples produced bands for ligands; *CXCL12*, *Jag-1* and *Ang-1*, and HSC niche molecules; *Notch-1* and *N-cad*. In addition, the primary OLCs produced a band for *Tie-2*. Therefore, the osteoblastic cells were positive for all ligands and some of the HSC niche molecules using endpoint PCR.

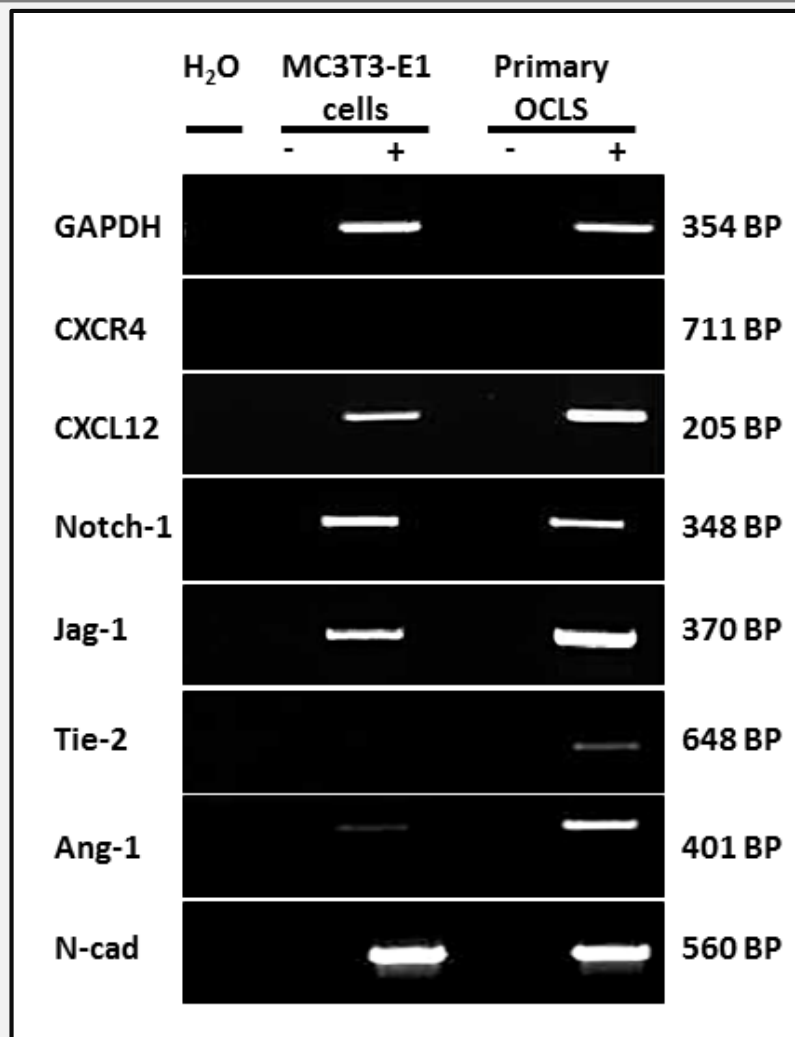


Figure 3.10: The murine osteoblastic cells expressed the complementary ligands and some of the HSC niche molecules using endpoint PCR. The endpoint PCR reactions were run using approximately 40 ng of RT+ cDNA samples. An equal volume of RT- and H₂O control samples were used to assess genomic and reagent contamination. The PCR reactions were run at 25 cycles for GAPDH and 35 cycles for the HSC niche molecules and ligands. The PCR product was separated by electrophoresis in a 1.6% agarose gel and visualised using a Bio-rad Gel Doc XR+ Imager system and Quantity One 4.6.8 software. Each row depicts an individual gel electrophoresis for GAPDH and each HSC molecule and ligand. The base pair (BP) number on the right corresponds to the size of bands visualised and band product was confirmed by in-house sequencing. Results are representative of three independent experiments.

3.4.7 Quantitative assessment of gene expression for the HSC niche molecules and ligands by MC3T3-E1 and primary osteoblast lineage cells using real-time PCR

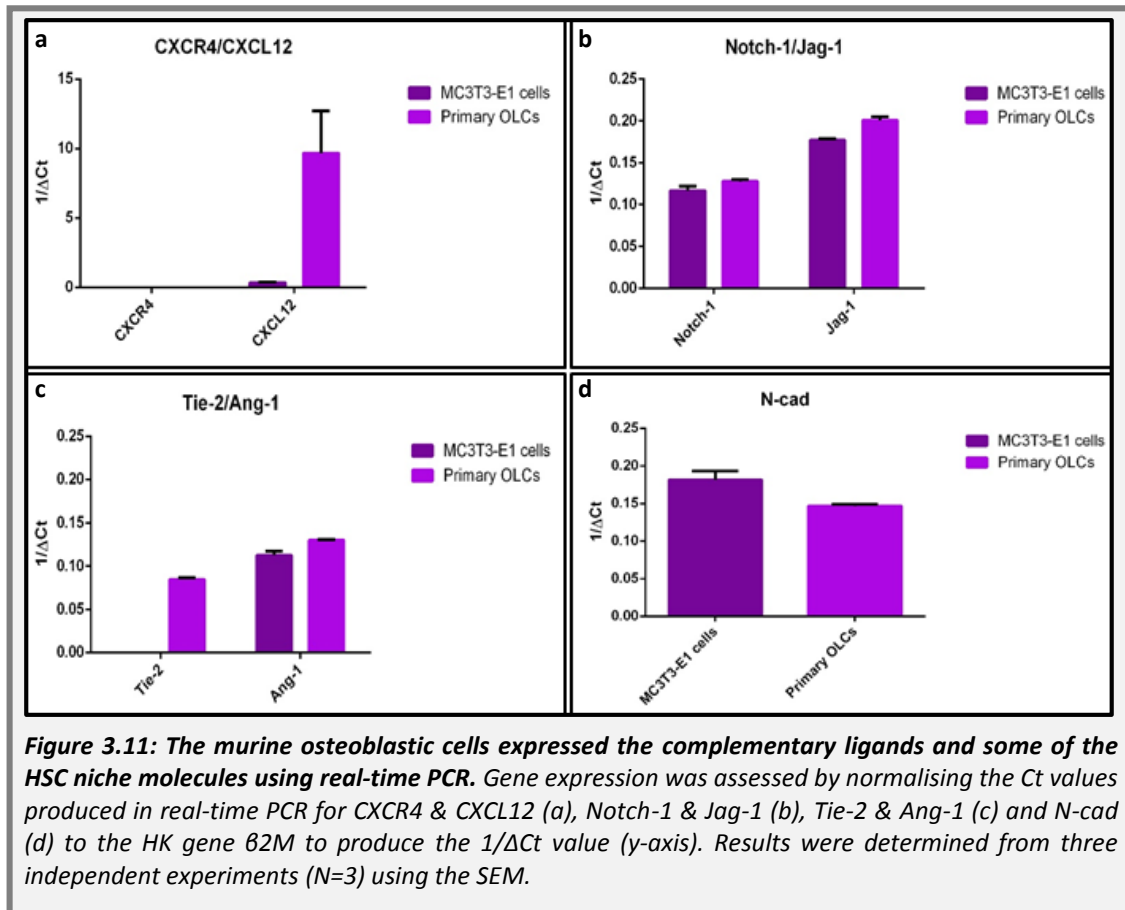
Real-time PCR was used to determine the quantitative expression of the HSC niche molecules and their ligands by MC3T3-E1 cells and OCLs. Table 3.5 demonstrates a summary of the absolute gene expression values (Ct values) and Figure 3.11 shows the 1/ Δ Ct values generated using real-time PCR.

Table 3.5: A summary of the absolute gene expression for the HSC niche molecules and ligands by MC3T3-E1 cells and primary osteoblast lineage cells using real-time PCR

Gene	MC3T3-E1	Primary OLCs
<i>β2M</i>	19 ± 0.94	17 ± 0.12
<i>HPRT</i>	25 ± 0.90	23 ± 0.08
<i>CXCR4</i>	UD	UD
<i>Notch-1</i>	28 ± 1.26	25 ± 0.34
<i>Tie-2</i>	UD	29 ± 0.37
<i>N-cad</i>	24 ± 1.28	23 ± 0.16
<i>CXCL12</i>	22 ± 1.18	17 ± 0.21
<i>Jag-1</i>	25 ± 0.98	22 ± 0.13
<i>Ang-1</i>	28 ± 1.31	25 ± 0.16

Mean Ct values ± SEM UD= Undetermined, Ct value > 35.

Both cell types expressed the HK genes *β2M* and *HPRT* as well as the ligands *CXCL12*, *Jag-1* and *Ang-1*. In addition, they both expressed the HSC niche molecules *Notch-1* and *N-cad*. The primary OLCs, also expressed *Tie-2*, whereas this was absent in the MC3T3-E1 cells. Both cell types did not express *CXCR4*. It is clear from these data that the primary OLCs expressed *CXCL12* at a greater level than the MC3T3-E1 cells and also had slightly higher expression of *Notch-1*, *Jag-1*, *Tie-2* and *Ang-1*, whereas, *N-cad* was more highly expressed in the MC3T3-E1 cells, however, statistical analysis was unable to be conducted.



3.4.8 Protein quantification of the HSC niche molecules and ligands by MC3T3-E1 and primary osteoblast lineage cells using flow cytometry

Flow cytometry was used to determine the number of MC3T3-E1 cells and primary OLCs, which were positive for the HSC niche molecules and their ligands. Figure 3.12a demonstrates an example of the flow cytometry plots produced for the staining of Jag-1 and the viability dye TO-PRO-3 using the MC3T3-E1 cells and primary OLCs. The mean percentage of cells, which were positive for each HSC niche molecule and ligand, are shown in Figure 3.12b. A summary of the percentages of cells which were positive for the HSC niche molecules and ligands is shown in Table 3.6. The MC3T3-E1 cells and primary OLCs were positive for the ligands CXCL12 and Jag-1 and the HSC molecule Notch-1 and neither cell type was positive for Tie-2. A slightly higher number of primary OLCs were positive for CXCL12 compared to the MC3T3-E1 cells, whereas, a greater number of MC3T3-E1 cells were positive for Notch-1 and Jag-1

compared to the primary OLCs, where the difference was particularly obvious for Jag-1, however, statistical analysis was unable to be conducted.

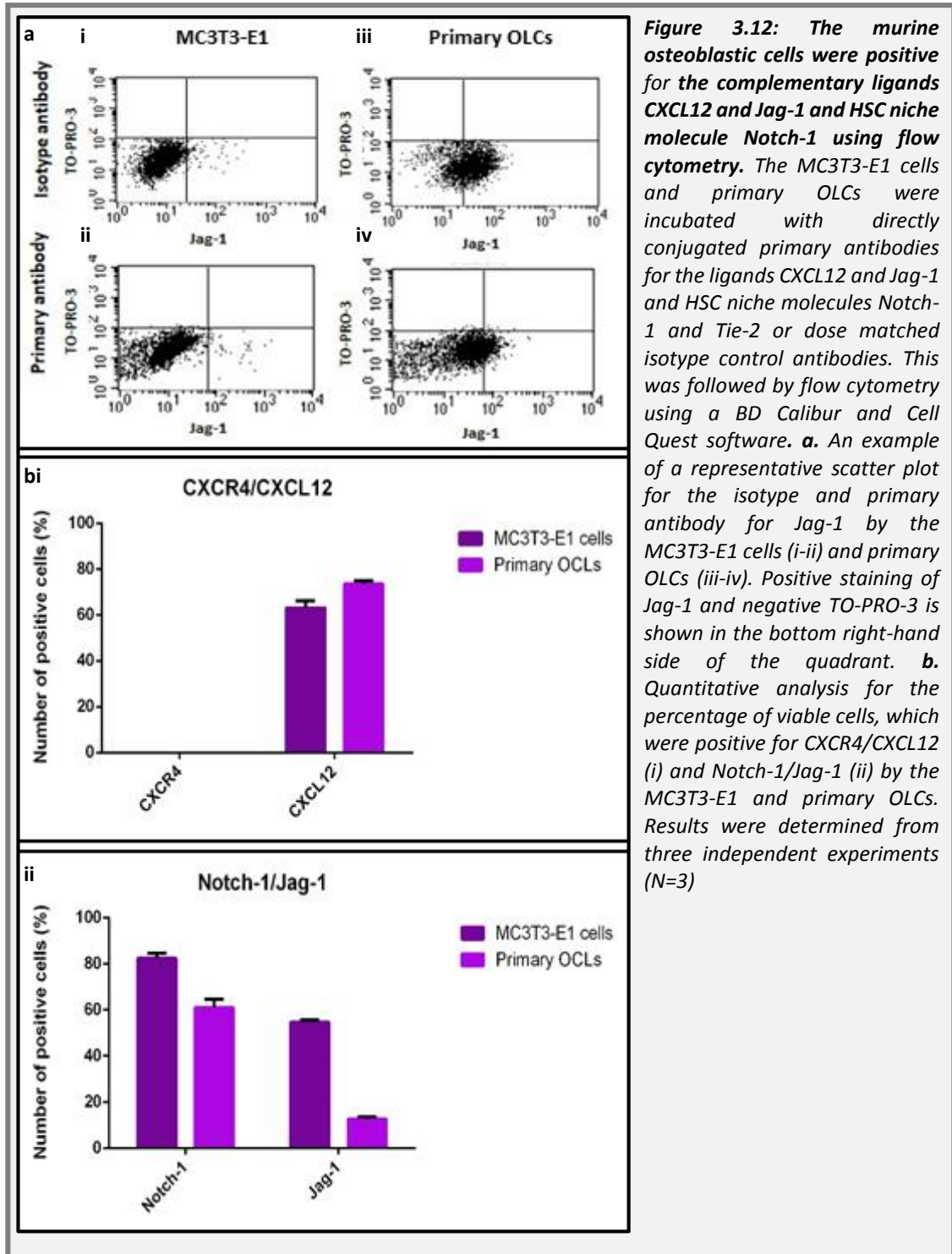


Table 3.6: A summary of the quantitative analysis for the percentage of MC3T3-E1 cells and primary osteoblast lineage cells, which were positive for the HSC niche molecules and ligands using flow cytometry.

Protein	MC3T3-E1	Primary OLCs
CXCL12	63.10 ± 3.10	75.53 ± 1.37
Jag-1	54.70 ± 0.95	12.63 ± 1.01
Notch-1	82.48 ± 0.75	61.03 ± 6.64
Tie-2	0.00 ± 0.00	0.00 ± 0.00

Mean percentage of positive cells ± SEM.

3.5 Discussion

The aim of this chapter was to determine whether the HSC niche molecules CXCR4, Notch-1, Tie-2 and N-cad were expressed by the 5T33MMvt and 5TGM1-GFP cell lines, and to determine the expression of their complementary ligands CXCL12, Jag-1, Ang-1 and N-cad by the MC3T3-E1 cells and murine primary OLCs *in vitro*.

Firstly, murine BM cDNA was used in PCR experiments, and murine BM, splenocytes and blood cells were used for flow cytometry as positive controls to ensure that the PCR and flow cytometry reagents and protocols were working effectively. The expression of each HSC niche molecule and ligand by the murine BM was demonstrated in my studies, using each methodology. However, when comparing the BM PCR and flow cytometry data, the number of positive cells did not correlate with the gene expression. For example there was high expression of *CXCL12* and *Notch-1* using PCR, whereas the number of cells positive for *CXCL12* and *Notch-1* was below 12% and 3% respectively using flow cytometry. This difference may potentially be due to the preparation of the samples i.e. the RBCs were lysed in the flow cytometry samples whereas the entire BM population was used for RNA extraction, or it may also be due to inefficiency of the antibodies. It is also possible that high transcript levels of *CXCL12* and *Notch-1* are present in the BM samples but only in particular sub-populations of cells. Therefore, this may account for high levels of

expression in the PCR but low numbers of positive cells using flow cytometry, as flow cytometry did not account for the level of protein present, only the number of positive cells.

A further explanation to account for differences in gene expression and presence of protein which has been highly explored in the literature, is that there is only a weak correlation between the levels of mRNA and protein within mammalian cells (209). Messenger RNA to protein studies were conducted using cells derived from a variety of different organisms including mouse, yeast and bacteria using specialised mRNA and protein quantification techniques. Results were analysed using both the Spearman rank coefficient and Pearson correlation coefficient statistical tests to compare mRNA and protein levels at one time by hundreds of genes and corresponding proteins. On average, a coefficient correlation value of 0.57 was established which illustrated a correlation of 57% between mRNA and protein levels in the different cell types (210). Therefore, mRNA and protein values were not directly correlated. Several factors have been implicated in this finding which included varying rates of mRNA synthesis and protein production, stability of the mRNA and protein, in addition to the state of mRNA synthesis (210). Previous studies found that mRNA was synthesised at a slower rate compared to proteins i.e. cells were found to produce two copies of mRNA per hour compared to a dozen copies of the corresponding protein (210). In one study, median translation rate was approximately 140 proteins per mRNA per hour however, this varied depending on the function of the proteins of interest; for example, proteins involved in translation regulation had much slower rates of translation (211). In addition, mRNA degrades quicker than proteins with a median half-life of 9 hours compared to proteins which are five times more stable with a median half-life of 46 hours (211). Housekeeping genes and small proteins were also found to be more stable (211), whereas genes and proteins for transcription factors and chromatic organisation were significantly less stable (211). In addition, the state of mRNA production when analysed influenced protein production. For example, if the cells were producing mRNA for a

particular protein at a steady state, the variability of protein production was high, whereas if the mRNA was synthesised at varying rates the corresponding protein output correlated well (212). These concepts provide an insight as to why differences in mRNA and protein expression occur. However, the general concept implies that mRNA production may be slower and prone to degradation and therefore, this does not provide a theory as to why the CXCL12 and Notch-1 mRNA expression by the BM was higher compared to the level of protein. However, as stated above, the rates of mRNA synthesis and translation may be gene and protein specific and highly variable.

Polymerase chain reaction, flow cytometry and IF were also used to determine the gene expression and presence of protein for the HSC molecules, ligands and CD138 in the MCs. Taken together, using both gene and protein methodologies, the MCs expressed all HSC niche molecules as well as the ligands CXCL12, Ang-1 and Jag-1. However, similar to the BM analysis, there were some discrepancies between the gene expression and presence of protein in the MCs using both PCR and flow cytometry. There were no bands present for *Tie-2*, *CXCL12*, *Ang-1* or *Jag-1* by endpoint PCR in any of the MCs and only marginal expression of *CXCL12*, *Tie-2* and *Ang-1* (which varied depending on the cell type) and UD expression of *Jag-1* in all MCs, by real-time PCR. Whereas, using flow cytometry, a high proportion of 5TGM1-GFP cells (64%) and a lower number of 5T33-WT and 5T33-GFP cells (32% and 4%, respectively) were positive for CXCL12, Tie-2 was present at a low frequency only in the 5T33-WT and 5TGM1-GFP cells (4-5%), and Jag-1 was present only in the 5TGM1-GFP cells (7%). The 5T33-GFP and 5TGM1-GFP cells were also positive for CXCL12 using IF, where staining seemed to exist as discrete foci and there was no staining of Jag-1 or Tie-2 in the 5T33-GFP cells and 5TGM1-GFP cells. Again, the positive CXCL12, Jag-1 and Tie-2 staining in the flow cytometry and/or IF may be due to non-specific binding of the antibodies and WB could be used to determine the specificity. Low expression of CXCL12 and Tie-2, and UD expression of Jag-1 by the MCs using endpoint and real-time PCR could also be due to the inefficiency of the primers and probes used. However, the primers for endpoint PCR worked successfully using the

BM cDNA and the efficiency of the CXCL12 and Jag-1 probes were within the normal range as shown in Appendix 2, Section 2.5. The difference in gene expression and presence of protein may also be due to differences in mRNA and protein production rates as stated above, which may account for lower mRNA levels of CXCL12, Tie-2 and Jag-1 compared to protein. In addition, sub-populations of cells could also be responsible. A small sub-population of MCs may express high levels of the molecules Tie-2 and Jag-1 however, because there are only low numbers of positive cells these are undetectable using real-time PCR.

Another theory with regards to CXCL12 and the conflicting results between gene expression and presence of protein in the MCs, is that CXCL12 is internalised from the FBS in the media that the MCs are cultured in, resulting in false positives using flow cytometry and IF. In support of this, Hatse *et al* (213), reported that CXCL12 was internalised in bovine endothelial cells and in the T lymphoblastic cell line SupT1, visualised by flow cytometry using a fluorescent recombinant CXCL12 protein. However, further work is required to test this hypothesis in MCs.

There were also some differences in the expression of some of the molecules and ligands between the MCs using real-time PCR, flow cytometry and IF. Differences between the cell types was particularly apparent with regards to N-cad using real-time PCR, CXCL12, Notch-1 and Jag-1 using flow cytometry and CXCL12 using IF. The differences observed between the MCs maybe caused by several factors. Firstly, differences between the 5T33-WT and GFP cells may be due to the selection process after the GFP had been transduced into the 5T33MMvt cells (the process for this is unknown as the cells were transduced outside of the University) or their characteristics may have changed due to *in vitro* cell culture. The 5TGM1-GFP cell line, which was derived from the 5T33MMvt cells, demonstrates different characteristics *in vivo*, such as bone lesions; therefore, it may be unsurprising that the expression of some of the molecules differs *in vitro*.

Flow cytometry was also used to detect the number of N-cad positive 5T33-GFP and 5TGM1-GFP cells. However, due to nonspecific binding of the primary antibody and unsuitable isotype control antibody, WB was used as an alternative. Western blotting was originally conducted using two different types of ECL. The ECL purchased from Thermo Scientific resulted in over-exposed bands despite less exposure time, whereas ECL purchased from Santa Cruz Biotechnology demonstrated more optimum band density despite a longer exposure time. Using both types of ECL, the 5T33-GFP lysates did not produce a band for N-cad whereas the 5TGM1-GFP lysates produced a band of the correct size. Therefore, these data correlated with the real-time PCR results where N-cad was not expressed in the 5T33-GFP cells but was detected in the 5TGM1-GFP cells. Western blotting is in some ways more advantageous than flow cytometry, because in addition to detecting the presence of protein it can also provide evidence for the specificity of the antibody. However, one of its limitations is that it is unable to provide a percentage of cells, which are positive for the protein of interest (POI). Therefore, from these studies it implies that N-cad is present in the 5TGM1-GFP cells but the percentage of positive cells is unknown.

Taken together, the PCR, flow cytometry and IF data demonstrated that the HSC niche molecules were expressed by or present on the 5T33-WT, 5T33-GFP and 5TGM1-GFP cells. These data are supported by previous studies, which have determined the expression of some of these molecules by MCs *in vitro*. CXCR4 expression was previously determined by the 5T2MM and 5T33MMvt cells (170) and various human MCs (193-195) *in vitro*. Notch-1 was expressed by human MC lines and patient cells (198, 199, 214) and Tie-2 was expressed by the XG-1 cell line *in vitro* (201). N-cad was also expressed by several different human cell lines as well as patient cells (205-207). The MCs were also potentially positive for the ligands CXCL12, Jag-1 and Ang-1. CXCL12 expression was previously shown in MCs such as ARH-77, WL2, JIMI, LP-1, NCI-H929 and RPMI-8266 cells using real-time PCR and in human MM cells using IHC (215). However, as stated previously it is uncertain whether the MCs in these studies are producing CXCL12 themselves or whether they are

internalising it from the FBS present in the media. Jag-1 protein expression has previously been demonstrated in primary patient MC samples (198, 214) and Ang-1 expression has also previously been shown in myeloma cell lines including RPMI-8226, U266, OPM-2, XG-1, and XG-6 as well as patient samples (201).

Endpoint and real-time PCR and flow cytometry demonstrated the expression of the ligands CXCL12, Jag-1, Ang-1 and N-cad and the receptor Notch-1 by both the MC3T3-E1 and primary OLCs, whereas Tie-2 was only expressed by the primary OLCs. However, some of the findings between gene expression and presence of protein did not entirely correlate. The real-time PCR results implied greater expression of all ligands with the exception of *N-cad* by the primary OLCs compared to the MC3T3-E1 cells (though these were not compared statistically). Whereas, using flow cytometry, the number of Notch-1 and Jag-1 positive cells were higher in the MC3T3-E1 cells compared to the primary OLCs, and Tie-2 staining was absent by flow cytometry in the primary OLCs, contradictory to the real-time PCR data. In addition, the difference in CXCL12 expression between the MC3T3-E1 cells and primary OLCs was obvious using real-time PCR however, by flow cytometry they differed only by 10 %. Again, inconsistencies between the gene expression and presence of protein may be due to differences in transcription and translation rates or the specificity of the PCR and flow cytometry reactions. The flow cytometry protocol may be particularly responsible for the contrasting results for Jag-1 and Tie-2. These are both membrane-bound proteins, and despite cautious efforts to retain its presence through careful dissociation of the cells from their flasks, the molecules may have been cleaved. This therefore may have resulted in the absence of Tie-2 and low Jag-1 positive cells in the primary OLCs using flow cytometry. In addition, flow cytometry only accounted for the number of cells, which were positive for each molecule, not the number of proteins present on a per cell basis therefore, this could result in differences between real-time PCR and flow cytometry.

The overall expression of the HSC niche molecules and ligands by osteoblastic cells are however, supported by the literature. Jag-1 expression has been detected in MC3T3-E1 cells (200, 216), BM stromal cells (199), C3H10T1/2 and C2C12 cell lines, murine primary osteoblastic cells (216) and osteoblasts in mice *in vivo* (82). Notch-1 expression has previously been identified in MC3T3-E1 cells (200, 216), C3H10T1/2 and C2C12 cell lines and murine primary osteoblastic cells (216). CXCL12 was expressed in MC3T3-E1 cells, human osteoblastic cells, stromal cells, MG63 cells (196) and by MSCs (217). Tie-2 is generally perceived as an endothelial marker however, Jeong *et al* (202) determined its expression in MC3T3-E1 cells, murine primary osteoblastic cells, C2C12 cells, C3H10T1/2 cells and ST-stromal cells. Ang-1 expression has previously been identified in murine primary osteoblastic cells, ST-stromal cells, C2C12 cells and C3H10T1/2 cells (202). N-cad expression has previously been identified in MC3T3-E1 cells, C3H10T1/2, ST-stromal cells, ATDC5 chondrogenic cells, NIH3T3 fibroblastic cells (218), KS483 osteoblastic cells (206), SAOS-2 cells (219) and by both oval and spindle shaped osteoblasts *in vivo* (83).

In conclusion, these data support the hypothesis that MCs express and produce the same repertoire of molecules as HSCs, which include CXCR4, Notch-1, Tie-2 and N-cad and that their complementary ligands; CXCL12, Jag-1, Ang-1 and N-cad are expressed by osteoblastic cells *in vitro*. However, their role within a MC niche is still unknown and therefore, further research is required to explore this.

**Chapter IV: The *ex vivo* and *in vivo* expression of HSC
niche molecules and their ligands by murine myeloma
cells**

4.1 Introduction

As discussed previously, it has been suggested that MCs may home to a BM microenvironmental niche similar to that occupied by HSCs. To achieve this it was hypothesised that MCs express the same repertoire of HSC niche molecules, which anchor MCs to the niche and induce MC dormancy.

Chapter III explored the expression and presence of the HSC niche molecules and complementary ligands in murine MCs (5T33-WT, 5T33-GFP and 5TGM1-GFP) and osteoblastic cells (MC3T3-E1 and primary OLCs) cultured *in vitro*. However, the expression of these molecules was not determined *ex vivo* or *in vivo*. It remains unknown whether the MCs express/utilise the same HSC niche molecules once injected into mice and also whether these molecules play a role in the homing, growth and subsequent survival of the MCs within the BM *in vivo*.

Previous studies have determined the expression of some of the HSC niche molecules and their ligands in MCs isolated from BM or peripheral blood of mice or patients analysed *ex vivo* or *in vivo* using BM sections.

Van de Broek *et al* (220) demonstrated that 59% of MM patients had CXCR4 positive BM MCs, when analysed *ex vivo* and this is supported by a separate study which found that 5/5 myeloma patient samples were positive for CXCR4 when isolated and analysed in a similar way (221). In addition, Alsayed *et al* (195) reported that both BM and peripheral blood MCs from MGUS and MM patients were positive for CXCR4 using flow cytometry, analysed *ex vivo*.

CXCL12 expression was detected in human BM cells isolated from healthy donors and specifically in sorted mononuclear cell fractions, analysed *ex vivo* (193). CXCL12 protein was also detected in human bone by immature osteoblastic cells lining the endosteum and stromal cells in the marrow space *in vivo* using IHC (111). In addition, the presence of CXCL12 was significantly higher in BM samples isolated from patients with MM compared to healthy controls and there were significantly higher levels of CXCL12 in the BM compared to samples from the peripheral blood (195).

Previous studies have also demonstrated the expression of Notch-1 and Jag-1 by MCs and osteoblastic cells *ex vivo* and *in vivo*. Patient MCs were isolated from BM samples by CD38^{high}/CD19^{low} flow cytometry sorting and were cytopspun on to slides followed by IHC staining for both Notch-1 and CD138. CD138 staining was observed on the membrane of the cells, whereas Notch-1 staining was cytoplasmic (198). The presence of Notch-1 protein in MCs was also visualised *in vivo* on BM trephines using IHC where 72 out of 78 (92.31%) MM patient samples were positive for Notch-1 (214). Jag-1, the ligand for Notch-1 was expressed by human BM stromal cells isolated from healthy donors and analysed by WB (199). Jag-1 staining was also present on osteopontin (Opn) positive osteoblasts situated on trabecular bone surfaces on histological slides using IHC (82).

As stated in Chapter III, there is little evidence in support of Tie-2 expression by MCs. However, Tie-2 expression was found in 4 out of 23 BM MC patient samples, determined by RT-PCR. In addition, 11 out of 22 samples also expressed Ang-1. Furthermore, stromal cells isolated from the BM of myeloma patients were positive for both Ang-1 and Tie-2 (201). In addition, the presence of Ang-1 protein was also detected by murine osteocalcin (Ocn) positive osteoblasts lining trabecular bone on histological slides *in vivo* (85).

N-cad expression has previously been observed in BM patient MCs as well as patient serum (205). N-cad was also implicated as a marker of prognosis, where patients with high circulating N-cad were found to have a poorer prognosis and a greater risk of death compared to those with low levels. In addition, N-cad protein was present in both spindle and oval-shaped osteoblasts *in vivo* (83) and by human primary OLCs isolated from trabecular bone chips using Northern blotting (152).

Taken together, these studies provide evidence that the HSC niche molecules CXCR4, Notch-1, Tie-2 and N-cad are expressed by patient MCs isolated from the BM or circulation and analysed *ex vivo*, as well as being present on patient MCs analysed *in vivo*. In addition, their complementary ligands CXCL12, Jag-1, Ang-1 and N-cad are expressed by osteoblastic cells isolated from patient BM and analysed *ex vivo* as well as osteoblastic cells *in vivo*.

While the above provides some evidence for the expression and activities of HSC niche molecules and ligands by both human and murine MCs, there is also little or no data, which systematically determines the expression or function of these molecules in the 5T33-GFP and 5TGM1-GFP models of myeloma either analysed *ex vivo* or *in vivo*.

In this chapter, I have determined the presence of protein for CXCR4, Notch-1, Tie-2 and N-cad in BM derived 5T33-GFP cells as well as BM and spleen derived 5TGM1-GFP cells analysed *ex vivo* using flow cytometry. In addition, I have also mapped the growth of the 5TGM1-GFP cells and the presence of the HSC niche molecules and ligands over-time *in vivo*.

4.2 Hypothesis, aims and objectives

4.2.1. Hypothesis and aims

The aim of these studies was to test the hypothesis that “Myeloma cells express the same repertoire of molecules as HSCs when analysed *ex vivo* and *in vivo*.”

4.2.2 Objectives

The hypothesis will be tested by the following objectives:

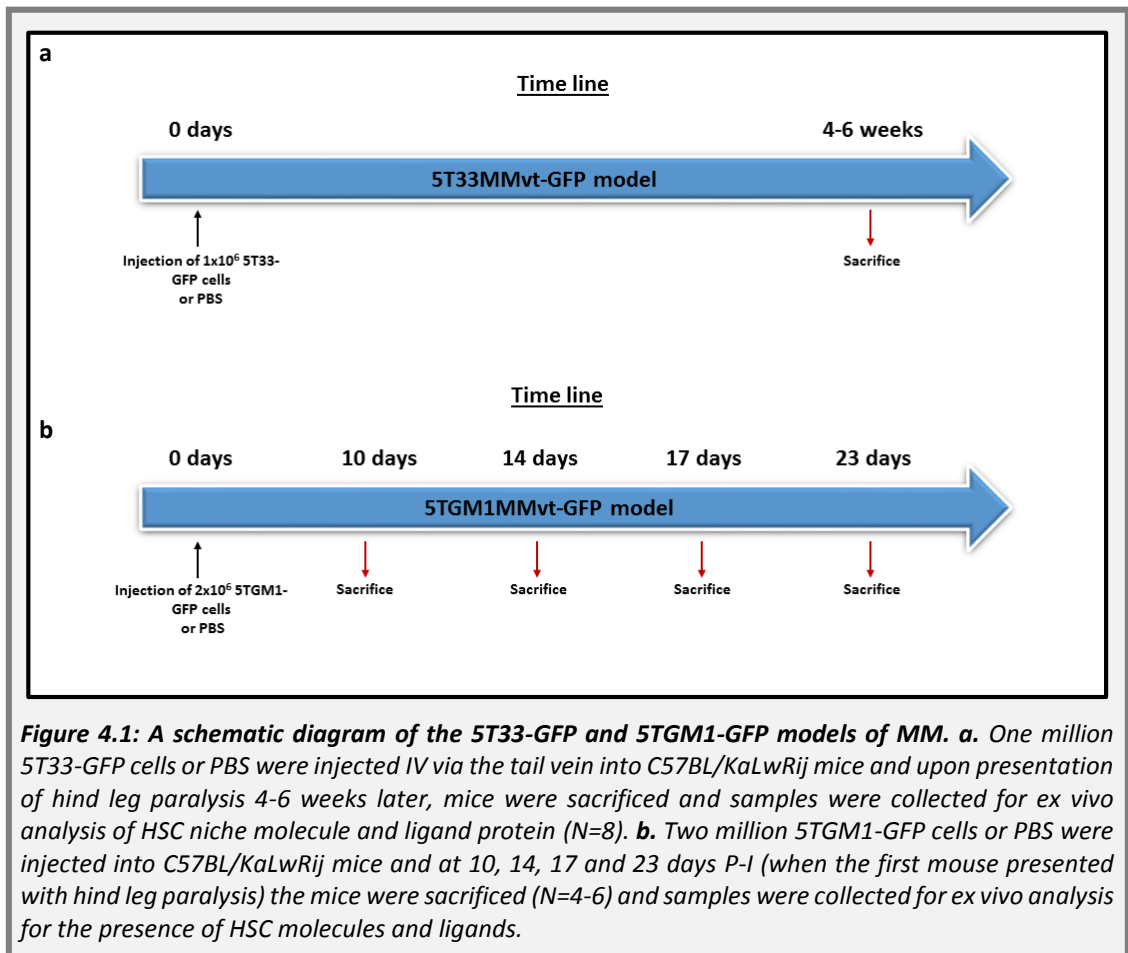
1. To determine the presence of protein for the HSC niche molecules; CXCR4, Notch-1 and Tie-2, complementary ligands; CXCL12 and Jag-1, and CD138 in the BM derived 5T33-GFP cells as well as BM and spleen derived 5TGM1-GFP cell lines analysed *ex vivo* using flow cytometry.
2. To determine the presence of CXCR4 and N-cad protein as well as CD138 by the 5TGM1-GFP cell lines grown *in vivo* over-time using IHC.

4.3 Methods

4.3.1 Murine models of multiple myeloma

The 5T33-GFP and the 5TGM1-GFP murine models of MM were used to determine the presence of protein in BM and spleen derived HSC niche molecules and ligands. The individual characteristics of each murine myeloma model are described in Chapter I Section 1.5 and the experimental design for these studies are shown below in Figure 4.1. The study design for the 5T33-GFP model of MM is shown in Figure 4.1a. Due to the variability of the tumour in this particular model, mice were sacrificed individually when they became ill and a control PBS treated mouse was sacrificed at the same time. The longitudinal study design for the 5TGM1-GFP model

of MM is shown in Figure 4.1b. At the final time point (23 days P-I) all mice were sacrificed at the same time rather than individually because the 5TGM1-GFP model was intrinsically less variable than the 5T33-GFP model.



4.3.2 Protein analysis of bone marrow and spleen derived myeloma cells, analysed *ex vivo*

4.3.2.1 Flow cytometry

Murine BM was isolated from the 5T33-GFP, 5TGM1-GFP and PBS injected mice, as described previously in Chapter II Section 2.2.1.4. In addition, splenocytes were also isolated from the mice injected with the 5TGM1-GFP cells and complementary PBS controls, as mice in the 5TGM1-GFP model develop splenomegaly due to infiltration of tumour cells at this site of haematopoiesis. The spleen was also analysed to

determine any differences in the presence HSC niche molecules and ligands between BM and spleen derived cells. The presence of these molecules on either of the cell types may highlight which molecules may or may not be important for tumour growth specifically in the BM. These samples were isolated as previously described in Chapter II Section 2.2.1.4.

Tumour burden was assessed using GFP expression as a marker for the percentage of MCs in each BM and spleen sample. The samples were also stained with the optimised quantity of antibody for the HSC niche molecules, ligands and CD138 as described in Chapter II Section 2.4.1.2. The number of GFP positive MCs, which were also positive for the HSC niche molecules and ligands, were measured using a FACS Calibur. Cell Quest software was used to analyse the data by gating against the negative isotype control antibodies, (which demonstrated less than 1% positive staining) to produce a percentage of cells, which were positive for each molecule. Each mouse was classed as a biological replicate to produce a mean percentage of cells, which were positive for each HSC niche molecule and ligand.

4.3.3 Protein analysis of bone marrow derived myeloma cells, analysed *in vivo*

4.3.3.1 IHC

Immunohistochemistry was conducted to visualise positive staining of the HSC niche molecules in the BM cells and MCs *in vivo*. C57BL/KaLwRij mice were injected with either 2×10^6 5TGM1-GFP cells or PBS IV and at 0, 3, 7, 10, 14, 17 and 21 days P-I (N=3-4 per group) mice were sacrificed as described previously. The hind limbs were dissected and then processed for histology, as described in Chapter II Section 2.4.3.2. Wax embedded sections from the 10-21 day time points were stained with anti-CXCR4, anti-N-cad or anti-CD138 antibodies or complementary isotypes to each primary antibody. Images of the staining were taken using an Aperio Scan Scope slide scanner and visualised using Image Scope software. These time points were used, as clear MC colonies were visible by eye.

CD138 staining by IHC was also analysed by Dr Shelly Lawson (*Department of Oncology, The University of Sheffield*) using Osteomeasure Software. The number of single cells, colony number and area were calculated after 0, 3, 7, 10, 14, 17 and 21 days P-I of 5TGM1-GFP cells (N=3-4 per group).

4.3.4 Statistics

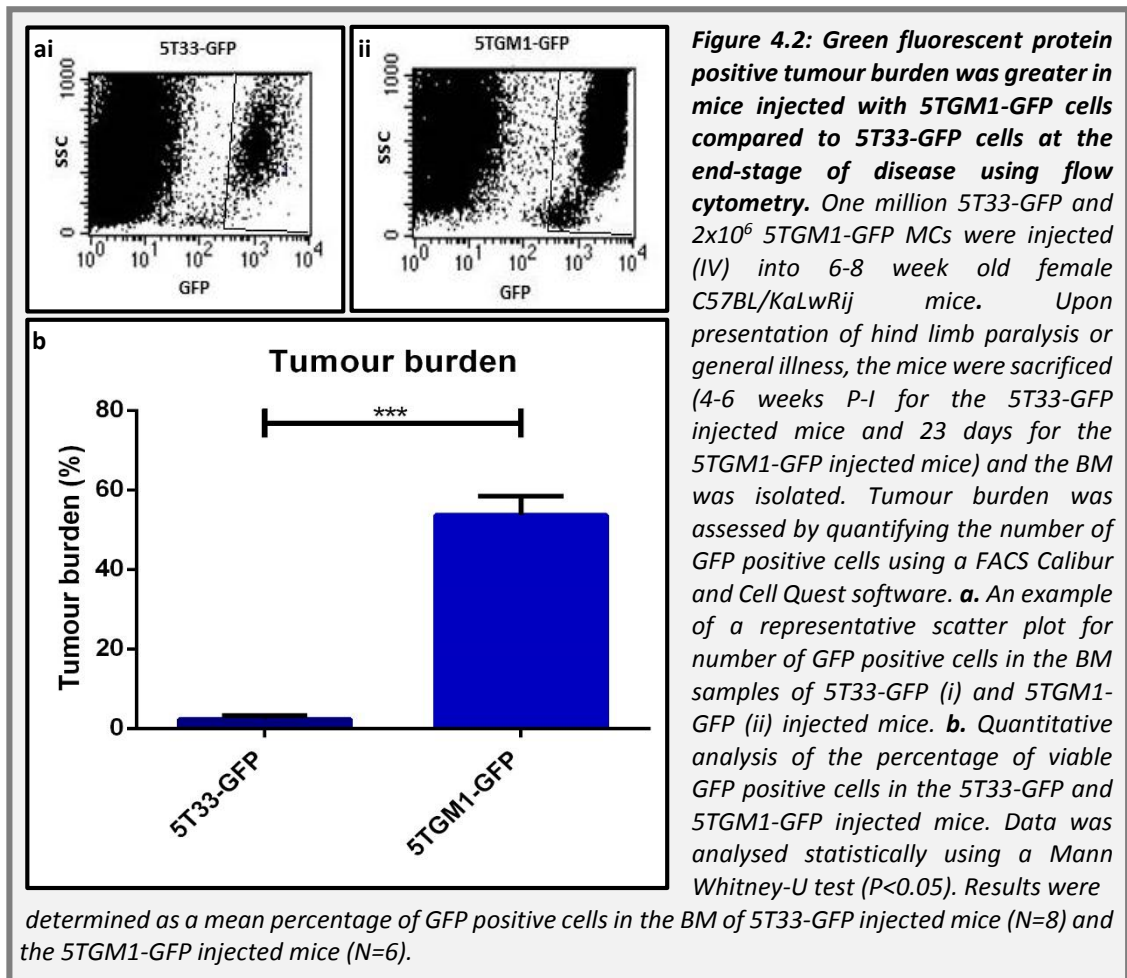
Where relevant, non-parametric statistical tests were used. A Kruskal-Wallis test followed by Dunn's post test ($P < 0.05$) was used to determine any differences in tumour burden and HSC niche molecule, ligand and CD138 protein frequency in the BM and spleen over-time. A Mann-Whitney U test ($P < 0.05$) was used to compare tumour burden in the BM of 5T33-GFP injected mice with 5TGM1-GFP injected mice at the end stage of disease. It was also used to compare the presence of HSC niche molecules, ligands and CD138 between the 5T33-GFP and 5TGM1-GFP cells at the end-stage of disease as well as between cells cultured *in vitro*. Where relevant, error bars were displayed on all graphs using the SEM, unless stated otherwise in the legend.

4.4 Results

4.4.1 Quantification of tumour burden at the end-stage of disease in the bone marrow of mice injected with 5T33-GFP and 5TGM1-GFP cells

Flow cytometry was used to determine the number of 5T33-GFP and 5TGM1-GFP cells present in the BM of C57BL/KaLwRij mice based upon GFP expression. Figure 4.2a shows an example of the flow cytometry profiles used to quantify the number of GFP positive MCs in both the 5T33-GFP and 5TGM1-GFP injected mice at the end-stage of disease. The 5TGM1-GFP injected mice had significantly greater numbers of GFP positive tumour cells ($53.71\% \pm 4.70$) ($P < 0.001$) present in their BM compared to the 5T33-GFP injected mice ($2.40\% \pm 0.90$). In addition, three of the 5T33-GFP injected mice included within the mean did not have obvious tumour burden from the flow

cytometry profiles with values less than 0.25% tumour burden. This contrasted with the mice injected with the 5TGM1-GFP cells, where all mice injected were positive for GFP positive tumour burden.



Flow cytometry was also used to determine the percentage of MCs present in the BM and spleen of mice injected with 5TGM1-GFP cells at 10, 14, 17 and 23 days P-I as shown in Figure 4.3. From the data, it was clear that there was a linear increase in GFP positive tumour burden in both the BM and spleen over-time. Statistically, there was significantly greater tumour burden at 23 days compared to 10 and 14 days in both the BM and spleen samples ($P < 0.05$). In addition, there seemed to be higher tumour burden in the BM compared to the spleen, particularly at 14, 17 and 23 days P-I.

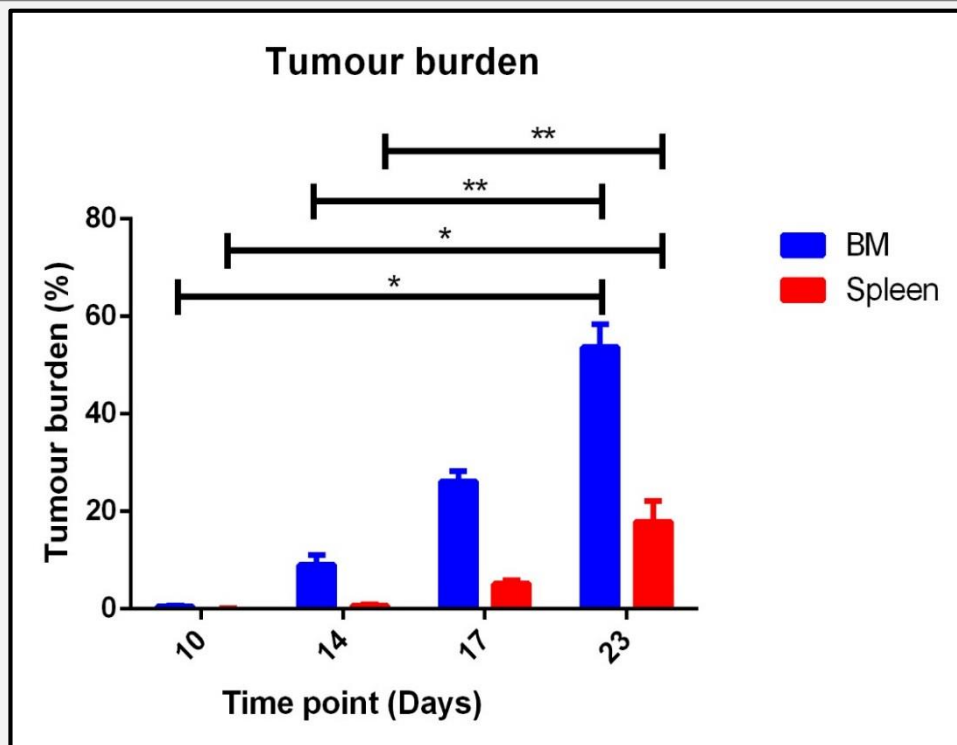


Figure 4.3: Green fluorescent protein positive tumour burden in the bone marrow and spleen of mice injected with 5TGM1-GFP cells increased over-time and was greater in the bone marrow compared to the spleen using flow cytometry. Two million 5TGM1-GFP cells were injected (IV) into 6-8 week old female C57BL/KaLwRij mice. At 10, 14, 17 and 23 days P-I, the mice were sacrificed and the BM and spleen were isolated. Tumour burden was assessed by quantifying the number of viable GFP positive cells in the BM and spleen of 5TGM1-GFP injected mice using a FACS Calibur and Cell Quest software and displayed as a mean percentage of tumour burden. Data was analysed statistically using a Kruskal-Wallis test followed by Dunn's correct test to compare the tumour burden in the BM and spleen separately over-time ($P < 0.05$).

4.4.2 Protein quantification of the HSC niche molecules, ligands and CD138 by 5T33-GFP and 5TGM1-GFP cells *ex vivo* using flow cytometry

Flow cytometric analysis was used to determine the number of BM derived 5T33-GFP and 5TGM1-GFP MCs that were positive for the HSC niche molecules, ligands and CD138, analysed *ex vivo*. Table 4.1 shows a summary of the percentage of BM derived 5T33-GFP and 5TGM1-GFP cells, which were positive for each HSC niche molecule, ligand and CD138, analysed *ex vivo*. Figure 4.4 shows the mean percentage of 5T33-GFP and 5TGM1-GFP cells, which were positive for each HSC niche molecule, ligand and CD138 at the end stage of disease, analysed *ex vivo* using flow cytometry. A high percentage of BM derived 5T33-GFP and 5TGM1-GFP cells were positive for the HSC niche molecules CXCR4, Notch-1 but <2% were positive for Tie-2. The 5T33-GFP cells were also positive for ligand CXCL12, which was only expressed at a low frequency in

the 5TGM1-GFP cells. Both cell types were also marginally positive for the ligand Jag-1 and highly positive for the plasma cell marker CD138. Statistically, a significantly greater number of 5T33-GFP cells were positive for HSC niche molecules CXCR4 and Notch-1 ($P < 0.05$) and ligands CXCL12 ($P < 0.05$) and Jag-1 ($P < 0.05$) compared to the 5TGM1-GFP cells. There was however, no statistical difference in the number of 5T33-GFP and 5TGM1-GFP cells, which were positive for Tie-2 or CD138.

Table 4.1: A summary of the quantitative analysis for the percentage of bone marrow derived myeloma cells, which were positive for the HSC niche molecules, ligands and CD138 using flow cytometry

Protein	5T33-GFP	5TGM1-GFP
CXCR4	99.53 ± 0.12	93.63 ± 2.05
Notch-1	99.09 ± 0.27	86.83 ± 1.54
Tie-2	1.91 ± 0.23	1.66 ± 0.62
CXCL12	38.18 ± 3.03	1.01 ± 0.39
Jag-1	8.55 ± 0.93	1.88 ± 0.37
CD138	93.28 ± 1.78	93.19 ± 0.70

Mean percentage of positive cells shown using the SEM.

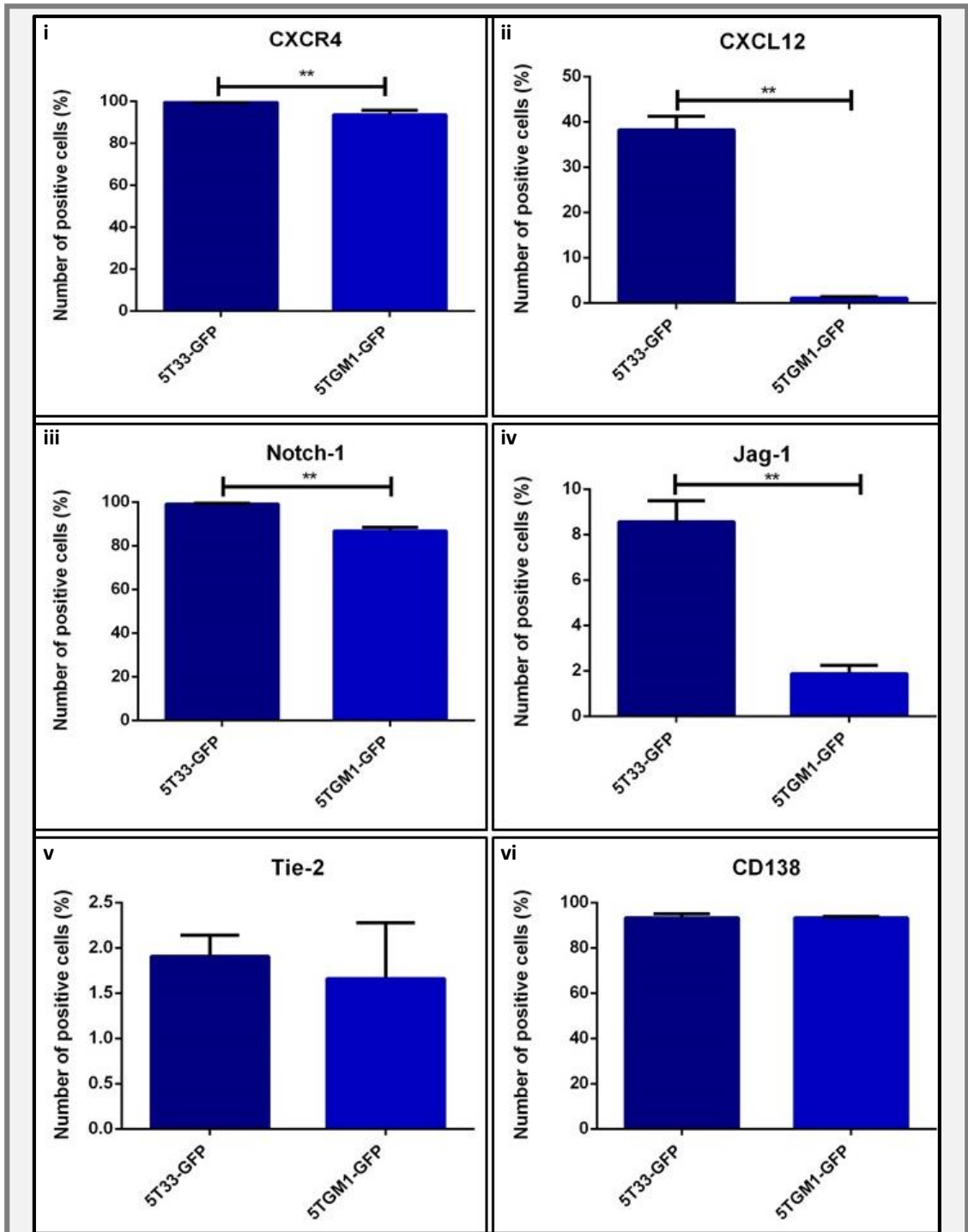


Figure 4.4: 5T33-GFP and 5TGM1-GFP cells isolated from the bone marrow of mice were positive for the HSC niche molecules and ligands at varying frequencies at the end-stage of disease, analysed *ex vivo* using flow cytometry. One million 5T33-GFP and 2×10^6 5TGM1-GFP MCs were injected (IV) into 6-8 week old female C57BL/KaLwRij mice. Upon presentation of hind limb paralysis or general illness, the mice were sacrificed (4-6 weeks P-I for the 5T33-GFP injected mice and 23 days for the 5TGM1-GFP injected mice) and the BM was isolated. Cells were incubated with directly conjugated primary antibodies for the HSC niche molecules CXCR4 (i), Notch-1 (iii) and Tie-2 (v), ligands CXCL12 (ii) and Jag-1 (iv) and CD138 (vi) and dose matched isotype control antibodies. This was followed by flow cytometry using a FACS Calibur and Cell Quest software. Data was analysed statistically using a Mann-Whitney U test ($P < 0.05$). Results were determined as a mean percentage of 5T33-GFP ($N=8$) and the 5TGM1-GFP ($N=6$) which were positive for each molecule.

The number of BM derived 5T33-GFP and 5TGM1-GFP cells which were positive for each HSC niche molecule, ligand and CD138 at the end-stage of disease were compared to the number of cells which were positive for these molecules *in vitro* (the results for this were originally shown in Chapter III, Section 3.4.3). This is displayed in Figure 4.5 for the 5T33-GFP cells and Figure 4.6 for the 5TGM1-GFP cells.

A significantly greater number of BM derived 5T33-GFP cells (“5T33-GFP *ex vivo*”) were positive for the HSC niche molecules CXCR4 (P<0.05), Notch-1 (P<0.05) and Tie-2 (P<0.05) compared to the 5T33-GFP cells cultured *in vitro* (“5T33-GFP *in vitro*”). There was also a significantly greater number of “5T33-GFP *ex vivo*” cells which were positive for the ligands CXCL12 (P<0.05) and Jag-1 (P<0.05) compared to the “5T33 *in vitro*” cells.

In contrast, significantly fewer BM derived 5TGM1-GFP cells (“5TGM1-GFP *ex vivo*”) were positive for the HSC niche molecules Notch-1 (P<0.05) and Tie-2 (P<0.05) compared to 5TGM1-GFP cells cultured *in vitro* (“5TGM1-GFP *in vitro*”). There was also a significantly lower number of “5TGM1-GFP *ex vivo*” cells which were positive for the ligands CXCL12 (P<0.05) and Jag-1 (P<0.05) compared to the “5TGM1-GFP cells *in vitro*” cells. In addition, there was a significant decrease in the number of “5TGM1-GFP *ex vivo*” cells which were positive for CD138 compared to the “5TGM1-GFP *in vitro*” cells (P<0.05).

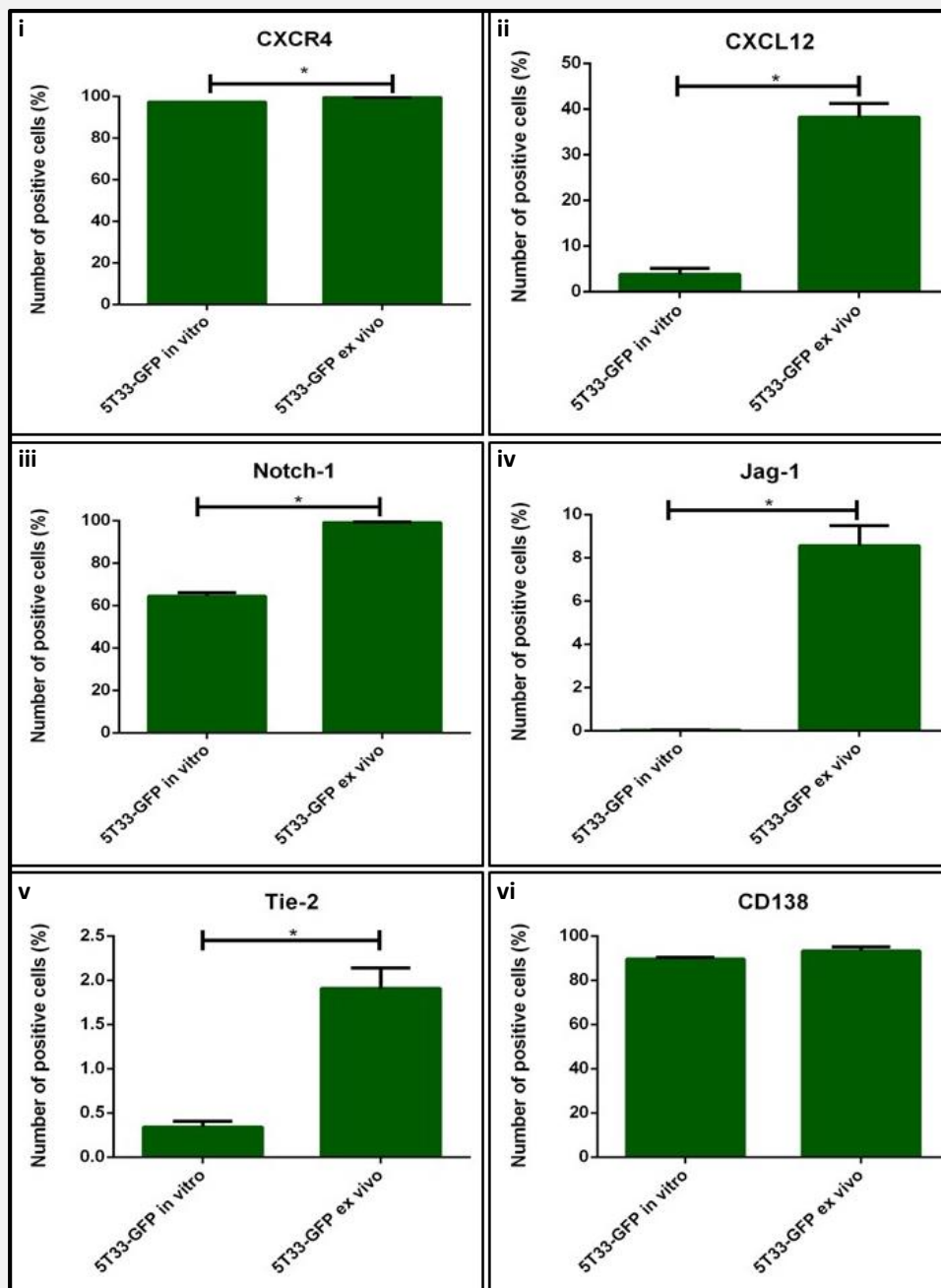


Figure 4.5: The presence of the HSC niche molecules and ligands was significantly higher in the bone marrow derived 5T33-GFP cells compared to in vitro 5T33-GFP cells by flow cytometry. 5T33-GFP cells were cultured in vitro (N=3), or in vivo, by injecting 6-8 week old female C57BL/KaLwRij mice with 1×10^6 5T33-GFP (N=8) cells. At the end-stage of disease (when mice demonstrated hind-leg paralysis), the BM was subsequently isolated for flow cytometry. Both the 5T33-GFP cells analysed ex vivo and in vitro were incubated with directly conjugated primary antibodies for the HSC niche molecules; CXCR4 (i), Notch-1 (iii) and Tie-2 (v), ligands; CXCL12 (ii) and Jag-1 (iv), and CD138 (vi) or dose matched isotype control antibodies. This was followed by flow cytometry using a FACS Calibur and Cell Quest software. Quantitative analysis for the percentage of viable 5T33-GFP cells analysed ex vivo and in vitro which were positive for each HSC niche molecule, ligand and CD138 was determined. Data was analysed statistically using a Mann-Whitney U test ($P < 0.05$) to compare the percentage of 5T33-GFP cells which were positive for each HSC niche molecule, ligand and CD138. Results were determined as a mean percentage of 5T33-GFP cells, which were positive for each molecule.

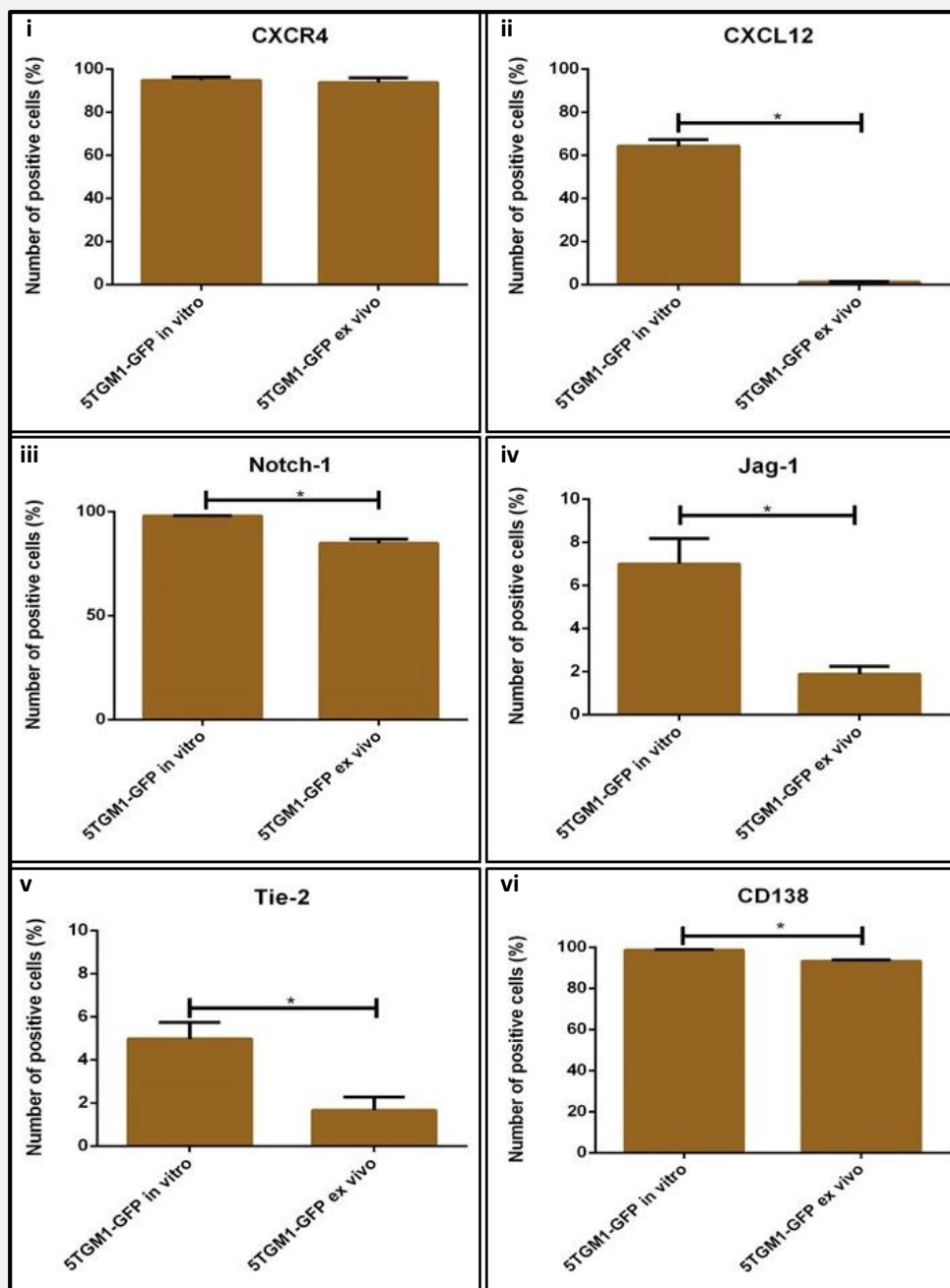


Figure 4.6: The presence of the HSC niche molecules and ligands was significantly decreased in the BM derived 5TGM1-GFP cells compared to in vitro 5TGM1-GFP cells by flow cytometry. 5TGM1-GFP cells were cultured in vitro (N=3), or in vivo, by injecting 6-8 week old female C57BL/KaLwRij mice with 2×10^6 5TGM1-GFP (N=6) cells. At the end-stage of disease (when mice demonstrated hind-leg paralysis), the BM was subsequently isolated for flow cytometry. Both the 5TGM1-GFP cells analysed ex vivo and in vitro were incubated with directly conjugated primary antibodies for the HSC niche molecules; CXCR4 (i), Notch-1 (iii) and Tie-2 (v), ligands; CXCL12 (ii) and Jag-1 (iv), and CD138 (vi) or dose matched isotype control antibodies. This was followed by flow cytometry using a FACS Calibur and Cell Quest software. Quantitative analysis of the percentage of viable 5TGM1-GFP cells analysed ex vivo and in vitro which were positive for each HSC niche molecule, ligand and CD138 was determined. Data was analysed statistically using a Mann-Whitney U test ($P < 0.05$) to compare the percentage of 5TGM1-GFP cells which were positive for each HSC niche molecule, ligand and CD138. Results were determined as a mean percentage of 5TGM1-GFP cells positive for each molecule.

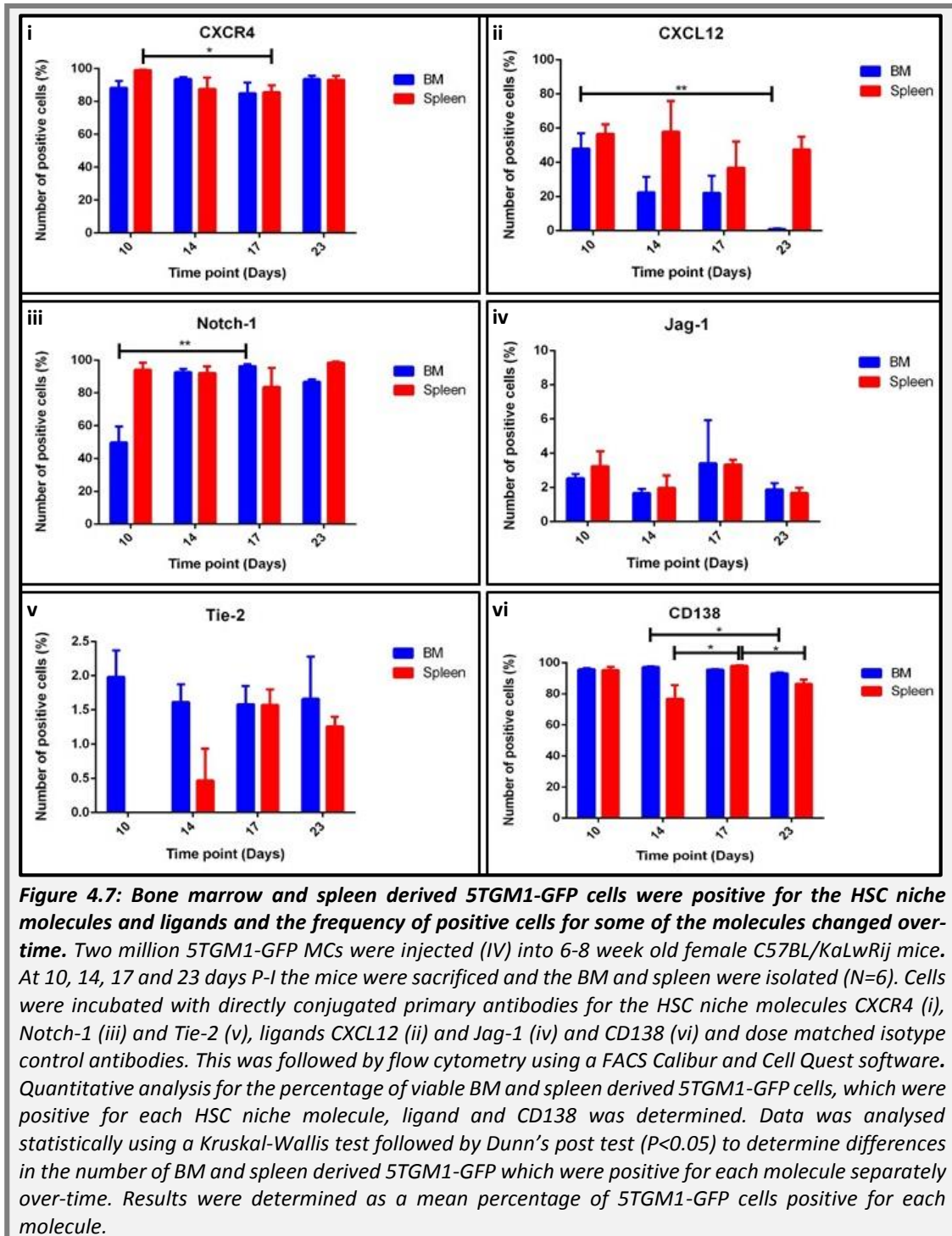
4.4.3 Protein quantification of the HSC niche molecules and ligands by the bone marrow and spleen-derived 5TGM1-GFP cells over-time analysed *ex vivo* using flow cytometry.

The presence of HSC molecules and ligands in the BM and spleen derived 5TGM1-GFP cells was also quantified using flow cytometry over-time at 10, 14, 17 and 23 days P-I of tumour cells, as shown in Figure 4.7. The HSC niche molecules CXCR4, Notch-1 and Tie-2, ligands CXCL12 and Jag-1, and plasma cell marker CD138 were present in both the BM and spleen derived 5TGM1-GFP cells at each time point.

Flow cytometry showed that there were no clear patterns with regards to the frequency of HSC niche molecule and ligand positive cells over-time, with the exception of CXCL12. Using a Kruskal-Wallis test followed by Dunn's post test there were significantly fewer BM derived 5TGM1-GFP cells, which were positive for CXCL12 after 23 days compared to 10 days and interestingly this reduced over the time course in a linear fashion. This pattern was however, only observed in the BM derived 5TGM1-GFP cells and not those isolated from the spleen. In addition, the frequency of Notch-1 positivity increased in the BM derived cells between 10 and 17 days and CD138 was reduced from 14 days to 23 days. The spleen derived 5TGM1-GFP cells also had significantly reduced numbers of cells, which were positive for CXCR4 between 10 and 17 days, and a significant increase in CD138 positive cells from 14 to 23 days.

Differences in the number of BM and spleen derived MCs, which were positive for the HSC niche molecules and ligands, were unable to be analysed as no suitable non-parametric two-way tests were available. However, from the data, there did seem to be fewer BM derived MCs which were positive for CXCL12 compared to those isolated from the spleen, particularly at 23 days P-I. Interestingly, the number of Notch-1 positive BM derived cells was lower at 10 days P-I compared to the spleen

derived cells and Tie-2 was absent in the spleen derived MCs at 10 days P-I, whereas a small proportion of BM derived cells were positive at this time point.



4.4.4 Protein visualisation of the HSC niche molecules CXCR4 and N-cad, and CD138 by the 5TGM1-GFP cells in histological bone sections, over-time using IHC

Immunohistochemistry was used to visualise the presence of protein for CXCR4, N-cad and CD138 *in vivo* over the disease course in histological bone sections taken from mice injected with 5TGM1-GFP cells or non-tumour bearing animals. Figure 4.8 illustrates CD138 staining in histological bone sections taken from mice injected with 5TGM1-GFP cells or PBS and stained by IHC at 10, 14, 17 and 21 days P-I. In the tibiae of PBS injected mice, only single cells were positive for CD138, unlike in the 5TGM1-GFP injected mice where discrete colonies were observed. 5TGM1-GFP cells were morphologically different to the normal constituents of the BM as they demonstrated an enlarged nucleus and some cells were also multi-nuclear. Staining at 10 days P-I showed small CD138 positive colonies, which were mostly adjacent to sinusoid structures and as the disease progressed over-time the number of colonies increased. From 17 to 21 days P-I, the CD138 positive colonies had merged and therefore, colony number decreased despite colony area increasing. Quantification of the colony number over-time is shown in Figure 4.9 (*analysed by Shelly Lawson, Department of Oncology, The University of Sheffield*). These were taken from bone sections from the same study however, staining was conducted on the early time points (0, 3 and 7 days P-I) as well as the latter time points (10, 17 and 21) and analysed using Osteomeasure software. At the early time points of 0, 3 and 7 days, single cells were observed which were either normal murine plasma cells or MCs, however, the two are indistinguishable. From 7 days onwards, some colonies were observed though they were small and not always distinct. Following 7 days there was a linear increase in tumour burden as seen previously with the flow cytometry tumour burden data.

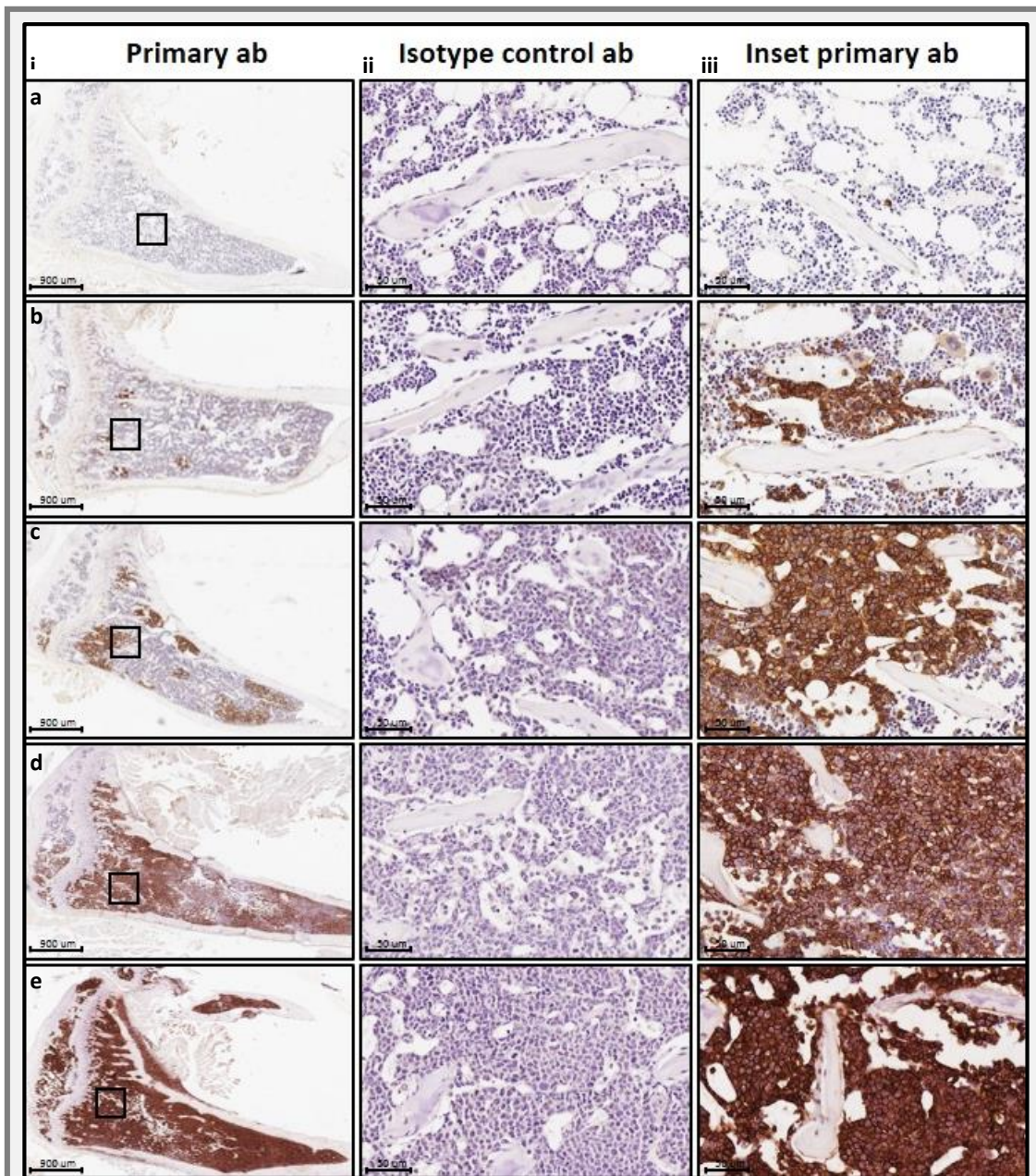


Figure 4.8: CD138 IHC staining increased over-time in the tibiae of 5TGM1-GFP injected mice. PBS (a) or 2×10^6 5TGM1-GFP cells (b-e) were injected into C57BL/KaLwRij mice and at 10 (b), 14 (c), 17 (d) and 21 (e) days P-I, mice were sacrificed and tibiae were dissected. The Tibiae were fixed, decalcified, processed, embedded and cut into $3 \mu\text{m}$ sections. Bone sections were stained by sandwich IHC using an anti-CD138 primary antibody or complementary isotype control antibody followed by biotinylated secondary antibody, streptavidin HRP and DAB substrate where positive staining is brown. Images of sections were taken using an Aperio Slide Scanner and subsequently visualised using Image Scope Software. At each time point, images were taken of primary antibody staining using a 2X magnification (i) followed by images using a 40X magnification of isotype (ii) and primary antibody (iii) staining of trabecular bone regions. Scale bars represent $900 \mu\text{M}$ (i) and $50 \mu\text{M}$ (ii and iii).

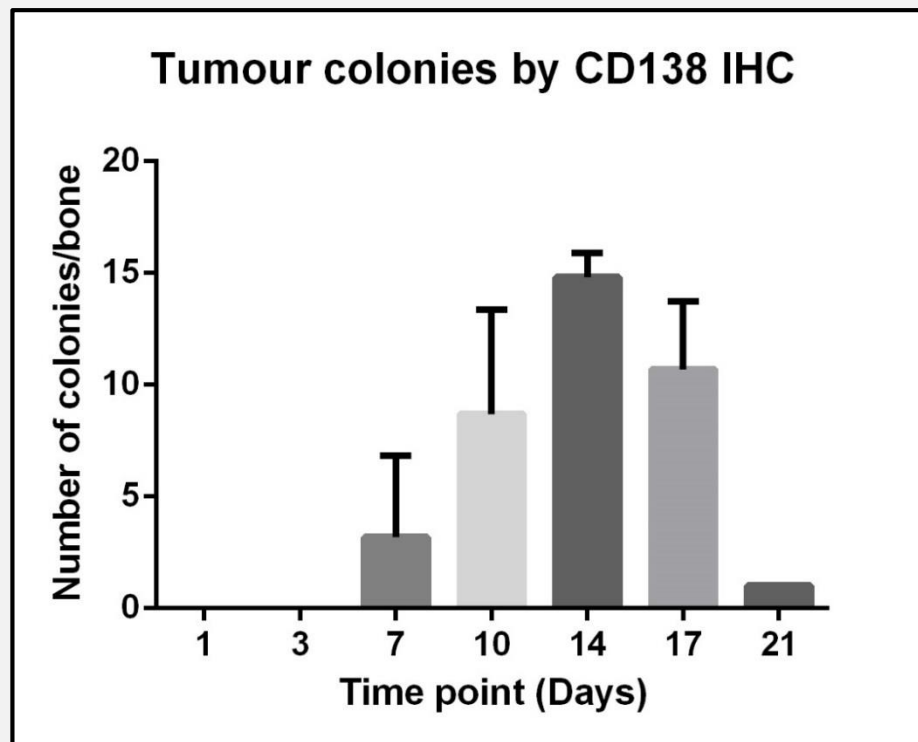


Figure 4.9: The number of CD138 colonies increased over-time before merging together. Bone sections of mouse tibiae, taken from mice injected with 5TGM1-GFP cells after 1, 3, 7, 14, 17 and 21 days P-I, were stained for CD138 by IHC. The staining was analysed using Osteomeasure software to quantify the number of CD138 positive stained colonies per bone. (Sections were stained by Julia Hough, Department of Human Metabolism, The University of Sheffield and analysed by Shelly Lawson, Department of Oncology, The University of Sheffield).

Figure 4.10 shows the positive staining of N-cad in histological bone sections of tibiae taken from mice injected with PBS or 5TGM1-GFP cells over-time. In the PBS control, positive staining for N-cad was visualised on what appeared to be osteoblastic cells lining both cortical and trabecular bone throughout the bone and staining was particularly intense in the growth plate region. In addition, the staining appeared to be primarily on the membrane of the cells.

In the bones of mice that had been injected with 5TGM1-GFP cells, staining again was observed in osteoblastic cells in trabecular and cortical regions. In addition, all MC colonies, identified by morphology, were also positive for N-cad but staining was not as intense as the CD138 IHC staining. There was also a direct correlation of tumour burden with N-cad staining and as the tumour burden increased so did the number of N-cad stained cells and tumour area. The staining pattern of N-cad also differed

between the osteoblastic and MCs. The osteoblastic staining for N-cad was highly membranous, whereas the staining of N-cad in the MCs seemed to be cytoplasmic. In addition, the intensity of the staining seemed to increase until day 14 and following this, at 17 and 21 days P-I the intensity of staining decreased.

Figure 4.11 illustrates IHC staining of CXCR4 in the BM of PBS or 5TGM1-GFP injected mice. Very little staining, if any, was present in the PBS injected mice, whereas in the 5TGM1-GFP injected mice the staining was highly selective for the 5TGM1-GFP cells. In addition, all 5TGM1-GFP cells seemed to be positive for CXCR4 and staining correlated with an increase in tumour burden over-time. The staining pattern within the MCs was quite unusual and unexpected. The cells had both cytoplasmic staining and intense nuclear staining, which is not typical of G-protein coupled receptors (GPCRs). In addition, the staining intensity seemed to increase as the tumours increased in size over-time.

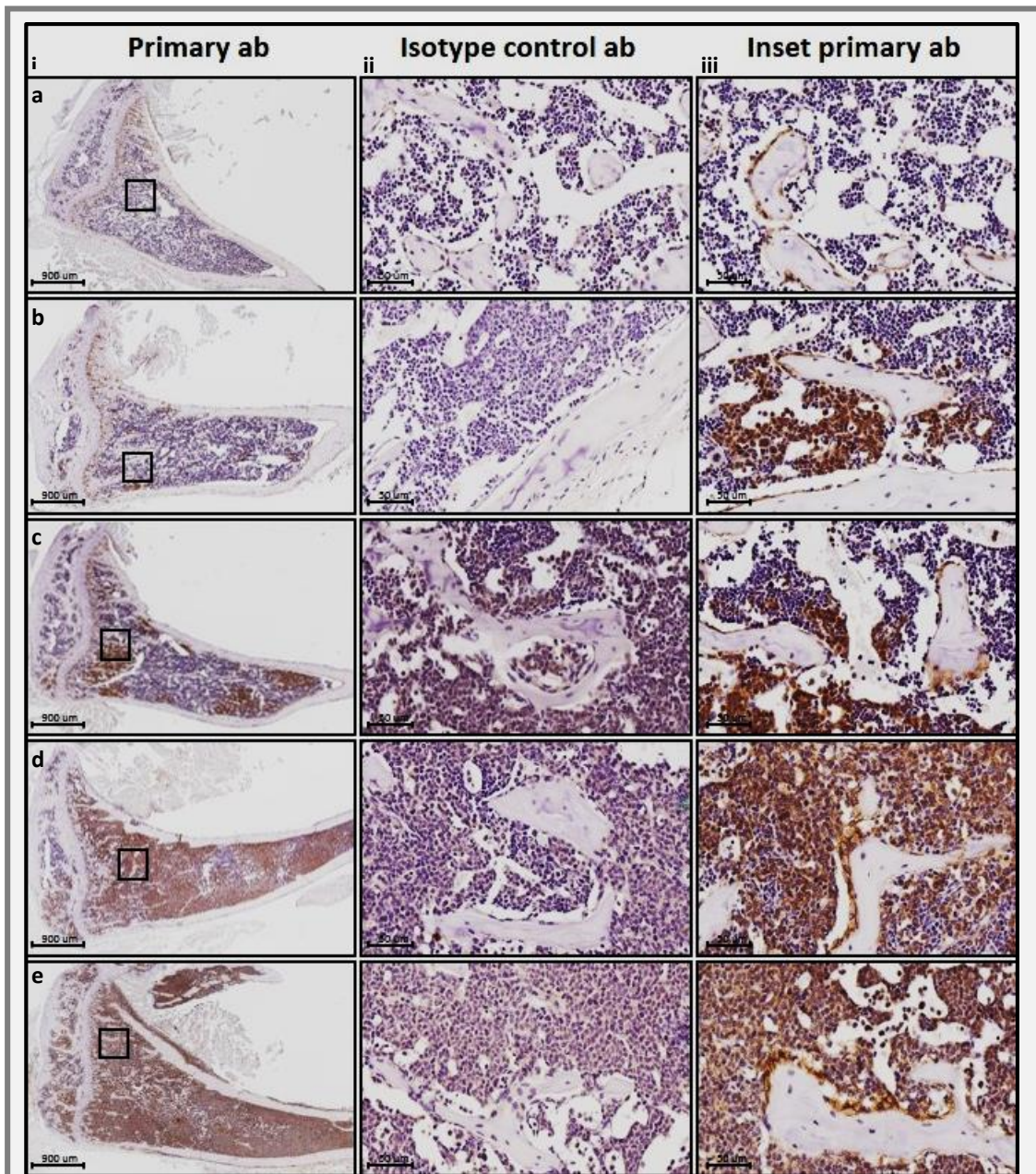


Figure 4.10: N-cad IHC staining increased over-time in the tibiae of 5TGM1-GFP injected mice. PBS (a) or 2×10^6 5TGM1-GFP cells (b-e) were injected into C57BL/KaLwRij mice and at 10 (b), 14 (c), 17 (d) and 21 (e) days P-I, mice were sacrificed and tibiae were dissected. The Tibiae were fixed, decalcified, processed, embedded and cut into $3 \mu\text{m}$ sections. Bone sections were stained by sandwich IHC using an anti-N-cad primary antibody or complementary isotype control antibody followed by biotinylated secondary antibody, streptavidin HRP and DAB substrate where positive staining is brown. Images of sections were taken using an Aperio Slide Scanner and subsequently visualised using Image Scope Software. At each time point, images were taken of primary antibody staining using a 2X magnification (i) followed by images using a 40X magnification of isotype (ii) and primary antibody (iii) staining of trabecular bone regions. Scale bars represent $900 \mu\text{m}$ (i) and $50 \mu\text{m}$ (ii and iii).

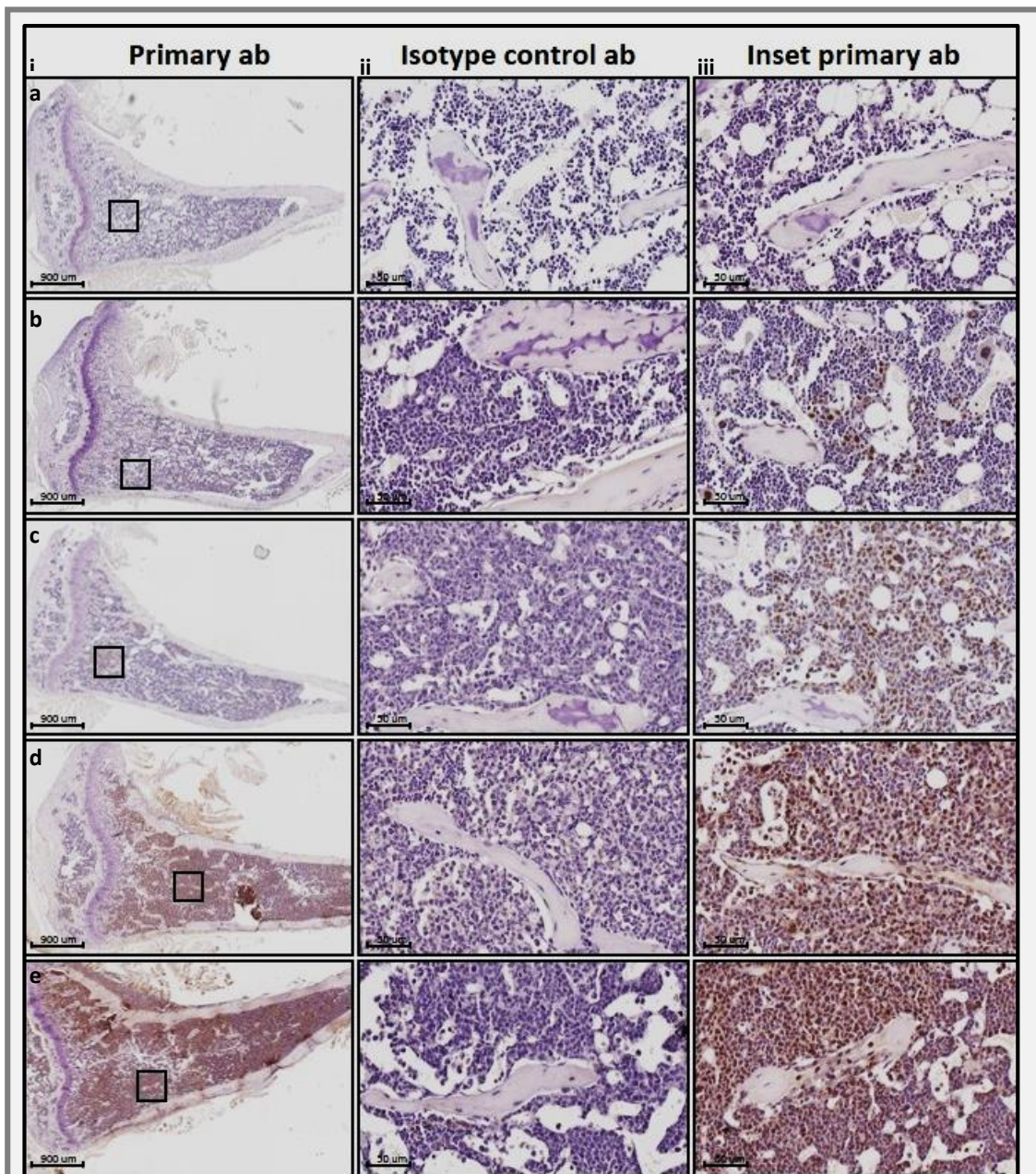


Figure 4.11: CXCR4 IHC staining increased over-time in the tibiae of 5TGM1-GFP injected mice. PBS (a) or 2×10^6 5TGM1-GFP cells (b-e) were injected into C57BL/KaLwRij mice and at 10 (b), 14 (c), 17 (d) and 21 (e) days P-I, mice were sacrificed and tibiae were dissected. The Tibiae were fixed, decalcified, processed, embedded and cut into $3 \mu\text{m}$ sections. Bone sections were stained by sandwich IHC using an anti-CXCR4 primary antibody or complementary isotype control antibody followed by biotinylated secondary antibody, streptavidin HRP and DAB substrate where positive staining is brown. Images of sections were taken using an Aperio Slide Scanner and subsequently visualised using Image Scope Software. At each time point, images were taken of primary antibody staining using a 2X magnification (i) followed by images using a 40X magnification of isotype (ii) and primary antibody (iii) staining of trabecular bone regions. Scale bars represent $900 \mu\text{M}$ (i) and $50 \mu\text{M}$ (ii and iii).

4.5 Discussion

The aim of this chapter was to determine the number of 5T33-GFP and 5TGM1-GFP cells, isolated from the BM and/or spleen and analysed *ex vivo*, which were positive for the HSC niche molecules. An additional aim was to determine the presence of protein for HSC niche molecules by 5TGM1-GFP cells in histological bone sections at different stages of disease.

Firstly, the tumour burden in the BM of mice injected with 5T33-GFP or 5TGM1-GFP cells was determined by GFP expression, using flow cytometry. Despite 5TGM1-GFP cells being a derivative of the 5T33MMvt cells (174) there were significant differences in tumour burden. The flow cytometry data demonstrated that the 5TGM1-GFP injected mice had significantly greater tumour burden in the BM compared to mice injected with 5T33-GFP cells. In addition, the take rate was 100% in the mice injected with 5TGM1-GFP cells whereas; the take rate was 63% for mice injected with 5T33-GFP cells. This was slightly unusual; however, the preparation of the 5TGM1-GFP cells differs to that of the 5T33-GFP cells. As described by Dallas *et. al* (222) the 5TGM1-GFP cells were “propagated by marrow transfer” in the C57BL/KaLwRij mice, by BM flushes followed by growth *in vitro* for 7 days and re-inoculation into mice, whereas the 5T33-GFP cells were continually cultured without *in vivo* passaging. Therefore, passaging through the animals may result in highly tumourgenic 5TGM1-GFP cells. It maybe that if the 5TGM1-GFP cells had been cultured extensively, as the 5T33-GFP cells had been, they would have lost certain characteristics required for the homing of cells to the BM and subsequent growth *in vivo*. Within our group, we have attempted to increase tumour take by *in vivo* passaging of the 5T33-GFP cells but with little success. However, continual *in vivo* passaging of the 5T33-GFP cells may be required to recapitulate the original tumourgenicity of these cells.

In the 5TGM1-GFP injected mice, tumour burden was observed in both the BM and spleen (sites of haematopoiesis in mice after birth), which is not typical of human myeloma disease. Tumour burden at both sites increased significantly over-time. The 5TGM1-GFP cells grew in a linear fashion with an initial lag phase between 10 and 14 days (the earliest time points where GFP positive cells were clearly visualised using flow cytometry) followed by an exponential growth phase from 14 days up until 23 days. Interestingly, there was less tumour burden in the spleen at each time point compared to the BM (though this could not be statistically compared). These data therefore, suggested that the 5TGM1-GFP cells may either initially home to the BM and subsequently migrate to the spleen, or that the MCs arrive in the BM and spleen but grow at a slower rate in the spleen compared to the BM. Oyajobi *et al* (223) observed a high number of 5TGM1-GFP cells in the BM of live mice (Light Tools Imaging system) whereas, only a low number of 5TGM1-GFP cells were seen in the spleen of animals 4 weeks P-I. However, again, it is uncertain whether fewer cells home to the spleen initially or whether they proliferate at a slower rate compared to those in the BM. Additional studies are therefore, required to ascertain the number of cells initially homing to both the BM and spleen.

The presence of HSC niche molecules; CXCR4, Notch-1 and Tie-2, their respective ligands; CXCL12 and Jag-1, and CD138 were shown in 5T33-GFP and 5TGM1-GFP cells isolated from the BM and analysed *ex vivo*. When the number of cells which were positive for the HSC niche molecules, ligands and CD138 were compared between the 5T33-GFP and 5TGM1-GFP cells isolated at the end stage of disease, several differences were identified. Significantly less BM derived 5TGM1-GFP cells were positive for CXCR4, Notch-1, CXCL12 and Jag-1 compared to the 5T33-GFP cells. Currently there is no data available that have compared the expression of these molecules between the two different MC lines. In my studies, differences between the cell lines at the time point when the 5TGM1-GFP treated animals were at end-stage disease may be due to the differences in tumour infiltration in the BM. These molecules may be important in the early establishment of disease and therefore are

more highly expressed in the 5T33-GFP cells compared to the 5TGM1-GFP cells, which had fully infiltrated the BM at this time of analysis. In previous studies, CXCR4, Notch and Tie-2 signalling have been associated with several different mechanisms in healthy cells as well as cancer cells. Specifically, CXCR4 is important for chemotaxis via the activation of PI3-K (105) and MAPK/ERK (103) signalling following CXCL12 stimulation of CXCR4. Notch-1 signalling also induces cell growth and enhances cell survival potentially via ERK and Akt signalling, following Notch-1 activation (224). Phosphatidylinositol 3-kinase and Akt signalling have also been associated with cell survival following activation of Tie-2 by Ang-1 (85). Chemotaxis, migration and proliferation are often mechanisms, which are important in the early time points of disease establishment therefore, it is likely that the molecules CXCR4, Tie-2, and Notch-1 which induce chemotaxis and/or proliferation are down-regulated in the 5TGM1-GFP cells, which have successfully homed and established full disease in the BM compared to the 5T33-GFP cells.

Previous studies have supported as well as disapproved the theory that early disease MCs have higher expression of the molecules CXCR4, Notch-1, Tie-2, CXCL12 and Jag-1 compared to MCs in established disease. With regards to Notch-1, Skrtic *et al* (2010) found that MGUS patients, with less than 10% tumour infiltration, had MCs which were Notch-1 negative, compared with symptomatic myeloma patients, who had high Notch-1 expression (214). This is similar to prostate cancer where 41% of patients with high-grade disease and 61% of patients with prostate metastasis had Notch-1 positive prostate cancer cells, compared with 23% of patient with low-graded prostate cancer (225). Taken together, this shows that Notch-1 seems to be present in latter stages of disease. The presence of Jag-1 on CD138 positive MCs has previously been demonstrated in primary patient samples (198) but previous studies have not identified its expression on murine 5T cells *in vitro*, *ex vivo* or *in vivo*. Jag-1 expression seems to be associated with disease progression in myeloma. Samples from MGUS patients were negative for Jag-1 staining using IHC whereas, samples from symptomatic myeloma patients were positively stained for Jag-1 (214). This was

also demonstrated in prostate cancer, where localised primary tumours and metastatic samples had higher intensity of Jag-1 staining compared to benign samples. High levels of Jag-1 also correlated with reoccurrence of disease assessed by prostate-specific antigen free survival (226). Taken together, this disapproves my findings of higher expression in the early stages of myeloma disease. However, when comparing the presence of protein for the molecules in the 5TGM1-GFP time-course experiment rather than between the 5T33-GFP and 5TGM1-GFP cells at the end-stage of disease the data, Notch-1 correlates with the experiments described above where Notch-1 expression was significantly lower at 10 days compared to 14 days.

It is also difficult to rationalise why the number of cells positive for CXCL12 were lower in the 5TGM1-GFP cells compared to the 5T33-GFP cells and also why the number of CXCL12 positive cells decreased linearly over-time in the 5TGM1-GFP cells grown in the BM. As stated in Chapter III, whether CXCL12 is produced by the 5T33MMvt and 5TGM1-GFP cells themselves or whether it is internalised from the local environment is uncertain. However, our hypothesis is that fewer 5TGM1-GFP cells were positive for CXCL12 towards the end-stage of disease because they no longer internalised CXCL12 from the BM environment. This may be because CXCL12 levels were reduced in the BM, as fewer CXCL12 producing cells were present due to the physical expansion of MCs and reduction in CXCL12 positive osteoblastic cells. The 5T33-GFP cells isolated from the BM however, had a higher frequency of CXCL12 positive cells than those cultured *in vitro*. This increase maybe due to induced production by the MCs themselves or because of the internalisation of CXCL12, which is still in abundance in the BM, due to low 5T33-GFP tumour burden. In support of CXCL12 internalisation, previous studies demonstrated that CXCL12 was internalised via CXCR4 in human and mouse ECs (93). In addition, previous studies showed internalisation of the receptor CXCR4 in MCs (195) and B lymphoblastic cells (227), which in turn may result in ligand internalisation, however these studies did not address that question.

The presence of protein for the HSC niche molecules, ligands and CD138 by the 5T33-GFP and 5TGM1-GFP cells were compared between the BM derived MCs at the end-stages of disease and the MCs cultured *in vitro*. In the 5T33-GFP cells, the HSC niche molecules; CXCR4, Notch-1 and Tie-2 and ligands; CXCL12 and Jag-1 were significantly up regulated in the BM derived cells compared to the 5T33-GFP cells cultured *in vitro*. Whereas, the HSC niche molecules; Notch-1 and Tie-2, ligands; CXCL12 and Jag-1, and CD138 were significantly down regulated in the BM derived 5TGM1-GFP cells compared to the 5TGM1-GFP cells cultured *in vitro*. The data were almost 'mirror images' of each other but again may reflect the difference in tumour growth rates in each cell line observed in my studies. As with the differences in protein frequency between the 5T33-GFP and 5TGM1-GFP, exactly why cells cultured *in vitro* have different numbers of positive cells to *ex vivo* cells is unknown. However, cell localisation in the BM to specific ligands or regulation by secreted factors would be likely to influence gene expression and protein production. Increases in the HSC molecules and ligands in the *ex vivo* 5T33-GFP cells but decreases in the 5TGM1-GFP cells again may be due to differences in the phase of cell growth. Whilst the 5T33-GFP cells have not established full tumour infiltration, they produce proteins that promote their growth whereas, the 5TGM1-GFP cells, which have already reached full capacity in the BM, down-regulate molecules, which they no longer require, as discussed above.

In addition, there were also several differences between the BM and spleen derived 5TGM1-GFP cells. Notch-1 was present in a greater number of spleen derived 5TGM1-GFP cells compared to the BM at 10 days P-I and also the number of cells positive for Tie-2 was greater in the BM compared to the spleen-derived cells at 10 days. Differences in the frequency of these molecules between BM and spleen derived 5TGM1-GFP cells have not been reported in the literature. However, again the stage of tumour progression may be important with regards to presence of the HSC niche molecules and ligands and may account for differences for the presence of Notch-1. The numbers of cells, which were positive for Tie-2, compared to the BM

and spleen was extremely interesting. At day 10 P-I, the spleen derived 5TGM1-GFP cells were negative for Tie-2, and it was not until day 17 that they showed similar numbers of Tie-2 positive cells compared to the BM derived cells. Tie-2 expression by the 5TGM1-GFP cells remains ambiguous due the lack of gene expression using RT-PCR. However, it remains interesting that Tie-2 positive cells were observed in the BM derived cells but were absent initially in spleen derived cells, indicating that Tie-2 may be a molecule required for initial tumour development specifically within the BM, opposed than the spleen.

The presence of CXCR4, N-cad and CD138 protein was visualised by 5TGM1-GFP cells *in vivo* by IHC of BM sections taken from mice injected with 5TGM1-GFP and sacrificed at various time points. Using IHC and Osteomeasure analysis, CD138 protein was mapped over-time in the 5TGM1-GFP infiltrated BM sections. The analysis showed that the tumour burden results correlated perfectly with the flow cytometry tumour burden data, whereby tumour increased exponentially over-time, therefore, highlighting the reliability of the staining.

The distribution of N-cad was also mapped using IHC and the staining showed that all MC colonies were positive for N-cad *in vivo* at each time-point and the intensity of N-cad staining reached its peak at 14 days P-I of 5TGM1-GFP cells. The pattern of staining was also interesting. The osteoblastic cells in the bone had very distinct membranous staining around the cell whereas; the N-cad positive MCs displayed cytoplasmic staining. The staining patterns observed correlated partially with the literature where OPM-1 MCs positive for N-cad demonstrated cytoplasmic staining, however, they also demonstrated membranous staining (206). This also correlates with staining observed in patient prostate biopsies where again N-cad staining was observed in the cytoplasm but also on the membrane (228). However, Zhang *et al* (2003) also showed N-cad staining that “asymmetrically localised to the cell surface” of HSCs and N-cad positive spindle-shaped osteoblasts, rather than inside the cell.

CXCR4 appeared to be present throughout the development of disease however; the staining patterns were not as expected. From the IF experiments in the Chapter III, CXCR4 staining was displayed as discrete membranous staining around the cell however, in the IHC sections, CXCR4 was situated within the nucleus of the cells. Differences may be due to sample preparation, as the bones were fixed, processed and the bones were cut into wax sections. This process eliminates the requirement of permeabilisation for antibody entry whereas, the cells for IF were not permeabilised and the CXCR4 antibodies would therefore be unable to enter the cell. Previous studies also showed that CXCR4 nuclear localisation arises due to stimulation using CXCL12 *in vitro*, where treatment of MCs or lymphoblastic cells with recombinant CXCL12 resulted in internalisation of CXCR4 (195, 227). In addition, previous studies have demonstrated that nuclear staining of CXCR4 may be a marker for prognosis however; this remains to be a controversial concept. CXCR4 nuclear IHC staining has been reported in cancer cells in colo-rectal cancer (229), gall bladder cancer (230) and interestingly solely in prostate cells in the bone compared to the primary site and lymph nodes (104) and it is associated with poorer patient outcome. However, Eaton *et al*, (231) noted that nuclear CXCR4 staining was removed when prostate samples were blocked with normal horse serum (presumably the serum block for the secondary antibody) opposed to casein. The different serum block resulted in fewer cells, which were positive, and cells that were positive did not display nuclear staining but demonstrated “cytoplasmic, membranous or punctate positive staining”. Therefore, this study implies that IHC methodology may result in false positives for CXCR4 (231). In my studies, the specificity of the antibody needs to be further evaluated. The antibody used seemed highly specific for the MCs, which express CXCR4 however, whether it is binding to the correct epitope is unknown. Therefore, further experiments are required to confirm that the antibody is specific, possibly by WB. Also further *in vitro* experiments to explore the effect of CXCL12 stimulation upon the localisation of CXCR4 in the 5TGM1-GFP cells could be conducted to determine whether CXCL12 is responsible for CXCR4 internalisation in these cell types.

In conclusion, these data support the hypothesis that BM derived MCs are positive for the same repertoire of molecules as HSCs when analysed *ex vivo* and *in vivo*. However, their role in a MC niche is still unknown and further functional studies are required to explore this.

Chapter V: Validating a model for primary osteoblast lineage cell differentiation *in vitro*, to determine the expression of HSC niche molecules and ligands, and to develop an osteoblastic and myeloma cell co-culture system

5.1 Introduction

Osteoblasts are the cells within the bone responsible for production of osteoid, primarily composed of type 1 collagen which forms mineralised bone when calcified with hydroxyapatite, $\text{Ca}_{10}(\text{PO}_4)_6(\text{OH})_2$. They are also one of the important components in the BM microenvironment, which are potentially required to establish a niche for HSCs, inducing their quiescence. Increases in osteoblast numbers by constitutively activating the PTH/PTHrP receptor (PPR), using the Col1-caPPR mouse model, also increased numbers of c-kit⁺, sca-1⁺, lin⁻ (KSL) HSCs *in vivo* and BM cells from transgenic mice had higher engraftment into irradiated recipients compared to wild-type control BM cells (82). In addition, inactivation of BMP receptor 1 A (BMPR1A) in transgenic mice, resulted in an increase in BM osteoblastic cells and ectopic bone which correlated with an increase in HSCs (83). However, currently it is unknown whether all cells of the osteoblast cell lineage are involved in the osteoblastic niche or whether there is a particular sub-set of osteoblasts, which are particularly important. Zhang *et al* (83) noted that HSCs seemed to selectively adhere to a sub-population of N-cad positive, spindle-shaped cells on both trabecular and cortical bone, clarified to be early osteoblastic cells by Xie *et al* (84), supported by Clark *et al* (232) who defined spindle-shaped osteoblastic cells as immature osteoblastic cells.

Osteoblasts originate from MSCs through a series of differentiation steps as shown in Figure 5.1, determined by Friedenstein *et al* (233).

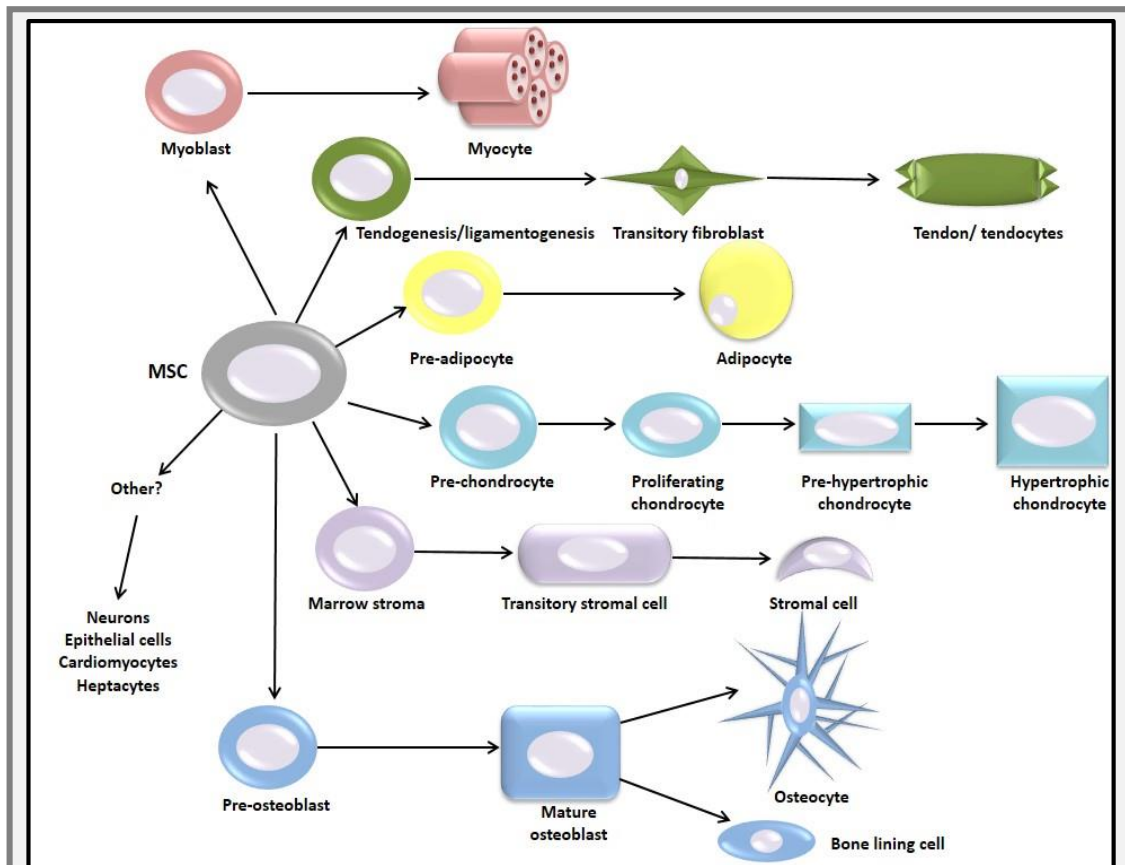


Figure 5.1: Mesenchymal stem cell differentiation. Mesenchymal stem cells differentiate through a series of different lineages to produce myocytes, tendocytes, adipocytes, chondrocytes, stromal cells and osteoblastic cells. In particular, mesenchymal stem cells form preosteoblasts, followed by mature osteoid producing osteoblasts, which differentiate into quiescent bone lining cells or osteocytes. Adapted from Harada and Rodan (234) and Caplan and Bruder (235).

Several transcription factors and cellular pathways have been associated with osteoblast differentiation. Transcription factors of particular importance are runt-related transcription factor-2 (Runx-2) also known as CBF1 α and osterix (Ostx).

Transgenic mice with a deletion for the *Runx-2* gene died shortly after birth and showed signs of dwarfism and an absence of bone formation. Very few osteoblasts were observed in the BM of embryo sections and those present had a flattened appearance with only marginal expression of the osteoblast marker osteopontin (Opn) and an absence of osteocalcin (Ocn) expression (a marker for late stage differentiation) by *in situ* hybridisation (78). This was confirmed also by Otto *et al* (236). Runx-2 also binds to the Ocn promoter, which stimulates late osteoblast

differentiation, and Runx-2 regulation also correlates with the expression of the bone differentiation markers; *Opn*, bone sialoprotein and TGF- β receptor I (237).

Osterix is an important transcription factor for osteoblast differentiation. Over-expression of *Ostx* in osteoblast cell lines C2C12 and C3H10T1/2 resulted in an increase in *collagen type I α I (COL1A1)* and *Ocn* expression. Whereas, when the *Ostx* gene was deleted in transgenic mice, the mice died postnatally and the embryos had a complete lack of mineralisation in the skeleton by alizarin red staining. In addition, *Ostx* null mice had reduced RNA expression of the early differentiation marker *COL1A1*, as well as undetectable *bone sialoprotein*, *osteonectin (On)*, *Opn* and *Ocn* expression. Therefore, demonstrating that both early and late markers of osteoblast differentiation were absent within the *Ostx* null mice. (238).

In addition, several pathways are important for osteoblast differentiation, which include the Wnt, TGF β and BMP pathways.

Osteogenic assays have been developed over approximately the last four decades. Three different primary sources have previously been used (239) including foetal calvarial cells by enzymatic digestion of calvarial bone (240), BM-derived stromal cells isolated from iliac crest aspirates or femoral heads during surgery (241, 242) and trabecular bone explants.

Differentiation has also been mapped over-time and was defined within three stages, as shown in Figure 5.2 (183, 240), using rat calvarial cells.

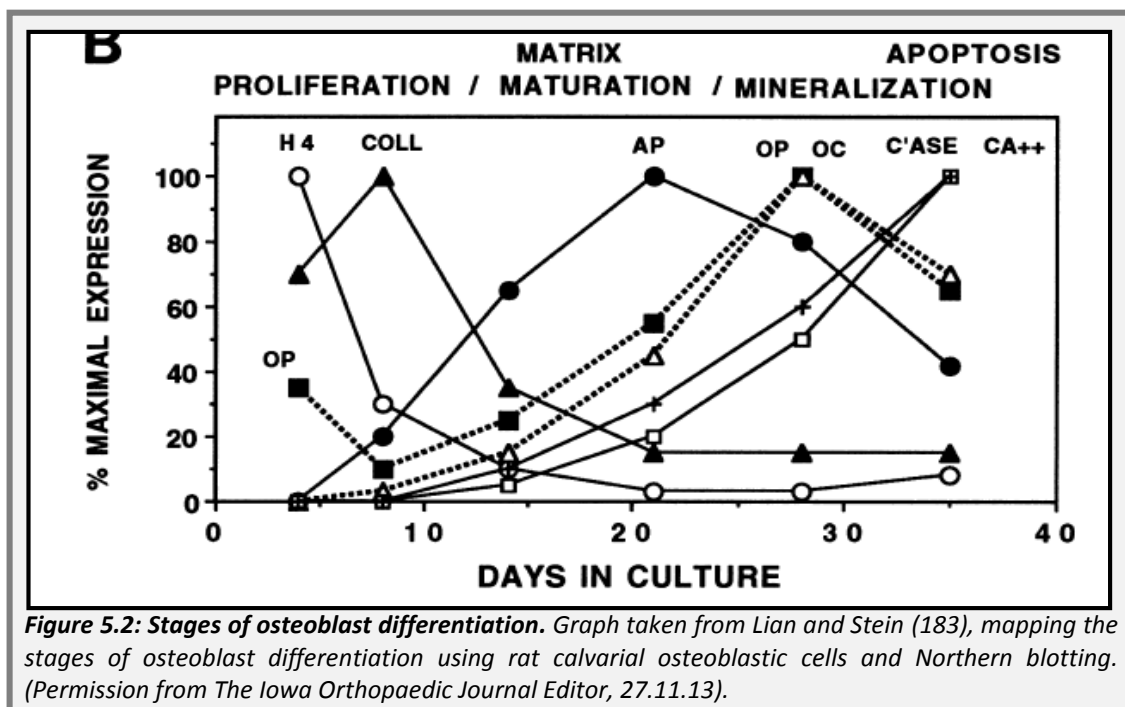
The main stages of differentiation are:

1. **Proliferation:** Genes such as histone genes (H4) (markers of mitosis) are at maximal levels at 5 days of differentiation. Active proliferation results in high

expression of *COL1A1*, *fibronectin* and *TGF-β* at approximately 10-12 days of differentiation.

2. **Proliferation decline:** Proliferation slows from approximately 10 days onwards and shortly afterwards collagen levels also decline at approximately 15-20 days, after which it plateaus and remains at a basal level for the remainder of differentiation. Once collagen reaches basal levels, *Alp* levels reach their maximal at approximately 20 days.

3. **Mineralisation:** Upon mineralisation, the *Alp* levels decline at approximately 28 days but late markers such as *Opn*, *bone sialoprotein* and *Ocn* reach maximal levels. (183, 240). Detection of mineralisation is commonly assessed by alizarin red staining, which binds to calcium deposits, and Von Kossa staining, used to visualise phosphate (239).



To induce osteoblast differentiation, human and rodent MSCs are generally cultured with osteogenic media (OGM) containing 10 mM of β -glycerophosphate (BGP) and

50 µg/ ml of ascorbic acid (asc). Beta-glycerophosphate is the source of phosphate to promote mineralisation whereas asc is responsible for collagen type I assembly (239). The addition of BGP in rat calvarial cultures resulted in the formation of mineral deposits compared to controls cultured in the absence of BGP (243). Bellows *et al* (244) noted that mineralisation increased in a dose dependent manner as the amount of BGP added to the media was increased.

Treatment of MC3T3-E1 cells with 50 µg/ml of asc alone resulted in an increase in *bone sialoprotein*, *Ocn*, *PTH* and *PTHrP* expression, which were not detected in cells cultured in the absence of asc (245). In addition, when BM MSCs were treated with OGM containing BGP, dexamethasone (dex) and increasing amounts of asc, it resulted in an increase in cell proliferation, particularly at 250 µM of asc, and it increased total phosphate and calcium staining particularly at 50 µM asc compared to controls (241). ST-2 cells cultured in asc alone had markedly increased Alp activity compared to those treated only with BGP, reaching maximal levels at 18 days. Ascorbic acid treatment using the ST-2 cells also resulted in increased *Ocn* mRNA expression at day 20 and calcium deposits which reached maximal levels at 75 µg/ml after 24 days (246).

Factors such as glucocorticoids including dex have also previously been used to enhance differentiation. Human MSCs treated with a combination of dex, asc and BGP were highly Alp positive at day 8 of culture and by day 12 a “bone-like material” had formed in the dish and mineralisation was evident (242). Alkaline phosphatase also increased in a dose dependent manner in MSCs, when cultured with BGP, asc and increasing doses of dex. The optimum concentration of dex was 10 mM for Alp and 1000 nM for mineralisation (242). In addition, when dex was administered alone, it resulted in an increase in Alp over-time in BM stromal cells compared to controls in standard media (247). Dexamethasone treatment also induced early expression of *Runx-2*, *Ostx*, *Ocn* and *bone sialoprotein* (248). Continuous combination

treatments of BGP, asc and dex using rat stromal cells isolated from the long bones also resulted in rapid proliferation in the first 24 hours, an increase in Alp production between 7-14 days for cells and *Ocn* expression between 14 and 21 days after treatment (249).

As described above, extensive research has previously been conducted to define the stages of osteoblast differentiation using both human and rodent osteoblastic cells. It is therefore desirable in these experiments to validate an *in vitro* osteoblast differentiation model using mouse calvarial cells which will enable us to investigate the effects of OGM on murine primary OLCs over-time. Specific time points can then be used to determine the effect of differentiation upon the expression of the HSC niche molecules and ligands implicated within a HSC niche and to determine whether MCs selectively adhere to *in vitro* osteoblastic cells at a particular stage of differentiation.

5.2 Hypothesis, aims and objectives

5.2.1 Hypothesis and aims

The aim of these studies was to test the following hypotheses:

1. "Treatment of murine primary osteoblast lineage cells (OLCs) with osteogenic media (OGM) will result in osteoblast differentiation".
2. "Differentiating OLCs express HSC niche molecules and ligands *in vitro*".
3. "Myeloma cells adhere to OLCs at different stages of differentiation *in vitro*".

5.2.2 Objectives

The hypothesis will be tested by the following objectives:

1. To determine whether treatment of murine primary OLCs with OGM results in osteoblast differentiation, tested by assessment of alkaline phosphatase (Alp) production, mineralisation and expression of differentiation bone markers by real-time PCR.
2. To determine whether OLCs express the HSC niche molecules; CXCR4, Notch-1, Tie-2 and N-cad and ligands; CXCL12, Jag-1, Ang-1 over the course of differentiation *in vitro*, using real-time PCR.
3. To establish whether differentiating OLCs adhere to 5TGM1-GFP cells at specified stages of differentiation *in vitro*.

5.3 Methods

5.3.1 Assessment of primary osteoblast lineage cell differentiation

5.3.1.1 Primary osteoblast lineage cell differentiation assay

Murine primary OLCs were isolated and cultured as described in Chapter II Section 2.1.2.7 and 2.2.1.2. Primary OLCs were initially seeded in quadruplicate at a density of 6000 cells/cm² (N=4) and cultured for 3 days before culturing with OGM containing 10 mM of BGP and 50 µg/ml of asc in MEM α -nuc (Day 0). The media was changed every 2-3 days over the course of 28 days.

5.3.1.2 Alkaline phosphatase analysis

Primary OLCs were seeded in quadruplicate into a 96 well plate using 150 µl standard or OGM. Cells were harvested on day 0, 3, 7, 10, 14, 21 and 28. At these time points, cells were lysed using 0.1% triton in PBS and Alp was detected using a PNPP reaction, assessed by spectroscopy using a SpectraMax 5Me plate reader over the course of 90 min and analysed using SoftMax Pro 5.2 software as described in Chapter II, Section 2.5.1.2. This was followed by DNA concentration determination using the

Invitrogen PicoGreen® reagent followed by fluorescent spectroscopy using the SpectraMax 5Me plate reader and analysed using SoftMax Pro 5.2 software as described in Chapter II, Section 2.5.1.3. This was used to normalise Alp production, the calculations for which are shown in Appendix 2, Section 2.8, Table 2.6. Results were based upon four independent experiments (N=4).

5.3.1.3 Mineralisation analysis

Primary OLCs were seeded in quadruplicate into a 12 well plate in 1 ml OGM. Mineralisation was determined on day 7, 14, 21 and 28 by alizarin red staining as described in Chapter II, Section 2.5.2.1. Plates were scanned using an Epson 4990 scanner and analysed using ImageJ software. Results were based upon four independent experiments (N=4).

5.3.1.4 Gene expression analysis by real-time PCR

Primary OLCs were seeded in quadruplicate into a T25 flask using 7 ml OGM. Primary OLCs were harvested at 7, 14, 21 and 28 days for gene expression analysis. Ribonucleic acid was extracted, cDNA was synthesised and real-time PCR was conducted (as described in Chapter II, Section 2.3.1.1, 2.3.2.1 and 2.3.5.2) to determine the expression of differentiation markers (*COL1A1* and *Runx-2*) and the HSC niche molecules and ligands. Data was analysed using the comparative $\Delta\Delta C_t$ method, by normalisation to $\beta 2M$. Data was expressed as a fold change of gene expression using the week 1 data as the comparator. Results were based upon four independent experiments (N=4).

5.3.2 Assessment of 5TGM1-GFP adhesion to primary osteoblast lineage cells at different stages of differentiation

5.3.2.1 Co-culture assessment

Primary OLCs were differentiated for 3, 14 and 28 days in OGM, after which 5×10^4 5TGM1-GFP cells were seeded onto the murine primary OLCs for 1 and 6 hours. The number of 5TGM1-GFP cells adhering to the primary OLCs was assessed by fluorescent microscopy using a Leica AF6000LX microscope, followed by quantification using Volocity software. Results were based upon four independent experiments (N=4).

5.3.3 Statistics

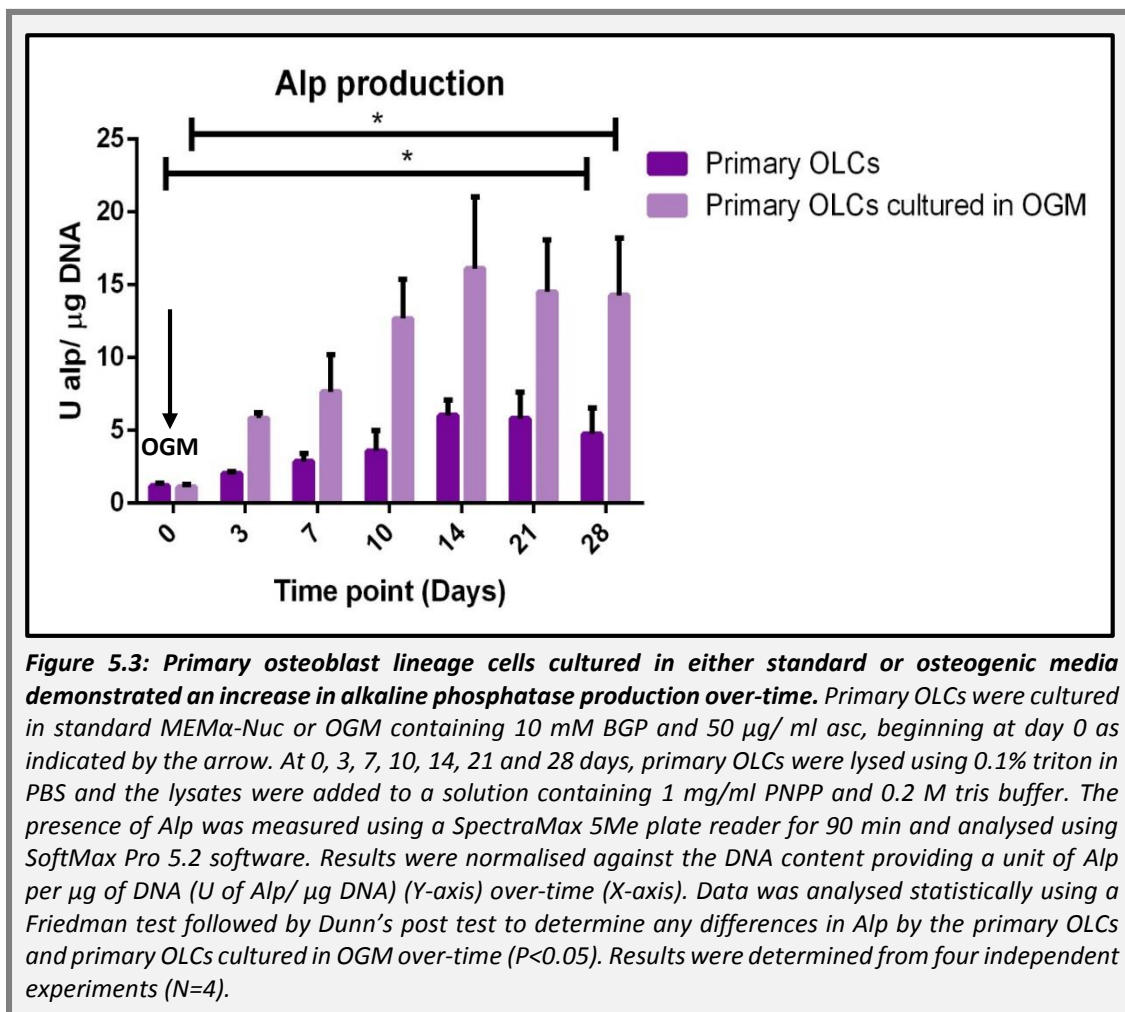
Where relevant, non-parametric statistical tests were used. A Friedman test followed by Dunn's post test ($P < 0.05$) was used to compare Alp production, DNA content, mineralisation, gene expression as well as 5TGM1-GFP cell adhesion to osteoblastic cells. In addition, a Wilcoxon Matched pairs signed rank test ($P < 0.05$) was used to determine differences in the adhesion of 5TGM1-GFP cells to primary OLCs after 1 and 6 hours. As a non-parametric paired two-way statistical test was unavailable, differences in the Alp production and DNA content between the primary OLCs cultured in standard and OGM media over-time was unable to be conducted. Where relevant, error bars were displayed on all graphs using the SEM, unless stated otherwise in the legend.

5.4 Results

5.4.1 Alkaline phosphatase production by primary osteoblast lineage cells cultured in standard or osteogenic media over-time

Figure 5.3 demonstrates the differences in Alp production between primary OLCs cultured in standard media and OGM over-time. From the graph, it is clear that Alp

production increased in the primary OLCs cultured in standard media as well as OGM until 14 days, after which Alp production reduced. Using a Friedman test followed by Dunn's post test, the changes in Alp production over-time were significant for both the sets of samples ($P < 0.05$) however, the Dunn's post test did not identify at which time points significant differences in Alp were apparent. It was also clear that Alp production was higher at each time-point in the OGM treated primary OLCs compared to the primary OLCs.



5.4.2 DNA content of primary osteoblast lineage cells cultured in standard or osteogenic media over-time

Figure 5.4 demonstrates the DNA content of the primary OLC samples cultured in standard media and OGM. From the graph, it is clear that as time progressed the

amount of DNA in both the primary OLC samples and primary OLCs cultured in OGM samples increased. Therefore, as this was used as a surrogate for cell counts, we can surmise that the number of cells increased over-time. Statistically, this increase was significant between days 0 and 28 for both the primary OLCs and primary OLCs cultured in OGM ($P < 0.05$). Interestingly from 7 days onwards the DNA content in the primary OLCs cultured in OGM was lower compared to the OLCs cultured in standard media, thus implying that proliferation in these cells may have decreased due to the addition of BG and Asc. This however, was not assessed statistically due to a lack of appropriate test.

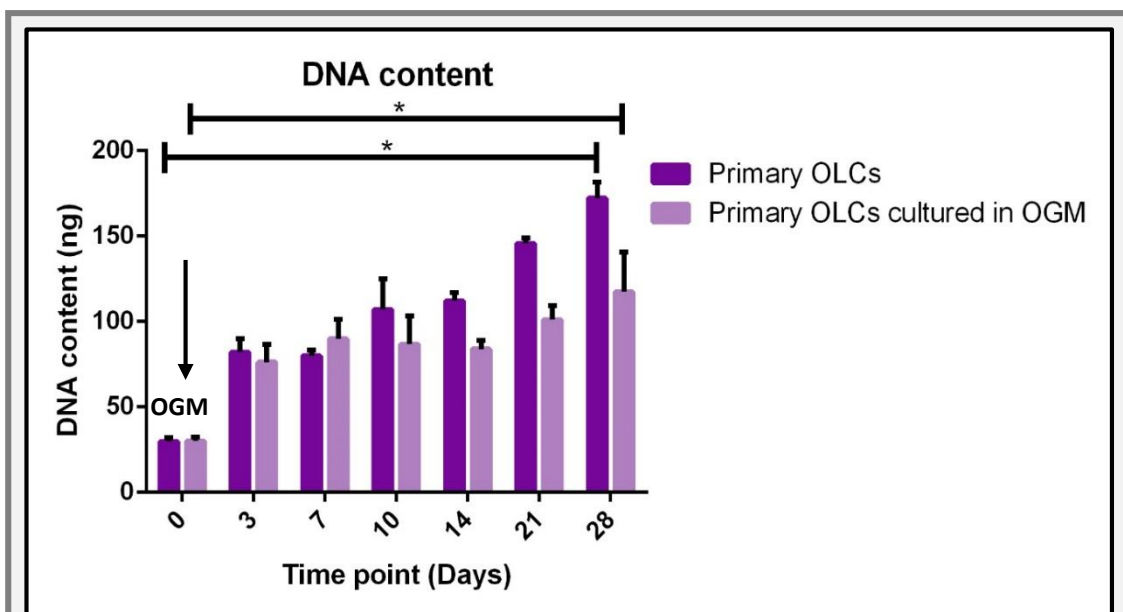
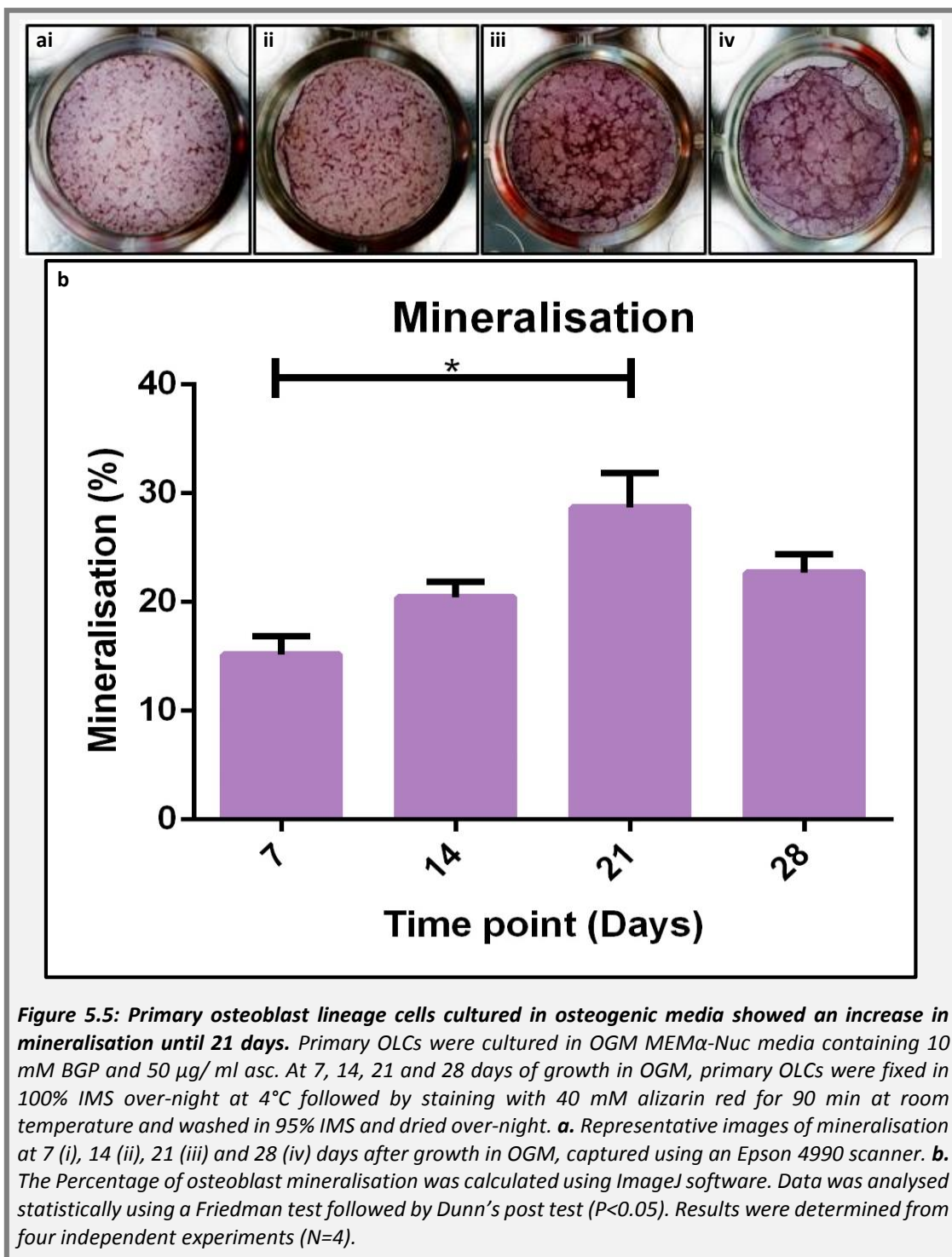


Figure 5.4: Primary osteoblast lineage cells cultured in osteogenic media demonstrated a reduction in proliferation over 28 days, assessed by DNA quantification. Primary OLCs were cultured in standard MEM α -Nuc or OGM MEM α -Nuc media containing 10 mM BGP and 50 μ g/ml asc, beginning at day 0 as indicated by the arrow. After 0, 3, 7, 10, 14, 21 and 28 days, primary OLCs were lysed using 0.1% triton in PBS and the DNA content was measured using the PicoGreen[®] reagent. The DNA present was measured by fluorescence using a SpectraMax 5Me plate reader. Results were calculated by extrapolation from a standard curve of known amounts of DNA (ng). Data was analysed statistically using a Friedman test followed by Dunn's post test ($P < 0.05$) to determine differences in DNA content over-time. Results were determined from four independent experiments ($N=4$)

5.4.3 Mineralisation of primary osteoblast lineage cells cultured in osteogenic media over-time

Mineralisation was quantified in the primary OLCs cultured in OGM over-time, as shown in Figure 5.5. Figure 5.5a demonstrates representative images of mineralisation, where mineralisation was visualised as small red nodules stained positive with alizarin red. Figure 5.5b shows the percentage of mineralisation, demonstrating a significant increase in the percentage of mineralisation between 7 and 21 days ($P < 0.01$) of OGM.



5.4.4 Gene expression of osteoblast differentiation markers and HSC niche molecules and ligands by primary osteoblast lineage cells cultured in osteogenic media over-time

Table 5.1 shows the Ct values generated using real-time PCR to determine the expression of the osteoblast differentiation markers *COL1A1* and *Runx-2*, and HSC niche molecules and ligands by primary OLCs cultured in OGM.

Table 5.1: A summary of the quantitative analysis for the absolute real-time PCR gene expression of the osteoblast differentiation markers, HSC niche molecules and ligands by primary osteoblast lineage cells cultured in osteogenic media over-time

Gene	7 days	14 days	21 days	28 days
<i>COL1A1</i>	18.11 ± 0.56	18.72 ± 0.50	18.84 ± 0.21	19.11 ± 0.16
<i>Runx-2</i>	24.16 ± 0.26	24.08 ± 0.38	23.80 ± 0.52	23.90 ± 0.45
<i>CXCR4</i>	33.25 ± 1.30	32.31 ± 0.17	31.10 ± 0.68	32.10 ± 0.56
<i>Notch-1</i>	26.12 ± 0.42	26.31 ± 0.52	26.01 ± 0.55	26.15 ± 0.52
<i>Tie-2</i>	28.53 ± 1.13	29.24 ± 1.43	28.59 ± 1.07	29.46 ± 1.25
<i>N-cad</i>	25.26 ± 0.20	25.42 ± 0.47	24.83 ± 0.25	25.97 ± 0.61
<i>CXCL12</i>	21.51 ± 1.08	22.55 ± 0.83	22.06 ± 0.98	21.52 ± 1.09
<i>Jag-1</i>	25.02 ± 0.25	25.93 ± 0.54	25.35 ± 0.35	25.95 ± 0.42
<i>Ang-1</i>	26.04 ± 0.42	26.74 ± 0.78	26.11 ± 0.47	25.95 ± 0.42

Mean Ct values ± SEM

Figure 5.6 demonstrates the results graphically using the fold change and percentage of gene expression above the columns using the comparative $\Delta\Delta\text{Ct}$ method, using Day 7 as the comparator. *CXCR4* was not shown graphically as the $\Delta\Delta\text{Ct}$ method of analysis could not be used, as some of the Ct values were undetermined (UD). The differentiation markers *COL1A1* and *Runx-2* were both highly expressed by the primary OLCs at each time point and *COL1A1* had the greatest expression. Over-time, *COL1A1* expression declined, although this change did not reach significance, whereas, *Runx-2* expression was stable across the time course. All of the HSC niche molecules were also expressed by the OLCs, though *CXCR4* expression was inconsistent across the time course, as some samples were UD. *Notch-1* and *N-cad* were highly expressed, whereas *Tie-2* and *CXCR4* were expressed at lower levels. The ligands *CXCL12*, *Jag-1* and *Ang-1* were also expressed by the primary OLCs at each

time point and CXCL12 was expressed at a higher level compared to both *Jag-1* and *Ang-1*. Statistically, there were no significant differences in the expression of the HSC niche molecules or ligands over-time in the primary OLCs cultured with OGM. In addition, no apparent trends in the gene expression of the HSC niche molecules and ligands were observed over the time course with the exception of *Jag-1* and *N-cad*, which decreased over-time.

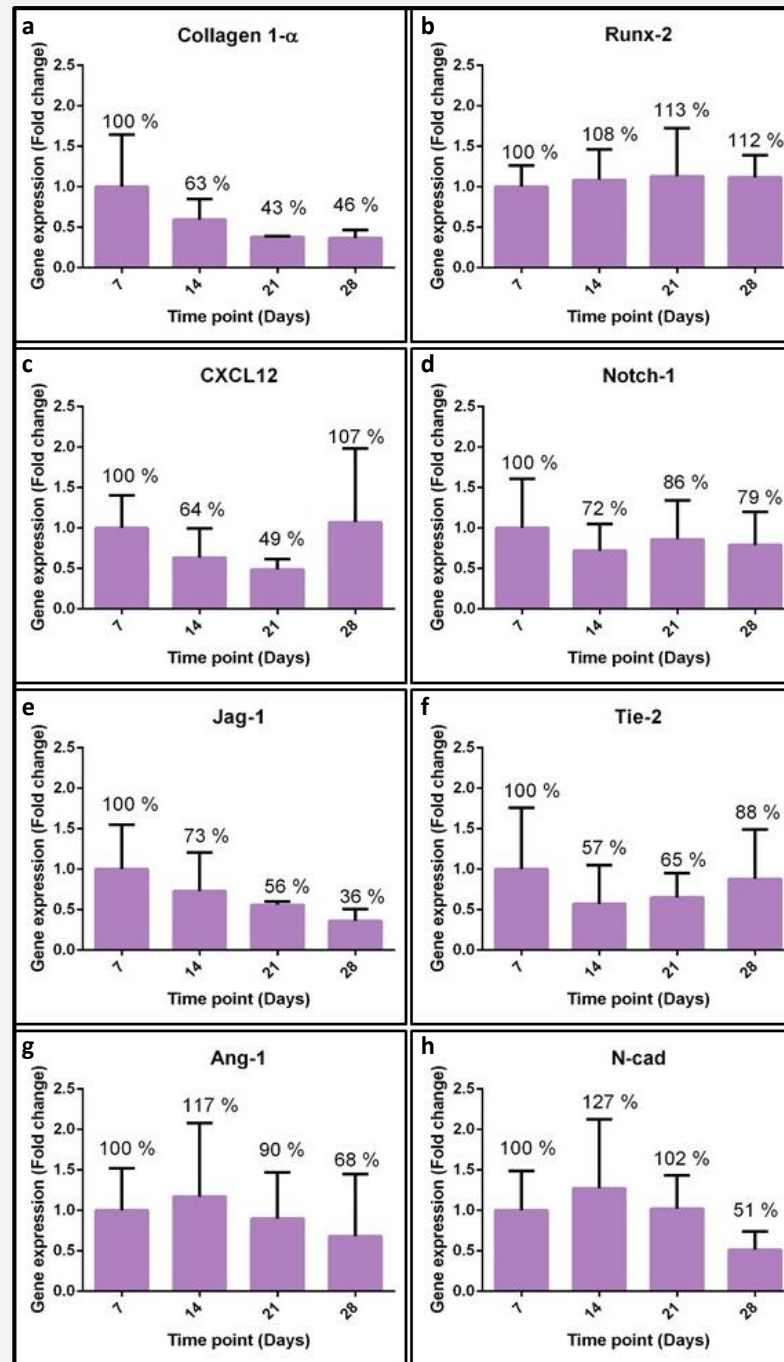
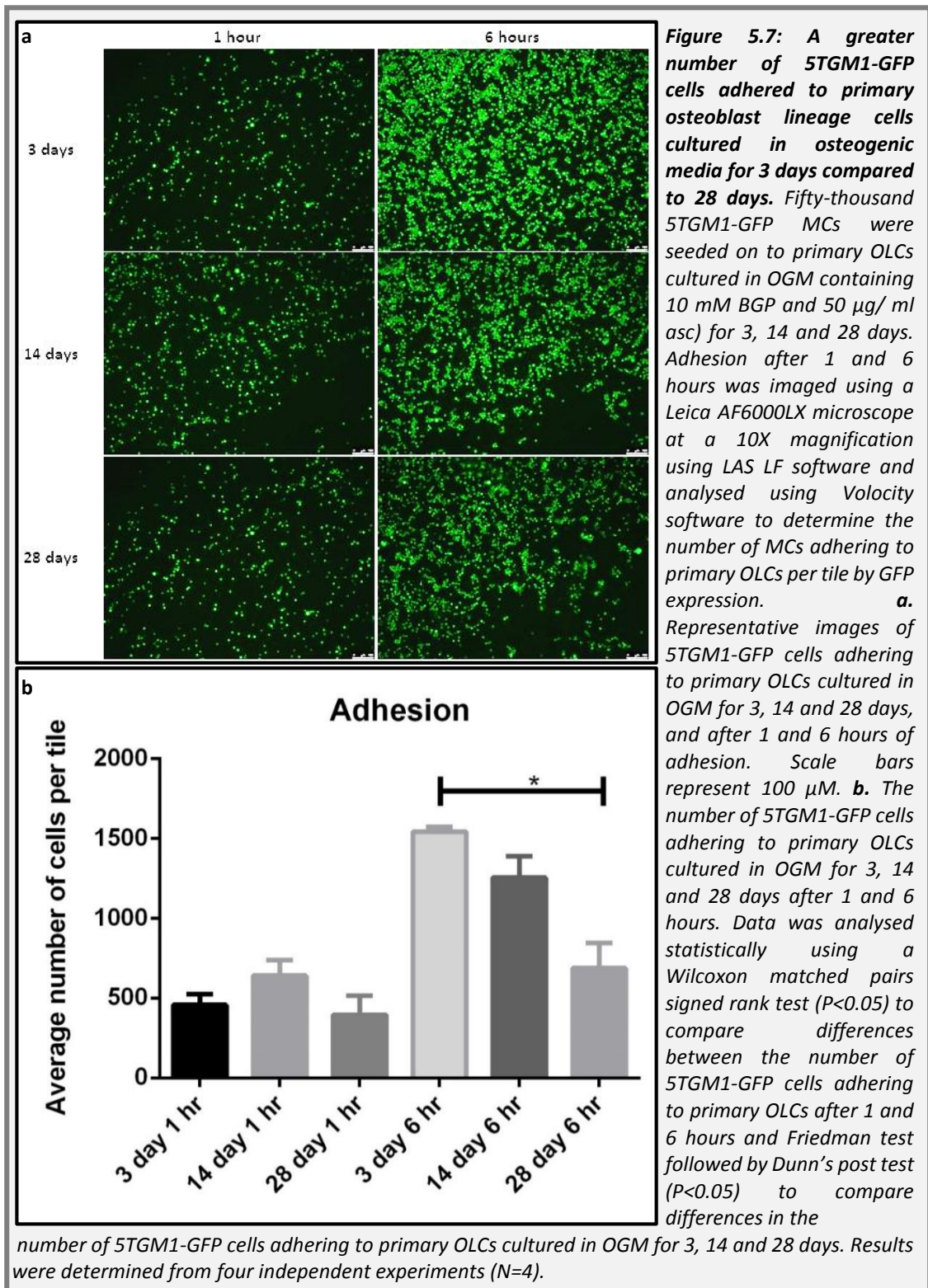


Figure 5.6: There were no significant changes in the gene expression of bone and HSC niche markers over-time by primary osteoblast lineage cells cultured in osteogenic media over 28 days. Primary OLCs were cultured in OGM containing 10 mM BGP and 50 μ g/ml asc. At 7, 14, 21 and 28 days, RNA was extracted, cDNA was synthesised and real-time PCR reactions were run using approximately 40 ng (2 μ l) of RT+ cDNA samples. An equal volume of RT- and H₂O control samples were used to assess genomic and reagent contamination. Real-time PCR reactions were run using an Applied Biosystems' 7900HT Real-Time PCR machine and Applied Biosystems' recommended settings. Data was analysed using the comparative $\Delta\Delta$ Ct method and shown graphically using the fold change, and the percentage of gene expression is shown above the columns for collagen-1 α (a), Runx-2 (b) CXCR4 (c), CXCL12 (d), Notch-1 (e), Tie-2 (f), Ang-1 (g) and N-cad (h). Data was analysed statistically using a Friedman test followed by Dunn's post test. Results were determined from four independent experiments (N=4).

5.4.5 Adhesion of 5TGM1-GFP cells to primary osteoblast lineage cells cultured in osteogenic media

Figure 5.7a demonstrates representative images showing the adhesion of 5TGM1-GFP cells to osteoblastic cells at the different time-points. Figure 5.7b shows the differences in the number of 5TGM1-GFP cells adhering to primary OLCs cultured in OGM for 7, 14 and 28 days after 1 and 6 hours. From the data, there seemed to be an increase in the number of 5TGM1-GFP cells adhering to the primary OLCs at 6 hours compared to 1 hour at each of the differentiation time points however, using a Wilcoxon matched pairs signed rank test this difference did not reach significance. When the number of 5TGM1-GFP cells adhering to the primary OLCs cultured in OGM over-time were compared there was a decrease in the number of 5TGM1-GFP cells adhering to primary OLCs cultured in OGM for 28 days compared to 3 days however, this was only significant at the 6 hour time point ($P < 0.05$).



5.5 Discussion

The aim of these experiments was to firstly, validate an in-house model to differentiate murine primary OLCs *in vitro* and secondly to use this system to determine whether changes in HSC niche molecules and ligand expression occurred at the different stages of differentiation and whether MCs adhered to a specific type of osteoblast *in vitro*, at a specific stage of differentiation.

Firstly, Alp levels were established using the PNPP assay. Alkaline phosphatase is an enzyme, which is bound to the surface of osteoblasts by a phosphoinositol bond and is also found within the bone matrix. It is thought to act by removing inhibitors of hydroxyapatite crystal growth and also by increasing concentrations of phosphorus at the site of bone formation, to increase bone mineralisation (232). Therefore, Alp production increases before mineralisation occurs.

In these experiments, murine primary OLCs were cultured with either standard MEM α -nuc or OGM. In both groups, there was an increase in Alp production until day 14 post treatment. However, this was to a lesser extent in the cells cultured in standard media compared to OGM. The increase in Alp over-time was also significant based on the Friedman statistical test however; a Dunn's post test was unable to identify the specific time points, which were significantly different. This may be due to the high variability of the results in these experiments. The variability seemed to be a result of the first two and latter two experiments being conducted using two separate isolates of calvarial osteoblasts. Therefore, there seems to be high variability between different batches of isolated osteoblasts and for future studies, it would be desirable to use cells from the same batch. This variability may be unsurprising as previous experiments have experienced variability even within

osteoblastic cell lines where sub-clones of MC3T3-E1 cells expressed different amounts of Alp, Ocn and bone sialoprotein when differentiated (245).

When comparing the pattern of Alp production over-time this varied slightly from results in the literature. Lian and Stein *et al* (240) and Lynch *et al* (250) reported maximal Alp production at 19-20 days of differentiation using rat calvarial osteoblasts, whereas, Alp peaked earlier at 14 days in these experiments. However, the results in this chapter seemed more so similar to differentiation experiments using rat stromal cells or MSCs, which demonstrated maximal Alp production between 14-21 days and 8-12 days respectively (242, 249).

It is also difficult to determine whether previous experiments support the raw Alp values seen in these experiments, as early experiments mainly use Alp staining and studies that do use PNPP biochemical staining generally normalise to mg of protein rather than DNA, therefore, they are not directly comparable. However, a recent paper by Wang *et al* (187) demonstrated levels of 0.8 Units of Alp production per μg of DNA after 7 days of culture in standard media using C57BL/6 murine calvarial osteoblasts, which was slightly lower but similar to the values calculated in the studies in this Chapter.

The presence of Alp and an increase in Alp over-time in osteoblastic cells cultured in standard media has also been described in previous experiments. Jaiswal *et al* (242) described how MSCs cultured in standard media, which didn't contain BGP and asc, produced Alp, though not to the extent of media containing BGP and asc. In addition, the type of media used also affected basal levels of Alp, where MSCs cultured in DMEM had the lowest basal levels whereas, cells cultured in MEM α had the highest (242).

In the experiments in this chapter, the statistical difference in the Alp produced by the cells cultured in OGM and standard media over-time could not be performed due to a lack of non-parametric paired two-way test, however from the graphs it is clear that the OGM cultured cells do produce higher Alp. Therefore, it can be concluded that the OGM is causing an increase in Alp production, and potentially inducing osteoblast differentiation.

Cell proliferation was also investigated in primary OLCs cultured with standard media and OGM. The concentration of DNA increased over-time significantly for both cell types from day 0 to day 28. However, again as a suitable test was unavailable to compare the two cell types it was difficult to confirm the differences in proliferation between cells culture in OGM compared to those cultured in standard media. However, by the patterns shown in the graphs it seemed that the OGM cultured cells had a lower DNA content than those cultured in standard media from 10 days onwards. Therefore, proliferation may be decreased in the OGM cultured cells. This is supported by studies conducted by Lian and Stein *et al* (240) who previously reported an initial increase in proliferation by histone determination in rat calvarial osteoblasts between days 5-10, which then reduced and plateaued for the remainder of the differentiation period examined, also reported by Choi *et al* (251) using MC3T3-E1 cells. However, experiments using human MSCs differentiated in OGM containing dex actually showed an increase in proliferation when measured by crystal violet staining of DNA (242). Therefore, the way in which proliferation is measured may provide a difference in determining whether proliferation remains active. Lynch *et al* (250) used fluorometric analysis of DNA from rat calvarial osteoblasts cultured in OGM and found an increase in DNA up to 21 days, supporting Jaiswal *et al* (242). Interestingly, in the same experiment, histone 4 was decreased from 5 days onwards, supporting Lian and Stein *et al* (240). In addition, the amount of FBS used in the culture may also affect proliferation rates. Previous papers have shown that some osteoblastic cells such as the cell line SAOS-2 are cultured in FBS at concentrations as

low as 0.5% (252), which slows proliferation and induces Alp production and mineralisation.

Mineralisation is a later marker of osteoblast differentiation, associated with a down-regulation of Alp and an up-regulation of Ocn, Opn and On (183, 240). Mineralisation in the experiments in this chapter occurred from the beginning of OGM treatment and peaked at 21 days. Therefore, mineralisation occurred earlier than previous reports, which showed mineralisation in rat calvarial osteoblastic cells and human osteoblastic cells at approximately 28 days onwards (183, 253). In addition, mineralisation usually begins when Alp decreases but mineralisation in these experiments continued to increase as Alp increased until 14 days. In support of my data, Nefussi *et al* (254) found that rat calvarial osteoblastic cells cultured in the presence of BGP demonstrated mineralisation within 14 days. One potential explanation for early mineralisation by the OLCs in these experiments is due to high basal levels of Alp present in the cells due to the type of media used and also, standard media contains phosphate which, combined with Alp, may stimulate immediate mineralisation (239).

In addition, inconsistencies in the literature as well as between my data and previous studies may again be due to the variability between samples and the heterogeneous nature of the cells. In addition, other groups have found that BGP may not be the best source of phosphate for mineralisation and Gartland *et al* (252) found that inorganic phosphate was more suitable. In addition, it is also difficult to conclude the effect of OGM on mineralisation as a standard media without BGP and asc control group was not used as a comparator in these experiments. The addition of this control would have provided evidence of basal levels of mineralisation in the presence of pre-existing phosphate in the media and therefore, the actual level of mineralisation due to OGM could have been assessed.

Real-time PCR was conducted to determine the gene expression of the differentiation markers *COL1A1* and *Runx-2* in primary OLCs cultured in OGM over-time. There were no significant differences in *COL1A1* and *Runx-2* expression over-time although; there was a slight decrease in *COL1A1* expression. At each time point, *COL1A1* expression was extremely high implying that the primary OLCs were secreting high amounts of collagen protein to begin with. Lian and Stein *et al* (183) previously described high *COL1A1* expression in the early time points of differentiation, which drastically dropped after 12 days in rat calvarial osteoblasts. This was supported by Choi *et al* (251) using MC3T3-E1 cells whereby *COL1A1* expression was highest between 10-15 days and reduced significantly after 15 days. Therefore, these results coincide with the maximal expression of *COL1A1* in the murine primary OLCs observed at 7 and 14 days. However, the drop after the maximal expression of *COL1A1* was not significant but a longer period of differentiation may be required to detect a further reduction in the future.

Runx-2 is an early marker of differentiation and its expression has been observed in a variety of primary OLCs at different stages as well as in MSCs. In the experiments in this chapter, *Runx-2* was expressed by the primary OLCs at each time point but there was also no significant difference between *Runx-2* expression over time. This is consistent with previous studies which found that the *Runx-2* isoform II mRNA was constitutively expressed by the human stromal cell line hMS2-15 when treated with BGP, asc and dex over a 14 day period, whereas, the isoform I was not expressed at all (255). Another study determined the expression of *Runx-2* in a variety of stromal and osteoblastic cells, which included “non-osteoblastic”; Cos-7, NIH3T3 and C3H10T1/2 cells, immature osteoblastic; ST-2 and MC3T3-E1 cells and mature osteoblastic; Ros 17/2.8, FRC, SaOS-2 and U2OS cells. Each cell type expressed the RNA (assessed by Northern blot) for *Runx-2* isoform I and both immature and mature osteoblastic cells expressed *Runx-2* isoform II, whereas the RNA from the non-osteoblastic cells for *Runx-2* isoform II was negative. In contrast, using PCR the mRNA from the non-osteoblastic cells was positive for *Runx-2* isoform II. The protein

expression was also different from the RNA and mRNA results where only the mature osteoblastic cells and the ROS 17/2.8 cells were positive for each isoform, whereas the immature osteoblastic cells were negative (256). This therefore, demonstrates the complexities of using *Runx-2* as a marker for osteoblast differentiation and it is difficult to determine whether *Runx-2* expression does differ over the course of differentiation due to the different isoforms and inconsistencies in RNA, mRNA and protein expression.

To assess differences in the expression of HSC niche molecules and ligands by OGM treated primary OLCs, real-time PCR was used. Interestingly, the murine primary OLCs expressed *CXCR4* at each time-point however; this was inconsistent as some values were UD between the different experiments. This was particularly interesting as previous experiments have focused upon the expression of its ligand *CXCL12*, shown to be expressed on endosteal osteoblasts, vessels and reticular cells *in vivo* (82, 196), and little emphasis has been placed on *CXCR4* expression by osteoblasts. A study by Ponomaryov *et al* (111) demonstrated low expression of *CXCR4* by MBA-15 and BM stromal cells. In the studies in this chapter, there was no difference in the expression of *CXCR4* over-time when treated with OGM, but this may be due to the heterogeneous nature of primary OLCs.

CXCL12 was also shown to be expressed by murine primary OLCs at each time point of OGM treatment and was surprisingly high. Expression of *CXCL12* by murine osteoblasts is consistent with previous experiments which demonstrated the expression of *CXCL12* by the BM stroma and endosteal osteoblasts *in vivo* (82, 111). There were no significant differences in the expression of *CXCL12* over-time implying that OGM treatment did not influence its expression. Interestingly, previous papers have categorised *CXCL12* expressing osteoblasts as immature osteoblastic cells opposed to mature osteoblasts (111). This is supported by studies, which have compared the levels of *CXCL12* between MG-63 and SAOS-2 cells. Previous studies

reported that SAOS-2 cells were more mature with high mineralisation compared to the MG63 cells which were described as immature and heterogeneous (196, 257). When the CXCL12 levels were compared, the more mature SaOS-2 cells had lower expression of CXCL12 compared to the immature MG-63 cells (111, 258). In addition, Jung *et al* (196) demonstrated that human osteoblastic cells, MG63 cells, BM stromal cells and MC3T3-E1 cells secreted SDF-1 in the early time points of differentiation (detected by enzyme-linked immunosorbent assay in conditioned media) and production of SDF-1 decreased over the time course, again highlighting that SDF-1 is produced in the early stages of osteoblastic differentiation. With regards to the experiments in this chapter, it may seem that the osteoblastic population used was still quite heterogeneous, particularly as *CXCL12* expression decreased after 7 days and then reached maximal levels at 28 days. In addition, only mRNA was detected therefore, protein production may have provided different results.

Notch-1 expression, was expressed by MC3T3-E1 osteoblastic cells (200), C3H10T1/2 and C2C12 cell lines and murine undifferentiated primary OLCs (216), therefore, *Notch-1* may be more prevalent in preosteoblastic cells rather than mature osteoblasts. *Notch-1* expression in the experiments in this chapter was detected in osteoblasts at all time-points and no significant changes in *Notch-1* expression over-time were observed. *Notch-1* expression did however, slightly decrease after 7 days but this was variable. If the experiment was conducted for a longer period, a further decrease may have been observed.

Jag-1 was expressed at similar levels to *Notch-1* at all time-points. *Jag-1* expression has been determined in a variety of different osteoblastic cells including MC3T3-1 E1 (200), BM stromal cells *in vitro* (199) and osteoblastic cells *in vivo* (82, 259). *Jag-1* expression levels by osteoblastic cells has not been associated with osteoblast differentiation states. Although, stromal cells and MC3T3-E1 cells are usually classed as immature osteoblasts or preosteoblasts, therefore, this correlates with the trend

observed whereby *Jag-1* expression decreased from 7 days onwards in the experiments in this chapter.

Tie-2 was expressed by the primary OLCs at each time-point. Its expression was particularly low and did not change over-time. *Tie-2* is typically a marker of ECs and has not been a key focus in osteoblastic cells. However, low expression of *Tie-2* was determined in MC3T3-E1 cells, murine primary OLCs, ST-stromal cells, C2C12 and C3H10T1/2 cells (202). Overall *Tie-2* expression was higher in the C3H10T1/2 cells (202), which may imply that *Tie-2* may be more prevalent in early mesenchymal progenitor cells, rather than immature or mature osteoblastic cells. However, this was contradicted in studies using primary osteoblastic cells and C2C12 cells, which seemed to demonstrate increased expression of *Tie-2* following three days of culture in OGM, therefore, *Tie-2* is present at higher levels in more differentiated cells in this instance (202). However, in the experiments in this chapter, no pattern of *Tie-2* expression was observed across the time course of differentiation, but again this could be due to the heterogeneity in the population.

Ang-1 was expressed over-time at similar levels to *Notch-1*, *Jag-1* and *N-cad*. Jeong *et al* (202) demonstrated an initial increase in *Ang-1* expression within the first three days of primary murine osteoblastic cell differentiation compared to day 0 and this was then maintained at the same level for a further 25 days. In these experiments, differences in *Ang-1* expression may not have been determined, as 7 days was the earliest time point used and any increase in *Ang-1* expression may have already occurred.

N-cad was expressed by the primary OLCs over-time. After 14 days of differentiation *N-cad* expression seemed to decrease however, this did not reach significance. *N-cad* was previously reported to be expressed by a variety of different MSC lineage cells

such as MC3T3-E1 cells, C3H10T1/2, ST-stromal cells, ATDC5 chondrogenic cells, NIH3T3 fibroblast cells (218) and KS483 osteoblastic cells (206). However, the effect of differentiation upon N-cad is currently unclear. Greenbaum *et al* (260) demonstrated expression of *N-cad* by primary murine osteoblastic cells which diminished following 15 days of differentiation whereas, Ferrari *et al* (219) demonstrated an increase in *N-cad* expression as SaOS-2 cells were differentiated over the course of 4 days. It is therefore, difficult to ascertain whether *N-cad* expression would increase upon differentiation stimuli. In the experiments in this chapter, no significant difference in *N-cad* expression was found over-time with OGM treatment. However, after 14 days there was a decrease in N-cad expression and again if the experiment was continued for a longer period, further declines may have been observed, correlating with the experiments conducted by Greenbaum *et al* (260).

Again, as these experiments lacked the suitable control of OLCs cultured in standard medium as a comparator at each of the times points it is difficult to draw substantial conclusions. For example, *Col1 α* and *Runx-2* levels did not significantly change over-time however; the levels of these may be significantly increased or decreased in OLCs cultured in OGM compared to OLCs cultured in control media, and similarly, the levels of HSC niche molecules and ligands may also be have significantly different between differentiating and non-differentiating OLCs. However, without the suitable non-OGM controls the actual effect of OGM and therefore differentiation upon bone marker or HSC niche molecule or ligand expression was unable to be suitably tested.

The adhesion of MCs to osteoblastic cells after treatment with OGM was then determined. A higher number of 5TGM1-GFP cells adhered to the primary OLCs after 6 hours compared to 1 hour although, this did not reach significance. In addition, significantly more MCs adhered to primary OLCs treated with OGM for 3 days compared to 28 days after 6 hours. This was quite interesting as it implies that MCs,

like HSCs, seem to preferentially adhere to osteoblastic cells in the early stages of differentiation, which is supported by Zhang *et al* (83) and Xie *et al* (84) when defining osteoblastic cells in the HSC niche. These results may also imply that the factors potentially responsible for this adhesion are not the HSC niche molecules or ligands described in this thesis, as no differences in their expression was seen over-time. However, as the day 3 time-point was not assessed by real-time PCR and as the standard media controls were not used, this cannot be completely concluded.

There are several disadvantages related to subjectivity using this adhesion technique that need to be noted. Firstly, washing the cells can severely affect the results, as washing the cells with slightly different forces may either detach or retain adhesion. In addition, results may be subjective as only 5 out of a 25 tile area were imaged, which was particularly subjective as the majority of cells were found around the edges of the wells compared to the centre, despite this, the same areas were imaged in each well. Also at 28 days, the primary OLCs had begun to detach at the edges of the wells, resulting in less area for the cells to adhere to, which may have also influenced the results. Mineralisation may have also interfered with MC adhesion, which was greatest at 21 days and again this could have provided less area for the cells to adhere to. In addition, it may also have been desirable to examine the effect of using PBS compared to media. PBS was previously used when investigating the adhesion of HSCs and osteoblastic cells (261) for a short adhesion time of 15 min, although 6 hours may be too long a time for MCs to survive in PBS as they have a short life span when not in media.

Survey of the literature did not provide a standardised time for the adhesion assays. Some experiments used 20 min (206), 2 hours, (262), 4 hours (263) or 6 hours (42). Therefore, an early (1 hour) and late (6 hours) time point was chosen. However, in retrospect, it may have been more desirable to look at the adhesion within the first 15 min, which could capture early simple associations and possibly even later than 6

hours such as 12 or 24 hours, which could potentially detect more complex interactions involving gene expression in interacting cells. In addition, the number of cells plated onto osteoblasts varied. Some studies used 1×10^5 (206, 261) and 5×10^6 /ml (263) in a 96 well plate. However, in these experiments 5×10^4 cells were used, as the 96 well plates did not have the capacity for greater numbers than this.

In conclusion, I have validated a model for the differentiation of murine primary OLCS *in vitro*. Some of the characteristics were similar to what has been previously reported using rat calvarial cells, BM stromal cells and osteoblastic cells however, there were also some inconsistencies particularly with respect to the mineralisation time points and peak expression of collagen. Treatment with OGM did not affect the expression of HSC molecules or ligands but despite this, MCs adhered highly to primary OLCS in the early time points of OGM treatment. Therefore, this may imply that other molecules besides the HSC niche molecules and ligands investigated here are important with regards to MC adhesion to osteoblasts, though as stated previous this isn't conclusive due to a lack of standard media controls.

Further research is now required to explore differences in the expression of other adhesion molecules using this system and also to further optimise the adhesion experiments. The assays used to determine the differentiation state of the BM cultures were population based and it would be have been helpful to assess differentiation in a per cell basis to determine the maturity of interacting cells. This was however beyond the scope of the present study, but should be considered in future studies.

**Chapter VI: The effect of knocking down HSC niche
molecules in myeloma cells upon adhesion to
osteoblast lineage cells *in vitro* and tumour burden *in*
*vivo***

6.1 Introduction

In the studies described in Chapter III-V, I determined the expression of several HSC niche molecules by the 5T33MMvt and 5TGM1-GFP cells. These studies collectively showed that MCs produced the HSC niche molecules CXCR4, Notch-1, Tie-2 and N-cad and the ligands CXCL12 and Jag-1. Expression of these molecules by MCs has previously been reported in the literature; however, the role of these molecules in a myeloma osteoblastic niche is yet to be determined.

Previous preclinical studies have shown the importance of the CXCR4/CXCL12 axis for its role in the mobilisation of CXCR4 positive HSCs (94, 112) and various cancer cells including prostate (258, 264), breast (265, 266) and MCs (170, 194) towards a high concentration gradient of CXCL12 *in vitro* and *in vivo*. In MM, *in vitro* transwell experiments showed that 5T2MM and 5T33MM cells specifically migrated towards fibroblast conditioned media containing CXCL12 and recombinant CXCL12. This was significantly inhibited using the peptide antagonist 4F-benzoyl-TN14003 (170). These observations were also supported by studies using human MC lines and primary patient samples, where recombinant CXCL12 or conditioned media induced chemotaxis (193, 194, 221) which was blocked by an anti-CXCR4 inhibitory antibody or the CXCR4 antagonist AMD3100 (195).

The interactions of Notch-1 and Jag-1 have also been investigated in MM. Activation of Notch-1 by Jag-1 and its effect upon cell proliferation is somewhat contradictory in the literature. Jundt *et al* (198) described a 2-fold increase in MC proliferation when stimulated with Jag-1, which was inhibited using the γ secretase inhibitor N-[(3,5-Difluorophenyl)acetyl]-L-alanyl-L-phenylglycine-1,1-dimethylethyl ester (DAPT). Whereas, Nefedova *et al* (199), described a reduction in proliferation and an increase in cells in the G₀ phase of cycling when cells were co-cultured with Jag-1 expressing stromal cells. In addition, the interaction of Jag-1 positive stromal cells

with MCs propagated chemoresistance when melphalan was administered (199). In a separate study, administration of a γ secretase inhibitor in combination with doxorubicin, also resulted in MC chemosensitisation and increased the percentage of apoptotic cells *in vitro* and *in vivo* (267).

N-cad expression and function has been implicated in several cancers including breast, prostate and melanoma, particularly in relation to metastasis. Hazan *et al* (268) demonstrated that N-cad expression in MCF-7 breast cancer cells induced both migration and invasion *in vitro* and an increase in metastasis upon injection *in vivo*. This was also supported by Nieman *et al* (204), who demonstrated that N-cad positive breast cancer cell lines had higher invasion and motility. In prostate cancer, 93% of patients with established metastasis had tumours which were positive for N-cad, whereas only 56% of patients who had no known metastasis had N-cad positive tumours (228). In addition, when N-cad was knocked-down in melanoma cells, this resulted in a reduction in transwell migration *in vitro* (269). Furthermore, when N-cad was blocked using an inhibitory antibody, this resulted in a reduction in melanoma cell adhesion to fibroblasts and endothelial cells, a reduction in migration towards fibroblasts *in vitro* and an increase in melanoma cell death (270).

N-cad has also been implicated in MC adhesion to osteoblastic cells and in the early stages of MC homing and survival in the BM. NCIH929 MCs adhered to recombinant N-cad and N-cad expressing C3H10T1/2 osteoblastic cells *in vitro* and this interaction was subsequently blocked using an N-cad inhibitory antibody (206). The KD of N-cad in NCIH929 cells also resulted in a reduction of MC homing or survival in the BM and an increase in the number of cells in the circulation when injected into mice (206). In addition, Sadler *et al* (207) demonstrated that inhibition of MC adhesion to stromal cells in culture using an anti-N-cad antibody resulted in increased proliferation of MCs, therefore, N-cad signalling may be important for cell proliferation and control of cell cycle.

As stated previously, Tie-2 and Ang-1 have not been highly studied in MM. They have activities typically associated with blood vessel development. Tie-2 is highly expressed in blood vessels and is required for vessel stability and integrity, which is stimulated by Ang-1 and inhibited by Ang-2. However, vessel stability is an important mechanism for the establishment of solid tumours and Vacca *et al* (271) reported an increase in micro-vessel area in myeloma patients. Therefore, Tie-2/Ang-1 interactions may be important in myeloma establishment in the BM.

Successful interventions of all the molecule interactions discussed above in disease have now also been translated into clinical trials for various types of cancer, discussed in detail in the general discussion, Chapter VII.

In this Chapter, I have used a shRNA gene KD strategy to suppress the expression of genes for CXCR4 and N-cad in 5TGM1-GFP cells. I then conducted functional studies to determine the effect of the KD on the adhesion of the MCs to the differentiated primary OLCs (optimised in Chapter V) and also the effect upon tumour growth *in vivo* in a pilot study. These experiments were conducted to determine the role of these molecules in a MC niche and to identify whether these molecules are important targets for future intervention studies. The 5TGM1-GFP model was used, as it is intrinsically less variable in terms of tumour burden and tumour take compared to the 5T33-GFP model. The 5T33-WT model was also used in this chapter as a control to test the transduction of GFP using the lentiviral system.

6.2 Hypothesis, aims and objectives

6.2.1 Hypothesis and aims

The aim of these studies was to test the hypothesis that “The knock-down (KD) of HSC niche molecules in MM cells, results in reduced myeloma cell (MC) adhesion to

primary osteoblast lineage cells (OLCs) *in vitro* and subsequent reduction in tumour burden *in vivo*".

6.2.2 Objectives

The hypothesis will be tested by the following objectives:

1. To KD HSC niche molecules in the 5TGM1-GFP cells using short hair-pin RNA (shRNA) and to transduce green fluorescent protein (GFP) into 5T33-WT cells. Gene KD will be validated using real-time PCR and Western blotting (WB), and GFP transduction will be confirmed using flow cytometry.
2. To determine the effect of knocking down HSC niche molecules on MC adhesion to primary OLCs *in vitro*.
3. To determine the effect of knocking down HSC niche molecules upon tumour burden *in vivo*.

6.3 Methods

6.3.1 Short hair-pin RNA knock-down strategy

6.3.1.1 Puromycin killing curves

5TGM1-GFP cells and 5T33-WT cells were seeded in triplicate at a density of 1×10^5 cells into a 12 well plate in 2 ml complete RPMI media containing either 0 (an equal volume of PBS), 0.5, 1.0, 2.5, 5.0, 7.5 and 10 $\mu\text{g}/\text{ml}$ puromycin and after 2 and 4 days the cell viability was determined using TO-PRO-3 staining followed by flow cytometry using a FACS Calibur and Cell Quest software. The lowest dose required for 100% cell death over a 4-day period was then established by analysing the number of viable cells remaining at the different concentrations of puromycin at 2 and 4-day time points. Results were based on three independent experiments (N=3). This is described in more detail in Chapter II, Section 2.6.2.2.

6.3.1.2 Polybrene optimisation

5TGM1-GFP and 5T33-WT cells were seeded in triplicate into a 48 well plate at a density of 5×10^4 in 500 μ l complete RPMI media containing 0 (PBS of the same volume), 2.5, 5.0, 7.5 and 10.0 μ g/ml polybrene and incubated for 24 hours. After 24 hours, the number of cells in each well were counted using a haemocytometer to establish whether high concentrations of polybrene were toxic. Results were established from three independent experiments (N=3). This was described in more detail in Chapter II, Section 2.6.3.1.

6.3.1.3 Lentiviral green fluorescent protein transduction

The 5T33-WT cells were seeded at a density of 2×10^4 cells in 100 μ l complete RPMI media containing 5.0 μ g polybrene (determined from the optimisation experiments) in a 96 well plate and the lentiviral particles for GFP and scrambled controls at a multiplicity of infection (MOI) of 5 (CTRL 5), 15 (CTRL 15) and 25 (CTRL 25) were added and then incubated for 20 hours. Green fluorescent protein expression was determined in puromycin resistant colonies (treated with 7.5 μ g puromycin) using flow cytometry. The stability of the GFP transduction was also established in cells in the absence of puromycin free media, four weeks after transduction. This was described in further detail in Chapter II, Section 2.6.4.1.

6.3.1.4 Lentiviral short hair-pin RNA transduction for CXCR4 and N-cad

The 5TGM1 cells were seeded at a density of 2×10^4 cells in 100 μ l complete RPMI media containing 5.0 μ g polybrene in a 96 well plate and the lentiviral particles containing shRNA for N-cad and CXCR4 at MOIs of 5 (KD 5), 15 (KD 15) and 25 (KD 25) or scrambled controls at the same MOIs were added and then incubated for 20 hours. Knock-down was detected in puromycin resistant colonies (treated with 5.0 μ g/ml puromycin) using real-time PCR and WB. The cells were then cultured in the absence of puromycin for four weeks to detect the stability of the KD, which was analysed

using real-time PCR and WB. This was described in further detail in Chapter II, Section 2.6.4.1.

6.3.2 Assessment of gene knock-down

6.3.2.1 Real-time PCR

For PCR analysis of the KD, 1×10^6 CXCR4 and N-cad KD 15 and 25 and CTRL 15 and 25 treated cells were taken in triplicate for RNA extraction. RNA was extracted, cDNA was synthesised and real-time PCR was conducted as described in Chapter II, Sections 2.3.1.1, 2.3.2.1 and 2.3.5.2. Real-time PCR was analysed using the comparative $\Delta\Delta C_t$ method by normalising to the HK gene β_2M and the percentage of KD was calculated as described in Chapter II, Section 2.6.4. Results were established from three independent experiments (N=3).

6.3.2.2 Western blotting

Western blotting was used to confirm the KD of protein in the 5TGM1-GFP cells. In each sample, 1×10^7 CTRL 15 and 25 and N-cad KD 15 and 25 cells were taken in triplicate and lysed using NP-40 buffer. The protein was quantified using a bicinchoninic acid (BCA) assay and run in a 7% resolving gel using 30% acrylamide by polyacrylamide gel electrophoresis (SDS-PAGE). The gel was transferred onto a nitrocellulose membrane and N-cad protein was determined using sandwich “immuno-blotting”. Results were visualised by chemoluminescence and quantified using ImageJ software to calculate band density. Knock-down was quantified by normalising to the HK protein β -actin and a percentage of protein KD was calculated. Results were established from three independent experiments (N=3). This is described in more details in Chapter II, Section 2.4.4.

6.3.3 Assessment of the *in vitro* effects of HSC niche molecule gene knock-down in transduced myeloma cells

6.3.3.1 Growth curves

To assess the effect of the HSC niche molecule KD upon cell proliferation *in vitro*, growth curve experiments were conducted, where 5×10^3 cells (5TGM1-GFP, CTRL 15 and 25 and KD 15 and 25) were seeded into a 96 well plate in 200 μ l complete RPMI media. Cell counts were recorded every 2 days for 12 days. Cell proliferation was presented in a graphical format to visualise each phase of growth and the doubling-time in the exponential phase was calculated using the formula shown in Chapter II section 2.4.5.1. Results were established from three independent experiments (N=3).

6.3.3.2 Adhesion experiments

To assess the effect of the HSC niche molecule KD upon MC adhesion to primary OLCs, the same method was used as developed previously in Chapter V. In brief, 5×10^4 cells (CTRL 15 and 25 and N-cad KD 15 and 25) were seeded in 200 μ l complete RPMI media onto primary OLCs differentiated in 10 mM BGP and 50 μ g/ml asc for 3, 14 and 28 days in a 96 well plate. After 1 and 6 hours, plates were washed and the remaining cells that adhered to the primary OLCs were visualised using a Leica AF6000 fluorescent microscope and LAS LF software. This is described in more detail in Chapter II, Section 2.5.3.2.

6.3.4 Assessment of the *in vivo* effects of HSC niche molecule gene knock-down in transduced myeloma cells

A pilot *in vivo* experiment using the N-cad KD cells was conducted to firstly, identify any differences in tumour burden between the transduced cells and standard 5TGM1-GFP cells (as it was suspected that prolonged *in vitro* culture may effect tumourgenicity) and secondly, to determine any differences in tumour burden between mice injected with CTRL 25 and N-cad KD 25 cells. Two million 5TGM1-GFP

cells (N=4), CTRL 25 (N=6) and KD 25 (N=6) cells were injected into 11 week old female C57BL/KaLwRij mice. When the first mouse became ill (at 25 days post injection), all mice were sacrificed and the hind limbs were dissected. The MM models are described in more detail in Chapter II, Section 2.2.2.1.

6.3.4.1 Tumour burden analysis

Both femurs from each mouse were flushed using PBS and analysed separately by flow cytometry to determine the percentage of GFP positive tumour cells in each femur as described in Chapter II, Sections 2.2.1.4 and 2.4.1.2. In addition, the left tibiae were fixed in 4% PFA, decalcified in PFA/EDTA and sections were cut and stained by CD138 IHC as described in Chapter II, Section 2.4.3.3. The stained slides were scanned using an Aperio Scan Scope slide scanner and tumour area and colony number were analysed manually using Image Scope software.

6.3.4.2 Bone disease analysis

The right tibia from each mouse was fixed in 10% formalin and scanned by μ CT using a SkyScan 1172 at 50 Kv, 200 μ A, an aluminium filter of 0.5 mm and pixel size of 4.3 μ m². Images were reconstructed using N-Recon Software. Trabecular bone 0.2 mm below the growth plate was analysed using Ct-an and Batman software to provide data for bone parameters including BV/TV, tb.n and tb.th. This is described in greater detail in Chapter II, Section 2.7.1.2. Lesion number and area were also calculated using Ct-an software by utilising reconstructed μ CT images of each tibiae. Following this, the images were resized; the cortical bone region of interest was selected for lesion analysis using ImageJ software. This is described in greater detail in Chapter II, Section 2.7.1.2.

6.3.5 Statistics

Non-parametric statistical tests were used where relevant. A Friedman test followed by Dunn's post test was used to determine differences in cell death between MCs treated with different concentrations of puromycin and polybrene and was also used to determine differences in GFP expression in MCs cultured in the absence of puromycin over-time. A Kruskal-Wallis test followed by a Dunn's post test was used to determine differences in cell proliferation between CTRL and KD cells over-time. A Mann-Whitney U test was used to compare differences in CTRL and KD MC adhesion to primary OLCs cultured in OGM for 3, 14 and 28 days and a Friedman test was used to determine differences in MC adhesion to primary OLCS cultured in OGM for 3, 14 and 28 days. In addition, a Mann-Whitney U test was used to compare tumour burden and bone disease between CTRL 25 and N-cad KD injected mice *in vivo*. A Fisher's exact test was also used to compare the tumour take.

Where relevant, error bars were displayed on all graphs using the SEM unless stated otherwise in the legend.

6.4 Results

6.4.1 Killing curves to determine the optimum concentration of puromycin using flow cytometry

Puromycin killing curves were conducted to determine the optimum concentration of puromycin to select for resistant colonies following lentiviral transduction for the KD of CXCR4 and N-cad by shRNA. Cell death was analysed by TO-PRO-3 staining using flow cytometry where non-viable cells were positive.

Figure 6.1 demonstrates the percentage of 5TGM1-GFP and 5T33-WT cell death after 2 and 4 days using increasing doses of puromycin. As the concentration of puromycin increased, the percentage of TO-PRO-3 positive 5TGM1-GFP and 5T33-WT cells also increased. After 2 days, the number of TO-PRO-3 positive 5TGM1-GFP cells increased between 0.0-5.0 µg/ml puromycin after which cell death plateaued at the remaining concentrations. Cell death was significant at 5.0, 7.5 and 10.0 µg/ml puromycin compared to the control ($P<0.05$). After 4 days again there was an increase in TO-PRO-3 positive cells, but the cell death plateaued earlier at 2.5 µg/ml, after which there was a 2% increase in cell death between 2.5 and 5.0 µg/ml puromycin. The mean percentage of cell death of 97% then remained constant for the remainder of the concentrations. Statistically, cell death was significant at 5.0 µg/ml puromycin compared to the control ($P<0.05$).

After 2 days, the 5T33-WT cells demonstrated an increase in TO-PRO-3 positive cells from 0.0-5.0 µg/ml. This was then followed by a 5% increase between 5.0 µg/ml and 7.5 µg/ml and a 2% increase between 7.5 µg/ml and 10.0 µg/ml. Statistically, there was a significant difference in the number of dead cells at 7.5 µg/ml ($P<0.05$) and 10.0 µg/ml ($P<0.01$) compared to the control, and also between 0.5 µg/ml and 10.0 µg/ml ($P<0.05$). After 4 days, the number of TO-PRO-3 positive cells increased between 0.0-5.0 µg/ml followed by a 2% increase between 5.0 µg/ml and 7.5 µg/ml and no increase between 7.5 µg/ml and 10.0 µg/ml puromycin. Statistically, there was a significant difference in cell death between 7.5 µg/ml ($P<0.01$) and 10.0 µg/ml ($P<0.05$) puromycin compared to the controls.

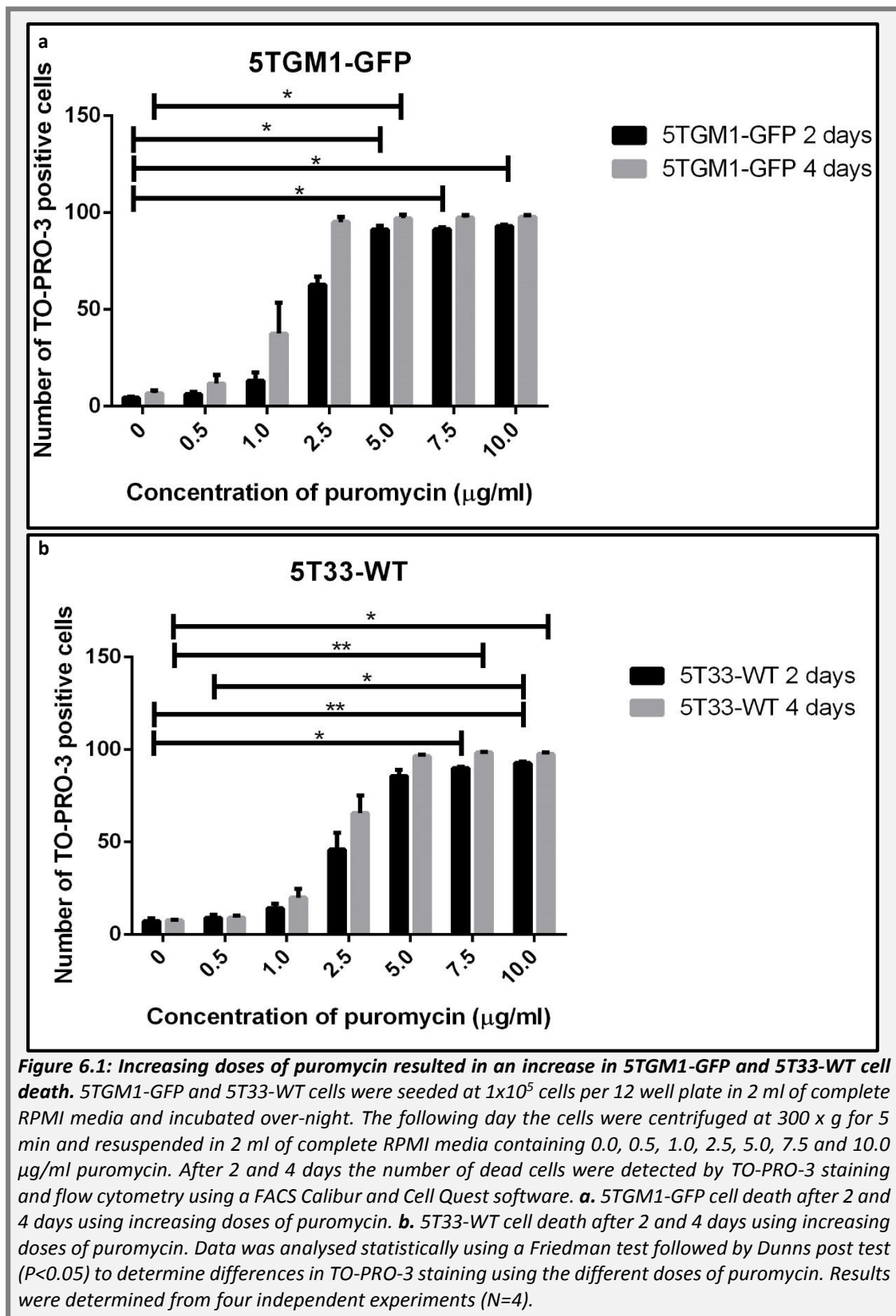


Figure 6.1: Increasing doses of puromycin resulted in an increase in 5TGM1-GFP and 5T33-WT cell death. 5TGM1-GFP and 5T33-WT cells were seeded at 1×10^5 cells per 12 well plate in 2 ml of complete RPMI media and incubated over-night. The following day the cells were centrifuged at $300 \times g$ for 5 min and resuspended in 2 ml of complete RPMI media containing 0.0, 0.5, 1.0, 2.5, 5.0, 7.5 and 10.0 µg/ml puromycin. After 2 and 4 days the number of dead cells were detected by TO-PRO-3 staining and flow cytometry using a FACS Calibur and Cell Quest software. **a.** 5TGM1-GFP cell death after 2 and 4 days using increasing doses of puromycin. **b.** 5T33-WT cell death after 2 and 4 days using increasing doses of puromycin. Data was analysed statistically using a Friedman test followed by Dunns post test ($P < 0.05$) to determine differences in TO-PRO-3 staining using the different doses of puromycin. Results were determined from four independent experiments ($N=4$).

From the data, it was also clear that a higher number of cells were TO-PRO-3 positive after 4 days compared to 2 days using each concentration of puromycin and cell type.

In addition, the 5T33-WT cells seemed to be more resistant to the puromycin compared to 5TGM1-GFP cells as higher concentrations of puromycin were required to kill the same number of cells. However, due to a lack of non-parametric two-way paired test, neither of these findings were analysed statistically.

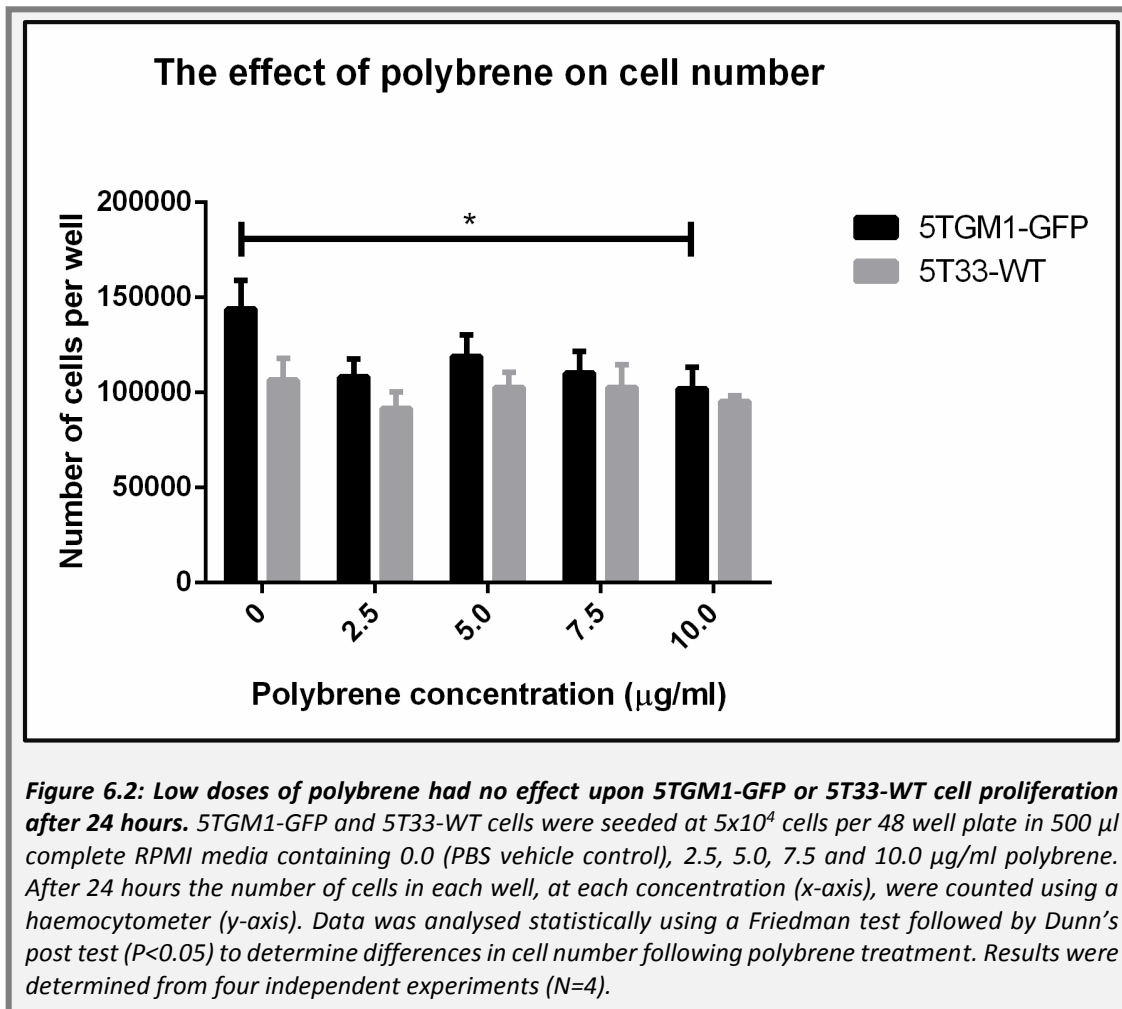
From these experiments, I was able to determine the suitable dose of puromycin for use in future experiments, required to select for resistant colonies in the KD experiments. In future experiments, I used a dose of 5.0 µg/ml of puromycin to select resistant colonies using the 5TGM1-GFP cells and 7.5 µg/ml of puromycin to select for resistant 5T33-WT cells. Both of these concentrations produced significantly greater cell death compared to the controls. In addition, the manufacturer recommended using a concentration which kills 100% of cells within four days and using these concentrations in my experiments a plateau in cell death was demonstrated with no increase in cell death after use at these concentrations.

6.4.2 The effect of polybrene upon cell viability after 24 hours of treatment

The effect of polybrene upon cell viability was tested after 24 hours of treatment at several different dose from 0.0 (PBS vehicle control), 2.5, 5.0, 7.5 and 10.0 µg/ml polybrene, by cell counting using a haemocytometer. Cell counts were used opposed to TO-PRO-3 staining, as polybrene acts by increasing pore sizes and upon using TO-PRO-3 and flow cytometry it resulted in false positives for dead cells.

Figure 6.2 shows the effect of polybrene upon cell number. Statistically, polybrene had no significant effect upon cell viability using any concentrations between 0.0 and 7.5 µg/ml in the 5TGM1-GFP cells, however, 10.0 µg/ml of polybrene resulted in a significant decrease in cell number ($P < 0.05$) after 24 hours. Polybrene however, had no effect upon 5T33-WT cell number after 24 hours at any dose (0.0-10.0 µg/ml). As polybrene had no significant effect on proliferation at any of the doses using the 5T33-WT cells and no affect upon proliferation up to 7.5 µg/ml using the 5TGM1-GFP

cells, the recommended dose by the manufacturer of 5.0 µg/ml was used for future experiments.



6.4.3 Green fluorescent protein transduction in the 5T33-WT cells as a proof of principal

A lentiviral GFP transduction system was used as a proof of principal to test whether lentiviral transduction using these particular reagents was possible in the MCs. The 5T33-WT cells were chosen, as we did not possess the non-GFP transduced 5TGM1 variety.

Lentiviral particles containing the GFP sequence and puromycin resistance vector were transduced into the polybrene (5.0 µg/ml) treated 5T33-WT cells at MOIs of 5, 15 and 25. This was followed by puromycin selection at 7.5 µg/ml, optimised as

shown in Chapter VI, Section 6.3.1, Figure 6.1. The cells treated with an MOI of 5 did not survive following puromycin selection whereas, those treated with an MOI of 15 and 25 were viable, indicating that transduction of the puromycin resistance vector was successful at the higher MOIs in the 5T33-WT cells.

Flow cytometry was used to detect the success of the GFP transduction in the 5T33-WT cells following puromycin selection (0 days). To determine the stability of the GFP transduction, cells were cultured in puromycin free media for 7, 14, 21 and 28 days, followed by flow cytometry. As shown in Figure 6.3, the 5T33-WT cells, transduced using both MOIs, expressed GFP after puromycin selection and also in puromycin free media over-time. Statistically, there were no significant differences in the expression of GFP over-time using MOIs of 15 and 25.

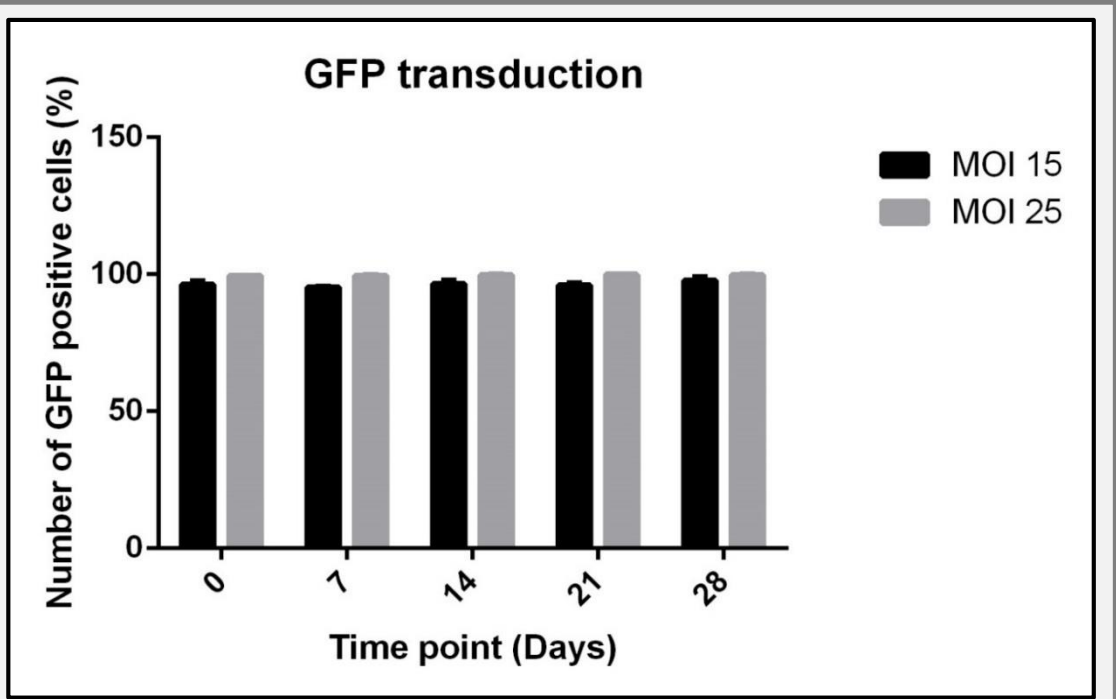


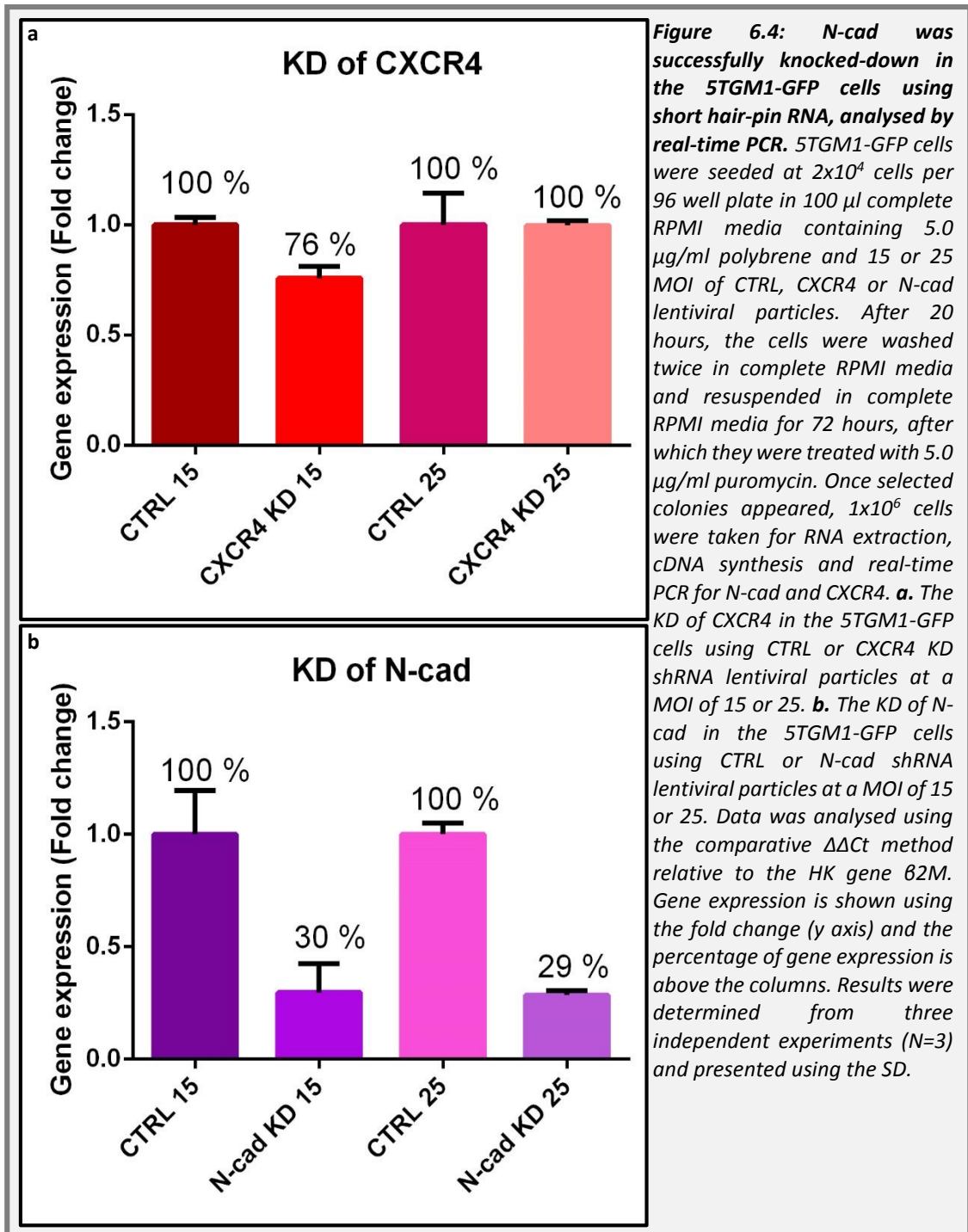
Figure 6.3: Green fluorescent protein was successfully transduced into 5T33-WT cells using lentiviral particles and analysed by flow cytometry. 5T33-WT cells were seeded at 2×10^4 cells per 96 well plate in 100 μ l complete RPMI media containing 5.0 μ g/ml polybrene and 15 or 25 MOI of lentiviral GFP particles. After 20 hours the cells were washed twice in complete RPMI media and resuspended in complete RPMI media for 72 hours, after which they were treated with 7.5 μ g/ml puromycin. Once selected colonies appeared, 1×10^6 cells were taken for flow cytometry (day 0) after which the cells were washed twice in RPMI media and cultured in complete media in the absence of puromycin for 7, 14, 21 and 28 days and at each time point the number of cells positive for GFP per 1×10^6 sample was assessed (y-axis) using a FACS Calibur and Cell Quest software. (x-axis). Data was analysed using a Friedman test followed by Dunn's post test ($P < 0.05$) to compare differences in GFP expression by the MOI 15 and 25 treated cells over-time. This experiment was conducted only once but set-up in triplicate.

6.4.4 Real-time PCR to establish the success of knocking-down CXCR4 and N-cad using the lentiviral short hair-pin RNA transduction system

The lentiviral shRNA system was used to KD the genes for CXCR4 and N-cad. Optimum conditions established using the 5T33-WT cells for GFP transduction were used. The 5TGM1-GFP cells were treated with polybrene and the lentiviral particles at MOIs 15 and 25. This was followed by puromycin selection at 5.0 μ g/ml.

The KD of CXCR4 and N-cad was determined using real-time PCR. Figure 6.4 demonstrates the effect of lentiviral shRNA transduction upon gene expression of CXCR4 (Figure 6.4a) and N-cad (Figure 6.4b) at MOIs of 15 and 25 after puromycin

selection. When the KD of CXCR4 was assessed, there was only a 24% reduction in CXCR4 expression at an MOI of 15 and no difference using the MOI of 25 compared to the control. At this stage, and after a number of attempts, it was clear that the KD of CXCR4 in the 5TGM1-GFP cells was unsuccessful, as assessed by real-time PCR. Therefore, the CXCR4 shRNA transduced cells were not used in future experiments. In contrast to CXCR4, when the KD of N-cad was assessed, there was a reduction in N-cad gene expression of 70% using the MOI of 15 and 71% using the MOI of 25, compared to their corresponding controls. According to the manufacturer's instructions, a successful KD is achieved if the KD is greater than 60%, therefore, KD of N-cad was successful at both MOIs and the N-cad shRNA transduced 5TGM1-GFP cells were used in future experiments.



6.4.5 Real-time PCR to establish the stability of N-cad knock-down in cells cultured in puromycin free media

Experiments were conducted to assess the stability of the N-cad KD in cells no longer cultured under puromycin selection. The rationale for this was to ensure that cells remained knocked-down for N-cad in the absence of puromycin because once injected *in vivo* they would no longer be under selection conditions.

Cells were cultured *in vitro* for 28 days without puromycin selection, followed by PCR analysis. This time-point was chosen due to the length of the 5TGM1-GFP *in vivo* model. Figure 6.5 demonstrates the effect of culturing the 5TGM1-GFP N-cad KD cells in the absence of puromycin after 28 days, upon N-cad gene KD. N-cad expression was reduced by 54% using a MOI of 15 and 75% using a MOI of 25. Therefore, after MC growth in complete media without puromycin, cells treated with a MOI of 15 were no longer suitably knocked-down as the reduction was no longer greater than 60% whereas, cells treated with an MOI of 25 remained successfully knocked-down with a reduction greater than 60%.

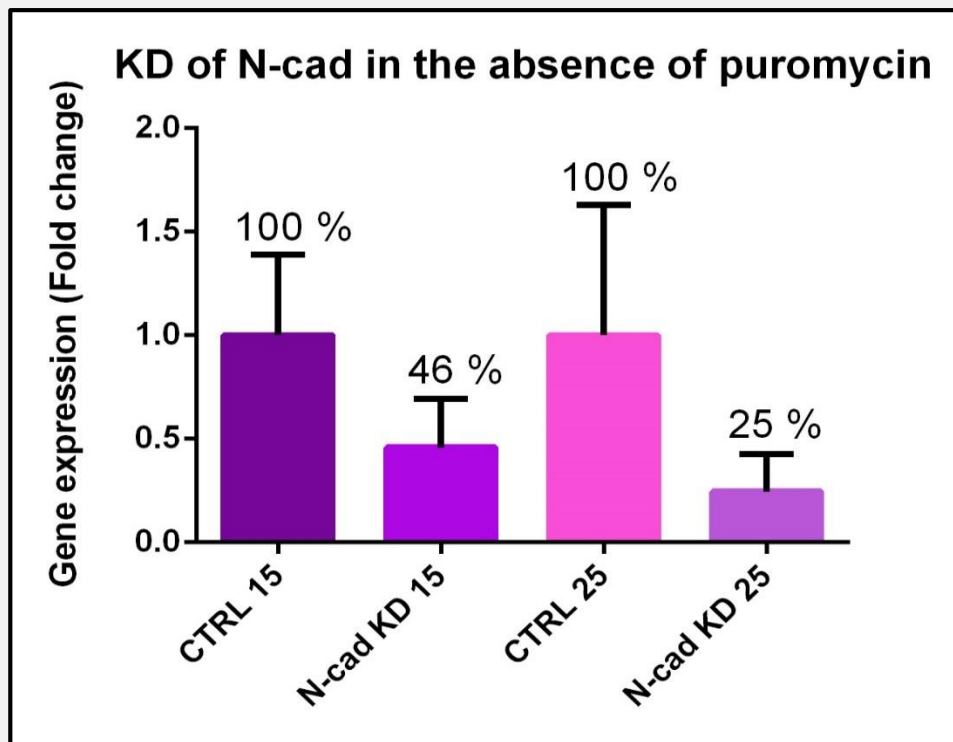
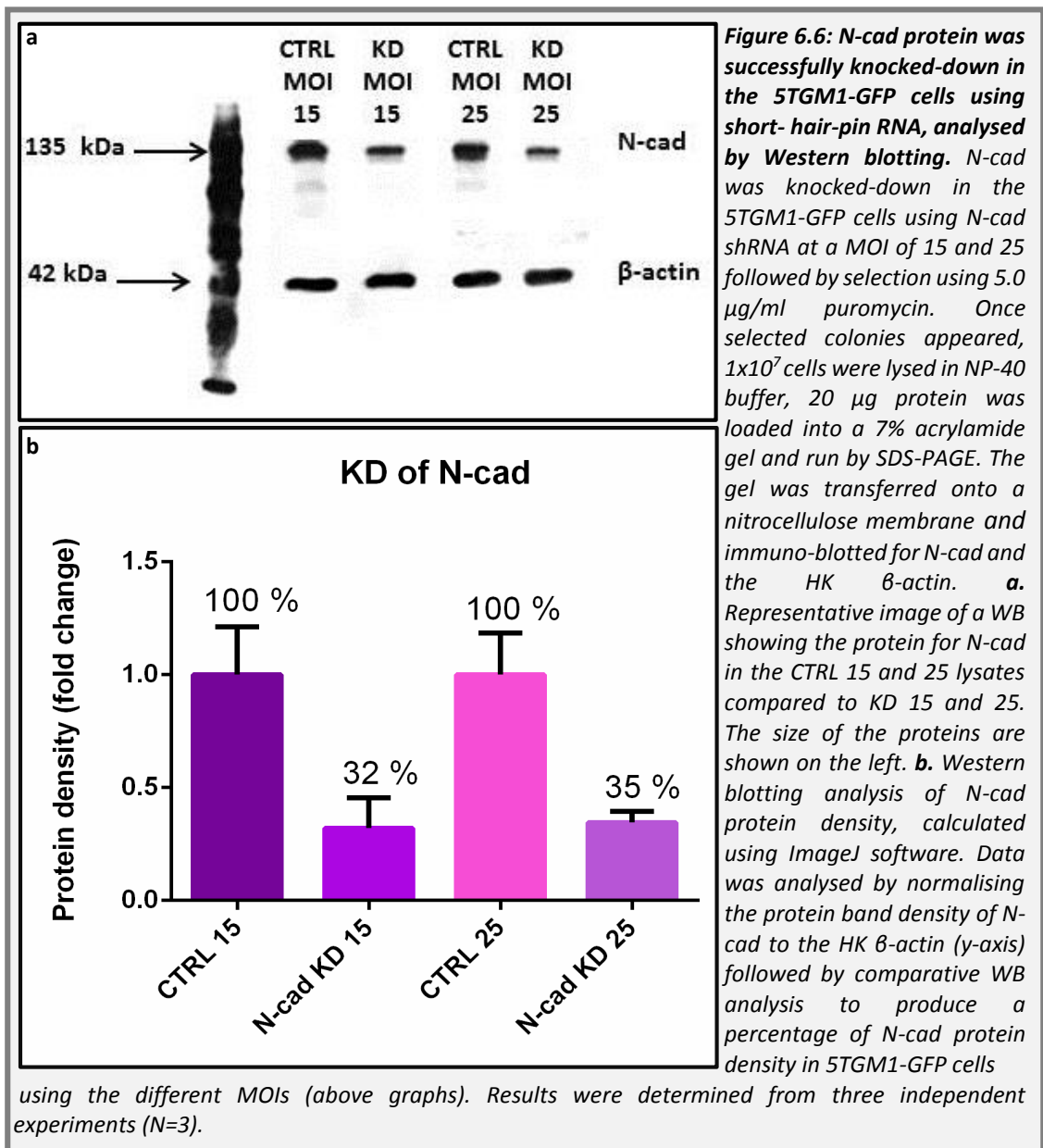


Figure 6.5: N-cad gene expression was stably knocked-down in the 5TGM1-GFP cells cultured in the absence of puromycin for 28 days, analysed by real-time PCR. 5TGM1-GFP CTRL 15 and 25 and KD 15 and 25 cells were cultured in puromycin free complete RPMI media for 28 days after which 1×10^6 cells were taken for RNA extraction, cDNA synthesis and real-time PCR for N-cad. Data was analysed using the comparative $\Delta\Delta C_t$ method relative to the HK gene $\beta 2M$. Gene expression is shown using the fold change (y axis) and the percentage of gene expression is above the columns. Results were determined from three independent experiments (N=3) and presented using the SD.

6.4.6 Western blotting to establish the success of knocking-down N-cad using the lentiviral short hair-pin RNA transduction system

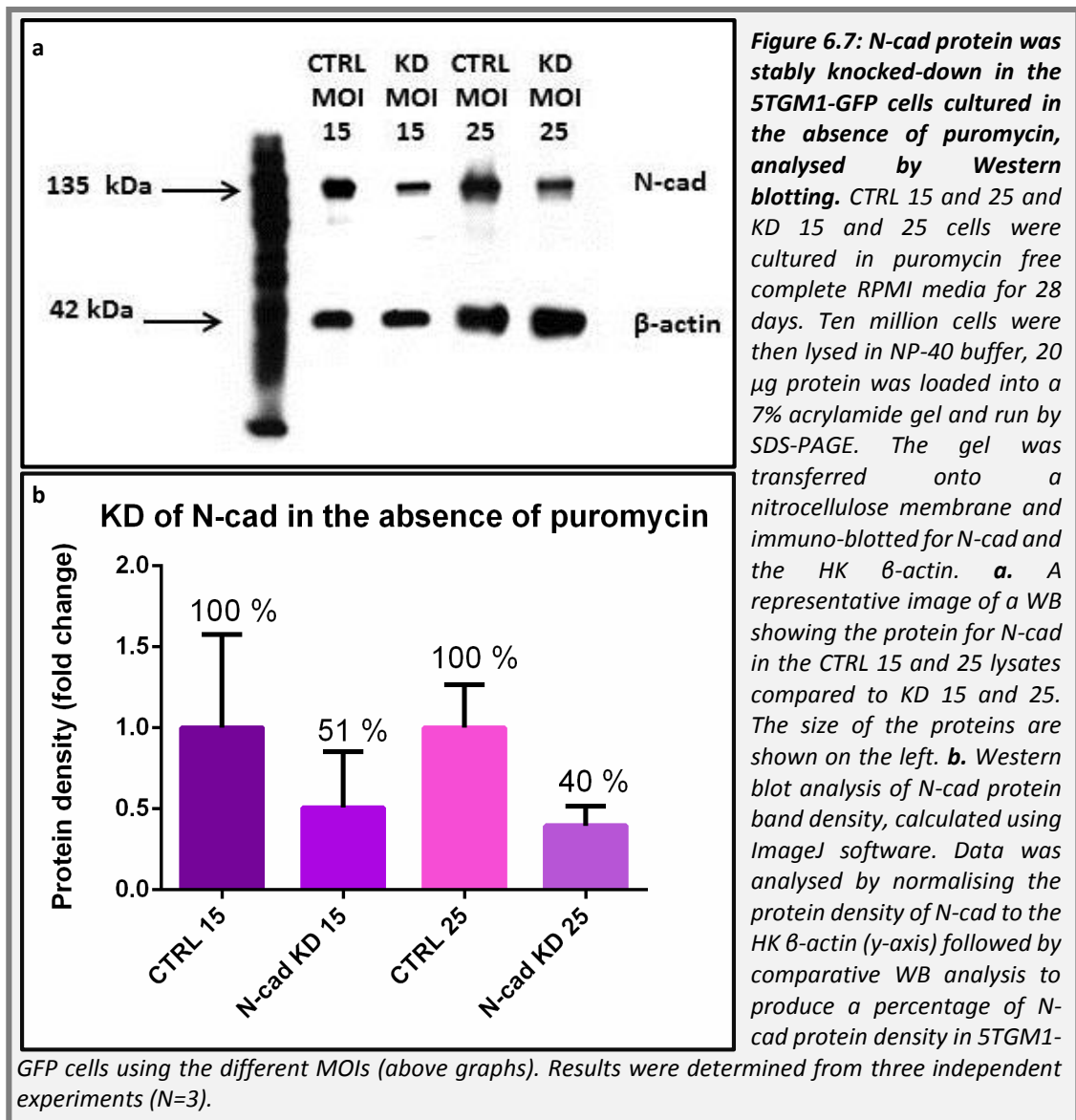
To further quantify the KD of N-cad in the 5TGM1-GFP KD cells, WB was used. Figure 6.6 shows the effect of shRNA treatment in the 5TGM1-GFP cells upon N-cad protein production at MOIs of 15 and 25 compared to the corresponding controls. Western blotting clearly shows a decrease in protein for N-cad at an MOI of 15 and 25, based upon band density (Figure 6.6a). When band density was analysed (Figure 6.6b) the N-cad KD cells at a MOI of 15 demonstrated a KD in protein of 68% whereas, the KD 25 cells demonstrated a KD of 65%. As with the real-time PCR data, N-cad KD was successful as KD was greater than 60%.



6.4.7 Western blotting to establish the stability of N-cad knock-down in cells cultured in puromycin free media

To determine the stability of N-cad protein KD in the 5TGM1-GFP cells, the cells were cultured for 28 days in the absence of puromycin, followed by WB analysis. Figure 6.7a demonstrates the WB of the CTRL and KD 5TGM1-GFP cells at MOIs of 15 and 25. Visually from the WB there was a reduction in N-cad protein in the cells at both the MOI of 15 and 25. Figure 6.7b demonstrates the quantification of N-cad protein KD in the 5TGM1-GFP cells at MOIs of 15 and 25. N-cad protein was reduced by 49% using the MOI of 15 and 60% using the MOI of 25. Therefore, as with the real-time

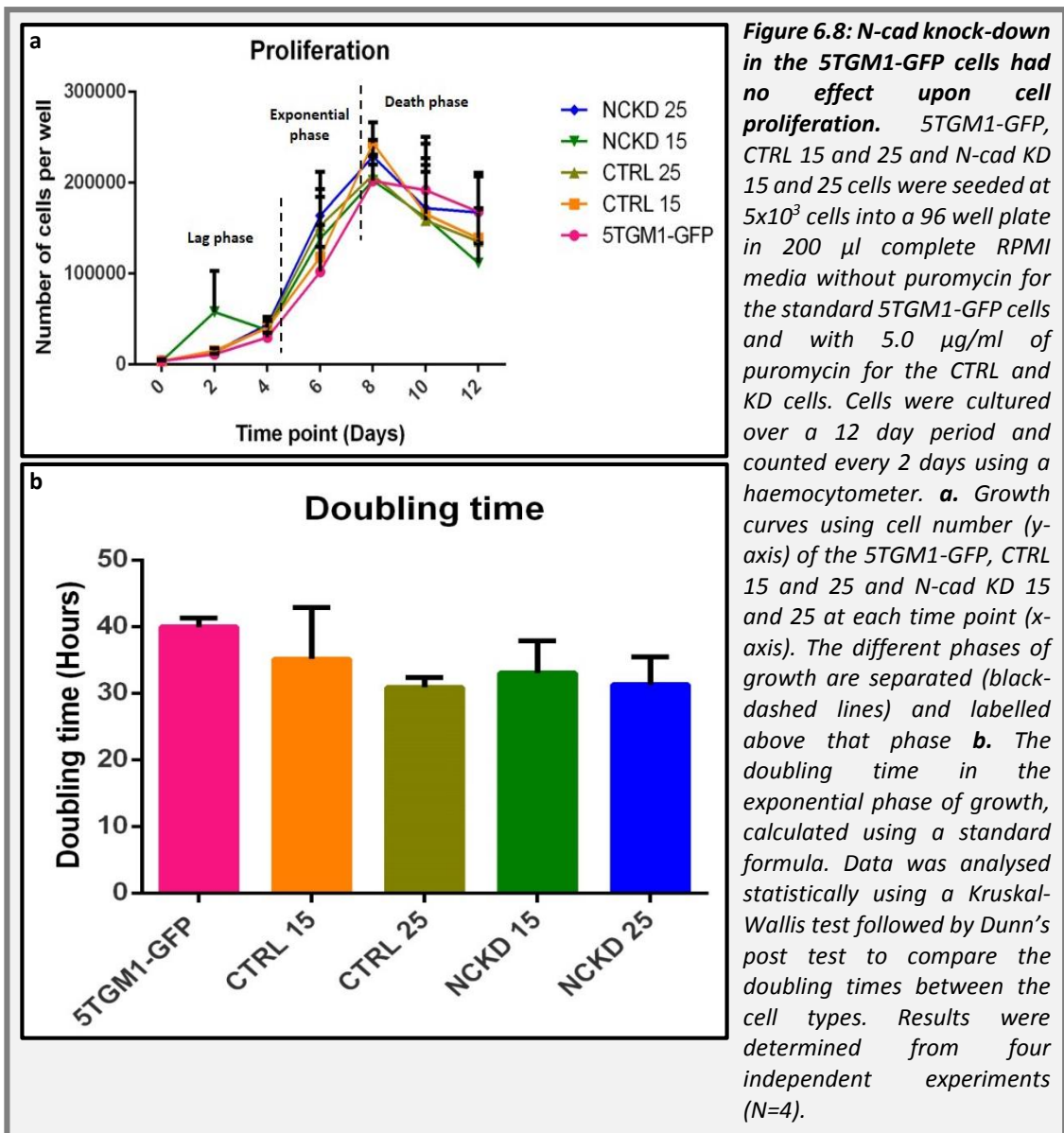
PCR analysis, the cells treated with a MOI of 15 and cultured in the absence of puromycin for 28 days, no longer have suitable protein KD for N-cad (reduction was less than 60%). Whereas, those treated with an MOI of 25 were still suitably knocked-down, with 60% reduction in N-cad protein after 28 days.



6.4.8 The effect of N-cad knock-down upon cell proliferation

In vitro experiments were conducted to determine any differences in cell proliferation due to the KD of N-cad in the 5TGM1-GFP KD cells transduced using an MOI of 15 and 25. Figure 6.8a demonstrates the growth curves produced over a 12-

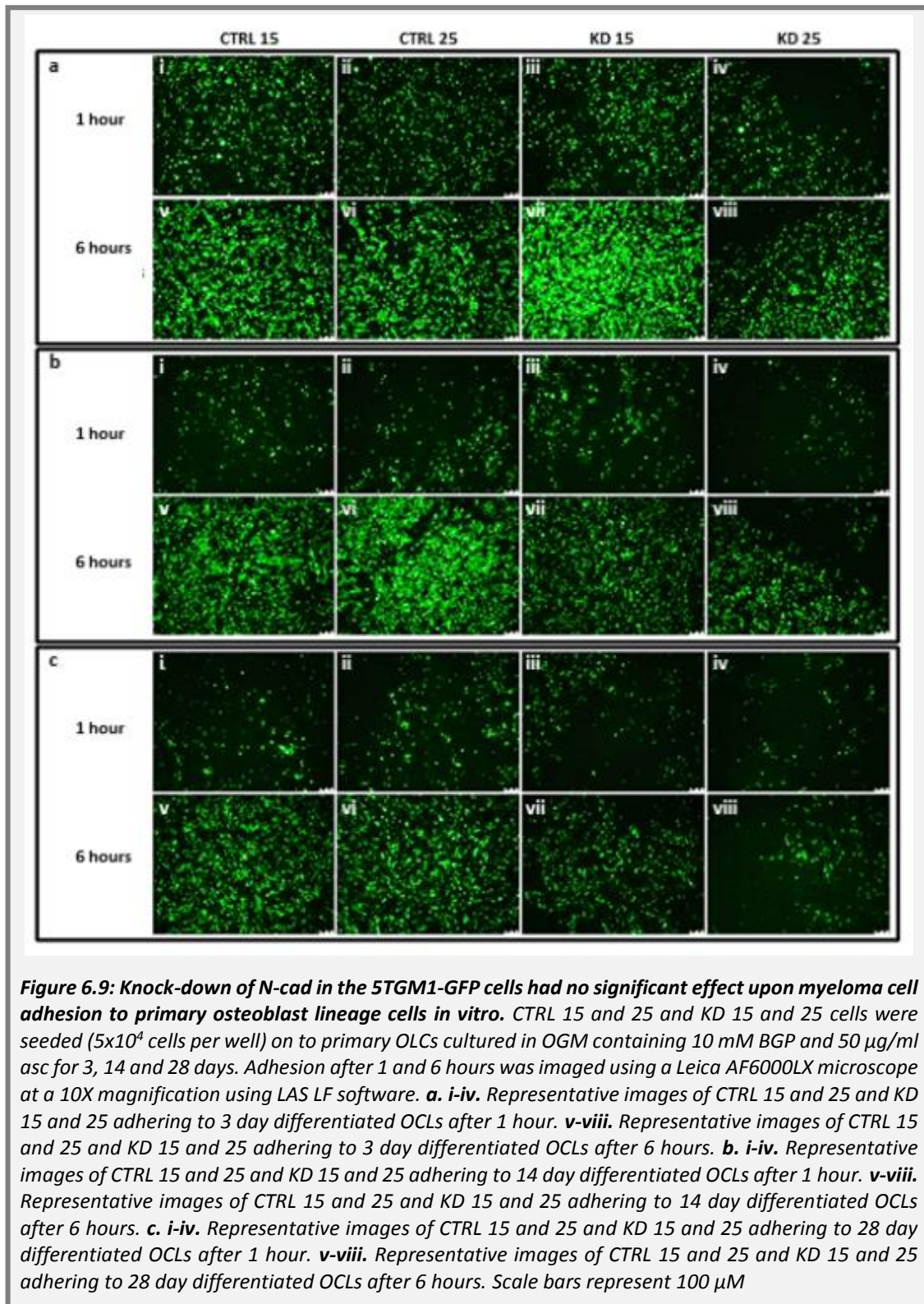
day period using the un-transduced 5TGM1-GFP cells and CTRL and N-cad KD cells at MOIs of 15 and 25, displayed using the cell number recorded at each time point. The growth curves displayed different stages of proliferation, whereby there was an initial lag phase between days 0-4, a short exponential phase between 4-8 days, followed by a death phase from 8-12 days. A plateau phase was not observed within these cells types, potentially due to how quickly the cells proliferate, which may result in quicker depletions in media. The doubling time was then calculated from the cells numbers in the exponential phase, as shown in Figure 6.8b. Statistically, there were no significant differences in the doubling times between the standard 5TGM1-GFP cells, transduced control cells and N-cad KD cells.



6.4.9 The effect of N-cad knock-down upon adhesion to primary osteoblast lineage cells *in vitro*

To test the effect of knocking-down N-cad in the 5TGM1-GFP cells upon adhesion to primary OLCs cells *in vitro*, using the same methodology developed in Chapter V, CTRL 15, CTRL 25, KD 15 and KD 25 cells were seeded onto primary OLCs which had been cultured in OGM for 3, 14 and 28 days.

The effect of knocking-down N-cad in the 5TGM1-GFP cells upon adhesion to primary OLCs *in vitro* was compared between the CTRL 15 and KD 15 cells and the CTRL 25 and KD 25 cells after 1 hour and 6 hours, as shown in representative fluorescent images in Figure 6.9 and quantitative analysis in Figure 6.10. There were no significant differences between the adhesion of KD 15 cells to OLCs at all time-points compared to CTRL 15 cells. There was however, a consistent but not significant reduction in the adhesion of KD 25 cells to OLCs at all time-points compared to the CTRL 25 cells. In addition, there was also a trend for less adhesion of CTRL 25 cells to OLCs across the time course with <50% adhesion on day 28 compared to day 3 but again these did not reach significance.



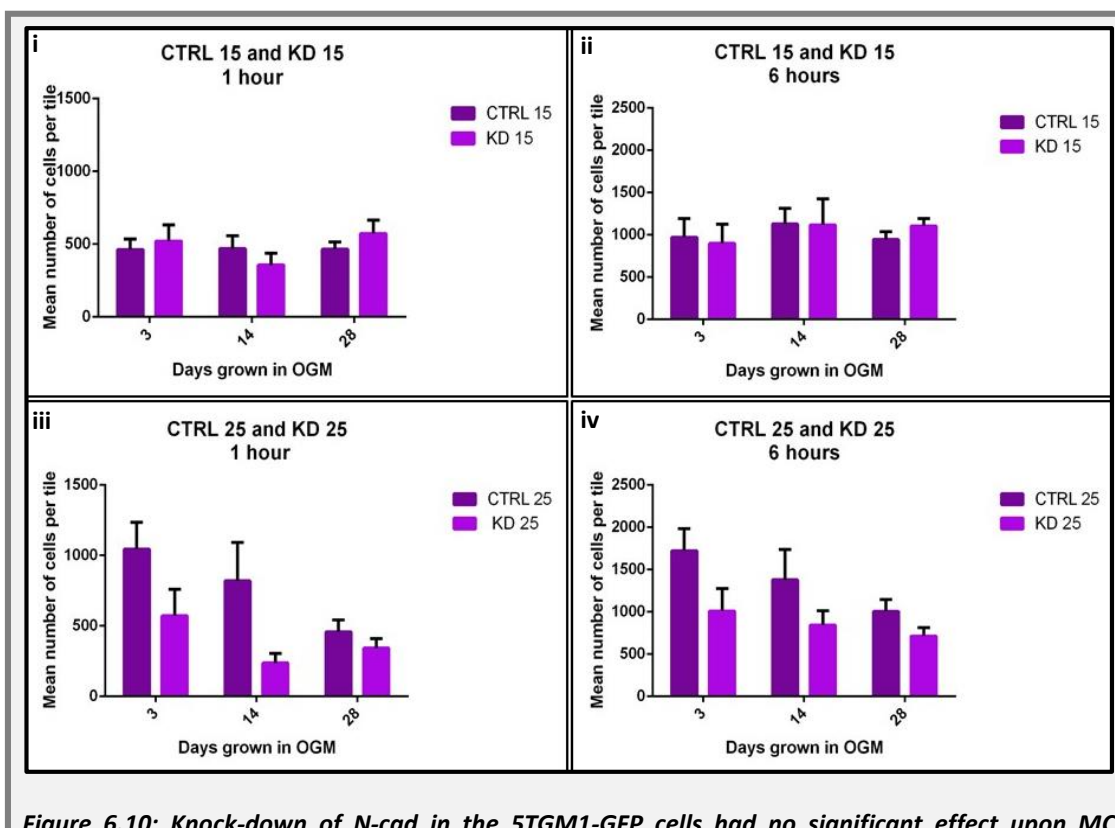


Figure 6.10: Knock-down of N-cad in the 5TGM1-GFP cells had no significant effect upon MC adhesion to primary osteoblast lineage cells *in vitro*. Fifty thousand CTRL 15 and 25 and KD 15 and 25 cells were seeded on to primary OLCs cultured in OGM containing 10 mM BGP and 50 µg/ml asc for 3, 14 and 28 days. Adhesion after 1 and 6 hours was imaged using a Leica AF6000LX microscope at a 10X magnification using LAS LF software and analysed using Volocity software to determine the number of MCs adhering to primary OLCs per tile. **i-ii.** A comparison between the number of CTRL 15 and KD 15 cells adhering to primary OLCs cultured in OGM for 3, 14 and 28 days after 1 hour (i) and 6 hours (ii). **iii-iv.** A comparison between the number of CTRL 25 and KD 25 cells adhering to primary OLCs cultured in OGM for 3, 14 and 28 days after 1 hour (iii) and 6 hours (iv). Data was analysed statistically using a Mann Whitney U test ($P < 0.05$) to determine any differences in the number of CTRL and KD cells adhering to primary OLCs cultured in OGM for at 3, 14 and 28 days after 1 and 6 hours. A Friedman test followed by Dunn's post test was used to determine any differences in MC adhesion to primary OLCs at 3, 14 and 28 days cultured in OGM ($P < 0.05$). Results were determined from four independent experiments ($N=4$).

6.4.10 Flow cytometry to determine the effect of knocking-down N-cad in the 5TGM1-GFP cells upon myeloma cell growth *in vivo*

An initial pilot study was conducted to firstly, determine whether the transduced CTRL 25 and KD 25 cells would home and grow in the BM of injected mice, as extensive time in culture could reduce tumourgenicity in these cells. Secondly, it was conducted to determine whether there was any difference in tumour load between the CTRL and KD groups.

The standard 5TGM1-GFP cells, CTRL 25 or KD 25 cells were injected into C57BL/KaLwRij mice and all groups were sacrificed when one of the mice became ill, which was at 25 days P-I in the 5TGM1-GFP injected group. The left and right femora were dissected from each mouse and the BM was isolated to detect GFP positive tumour cells by flow cytometry. Figure 6.11 shows representative flow cytometry profiles of the BM from mice injected with standard 5TGM1-GFP cells, CTRL 25 and KD 25 cells.

The GFP positive tumour cell number was assessed by flow cytometry, as shown in Figure 6.11b. The data demonstrated a higher number of GFP positive tumour cells in the BM of the 5TGM1-GFP injected animals ($32.90\% \pm 3.7$, data not shown) compared to the CTRL 25 injected animals ($0.6\% \pm 0.59$) and GFP positive KD 25 cells were not detected in the animals injected with KD 25 cells ($0.01\% \pm 0.00$) using flow cytometry. Interestingly, there was a significant reduction in KD 25 cells present in the BM of mice compared to CTRL 25 cell injected animals ($P < 0.05$).

Tumour take was assessed using a Fisher's exact test, to compare the number of mice and number of bones (as two femurs were used) with positive tumour burden between the groups. Bones with more than 0.05% GFP positive cells were deemed positive for tumour burden. As shown in Figure 6.11c, each mouse in the 5TGM1-GFP group was positive for GFP (100%), in the CTRL 25 injected group 4 out of 6 mice had GFP positive tumour burden (67%) and no mice in the KD 25 demonstrated tumour burden greater than 0.05% (0%). When compared using the Fisher's exact test there was a significant difference in the number of mice with tumour in the 5TGM1-GFP injected group compared to the KD 25 injected group ($P < 0.0048$). However, there was no significant difference between the 5TGM1-GFP and CTRL 25 injected group ($P < 0.4667$) or between the CTRL 25 and KD 25 groups ($P < 0.0606$).

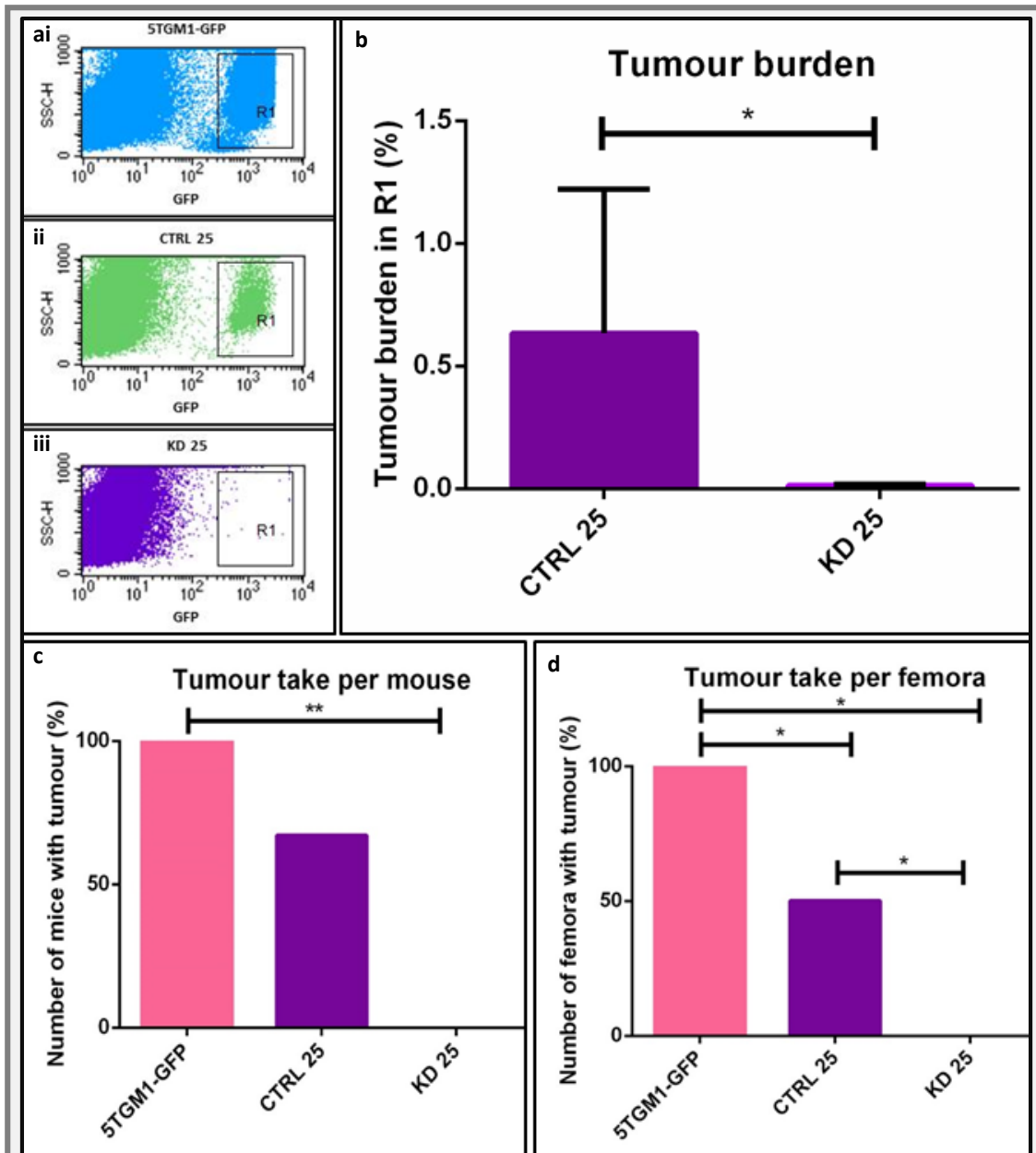


Figure 6.11: Mice injected with N-cad KD 25 cells had less tumour and reduced tumour take compared to mice injected with CTRL 25 cells, analysed by flow cytometry. 5TGM1-GFP (N=4), CTRL 25 (N=6) and N-cad KD 25 (N=6) cells (2×10^6) were injected (IV) into 11 week old C57BL/KaLwRij mice. At 25 days P-I (when the first mouse developed hind limb paralysis) all mice were sacrificed. The left and right femora were dissected and the BM was isolated. Flow cytometry was used to quantify the number of GFP positive cells in the BM using a FACS Calibur and Cell quest software. **a** Representative flow cytometry plots demonstrating the GFP positive tumour in the 5TGM1-GFP (i), CTRL 25 (ii) and KD 25 (iii) injected mice. **b**. The percentage of GFP positive tumour burden (in R1 of the FACS plot) in mice injected with 5TGM1-GFP, CTRL 25 and KD 25 cells. **c**. The percentage of tumour take per mouse, in mice injected with 5TGM1-GFP, CTRL 25 and N-cad KD 25 cells. **d**. The percentage of tumour take per femora, in mice injected with 5TGM1-GFP, CTRL 25 and N-cad KD 25 cells. Data was analysed using a Mann-Whitney U test to compare tumour burden between mice injected with CTRL 25 and N-cad KD 25 cells. A Fisher's exact test was used to compare the number of mice and femora with positive tumour burden between the 5TGM1-GFP, CTRL 25 and N-cad KD 25 injected mice. Each mouse was a biological replicate.

When the number of femora, which were positive for GFP was calculated, each femora in the 5TGM1-GFP injected mice group was positive for GFP positive (100%), 6 out of 12 femora were positive for GFP in the CTRL 25 groups (50%) and again no bones were positive for GFP in the KD 25 group (0%), as demonstrated in Figure 6.11d. Using the Fisher's exact test there were significantly less femora which were positive in the CTRL 25 ($P < 0.0445$) and KD 25 ($P < 0.0001$) injected mice compared to the 5TGM1-GFP injected mice. There were also significantly less femora which were positive for GFP in the KD 25 injected group compared to the CTRL 25 injected group ($P < 0.0137$).

6.4.11 IHC to determine the effect of knocking-down N-cad in the 5TGM1-GFP cells upon myeloma cell growth *in vivo*

Immunohistochemistry was also used to assess tumour burden. Figure 6.11a demonstrates representative images of histological sections of tibiae stained for CD138, taken from mice injected with CTRL 25 and N-cad KD 25 injected mice. Discrete tumour colonies were not observed in any of the KD 25 mice tibiae, though some CD138 staining was present in some of the bones as shown in Figure 6.12a-iii-iv. However, the staining present was not discrete membranous staining as observed in the CTRL 25 sections. In addition, all 5TGM1-GFP injected mice had fully infiltrated bones (data not shown), which correlated with the flow cytometry shown in Figure 6.12.

When tumour colony area and number was analysed using the Image Scope software there was interestingly, a significant decrease in tumour area in mice injected with N-cad KD cells compared to CTRL injected mice ($P < 0.0043$) (Figure 6.12b). However, the 5TGM1-GFP injected mice had fully infiltrated bones with between 80.78-99.77% (colony area) (data not shown), compared to the low percentage in the CTRL 25 injected mice. There was also a decrease in the number of colonies present in the BM of mice injected with CTRL 25 or KD 25 cells (Figure 6.12c) but this failed to reach significance.

When the number of mice which demonstrated positive tumour burden by CD138 staining (positive tumour burden was classed as colony area greater than 0.2%) were compared between the groups using a Fisher's exact test, significantly more mice (expressed as a percentage) in the CTRL 25 group had tumour compared to the KD 25 group ($P < 0.0152$), shown in Figure 6.12d.

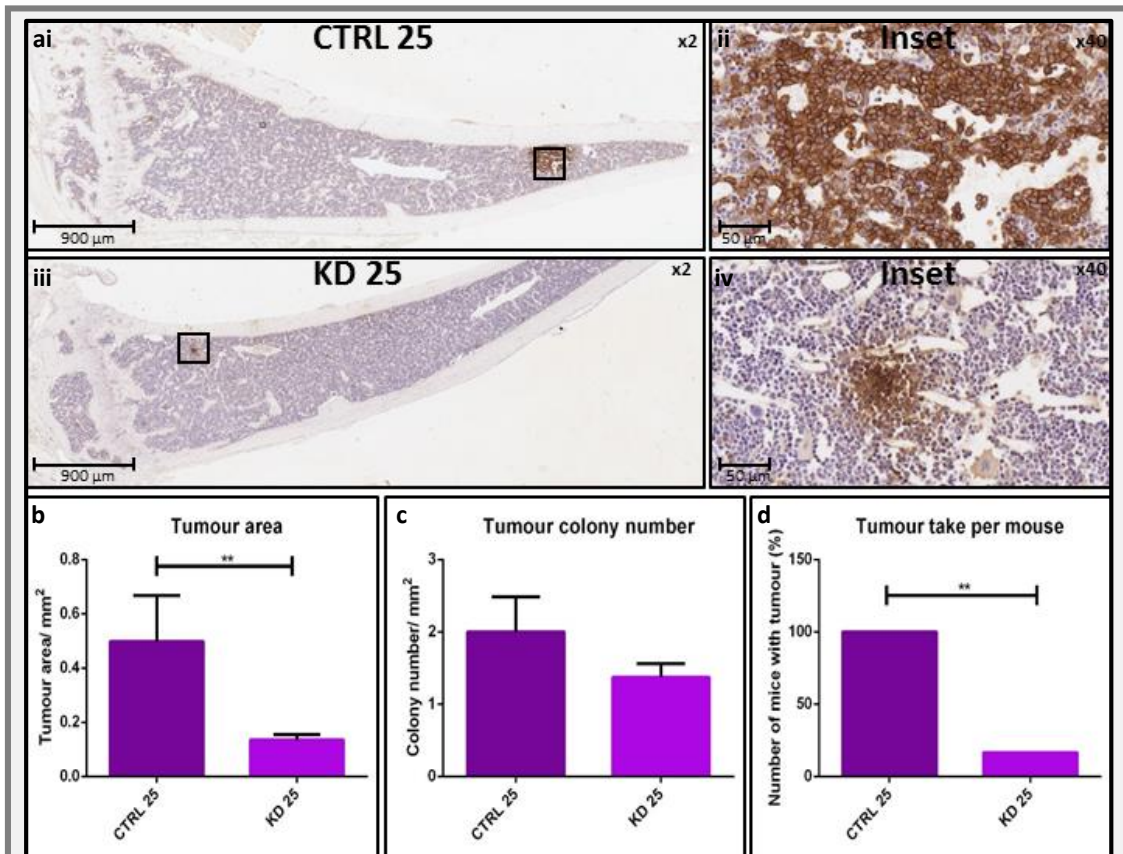
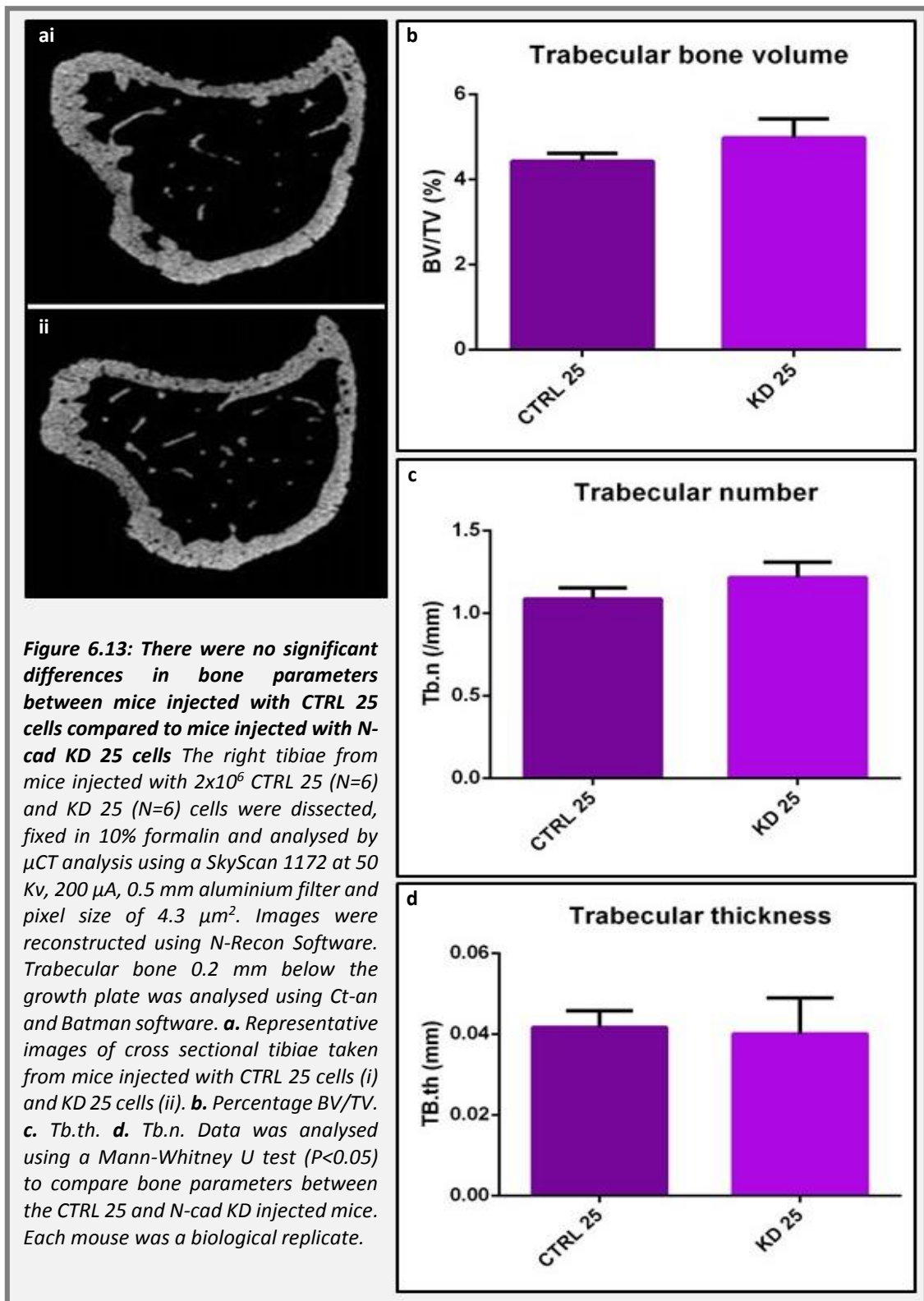


Figure 6.12: Mice injected with N-cad KD 25 cells had significantly less tumour compared to mice injected with CTRL 25 cells, analysed by IHC. Two million CTRL 25 (N=6) and KD 25 (N=6) cells were injected (IV) into 11 week old C57BL/KaLwRij mice. At 25 days P-I (when the first mouse developed hind limb paralysis) all mice were sacrificed. The left tibia was dissected and processed for histology by fixation for 24 hours in 4% PFA, decalcification for 2 weeks in 0.5% PFA/0.5 M EDTA followed by dehydration and processing into wax. Sections were cut (3 μ m) and stained by sandwich IHC for CD138. Sections were analysed using an Aperio Scan Scope slide scanner and Image Scope software to determine tumour colony area and number per mm² of BM. **a** Representative images of CD138 stained sections of tibiae from mice injected with CTRL 25 cells (i-ii) and KD 25 cells (iii-iv). **b**. The percentage of total colony area in mice injected with CTRL 25 and KD 25 cells **c**. The number of tumour colonies present in mice injected with CTRL 25 and KD 25 cells. **d**. Tumour take in mice injected with CTRL 25 and N-cad KD 25 cells. Data was analysed using a Mann-Whitney U test to compare colony area and number between the groups and a Fisher's exact test was used to compare the number of mice with tumour between the CTRL 25 and KD 25 injected mice. Each mouse was a biological replicate.

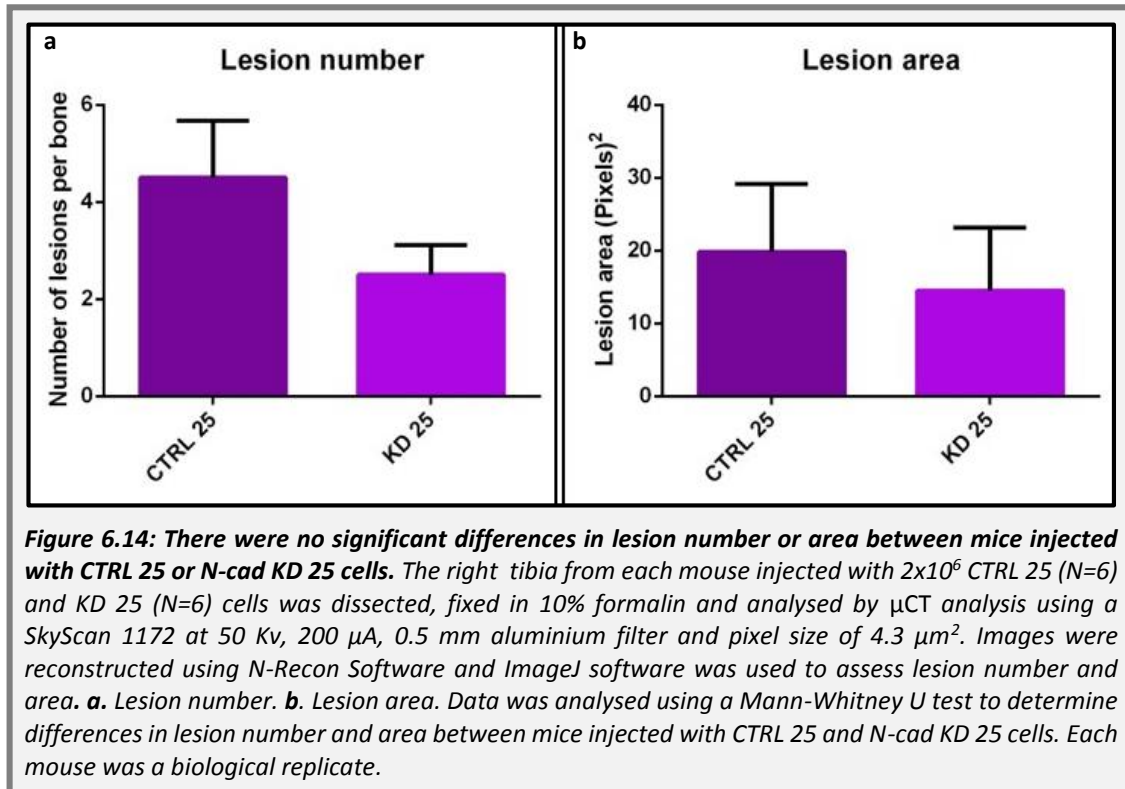
6.4.12 Micro-computed tomography to determine the effect of knocking-down N-cad in the 5TGM1-GFP cells upon bone parameters *in vivo*

To assess any differences in bone parameters between the groups μ CT was used. Figure 6.13 demonstrates the percentage of trabecular bone volume (BV/TV), trabecular number (tb.n) and trabecular thickness (tb.th) for the tibiae of mice injected with CTRL 25 and KD 25 cells. Statistically, there were no significant differences in percentage BV/TV, tb.n and tb.th between the CTRL 25 and KD 25 injected mice. However, there did seem to be a slight trend whereby the N-cad KD 25 cell injected mice had slightly higher values for the percentage BV/TV and tb.n, compared to the CTRL 25 injected mice.



Lesion number and area were calculated using ImageJ software, as shown in Figure 6.14. There was a trend towards a reduction in lesion number and area in mice

injected with the KD 25 cells compared to the CTRL 25 cells however, this did not reach significance.



6.5 Discussion

The aims of this chapter were to determine the role of HSC niche molecules in MC adhesion to osteoblastic cells *in vitro* as well as tumour growth *in vivo*. To achieve these aims, lentiviral particle shRNAs were used to KD HSC molecules in the 5TGM1-GFP cells. Before transduction, optimisation of the technique was conducted to determine the optimum dose of puromycin and polybrene and also a suitable MOI of virus using GFP transduction.

Firstly, puromycin concentrations were determined by conducting dose titration killing curves using TO-PRO-3 and flow cytometry. The final concentration of

puromycin used for the 5TGM1-GFP cells was 5.0 µg/ml and 7.5 µg/ml was used for the 5T33-WT cells. These concentrations produced significantly more cell death compared to the control and they were also the lowest doses required to kill the maximum amount of cells within four days, as suggested by the manufacturer. The potency of puromycin seemed to vary depending on the cell type, as shown by the higher dose required to kill the maximum amount of 5T33-WT cells. However, this higher dose was also used in previous studies where Glick *et al* (172) used puromycin at 7.0 µg/ml for the 5T33-WT cells. The difference between the sensitivity of MCs to puromycin has not previously been reported, but it was interesting that the 5TGM1-GFP cells seemed to be more sensitive to puromycin compared to the 5T33-WT cells.

Polybrene optimisation was then conducted by assessing differences in cell number following polybrene treatment after 24 hours. As there was no significant effect upon cell number following treatment, with the exception of 10.0 µg/ml using the 5TGM1-GFP cells, 5.0 µg/ml was used as advised by the manufacturer. Further experiments could have been investigated to determine long-term effects of polybrene treatment although, the polybrene was only required to be incubated with the cells for 24 hours and the manufacturer reported no effects of toxicity at the 5.0 µg/ml dose.

Following puromycin and polybrene optimisation, GFP transduction was conducted in the 5T33-WT cells as a proof of principal that the transduction technique would work in the MCs. Green fluorescent protein transduction was successful at MOIs of 15 and 25 but not at a MOI of 5 due to a lack of resistance to the puromycin treatment. This implies that the lentiviral particles were either not successfully transduced or that the number of puromycin resistance gene sequences integrated into the host genome using a MOI of 5 was not sufficient to incur resistance to puromycin, resulting in cell death. Therefore, this suggests that at the higher doses of virus, an adequate amount of the puromycin resistance gene was integrated into

the genome to inhibit the effect of puromycin on protein synthesis, preventing cell death.

These optimal conditions were used to KD N-cad and CXCR4 in the 5TGM1-GFP cells. N-cad was chosen due to its novelty in MM, as previous data is limited. CXCR4 was chosen as previous studies had largely focussed upon the role of CXCR4 in homing, but not in the context of a myeloma niche. Previous studies have also used compounds rather than KDs to block all CXCR4 positive cells, whereas, the KDs used here, were specific for the MCs.

N-cad was successfully knocked-down at MOIs of 15 and 25 whereas, CXCR4 was slightly knocked-down at an MOI of 15 (24%) and there was no KD at all using a higher MOI of 25. From these experiments, it can be concluded that increasing the MOI did not increase CXCR4 KD. Therefore, increasing the numbers of sequence insertions into the host's genome made no difference, implying that the shRNA sequences used were not effective at knocking down the gene. The lentiviral particles contained three different shRNA constructs, therefore, three different siRNAs would bind to three different sequences on the mRNA for CXCR4, increasing the probability that one sequence would result in the degradation of CXCR4 mRNA. However, in these experiments these sequences were not effective at knocking-down CXCR4. To improve this in the future, custom made shRNAs may be required with particular care to account for splice variants, which do occur within murine CXCR4. It may also help to use a different promoter such as the U6 rather than the H1, which was reported to be more effective (188).

As the real-time PCR for N-cad was successful, further validation was conducted using WB, which confirmed the results found in the real-time PCR. Western blotting showed that there was a protein KD of 68% and 65% in the 5TGM1-GFP cells at MOIs of 15 and 25, respectively. However, when the cells were cultured in the absence of

puromycin this resulted in some loss of N-cad KD in the KD 15 cells using both real-time PCR and WB whereas, using the KD 25 cells the gene and protein KD was stable. This implies that perhaps the amount of shRNA incorporated into the host DNA at the MOI of 15 was not sufficient to sustain the KD or that the original selection process was not selective enough, resulting in the expansion of cells without the shRNA, therefore, reducing the percentage of population KD.

To confirm any effect upon proliferation in the N-cad KD cells, growth curves were conducted using the CTRL and N-cad KD cells. There were no significant differences in proliferation between the CTRL 15 and KD 15 and CTRL 25 and KD 25 cells with regards to doubling time. This is supported by Groen *et al* (206) who found that inhibition of N-cad using an antibody or by knocking-down N-cad in NCI-H929 MCs had no effect upon proliferation. Whereas, in prostate cancer, antibody inhibition of N-cad using 1H7 and 2A9 clones resulted in a significant reduction in PC3 and LNCAP-C1 cell proliferation (203). However, these cells are highly adherent compared to the MCs, which may influence their requirement for N-cad signalling as a stimulant for proliferation.

To test the effect of N-cad KD upon MC adhesion to osteoblastic cells, co-culture experiments were conducted using the conditions from Chapter V. Knock-down of N-cad in the 5TGM1-GFP did not significantly impair their ability to adhere to primary OLCs cultured in OGM for 3, 14 and 28 days. There was however, a trend decrease in adhesion of KD 25 cells to primary OLCs at each of the time points compared to the CTRL 25 cells. Whereas, there was no obvious difference between the CTRL 15 and KD 15 cells. The difference between the MOI 15 and 25 cells may be due to the stability of the KD in the cells. As identified previously, N-cad KD using the MOI of 15 was unstable compared to the MOI of 25 and therefore, the increase in N-cad protein could remove any inhibitory effect in the adhesion to the primary OLCs. As only a trend was observed towards a decrease in the adhesion of the KD 25 cells to the

primary OLCs this might imply that the N-cad is not the sole molecule responsible for MC adhesion to osteoblastic cells. Other molecules previously implicated in this interaction are; Notch-1 and Jag-1 (described for their role in osteoblast adhesion), intercellular adhesion molecule (ICAM) 1 (expressed by osteoblastic cells) (272) and LFA-4 (expressed by MCs) (273) and vascular cell adhesion molecule-1 (VCAM-1) (expressed by BM stromal cells) (274) and VLA-4 (expressed by MCs) (275).

A lack of significance between N-cad KD and controls may also be due to the percentage of N-cad KD in the cells. N-cad has not been knocked-out but knocked-down and using RT-PCR and WB it is uncertain whether 71% of cells are knocked-down or whether protein within each individual cells is knocked-down by 71%. This therefore, means that N-cad is still present to a certain extent and therefore, even low levels may result in adhesion of MCs to the primary OLCs. However, to disprove this point, a previous paper has shown a significant reduction in the adhesion of N-cad KD NCI-H929 MCs to C3H10T1/2 cells (206). Although, as the C3H10T1/2 cells are MSCs as opposed to preosteoblasts or mature osteoblasts, this could be a potential explanation as to why these results differ from my own. As stated previously in Chapter V this technique may also not provide reliable results due to elements within the technique, which may need further optimisation, such as the wash steps, cell numbers and types of media or FBS used.

An initial pilot study was conducted, firstly, to test whether the CTRL 25 and KD 25 cells, which had been cultured extensively *in vitro*, still homed and grew in the BM and secondly, to determine whether there was a difference in tumour burden between the mice injected with the KD 25 cells compared to those injected with the CTRL 25 cells. CTRL and KD 25 cells were used due to their high level of gene and protein KD and low gene and protein KD variability when in puromycin free conditions compared to the CTRL 15 and KD 15 cells. The flow cytometry data confirmed that the CTRL 25 and KD 25 cells cultured extensively *in vitro* did not either

home to the bone as effectively or grow as quickly *in vivo* compared to the normal 5TGM1-GFP cells. This was shown by higher tumour take and tumour burden in the 5TGM1-GFP injected mice compared to the CTRL 25 and N-cad KD 25 injected animals. As stated previously this was expected, as the 5TGM1-GFP cells require *in vivo* passaging to remain tumourgenic.

The aspect of the data that was of most interest was the difference in tumour take and tumour burden between the CTRL 25 and KD 25 injected mice by flow cytometry and IHC. However, as stated previously, this was an initial pilot study and therefore, may need to be repeated to assess reproducibility. Based on the flow cytometry data there was a significant reduction in tumour burden in the mice injected with the KD 25 cells compared to those injected with the CTRL 25 cells. When the number of mice with tumour were compared, 67% of the mice in the CTRL 25 group were positive compared to 0% of mice injected with KD 25 cells. Although, this difference was not significant as two mice in the CTRL group did not have tumour. However, when the number of bones with tumour rather than per mouse were analysed, (as two femora per mouse were analysed), significantly fewer femora in the KD 25 injected group were positive for tumour compared to the CTRL 25 group. In addition, the IHC staining supported the flow cytometry results in the pilot study. Firstly, full infiltration of the BM was observed in all of the 5TGM1-GFP injected mice by CD138 staining. In the CTRL 25 injected mice, distinct colonies were visualised whereas, in the KD 25 injected mice, only small less discrete colonies were observed. This slightly contradicts the flow cytometry data where no GFP positive tumour cells were present in the KD 25 injected mice. However, flow cytometry can be limiting, firstly due to the way the BM is flushed and secondly due to the sensitivity of detecting low numbers of GFP by the machinery and the software. Despite differences in techniques, both the flow cytometry and IHC results suggested that there was a significant reduction in tumour burden in the KD 25 injected mice compared to the CTRL 25 injected mice and there was also a trend towards fewer tumour colonies present in the KD 25 injected mice by IHC. These data may potentially suggest a role

for N-cad with regards to MC homing, MC survival in the BM following injection as well as MC proliferation, though the latter may be questionable as no proliferative effects were observed in the N-cad KD cells *in vitro*, though factors *in vivo* may affect this.

Micro-CT was also conducted to examine the effect of N-cad KD upon bone disease, as the 5TGM1-GFP model results in lytic lesions in the mice. When comparing the CTRL 25 and KD 25 trabecular bone parameters, there were no significant differences between these groups. However, there was a slight trend towards an increase in the BV/TV, trabecular number, lesion number and lesion area in the KD 25 injected animals compared with the CTRL 25 group, which correlated with tumour burden. However, as little tumour burden was present in the mice it was unsurprising that no significant differences were found, as there may have not been sufficient tumour present to induce increases in osteoclastic bone resorption and decreases in osteoblastic bone formation. In addition, as a naïve mouse group was not used in this study there was also no comparator for normal bone parameters, therefore, whether either group of mice had evident bone disease was undetermined.

The data in this chapter, particularly with regards to the pilot *in vivo* study, provides evidence in support of the hypothesis that N-cad is important for myeloma development. From these studies, the precise role of N-cad in myeloma development is unknown but these experiments may imply that N-cad is involved in MC homing, survival and/or proliferation; however, due to poor tumour burden and low N numbers these findings are not completely conclusive. Currently, very little evidence is available to determine the role of N-cad in MM and no studies have looked at the effect of knocking N-cad down in MM upon tumour burden at the end-stage of disease. Groen *et al* (206) has however, examined the effect of knocking-down N-cad in NCI-H929 cells upon the number of MCs in the BM after 3 days post-injection and found that fewer N-cad KD NCI-H929 cells were present in the bone and more of

these cells were in the circulation compared to control NCI-H929 cells. Therefore, N-cad may be important for homing of MCs to the BM as well as attachment to a MC niche and MC survival. In addition, Sadler *et al* (207) found that inhibition of MC adhesion to stromal cells *in vitro* using an anti-N-cad antibody resulted in increased proliferation implying that MC attachment to stromal cells via N-cad is important for control of cell proliferation and cell cycle. However, this is contradictory to the experiments conducted in this chapter, which demonstrated reduced TB in mice injected with N-cad KD cells. However, as stated previously it is unknown as to whether the reduction in TB is due to reduced MC homing, survival or proliferation in the BM post-injection, and also as this is a KD not KO, cells arriving in the BM maybe N-cad positive and so no effect on proliferation would be observed. In addition, the experiment conducted by Sadler *et al* was conducted *in vitro*, and therefore, the behaviour of these cells *in vivo* may not be comparable.

Previous studies also determined that N-cad was an important molecule with regards to cancer cell growth and metastasis as described in the introduction. Tanaka *et al* (203) demonstrated that inhibition of N-cad using two different monoclonal antibodies significantly inhibited PC3 and LAPC9-CR (prostate cell lines) invasion, proliferation and attachment to fibronectin *in vitro* and significantly reduced tumour volume of both PC3 and LAPC9-CR subcutaneous tumours as well as preventing metastasis to the lymph nodes *in vivo*. N-cad expression in breast cancer cell lines including MDA-MB-435, SUM-159 cells and MCF-7 cells was associated with higher motility and invasion *in vitro* (204, 268) and increased metastasis *in vivo* (268). N-cad expression has also been implicated in melanoma whereby inhibition of N-cad in melanoma cell lines using an inhibitory antibody reduced adhesion and migration to fibroblasts *in vitro* (270).

In conclusion, I have been able to optimise a technique for the successful KD of one of the HSC niche molecules in the 5TGM1-GFP cells. However, the effect of the KD of

N-cad in the MCs with regards to adhesion to osteoblasts and its effect upon *in vivo* are still not completely conclusive. Therefore, further experiments are required to provide more conclusive evidence for the role for N-cad in an osteoblastic niche in bone using either the KD cells developed here or an N-cad inhibitor.

Chapter VII:
General discussion

7.1 General discussion

To date, MM is an incurable disease whereby only 5% of patients survive 5 years post-diagnosis. It results in severe disorders such as renal failure, lytic bone disease and susceptibility to infection, which in turn cause morbidity. It has been speculated that high rates of patient relapse in MM patients are due to a chemoresistant population of myeloma cells, which are able to survive even after treatment, rendering current chemotherapeutic strategies ineffective at completely eradicating disease. Therefore, new treatment strategies are required in an attempt to provide curative treatments. In addition, preventative strategies are required to stop the progression of MGUS to symptomatic myeloma and asymptomatic to symptomatic myeloma, which have a 1% chance within one year post-diagnosis, and 10% chance within five years post-diagnosis, of progression respectively (276).

Due to the potential survival of chemoresistant cells in patients after treatment, this led to the hypothesis that MM cells exist in a niche in the BM, which determines their proliferation, and promotes survival upon treatment with chemotherapeutic agents. This rationale was based upon previous studies, which identified a HSC niche in the BM. This HSC niche firstly; demonstrated the requirement of osteoblastic cells for HSC survival in the BM by a series of studies which reduced (71, 78, 79) or increased (81, 82) osteoblastic cell number using murine transgenic studies and hormone treatments. Secondly; HSCs seemed to localise and adhere specifically to osteoblastic cells (83) as well as endothelial cells (88, 89, 277) *in vivo*, which seemed a critical interaction for their survival. In addition, HSCs adhering to osteoblastic cells in the BM resided in a quiescent state but once activated began to proliferate (73, 142).

To firstly provide evidence of MM cell localisation to osteoblastic cells in a similar way to HSCs, several *in vivo* studies were conducted by members of the myeloma research group at The University of Sheffield and The Garvan Institute, Sydney Australia (Paper in submission "A Novel Method for Longitudinal Tracking of Dormant

Cancer Cell Activation in the Skeleton as a Platform for Drug Discovery”). C57BL/KaLwRij mice were injected with 1,1'-dioctadecyl-3,3,3',3'-tetramethylindodicarbocyanine perchlorate (DiD) labelled 5TGM1-GFP cells and after 18 and 72 hours single labelled MCs were found in close proximity to bone. However, over a time course, the majority of cells moved away from the bone surface and began to proliferate whereas, only single un-dividing DiD labelled cells, which were potentially quiescent, were still adjacent to the bone surface. Therefore, these data may imply that the MCs that were in contact with bone were dormant, whereas those that were further away from the bone were actively dividing. However, without staining these cells with cell cycle dyes it is difficult to conclude whether these cells are actively dividing or quiescent. In support of this work, Chen *et al* (70) found that PKH26 labelled MCs were found in close proximity to osteoblastic cells in the bone and a higher frequency of PKH26 positive cells were present in osteoblastic niches compared to vascular and splenic niches *in vivo*. In addition, PKH26 positive cells were more resistant to chemotherapeutics *in vitro* compared to PKH26 negative MCs. Therefore, this supports the hypothesis that MCs reside in osteoblastic niches, which may result in MC chemoresistance, potentially mediated by cellular quiescence.

Within my experiments in this thesis, I conducted *in vitro* experiments to determine whether the 5TGM1-GFP cells adhered to primary OLCs, as this again would provide evidence for the adhesion of MCs to osteoblastic cells (Chapter V). A large proportion of 5TGM1-GFP cells adhered to primary OLCs *in vitro* and the adhesion was highest when the OLCs had been differentiated for 3 days and 14 days compared to 28 days. This suggested that early primary OLCs may be more important for MM cell adhesion as described by Zhang *et al* (83) and Xie *et al* (84) in the HSC niche.

To determine what molecule interactions may result in the adhesion of MM cells to osteoblastic cells, the expression of the HSC niche molecules and ligands was analysed using 5T33-WT, 5T33-GFP and 5TGM1-GFP cells. In addition, the expression of complementary ligands was explored using murine primary OLCs and MC3T3-E1

osteoblastic cells. It was hypothesised that the MM cells expressed the same repertoire of molecules as the HSCs and that their complementary ligands were expressed by osteoblastic cells.

Within my studies, I determined the expression of the HSC niche molecules; CXCR4, Notch-1, Tie-2 and N-cad, and the complementary ligands; CXCL12 and Jag-1 by the MCs cultured *in vitro* (Chapter III), collectively using RT-PCR (endpoint and real-time), flow cytometry and IF. In addition, BM-derived *ex vivo* 5T33-GFP and 5TGM1-GFP cells also expressed the HSC niche molecules CXCR4, Notch-1, Tie-2 and complementary ligands CXCL12 and Jag-1 by flow cytometry, and BM sections infiltrated with 5TGM1-GFP cells also expressed CXCR4 and N-cad *in vivo* (Chapter IV). In addition, the expression of each of these molecules (excluding CXCR4) was reduced in the BM-derived 5TGM1-GFP at the end-stage of disease compared to the *in vitro* cells whereas, the protein frequency of all HSC niche molecules increased in the BM-derived 5T33-GFP cells compared to the 5T33-GFP cells cultured *in vitro*. Therefore, these data suggest that the expression of these molecules may be important in disease progression.

The expression of these molecules by MCs is supported by a variety of studies. CXCR4 was expressed by MC lines (170, 193-195) and primary patient MCs (195, 221) and its ligand CXCL12 was also expressed in human MC lines and patient samples (215). Notch-1 was expressed by several human MC lines (197) and patient MCs (198) and expression of Jag-1 was demonstrated in patient MC samples (198, 214). Tie-2 was also present in human MC lines and patient samples (201) as was Ang-1 (201). N-cad expression was also determined in patient MM cells (205) and the human MC lines (206, 207).

I also analysed the expression of the complementary ligands CXCL12, Jag-1, Ang-1 and N-cad, as well as the HSC niche molecules CXCR4, Notch-1 and Tie-2 using the MC3T3-E1 cells and primary OLCs (Chapter III). Each cell type expressed each complimentary ligand as well as the HSC niche molecule Notch-1 and the primary OLCs also expressed Tie-2. When the primary OLCs were cultured with OGM (Chapter

V), there were no significant differences in the expression of the HSC niche molecules or ligands, though there was a trend towards a decrease in Jag-1 and N-cad expression over-time. Therefore, differentiation of these cells did not significantly affect HSC niche and ligand expression, though as stated previously without the suitable controls this is difficult to conclude.

The expression of each of the complementary ligands by osteoblastic cells was supported by previous studies. CXCL12 was expressed by human and murine osteoblast cell lines (111, 196); Jag-1 was expressed by human primary BM stromal cells (199) and the MC3T3-E1 osteoblastic cells (200); Ang-1 was expressed by murine primary osteoblasts (85); and N-cad was expressed by several stromal and osteoblast cell lines (206, 208, 219).

Taken together, these studies supported the hypothesis that MCs express the same repertoire of niche molecules as HSCs and that their complementary ligands are expressed by osteoblastic cells. However, the function of each of these molecules in a MM cell niche was unknown. Therefore, to determine the role of these molecules I attempted to KD both CXCR4 and N-cad in the 5TGM1-GFP cells, with a successful KD of both gene and protein using N-cad shRNA (Chapter VI). As stated previously, these molecules were chosen, as little is known about the role of N-cad in MM, particularly as a candidate molecule in a MC niche. Whereas, CXCR4 has been highly studied with regards to mobilisation of MCs as well as other cell types, however, it has not been implicated specifically in an osteoblastic niche in MM. In addition, previous pre-clinical and clinical studies have focussed on inhibiting CXCR4/CXCL12 signalling using antibodies and inhibitors such as AMD3100, which target all CXCR4 positive cells, however, previous studies have not targeted CXCR4 specifically on the MCs, which the gene KD would achieve.

I then determined the effect of knocking down N-cad in the 5TGM1-GFP upon adhesion to primary osteoblastic cells *in vitro* (Chapter VI). In these experiments a consistent trend towards a reduction in the adhesion of KD 25 cells to OLCs at all time-points compared to the CTRL 25 cells was observed, however this did not reach

significance. This trend is supported by other studies which showed that KD of N-cad significantly reduced MC adhesion to osteoblastic cells however, this was using the human MC line NCI-H929 and C3H10T1/2 stromal cells (206). My results may imply that N-cad is not the only molecule responsible for MC adhesion to osteoblastic cells and as this is a KD of protein rather than KO, residual N-cad expression may still result in myeloma adhesion to osteoblastic cells.

An initial *in vivo* pilot study was then conducted to test firstly, whether extensive growth of the CTRL 25 and KD 25 *in vitro* would affect their ability to home and grow in the BM and secondly to determine any differences in tumour burden in mice injected with CTRL and N-cad KD cells. I hypothesised that the cells that had been cultured extensively *in vitro* would not home and/or grow at the same rate as the standard 5TGM1-GFP cells. I also hypothesised that tumour burden would be reduced in the mice injected with the KD 25 cells compared to CTRL cells. In support of these hypotheses, mice that had been injected with either the CTRL 25 or KD 25 cells, had significantly less tumour take (determined by flow cytometry and IHC) compared to the mice injected with the standard 5TGM1-GFP cells. Interestingly, to support the second part of the hypothesis, mice injected with the KD 25 cells had no GFP positive tumour determined by flow cytometry and a significant reduction in tumour area compared to mice injected with CTRL 25 cells. In addition, mice injected with the KD 25 cells also had a significantly lower take rate and fewer bones with tumour present compared to CTRL 25 injected mice using flow cytometry and IHC. This pilot study therefore, highlights the potential importance of N-cad for myeloma tumour development in the BM. However, as stated previously these results are not entirely conclusive due to poor tumour take and low N numbers. These results are however, supported by previous studies, which have explored the role of N-cad in other cancers such as breast, prostate and melanoma. In previous studies, N-cad expression was important for prostate and breast cancer cell invasion and metastasis (203, 204, 268), and interventions of N-cad inhibited tumour cell growth and metastasis in prostate and melanoma (203, 278). In addition, Groen *et al* (206), demonstrated that N-cad KD in the NCI-H929 MCs resulted in fewer cells homing to and/or surviving in the BM *in vivo*, and also found a higher number of these cells

present in the circulation. Therefore, N-cad may potentially be important for trans-endo migration or adhesion to osteoblastic cells in the BM and subsequent survival.

As this was a pilot study, this experiment needs to be repeated to confirm the results. In addition, future studies need to focus on the localisation of MCs with the hypothesis that KD of N-cad will prevent MC attachment to an osteoblastic niche in the BM, which is required for MC development. In this pilot study, only the latter time points of active cell growth were determined rather than the initial homing and colonisation of cells to the bone. Therefore, future studies also need to concentrate on the early time points of disease to determine differences in the number of cells originally homing to the bone and also assessing their localisation to osteoblastic cells at that time.

Other unanswered questions, which this study does not address is the potential for N-cad positive cells to promote chemoresistance in MCs. In addition, N-cad also seems to play an important role in epithelial-mesenchymal transition, where the switching between E-cadherin (E-cad) and N-cad determines the proliferative and metastatic state of the cells. In prostate cancer, high N-cad expression was associated with low E-cad expression in prostate cancer biopsies, which correlated with increasing severity of the prostate cancers (228, 279, 280) which were also associated with poorer patient outcome. In breast cancer, a reduction of E-cad staining in patient breast biopsies also correlated with increased severity of disease (281) and, several breast cancer cell lines which were positive for N-cad but had no evidence of E-cad expression were more invasive *in vitro* (204), suggesting again that cadherin switching may be important for tumour invasion and metastatic potential. Therefore, this suggests that the relationship between E-cad and N-cad may also be an important mechanism potentially in MM, where E-cad expression may precede N-cad expression in quiescent tumour cells after which they may be activated resulting in cadherin switching from E-cad to N-cad triggering proliferation. Therefore, it would be of interest to determine whether a cadherin switch occurs throughout the

different stages of myeloma progression and whether it is the initial E-cad positive cells, which promote quiescence, followed by N-cad expression, which results in proliferation. In addition, future experiments could also focus on MC survival *in vivo* following chemotherapeutic treatment and identifying whether these cells are N-cad positive and also whether these cells reside in a quiescent state adjacent to osteoblastic cells, which facilitates resistance. This would then provide the rationale to inhibit the interaction between the MCs and osteoblastic cells using a potential N-cad inhibitor, followed by chemotherapy. These are important questions to explore in the future to further characterise the role of N-cad in MM and a more detailed plan and further study modifications are discussed in Section 7.2, Future Work.

The majority of functional studies conducted within this thesis focused upon the role of N-cad in MM rather than the other molecules and ligands. However, it is highly likely that N-cad is not the sole molecule, which will influence MC adhesion to osteoblastic cells as well as proliferation *in vivo*. Clinical trials have previously explored, or are currently being conducted, to determine the role of CXCR4/CXCL12, Notch-1/ Jag-1 and Tie-2/ Ang-1 in cancer. Inhibition of CXCR4/CXCL12 signalling has also been translated into several different clinical trials. For example, inhibition of CXCR4 using AMD3100 has been used to mobilise HSCs from the BM into the blood for HSC harvesting in healthy volunteers (282) and has now also been assessed in phase three trials in combination with granulocyte colony-stimulating factor (G-CSF) to mobilise HSCs from myeloma patients before receiving chemotherapy (283). Furthermore, an anti-CXCR4 antibody, known as BMS-936564, inhibited CXCL12 induced migration of B lymphoblast Burkitt lymphoma and T lymphoblast leukaemia cells *in vitro* and resulted in a decrease in the volume of subcutaneous tumours using a myeloma xenograft model (284). The inhibitory peptide, 4F-benzoyl-TN14003, also known as BKT140, originally used by Menu *et al* (170) in pre-clinical studies to treat MM, also inhibited the growth of human non-small cell lung carcinoma cells *in vitro* and enhanced chemosensitisation (285) *in vivo* and reduced the size of subcutaneous tumours in myeloma xenograft models (286).

Several clinical trials are currently underway, using γ secretase inhibitors such as PF-03084014 and R04929097, to inhibit Notch-1 signalling. PF-03084014, is currently in phase I trials for use in patients with grade III breast cancer and T-cell leukaemic patients. Previous studies have shown a reduction in Notch-1 intracellular signalling which resulted in inhibition of cell growth and an increase in apoptosis *in vitro* as well as a reduction in tumour volume *in vivo*, using T-cell leukaemic cells (287, 288), as well as in breast cancer cells (289). In addition, the γ secretase inhibitor R04929097, is also currently in phase I clinical trials for use in lymphomas as well as a variety of metastatic solid tumours. In previous studies, this γ secretase inhibitor also inhibited tumour growth in human non-small cell lung carcinoma cell xenograft models and in some cases of solid tumours in humans (290, 291). The effects of these γ secretase inhibitors are yet to be explored in myeloma but may be of interest in the future.

Arcari *et al* (292) developed a series of Tie-2 inhibitors some of which reduced tumour volume in a rat glioblastoma model. Trebananib, a peptide Tie-2 inhibitor has also been tested in phase I clinical trials. However, use of this peptide did not considerably reduce progression free survival or overall survival in colorectal cancer patients (293). Whereas, the Tie-2 inhibitor, CEP-11981, also in clinical trials, reduced tumour volume and increased survival of animals in both glioblastoma and melanoma models *in vivo* (294). The mechanism of tumour reduction in these studies was not determined but a decrease in angiogenesis was speculated. Therefore, Tie-2 inhibition could be a future treatment strategy in myeloma, as inhibition may result in a reduction in angiogenesis, which is increased in myeloma patients (271) and this may result in a reduction in tumour load.

From the data collected in these studies there are several limitations, which need to be considered. Firstly, all of the experiments were conducted using murine MCs as opposed to human cells. The 5TGM1-GFP model has several advantages including excellent tumour take rate and growth in the BM of C57BL/KalwRij mice as well as producing osteolytic disease. This model is also fairly representative of patient

myeloma, particularly concerning tumour infiltration and bone disease, though it is more aggressive than MM disease occurring in patients. Another approach to investigate MM in pre-clinical studies is to use xenograft models of MM where, human cell lines and primary MM samples are injected into SCID mice (157-162, 165, 295). I could therefore, in future experiments use human cell lines and patients samples to assess the expression of the HSC niche molecules and ligands and to explore the importance of N-cad *in vivo* in xenograft models of MM. However, these models also have limitations in that immune-compromised mice are used as opposed to mice with an intact immune system and again isn't completely representative of human disease.

In addition, as mentioned previously, the use of KD cells as opposed to clinically relevant inhibitors are another limitation. Knock-down of genes to determine the role of the corresponding protein is a good proof of principal experiment. However, from these experiments it seemed to produce quite high variability in both the *in vitro* KD experiments and in the *in vivo* experiment. This was possibly due to the percentage of KD, which was not 100% as well as extensive cell growth *in vitro* and antibiotic selection. Knock-down experiments also inevitably will require interventions using compounds or antibodies. Therefore, for future experiments it may also be desirable to use peptides as well as functional inhibitory antibodies. Currently, an N-cad inhibitory peptide, known as adherin-1 (ADH-1), is in clinical trials for use in treating patients with solid tumours. Adherin-1 is a cyclic peptide with a specific "HAV" amino acid sequence which inhibits N-cad and its function was originally determined within retinal explants, resulting in a reduction in neurite outgrowth and a reduction in adhesion of LN-229 cells (a glioblastoma cell line) to recombinant N-cad *in vitro* (296). The use of this peptide was particularly beneficial in rats treated with melanoma DM366 cells by subcutaneous injection, followed by ADH-1 and melphalan treatment. Rats with melanoma, when treated with ADH-1 and melphalan in combination, had significantly lower tumour volume compared to those treated with ADH-1 and melphalan alone (278). Again this compound may be a suitable therapeutic in MM.

In conclusion, these experiments provide evidence in support of the overall hypothesis, that “myeloma cells exist within an osteoblastic niche similar to that occupied by HSCs”. Within these experiments, MCs expressed the same repertoire of molecules expressed by HSCs, and their complementary ligands were expressed by osteoblastic cells at varying stages of differentiation. In addition, the KD of one of these key molecules, N-cad, reduced (though not significantly) the adhesion of MCs to osteoblastic cells *in vitro* and potentially reduced tumour growth *in vivo*. This reduction may be due to fewer cells originally homing to the BM or inhibition in the adhesion of MCs to osteoblastic cells, which may be an essential interaction for MC survival in the BM. However, further experiments are required to confirm the role of N-cad in myeloma development and to determine the precise role of osteoblastic cells in this interaction. These studies do however; provide the rationale to continue to target the niche with the theory that detaching cells from the niche will result in chemosensitisation, which can be targeted by conventional chemotherapies. However, it is currently unknown if this would in fact increase tumour growth (as seen by Sadler *et al* (207) *in vitro*), and so one would have to proceed with caution by extensively testing such treatment strategies in preclinical models. In addition, it is also unlikely that one molecule alone will facilitate MC attachment to a niche in the BM and in future experiments using a combination of molecule interventions will be required. Therefore, future experiments aim to establish treatment strategies, which could more effectively kill MCs and prevent chemo-evasion.

7.2 Future studies

To assess the effect of knocking-down N-cad in the 5TGM1-GFP cells on homing, localisation and growth over-time *in vivo*

To further assess the effect of knocking-down N-cad in the 5TGM1-GFP cells upon tumour growth *in vivo*, certain aspects of the pilot study need to be repeated and additional aspects need to be investigated. Firstly, it would be desirable to determine whether different numbers of 5TGM1-GFP cells home to the BM. This could be done

by labelling the 5TGM1-GFP cells with the membrane dye DiD prior to injection. Three days after injection, labelled 5TGM1-GFP cells in the BM or circulation could be quantified by flow cytometry and their location could be determined using multi-photon microscopy. Secondly, analysis at the end stage of disease would be repeated. However, rather than sacrificing the mice at 3 weeks P-I the experiment would continue until the first mouse in either the CTRL 25 or KD 25 group became ill, as the standard 5TGM1-GFP group would no longer be required. Tumour burden would be quantified using IHC and flow cytometry and as the length of the study would be extended this would allow larger tumours to form in the CTRL 25 group, which may reduce variability in the tumour burden analysis. Another endpoint would be to analyse the number of single DID labelled cells present in the bones of mice at the end stage of disease and to determine the proliferative state of these cells to establish whether they are quiescent. To reduce variability, mouse numbers in the groups would be increased. This would be based on power calculations using standard deviations from the pilot study. A PBS control group would also be used to provide background CD138 positive plasma cell analysis to quantify CD138 staining at the early time points of disease by IHC as well as providing basal trabecular bone parameter values to determine any differences between the PBS control group and the CTRL 25 and KD 25 injected mice.

Determining the effects of a clinically relevant inhibitor of N-cad upon myeloma cell homing, colonisation and subsequent growth in the bone marrow

The N-cad KD experimental design could also be used to determine the effects of a clinically relevant inhibitor of N-cad upon MC homing, colonisation and subsequent growth in the BM. Initially, optimisation experiments to determine a suitable dose of an inhibitor, such as ADH-1 or inhibitory antibodies, would be required to assess toxicity and whether the compounds have any effect on tumour burden at the end stage of disease. If differences were seen, it would then be desirable to analyse the early stages of disease, using DID labelled MCs to establish whether treatment of mice with an N-cad inhibitor prevented MC homing to the BM and also to determine the localisation of the MCs in the BM *in vivo*. A potential limitation to this study would be that the detachment of MCs from the niche might induce proliferation of these

“dormant” cells increasing tumour burden as well as the potential to increase metastasis.

Quantifying and profiling the myeloma cells present in the bone marrow following chemotherapy

To assess whether N-cad or the other HSC niche molecules are important with regards to MC chemoresistance, further *in vitro* and *in vivo* studies are required. Firstly *in vitro* chemo-titration studies could be conducted to examine the effect of different doses upon MC death, using modern chemotherapies such as lenalidomide or pomalidomide. This would be followed by treatment of cells with optimised doses of chemotherapies followed by genetic profiling of cells before and after therapy to determine any key molecules, which may enable chemoresistance.

This would then be translated into *in vivo* experiments, to establish the genetic profile of the cells surviving after chemotherapeutic treatment *in vivo* (identified by DID labelling), which would include analysing the expression of the HSC niche molecules. In addition, molecules involved in cell signalling pathways could also be assessed in the chemoresistant cells to determine whether any of these pathways are activated following chemotherapeutic intervention.

Determining the effect of N-cad intervention in combination with chemotherapeutic treatment

Following on from both the separate N-cad intervention studies and chemo-titration experiments, both of these could be combined to form a new treatment strategy.

Mice could be injected with 5TGM1-GFP cells and upon colonisation at approximately 10 days P-I; they could then be treated with the N-cad inhibitor (inhibitory peptide or antibody), which may potentially dislodge the attachment of MCs from BM niches, rendering them more chemosensitive. This could then be followed by chemotherapeutic intervention using modern agents such as lenalidomide or pomalidomide as well as potentially in combination with proteasome inhibitors such

as bortezomib or carfilzomib. Following the combination treatment, the mice could be maintained in a survival study to determine whether mice, which received the combination treatment, survive longer or do not relapse compared to mice receiving chemotherapy alone. At the end of these studies the long bones could then be analysed for DID labelled cell number analysis as well as CD138 IHC to determine whether any MCs had remained in the BM following chemotherapy or N-cad intervention treatments. As already discussed, this strategy could be quite unsafe due to detachment of cells from the niche, which may result in cell proliferation and an increase in metastasis. However, if the chemotherapeutic strategy is at the correct dose these cells should be targeted.

Appendices

Appendix 1: Equipment, materials and reagents

1.1 Tissue culture

Table 1.1: Equipment, materials and reagents required for tissue culture

Item	Supplier
Disposable tips (10, 200 & 1000 µl)	Star labs
Eppendorph tubes (0.5 ml & 1 ml)	Sarstedt
Flasks (T25, T75 & T175)	Nalgene Nunc Ltd
Falcon tubes (50 ml)	BD Pharmingen
Universal tubes (20 ml)	Costar
15 ml tubes	BD Pharmingen
Bijoux tubes	Costar
Petri dishes (60 and 100 mm)	Nunc
Multi-well plates (6, 12, 24, 48, 96)	Nalgene Nunc Ltd.
Cryovials (1.5 ml)	Nalgene Nunc Ltd
Cell scrapers	Corning
Syringes	BD Pharmingen
MEM α medium (GlutaMAX and phenol red)	Gibco
MEM α -Nuc medium (GlutaMAX, deoxyribonucleosides, ribonucleosides and phenol red)	Gibco
RPMI 1640 medium (GlutaMAX and Phenol red)	Gibco
FBS	Gibco
NEAA (100X)	Gibco
NaP (100mM of sodium pyruvate)	Gibco
PS (10,000 units of penicillin and 10,000 µg/ml of streptomycin)	Gibco
FZ (250 µg of Amphotericin B and 205 µg of sodium deoxycholate/ml)	Gibco
PBS	Gibco
Trypsin/ EDTA (2.5 g trypsin, 0.38 g EDTA and 4Na per litre of Hank's balanced salt solution per litre)	Gibco
Trypan blue	Sigma Aldrich
DMSO	Sigma Aldrich
70 IMS	Fisher Scientific
Haemocytometer	Neubauer
Cover-slips	Fisher Scientific

1.2 Animal cell isolation

Table 1.2: Equipment, materials and reagents required for animal cell isolation

Item	Supplier
HBSS (calcium and magnesium)	Gibco
Collagenase Type II	Gibco
EDTA	Fluk analytical
Insulin Myjector needles (27 Gauge)	Terumo
Vacutainers	BD Pharmingen
RBC lysis (10X) and wash buffer (10X)	R & D Systems
DMEM media containing Pentobarbitone (concentration)	Gibco
	J M Loveridge Ltd

1.3 RNA extraction

Table 1.3: Materials and reagents required for RNA extraction

Item	Supplier
Ultra spec (A 14 M guanidine salt/urea RNA isolation system)	BioTecx
Molecular grade chloroform	Sigma Aldrich
Molecular grade 2-propanol	Sigma Aldrich
Molecular grade ethanol	Sigma Aldrich
DEPC water	Ambion
RNase Zap	Ambion

1.4 Reverse transcription

Table 1.4: Equipment, materials and reagents required for reverse transcription

Item	Supplier
0.5 ml RNase and DNase free tubes	Alpha laboratories
PTC 200 thermal cycler	MJ Research
UV hood	Jencons
Nuclease free water	Ambion
Random primers (500 ng/ μ l)	Promega
RNasin (40 U/ μ l)	Promega
SuperScript III first-strand synthesis system, Reverse transcriptase (200 U μ l)	Life Technologies
DTT (100 mM)	Life Technologies
First strand buffer (5X solution containing 250 mM Tris-HCl (pH 8.3), 375 mM potassium chloride (KCl), 15 mM MgCl ₂)	Life Technologies
dNTPs (100 mM),	Bioline

1.5 Endpoint PCR

Table 1.5: Materials and reagents required for endpoint PCR

Item	Supplier
RT-PCR H ₂ O	Ambion
MgCl ₂ (50 mM)	Bioline
Ammonium reaction buffer (10X)	Bioline
Taq polymerase (5 U/μl)	Bioline
Murine PCR primers (5 μM)	Thermo Scientific and Life Technologies

1.6 Gel electrophoresis

Table 1.6 Equipment, materials and reagents required for gel electrophoresis

Item	Supplier
Electrophoresis tank	Biorad
PowerPac	Biorad
Gel combs	Biorad
Gel casting mould	Biorad
Trizma base	Sigma Aldrich
Hyperladder IV 100-1000 BP	Bioline
Loading buffer (5X)	Bioline
Ultra-pure agarose	Sigma Aldrich
Glacial acetic acid	Fisher Scientific
Ethidium bromide (10 mg/ml)	Life Technologies

1.7 Real-time PCR

Table 1.7: Equipment, materials and reagents required for real-time PCR

Item	Supplier
384 well plates	Greiner Bio-one Ltd
Micro-seal adhesive covers	Bio-Rad
7900 Ht real-time PCR machine	Life Technologies
Endogenous control assays and experimental probes (20X)	Life Technologies
Real-time PCR Master Mix: (2x containing AmpliTaq GoldDNA Polymerase, Uracil DNA Glycosylase, dNTPs deoxyuridine triphosphate (dUTP))	Life Technologies

1.8 Flow cytometry

Table 1.8: Equipment, materials and reagents required for flow cytometry

Item	Supplier
FACS Calibur machine	BD Pharmingen
96 V bottom well plate	Sterilin
Flow cytometry tubes	Elkay Laboratory Products
Cell strainers	BD Pharmingen
Goat serum	Vector Laboratories
BSA	Sigma Aldrich
Cell dissociation solution	Sigma Aldrich
Fixation buffer (4% PFA)	BD Pharmingen
Permeabilisation buffer (Saponin) (10X)	BD Pharmingen
Fluorescent antibodies	Various suppliers-see Table 2.23
PI (1 mg/ml)	Life Technologies
TO-PRO-3 (1 mM)	Life Technologies

1.9 Immunofluorescence

Table 1.9: Equipment, materials and reagents required for immunofluorescence

Item	Supplier
Hydrophobic barrier pen	Vector Laboratories
Super-frost slides	VWR International
Cover-slips (22 x 22 mm)	Menzel glaser
Cytospin equipment and machine	Shandon
Hot plate	Thermo Scientific
Leica AF6000 microscope	Leica Microsystems
PBS tablets	Oxoid
Paraformaldehyde	Fisher Scientific
NaOH	Fisher Scientific
Prolong gold anti-fade aqueous mounting media with 4',-6-diamidino-2-phenylindole (DAPI)	Life Technologies
Tween	Fisher Scientific
Nail varnish	Boots Pharmacy

1.10 IHC

Table 1.10: Equipment, materials and reagents required for IHC

Item	Supplier
Processing cassettes	Leica Microsystems
Processing carousel Leica TP2010	Leica Microsystems
Blocking System II embedder	Raymond Lamb
Leica RM 2265 microtome	Leica Microsystems
Hot plate	Raymond Lamb
Water baths	Raymond Lamb
Oven	Scientific Laboratory Supplies
Processing wax	
Xylene	Fisher Scientific
Alcohols	Fisher Scientific
EDTA	Fisher Scientific
Trypsin antigen retrieval kit	A.Menarini Diagnostics
H ₂ O ₂	VWR
Streptavidin horse radish peroxidase	Dakocytomation
DPX mountant	VWR international
Primary antibodies- see table 2.12	Various suppliers- see table 2.12
Goat anti-rat biotinylated secondary antibody	Santa Cruz Biotechnology
Goat anti-rabbit biotinylated secondary antibody	Vector Laboratories
DAB peroxidase substrate kit	Vector Laboratories
Gill's haematoxylin	Fisher Scientific

1.11 Western blotting

Table 1.11: Equipment, materials and reagents required for Western blotting

Item	Supplier
Mini protean WB equipment: gel casting stands, casting frames, electrophoresis tank and electrode assembly, transfer cassettes, transfer electrodes	Bio-Rad
1.5 mm separator and cover plate	Bio-Rad
1.5 mm combs (15 wells)	Bio-Rad
Filter paper	Whatman
Teflon pads	Bio-Rad
Tris HCl	Sigma Aldrich
BCA	Sigma Aldrich
NaCl	Sigma Aldrich
Glycine	Fisher Scientific
NP-40 substitute	Fuka Biochemika
TEMED	Sigma Aldrich
Laemmli sample buffer (4X)	Biorad
PIC	Calbiochem
Acrylamide	National Diagnostics
APS	Bioproducts ltd
β -mercaptoethanol	Sigma Aldrich
SDS	Sigma Aldrich
Milk powder	Cooperative supermarket
Goat anti-rabbit horse radish peroxidase antibody	Dako cytomation
Anti-biotin antibody HRP	Cell signalling
Rabbit anti β -actin antibody	Abcam
Pre-stained all Blue protein ladder	Bio-rad
Biotinylated molecular weight standards	Cell signalling
Nitrocellulose membranes	Amersham
Methanol	Fisher Scientific
Luminol reagent (ECL)	Santa Cruz Biotechnology
Luminol reagent (ECL)	Thermo Scientific
Hyper film	Amersham
Developing solutions	AGFA

1.12 Primary osteoblast lineage cell differentiation

Table 1.12: Equipment, materials and reagents required for primary osteoblast lineage cell differentiation

Item	Supplier
Spectra Max M5e plate reader	Molecular devices
BGP	Sigma Aldrich
Asc	Sigma Aldrich
PNPP tablets, containing PNPP (20 mg/ml) and tris buffer tablets (4 M)	Sigma Aldrich
Alizarin red	Sigma Aldrich
Quant-it Pico green reagent: containing the dsDNA picogreen component, tris/EDTA buffer (20X) containing 200 mM Tris-HCl, 20 mM EDTA pH 7.5 and the lambda DNA standards (100 µg/ml)	Life Technologies

1.13 Gene knock-down using short hair-pin RNA

Table 1.13: Materials and reagents required for short hair-pin RNA knock-down

Item	Supplier
Puromycin (25 mg/ml)	Santa Cruz Biotechnology
Polybrene (10 mg/ml)	Santa Cruz Biotechnology
CXCR4 and N-cad shRNA lentiviral particles	Santa Cruz Biotechnology
GFP lentiviral particles	Santa Cruz Biotechnology
Scrambled control lentiviral particles	Santa Cruz Biotechnology

1.14 Micro-computed tomography

Table 1.14: Equipment, materials and reagents required for micro-computed tomography

Item	Supplier
SkyScan 1172 µCT machine	SkyScan
Sodium dihydrogen orthophosphate dihydrate	VWR international
Disodium hydrogen orthophosphate dihydrate	VWR international
Concentrated formaldehyde (i.e. 37-41%)	VWR international

Appendix 2: Additional information for methodologies

2.1 RNA quantification and contamination analysis

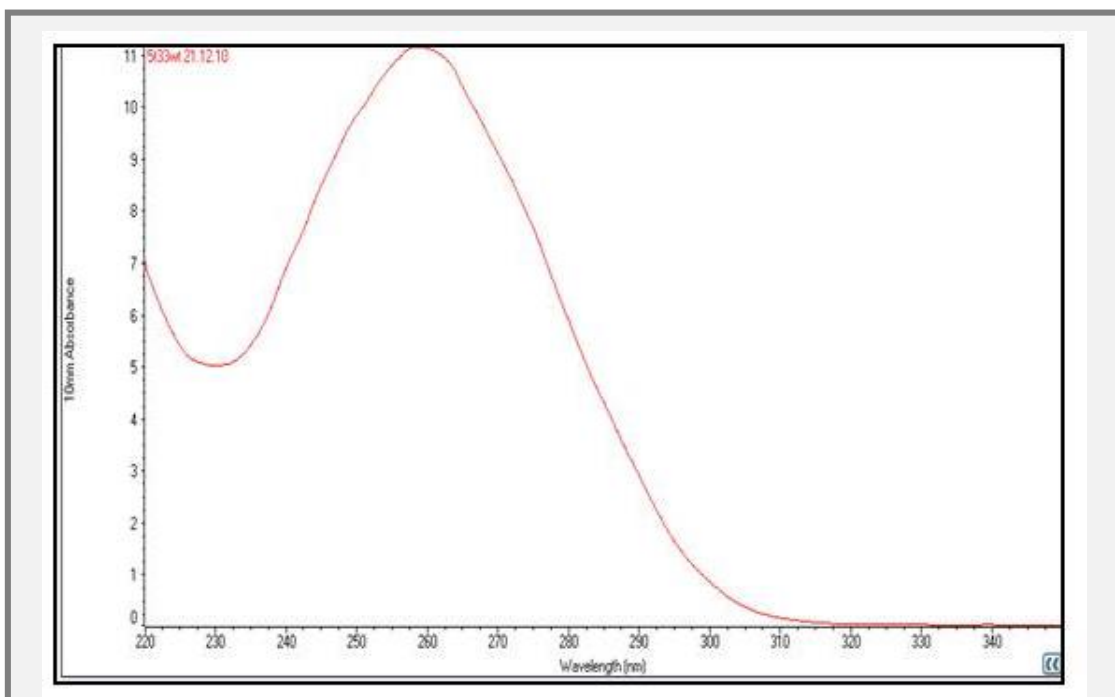


Figure 2.1: An example of a RNA spectrophotometry curve to detect contaminants. Ribonucleic acid was extracted and analysed using a NanoDrop 2000 and NanoDrop 2000 software. A graph was generated which summarised the quality of the RNA and generated contamination ratios (260:280, 260:230).

2.2 RNA fragment length analysis

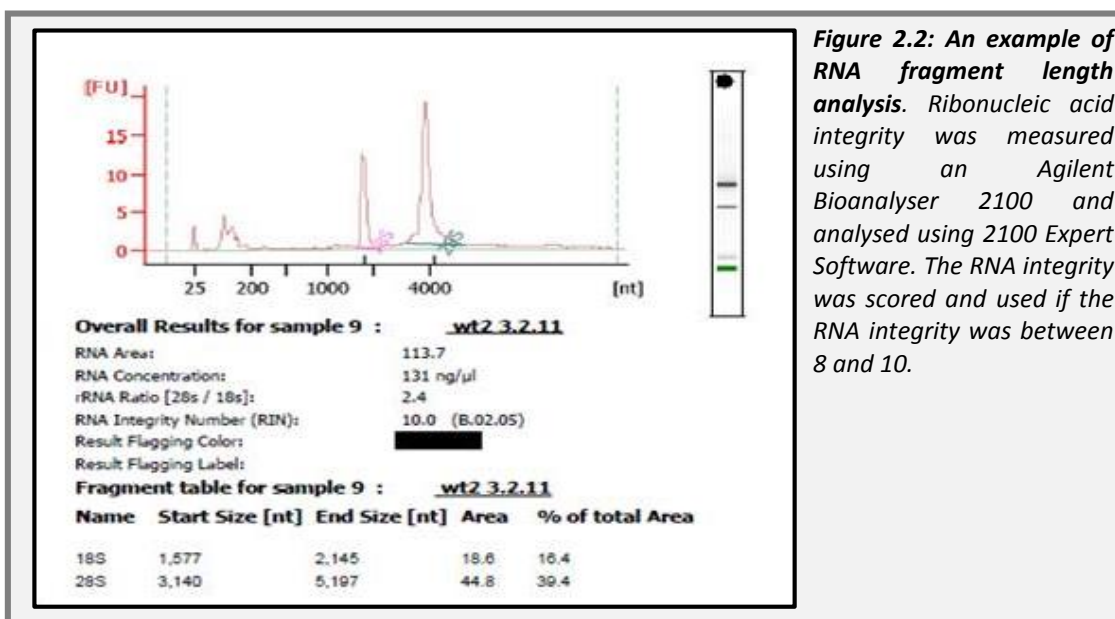


Figure 2.2: An example of RNA fragment length analysis. Ribonucleic acid integrity was measured using an Agilent Bioanalyser 2100 and analysed using 2100 Expert Software. The RNA integrity was scored and used if the RNA integrity was between 8 and 10.

2.3 Endpoint PCR primer information

Table 2.1: Primer annealing temperatures, cycle number and product size for endpoint PCR

Gene	Primer annealing temperature (°C)	Cycle number	Product size (BP)
<i>GAPDH</i>	53	25	354
<i>CXCR4</i>	48	35	711
<i>CXCL12</i>	48	35	205
<i>Notch-1</i>	48	35	348
<i>Jag-1</i>	48	35	370
<i>Tie-2</i>	48	35	648
<i>Ang-1</i>	48	35	401
<i>N-cad</i>	55	35	560
<i>CD138</i>	48	35	559

2.4 Endpoint PCR primer sequence information

Table 2.2: Endpoint PCR primer sequences, gene accession numbers and primer melting temperatures

Primer	Primer annealing Sequence	Accession number (NM)	T _m (°C)
Sense <i>GAPDH</i>	5'-TTGTCAGCAATGCATCCTGC-3'	008084	53
Anti-sense <i>GAPDH</i>	5'-GCTTCACCACCTTCTTGATG-3'	008084	53
Sense <i>CXCR4</i>	5'-ATGGAACCGATCAGTGTGAG-3'	009911	49
Anti-sense <i>CXCR4</i>	5'-CTTGGAGTGTGACAGCTTAG-3'	009911	45
Sense <i>CXCL12</i>	5'-TCAGTGACGGTAAACCAGTC-3'	021704	47
Anti-sense <i>CXCL12</i>	5'-GCTTCTCCAGGTACTCTTG-3'	021704	46
Sense <i>Notch-1</i>	5'-TAATGAGTGCAGCCAGAACC-3'	008714	50
Anti-sense <i>Notch-1</i>	5'-TCCTCTGTACAGTACTGACC-3'	008714	41
Sense <i>Jag-1</i>	5'-AGATCCTGTCCATGCAGAAC-3'	013822	49
Anti-sense <i>Jag-1</i>	5'-ATCATGCCTGAGTGAGAAGC-3'	013822	49
Sense <i>Tie-2</i>	5'-GTTTCGAGGACAGGCTATAAG-3'	013690	46
Anti-sense <i>Tie-2</i>	5'-CTTTCATTGGTACAGTGGC-3'	013690	47
Sense <i>Ang-1</i>	5'-CATTCTCCAGAACACGACG-3'	009640	51
Anti-sense <i>Ang-1</i>	5'-GGAGAAGTTGCTTCTTAGC-3'	009640	45
Sense <i>N-cad</i>	5'-CAGGTAGCTGTAAACCTGAG-3'	007664	55
Anti-sense <i>N-cad</i>	5'-CCATTCAGGGCATTGGATC-3'	007664	55
Sense <i>CD138</i>	5'-TGTTCTCCTGAAGATCAGG-3'	011519	49
Anti-sense <i>CD138</i>	5'-TGATTGGCAGTCCATCCTC-3'	011519	52

2.5 Probes used for real-time PCR

Table 2.3: Probes used for real-time PCR

Gene	Reference number
<i>β2M</i>	Mm00437762_m1
<i>HPRT</i>	Mm00446968_m1
<i>TFRC</i>	Mm00441941_m1
<i>Col1A1</i>	Mm00801666_g1
<i>Runx-2</i>	Mm00501584_m1
<i>CXCR4</i>	Mm01292123_m1
<i>CXCL12</i>	Mm00445552_m1
<i>Notch-1</i>	Mm00435249_m1
<i>Jag-1</i>	Mm00496902_m1
<i>Tie-2</i>	Mm00443243_m1
<i>Ang-1</i>	Mm00456503_m1
<i>N-cad</i>	Mm01162497_m1
<i>CD138</i>	Mm00448918_m1

2.6 Real-time PCR probe efficiencies

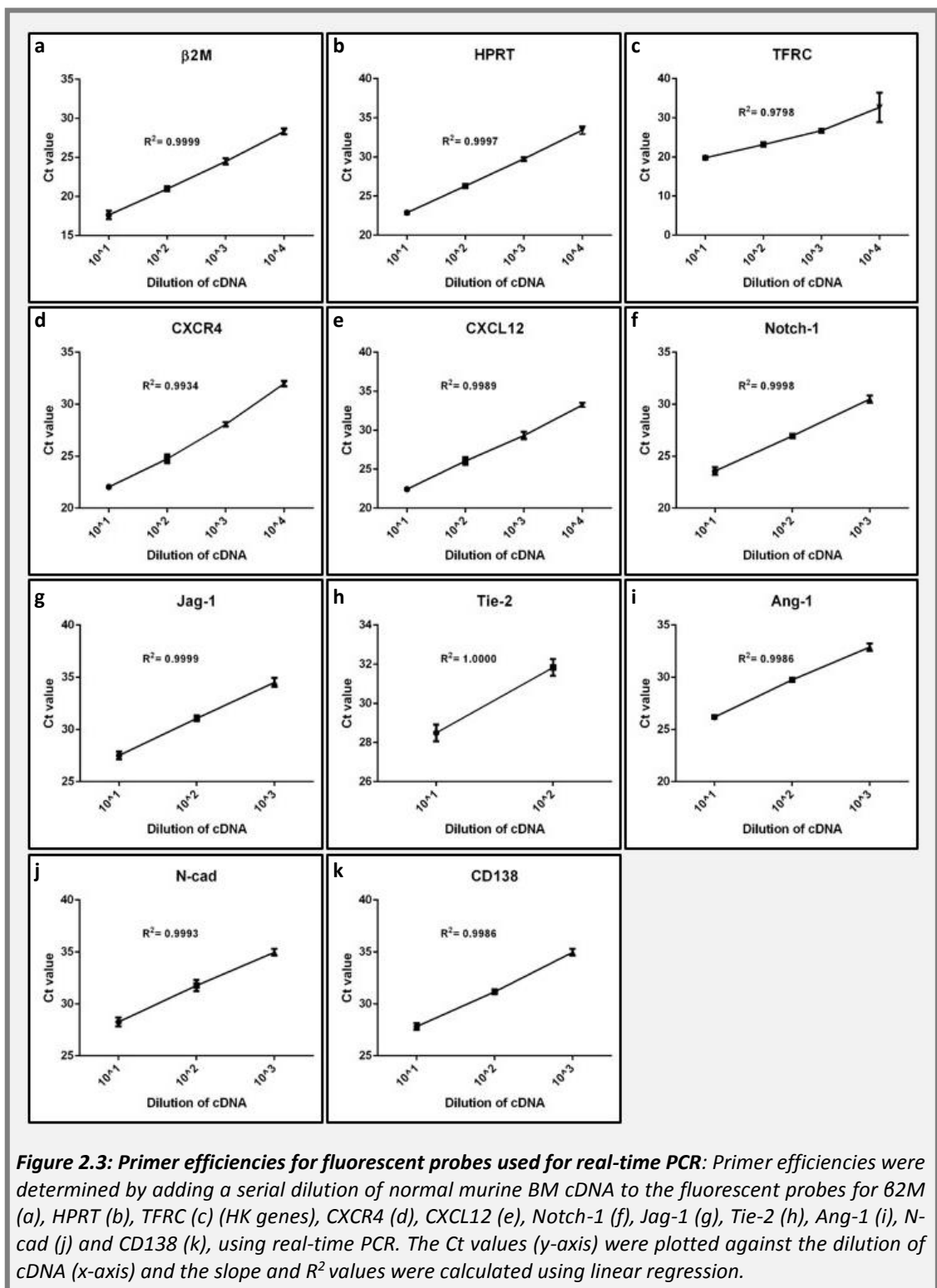


Table 2.6: The percentage of fluorescent probe efficiency

Gene	Primer efficiency (%)
<i>β2M</i>	93.12
<i>HPRT</i>	107.55
<i>TFRC</i>	72.66
<i>CXCR4</i>	100.16
<i>CXCL12</i>	90.57
<i>Notch-1</i>	94.50
<i>Jag-1</i>	93.09
<i>Tie-2</i>	99.18
<i>Ang-1</i>	98.84
<i>N-cad</i>	98.89
<i>CD138</i>	90.66

The percentage of fluorescent probe efficiency was calculated using the equation: $\text{Efficiency} = 10^{(-1/\text{slope})} - 1 * 100$, using the slope from the graphs calculated in Appendix Figure 2.3. Probes within a range of 90-110% were used in real-time PCR.

2.7 Optimisation experiments to determine the optimum amount of protein required to visualise N-cad using Western blotting

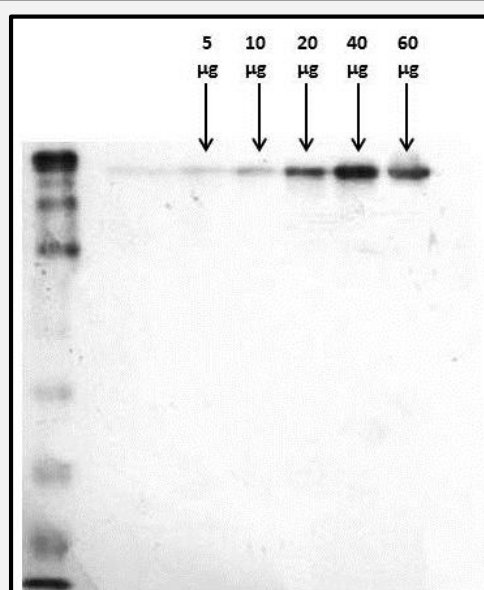


Figure 2.4: Western blotting to optimise the amount of protein used to detect N-cad in 5TGM1-GFP cells. Increasing amounts of 5TGM1-GFP protein (5, 10, 20, 40 and 60 µg) were loaded and run by SDS-PAGE and blotted using an anti-N-cad primary antibody followed by anti-rabbit HRP conjugated secondary Blots were visualised using ECL purchased from Santa Cruz.

2.8 Alkaline phosphatase analysis

Table 2.6: An example of alkaline phosphatase calculations used to determine differences in primary osteoblast lineage cell differentiation

OD End	OD Start	A= OD end- OD start	B=A* V	C= T*E*L	U=B/C (nmol/min)	DNA amount (ng)	DNA amount with dilution factor (ng)	U/ ng	U/ μg
0.32	0.11	0.21	46.90	1048.95	0.04	16.17	71.17	0.00063	0.62833
0.35	0.12	0.23	51.41	1048.95	0.05	17.78	78.25	0.00063	0.62642
0.32	0.11	0.21	45.32	1048.95	0.04	17.49	76.96	0.00056	0.56136
0.29	0.11	0.18	39.27	1048.95	0.04	16.23	71.39	0.00052	0.52437
0.32	0.11	0.21	0.00	1048.95	0.00	16.92	74.44	0.00	0.00

V=Volume (μL)	T= Time (Mins)	E=Molar coefficient ($\text{Mm}^{-1}\text{cm}^{-1}$)	L= Path length (Cm)
220	90	18.5	0.63

References

1. Sheridan CA. Multiple myeloma. *Seminars in Oncology Nursing*. 1996;12(1):59-69.
2. Streetly MJ. Myeloma and MGUS. *Medicine*. 2013;41(5):295-8.
3. Koura DT, Langston AA. Inherited predisposition to myeloma. *Therapeutic Advances in Hematology*. 2013.
4. Anderson KC, Alsina M, Bensinger W, Biermann JS, Cohen AD, Devine S, et al. Multiple myeloma, version 1.2013. *Journal of the National Comprehensive Cancer Network*. 2013;11(1):11-7.
5. Bird JM, Owen RG, D'Sa S, Snowden JA, Pratt G, Ashcroft J, et al. Guidelines for the diagnosis and management of multiple myeloma 2011. *British journal of haematology*. 2011;154(1):32-75.
6. Baker A, Braggio E, Jacobus S, Jung S, Larson D, Therneau T, et al. Uncovering the biology of multiple myeloma among African Americans: a comprehensive genomics approach. *Blood*. 2013;121(16):3147-52.
7. DeSantis C, Naishadham D, Jemal A. *Cancer Statistics for African Americans, 2013*. CA: a cancer journal for clinicians. 2013.
8. Calame K. Plasma cells: finding new light at the end of B cell development. *Nature immunology*. 2001;2(12):1103-8.
9. Di Noia J, Neuberger M. Molecular mechanisms of antibody somatic hypermutation. *Biochemistry*. 2007;76(1):1.

10. Goldsby RA, Kindt T.J, Osborne B. A. Kuby Immunology. 2nd ed. New York: Freeman and Company; 2000 2000. 1 p.
11. Morgan GJ, Walker BA, Davies FE. The genetic architecture of multiple myeloma. *Nature Reviews Cancer*. 2012;12(5):335-48.
12. Hallek M, Leif Bergsagel P, Anderson K. Multiple myeloma: increasing evidence for a multistep transformation process. *Blood*. 1998;91(1):3.
13. Seidl S, Kaufmann H, Drach J. New insights into the pathophysiology of multiple myeloma. *The Lancet Oncology*. 2003;4(9):557-64.
14. Mitsiades C, Mitsiades N, Munshi N, Anderson K. Focus on multiple myeloma. *Cancer cell*. 2004;6(5):439.
15. Hoffbrand A.V M, P.A.H, Pettit J.E. *Essential Haematology*. Fifth ed. Oxford: Blackwell Publishing LTD; 2006. 1 p.
16. Korbet SM, Schwartz MM. *Renal Disease in Multiple Myeloma*. 2006.
17. Wirk B. Renal failure in multiple myeloma: a medical emergency. *Bone marrow transplantation*. 2011;46(6):771-83.
18. Raje N, Roodman GD. Advances in the biology and treatment of bone disease in multiple myeloma. *Clinical Cancer Research*. 2011;17(6):1278-86.
19. Taberner D, San Miguel JF, Garcia-Sanz M, Najera L, García-Isidoro M, Perez-Simon JA, et al. Incidence of chromosome numerical changes in multiple myeloma: fluorescence in situ hybridization analysis using 15 chromosome-specific probes. *The American journal of pathology*. 1996;149(1):153.
20. Rajkumar SV. Multiple myeloma: 2012 update on diagnosis, risk-stratification, and management. *American journal of hematology*. 2012;87(1):78-88.

21. Rajan AM, Rajkumar SV. Diagnostic Evaluation of Monoclonal Gammopathy of Undetermined Significance. *European journal of haematology*. 2013.
22. Landgren O, Kyle RA, Pfeiffer RM, Katzmann JA, Caporaso NE, Hayes RB, et al. Monoclonal gammopathy of undetermined significance (MGUS) consistently precedes multiple myeloma: a prospective study. *Blood*. 2009;113(22):5412-7.
23. Waxman AJ, Kuehl M, Balakumaran A, Weiss B, Landgren O. Smoldering (asymptomatic) multiple myeloma: revisiting the clinical dilemma and looking into the future. *Clinical Lymphoma Myeloma and Leukemia*. 2010;10(4):248-57.
24. Smith A, Wisloff F, Samson D. Guidelines on the diagnosis and management of multiple myeloma 2005. *British journal of haematology*. 2006;132(4):410-51.
25. Kyle R, Child J, Anderson K, Barlogie B, Bataille R, Bensinger W, et al. Criteria for the classification of monoclonal gammopathies, multiple myeloma and related disorders: a report of the International Myeloma Working Group. *British journal of haematology*. 2003;121(5):749-57.
26. Durie B, Salmon S. A clinical staging system for multiple myeloma correlation of measured myeloma cell mass with presenting clinical features, response to treatment, and survival. *Cancer*. 1975;36(3):842-54.
27. Paget J. The distribution of secondary growth in cancer of the throat. *Lancet*. 1889;1:571.
28. Rhodin J. *Histology: a text and atlas*: Oxford University Press New York; 1974.
29. Teitelbaum SL. Bone resorption by osteoclasts. *Science*. 2000;289(5484):1504-8.

30. Pivonka P, Zimak J, Smith D, Gardiner B, Dunstan C, Sims N, et al. Model structure and control of bone remodeling: A theoretical study. *Bone*. 2008;43(2):249-63.
31. Proff P, Römer P. The molecular mechanism behind bone remodelling: a review. *Clinical oral investigations*. 2009;13(4):355-62.
32. Croucher P, Shipman C, Lippitt J, Perry M, Asosingh K, Hijzen A, et al. Osteoprotegerin inhibits the development of osteolytic bone disease in multiple myeloma. *Blood*. 2001;98(13):3534.
33. Galson DL, Silbermann R, Roodman GD. Mechanisms of multiple myeloma bone disease. *BoneKEy reports*. 2012;1(8).
34. Sezer O, Heider U, Jakob C, Zavrski I, Eucker J, Possinger K, et al. Immunocytochemistry reveals RANKL expression of myeloma cells. *Blood*. 2002;99(12):4646-7.
35. Han J, Choi S, Kurihara N, Koide M, Oba Y, Roodman G. Macrophage inflammatory protein-1 {alpha} is an osteoclastogenic factor in myeloma that is independent of receptor activator of nuclear factor {kappa} B ligand. *Blood*. 2001;97(11):3349.
36. Oyajobi BO, Franchin G, Williams PJ, Pulkrabek D, Gupta A, Munoz S, et al. Dual effects of macrophage inflammatory protein-1 α on osteolysis and tumor burden in the murine 5TGM1 model of myeloma bone disease. *Blood*. 2003;102(1):311-9.
37. Filella X, Blade J, Guillermo A, Molina R, Rozman C, Ballesta A. Cytokines (IL-6, TNF-alpha, IL-1alpha) and soluble interleukin-2 receptor as serum tumor markers in multiple myeloma. *Cancer detection and prevention*. 1995;20(1):52-6.

38. Yamamoto I, Kawano M, Sone T, Iwato K, Tanaka H, Ishikawa H, et al. Production of interleukin 1 β , a potent bone resorbing cytokine, by cultured human myeloma cells. *Cancer research*. 1989;49(15):4242-6.
39. Lee JW, Chung HY, Ehrlich LA, Jelinek DF, Callander NS, Roodman GD, et al. IL-3 expression by myeloma cells increases both osteoclast formation and growth of myeloma cells. *Blood*. 2004;103(6):2308-15.
40. Sati HI, Apperley JF, Greaves M, Lawry J, Gooding R, Russell RGG, et al. Interleukin-6 is expressed by plasma cells from patients with multiple myeloma and monoclonal gammopathy of undetermined significance. *British journal of haematology*. 1998;101(2):287-95.
41. Yaccoby S, Wezeman MJ, Henderson A, Cottler-Fox M, Yi Q, Barlogie B, et al. Cancer and the Microenvironment Myeloma-Osteoclast Interactions as a Model. *Cancer Research*. 2004;64(6):2016-23.
42. D'Souza S, Kurihara N, Shiozawa Y, Joseph J, Taichman R, Galson DL, et al. Annexin II interactions with the annexin II receptor enhance multiple myeloma cell adhesion and growth in the bone marrow microenvironment. *Blood*. 2012;119(8):1888-96.
43. Abe M, Hiura K, Wilde J, Shioyasono A, Moriyama K, Hashimoto T, et al. Osteoclasts enhance myeloma cell growth and survival via cell-cell contact: a vicious cycle between bone destruction and myeloma expansion. *Blood*. 2004;104(8):2484-91.
44. Moreaux J, Cremer FW, Reme T, Raab M, Mahtouk K, Kaukel P, et al. The level of TACI gene expression in myeloma cells is associated with a signature of microenvironment dependence versus a plasmablastic signature. *Blood*. 2005;106(3):1021-30.

45. Boyle W, Simonet W, Lacey D. Osteoclast differentiation and activation. *Nature*. 2003;423(6937):337-42.
46. Nakamura M, Udagawa N, Matsuura S, Mogi M, Nakamura H, Horiuchi H, et al. Osteoprotegerin regulates bone formation through a coupling mechanism with bone resorption. *Endocrinology*. 2003;144(12):5441-9.
47. Seidel C, Hjertner Ø, Abildgaard N, Heickendorff L, Hjorth M, Westin J, et al. Serum osteoprotegerin levels are reduced in patients with multiple myeloma with lytic bone disease. *Blood*. 2001;98(7):2269-71.
48. Tian E, Zhan F, Walker R, Rasmussen E, Ma Y, Barlogie B, et al. The role of the Wnt-signaling antagonist DKK1 in the development of osteolytic lesions in multiple myeloma. *The New England journal of medicine*. 2003;349(26):2483.
49. Heath DJ, Chantry AD, Buckle CH, Coulton L, Shaughnessy JD, Evans HR, et al. Inhibiting Dickkopf-1 (Dkk1) Removes Suppression of Bone Formation and Prevents the Development of Osteolytic Bone Disease in Multiple Myeloma. *Journal of Bone and Mineral Research*. 2009;24(3):425-36.
50. Oshima T, Abe M, Asano J, Hara T, Kitazoe K, Sekimoto E, et al. Myeloma cells suppress bone formation by secreting a soluble Wnt inhibitor, sFRP-2. *Blood*. 2005;106(9):3160.
51. Siegel R, Naishadham D, Jemal A. Cancer statistics, 2012. *CA: a cancer journal for clinicians*. 2012;62(1):10-29.
52. Palumbo A, Bringhen S, Ludwig H, Dimopoulos MA, Bladé J, Mateos MV, et al. Personalized therapy in multiple myeloma according to patient age and vulnerability: a report of the European Myeloma Network (EMN). *Blood*. 2011;118(17):4519-29.
53. Nau K, Lewis W. Multiple myeloma: diagnosis and treatment. *American family physician*. 2008;78(7):853.

54. Cavo M, Rajkumar SV, Palumbo A, Moreau P, Orłowski R, Bladé J, et al. International Myeloma Working Group consensus approach to the treatment of multiple myeloma patients who are candidates for autologous stem cell transplantation. *Blood*. 2011;117(23):6063-73.
55. Mitsiades N, Mitsiades CS, Poulaki V, Chauhan D, Richardson PG, Hideshima T, et al. Apoptotic signaling induced by immunomodulatory thalidomide analogs in human multiple myeloma cells: therapeutic implications. *Blood*. 2002;99(12):4525-30.
56. Hideshima T, Chauhan D, Shima Y, Raje N, Davies FE, Tai Y-T, et al. Thalidomide and its analogs overcome drug resistance of human multiple myeloma cells to conventional therapy. *Blood*. 2000;96(9):2943-50.
57. Zangari M, Yaccoby S, Cavallo F, Esseltine D, Tricot G. Response to bortezomib and activation of osteoblasts in multiple myeloma. *Clinical Lymphoma and Myeloma*. 2006;7(2):109-14.
58. Roccaro AM, Hideshima T, Raje N, Kumar S, Ishitsuka K, Yasui H, et al. Bortezomib mediates antiangiogenesis in multiple myeloma via direct and indirect effects on endothelial cells. *Cancer Research*. 2006;66(1):184-91.
59. Yeh H, Berenson J. Myeloma bone disease and treatment options. *European Journal of Cancer*. 2006;42(11):1554-63.
60. Russell R. Bisphosphonates: mode of action and pharmacology. *Pediatrics*. 2007;119(Supplement):S150.
61. Luckman S, Hughes D, Coxon F, Russell R, Rogers M. Nitrogen Containing Biphosphonates Inhibit the Mevalonate Pathway and Prevent Post Translational Prenylation of GTP Binding Proteins, Including Ras. *Journal of Bone and Mineral Research*. 2005;20(7):1265-74.

62. . !!! INVALID CITATION !!!

63. Shipman C, Rogers M, Apperley J, Russell R, Croucher P. Bisphosphonates induce apoptosis in human myeloma cell lines: a novel anti-tumour activity. *British journal of haematology*. 1997;98(3):665-72.

64. Croucher P, De Raeve H, Perry M, Hijzen A, Shipman C, Lippitt J, et al. Zoledronic Acid Treatment of 5T2MM Bearing Mice Inhibits the Development of Myeloma Bone Disease: Evidence for Decreased Osteolysis, Tumor Burden and Angiogenesis, and Increased Survival. *Journal of Bone and Mineral Research*. 2003;18(3):482-92.

65. Kellner J, Liu B, Kang Y, Li Z. Fact or fiction-identifying the elusive multiple myeloma stem cell. *Journal of hematology & oncology*. 2013;6(1):1-10.

66. Prabhala RH, Neri P, Bae JE, Tassone P, Shamma MA, Allam CK, et al. Dysfunctional T regulatory cells in multiple myeloma. *Blood*. 2006;107(1):301-4.

67. Dhodapkar MV, Geller MD, Chang DH, Shimizu K, Fujii S-I, Dhodapkar KM, et al. A reversible defect in natural killer T cell function characterizes the progression of premalignant to malignant multiple myeloma. *The Journal of experimental medicine*. 2003;197(12):1667-76.

68. Moser K, Tokoyoda K, Radbruch A, MacLennan I, Manz RA. Stromal niches, plasma cell differentiation and survival. *Current opinion in immunology*. 2006;18(3):265-70.

69. Wang LD, Wagers AJ. Dynamic niches in the origination and differentiation of haematopoietic stem cells. *Nature Reviews Molecular Cell Biology*. 2011;12(10):643-55.

70. Chen Z, Orłowski RZ, Wang M, Kwak L, McCarty N. Osteoblastic niche supports the growth of quiescent multiple myeloma cells. *Blood*. 2014:blood-2013-07-517136.

71. Visnjic D, Kalajzic Z, Rowe D, Katavic V, Lorenzo J, Aguila H. Hematopoiesis is severely altered in mice with an induced osteoblast deficiency. *Blood*. 2004;103(9):3258.
72. Schofield R. The relationship between the spleen colony-forming cell and the haemopoietic stem cell. *Blood cells*. 1978;4(1-2):7.
73. Nilsson S, Johnston H, Coverdale J. Spatial localization of transplanted hemopoietic stem cells: inferences for the localization of stem cell niches. *Blood*. 2001;97(8):2293.
74. Reya T, Morrison S, Clarke M, Weissman I. Stem cells, cancer, and cancer stem cells. *Nature*. 2001;414(6859):105-11.
75. Suda T, Arai F, Hirao A. Hematopoietic stem cells and their niche. *Trends in immunology*. 2005;26(8):426-33.
76. Shiozawa Y, Taichman RS. Getting blood from bone: An emerging understanding of the role that osteoblasts play in regulating hematopoietic stem cells within their niche. *Experimental Hematology*. 2012;40(9):685-94.
77. Kiel MJ, Radice GL, Morrison SJ. Lack of evidence that hematopoietic stem cells depend on N-cadherin-mediated adhesion to osteoblasts for their maintenance. *Cell stem cell*. 2007;1(2):204-17.
78. Komori T, Yagi H, Nomura S, Yamaguchi A, Sasaki K, Deguchi K, et al. Targeted disruption of *Cbfa1* results in a complete lack of bone formation owing to maturational arrest of osteoblasts. *Cell*. 1997;89(5):755-64.
79. Deguchi K, Yagi H, Inada M, Yoshizaki K, Kishimoto T, Komori T. Excessive extramedullary hematopoiesis in *Cbfa1*-deficient mice with a congenital lack of bone marrow. *Biochemical and biophysical research communications*. 1999;255(2):352-9.

80. Visnjic D, Kalajzic I, Gronowicz G, Aguila H, Clark S, Lichtler A, et al. Conditional ablation of the osteoblast lineage in Col2. 3 tk transgenic mice. *Journal of Bone and Mineral Research*. 2001;16(12):2222-31.
81. Calvi L, Sims N, Hunzelman J, Knight M, Giovannetti A, Saxton J, et al. Activated parathyroid hormone/parathyroid hormone-related protein receptor in osteoblastic cells differentially affects cortical and trabecular bone. *Journal of Clinical Investigation*. 2001;107(3):277-86.
82. Calvi L, Adams G, Weibrecht K, Weber J, Olson D, Knight M, et al. Osteoblastic cells regulate the haematopoietic stem cell niche. *Nature*. 2003;425(6960):841-6.
83. Zhang J, Niu C, Ye L, Huang H, He X, Tong W, et al. Identification of the haematopoietic stem cell niche and control of the niche size. *Nature*. 2003;425(6960):836-41.
84. Xie Y, Yin T, Wiegraebe W, He X, Miller D, Stark D, et al. Detection of functional haematopoietic stem cell niche using real-time imaging. *Nature*. 2008;457(7225):97-101.
85. Arai F, Hirao A, Ohmura M, Sato H, Matsuoka S, Takubo K, et al. Tie2/angiopoietin-1 signaling regulates hematopoietic stem cell quiescence in the bone marrow niche. *Cell*. 2004;118(2):149-61.
86. Kopp H, Avecilla S, Hooper A, Rafii S. The bone marrow vascular niche: home of HSC differentiation and mobilization. *Physiology*. 2005;20(5):349.
87. Li W, Johnson S, Shelley W, Yoder M. Hematopoietic stem cell repopulating ability can be maintained in vitro by some primary endothelial cells. *Experimental hematology*. 2004;32(12):1226-37.

88. Cardier J, Barberá-Guillem E. Extramedullary hematopoiesis in the adult mouse liver is associated with specific hepatic sinusoidal endothelial cells. *Hepatology*. 1997;26(1):165-75.
89. Ding L, Saunders TL, Enikolopov G, Morrison SJ. Endothelial and perivascular cells maintain haematopoietic stem cells. *Nature*. 2012;481(7382):457-62.
90. Bacon K, Baggiolini M, Broxmeyer H, Horuk R, Lindley I, Mantovani A, et al. Chemokine/chemokine receptor nomenclature. *Journal of Leukocyte Biology*. 2001;70(3):465.
91. Baggiolini M, Dewald B, Moser B. Human chemokines: an update. *Immunology*. 1997;15(1):675.
92. Kortesidis A, Zannettino A, Isenmann S, Shi S, Lapidot T, Gronthos S. Stromal-derived factor-1 promotes the growth, survival, and development of human bone marrow stromal stem cells. *Blood*. 2005;105(10):3793.
93. Dar A, Goichberg P, Shinder V, Kalinkovich A, Kollet O, Netzer N, et al. Chemokine receptor CXCR4-dependent internalization and resecretion of functional chemokine SDF-1 by bone marrow endothelial and stromal cells. *Nature immunology*. 2005;6(10):1038-46.
94. Sugiyama T, Kohara H, Noda M, Nagasawa T. Maintenance of the hematopoietic stem cell pool by CXCL12-CXCR4 chemokine signaling in bone marrow stromal cell niches. *Immunity*. 2006;25(6):977-88.
95. Balabanian K, Lagane B, Infantino S, Chow KY, Harriague J, Moepps B, et al. The chemokine SDF-1/CXCL12 binds to and signals through the orphan receptor RDC1 in T lymphocytes. *Journal of Biological Chemistry*. 2005;280(42):35760-6.
96. Rosenbaum DM, Rasmussen SG, Kobilka BK. The structure and function of G-protein-coupled receptors. *Nature*. 2009;459(7245):356-63.

97. Wu B, Chien EY, Mol CD, Fenalti G, Liu W, Katritch V, et al. Structures of the CXCR4 chemokine GPCR with small-molecule and cyclic peptide antagonists. *Science*. 2010;330(6007):1066-71.
98. Rosu-Myles M, Gallacher L, Murdoch B, Hess D, Keeney M, Kelvin D, et al. The human hematopoietic stem cell compartment is heterogeneous for CXCR4 expression. *Proceedings of the National Academy of Sciences of the United States of America*. 2000;97(26):14626.
99. Wright D, Bowman E, Wagers A, Butcher E, Weissman I. Hematopoietic stem cells are uniquely selective in their migratory response to chemokines. *The Journal of experimental medicine*. 2002;195(9):1145.
100. Teicher BA, Fricker SP. CXCL12 (SDF-1)/CXCR4 pathway in cancer. *Clinical Cancer Research*. 2010;16(11):2927-31.
101. Thelen M. Dancing to the tune of chemokines. *Nature immunology*. 2001;2(2):129-34.
102. Sodhi A, Montaner S, Gutkind JS. Viral hijacking of G-protein-coupled-receptor signalling networks. *Nature Reviews Molecular Cell Biology*. 2004;5(12):998-1012.
103. Bendall LJ, Baraz R, Juarez J, Shen W, Bradstock KF. Defective p38 mitogen-activated protein kinase signaling impairs chemotactic but not proliferative responses to stromal-derived factor-1 α in acute lymphoblastic leukemia. *Cancer research*. 2005;65(8):3290-8.
104. Domanska UM, Timmer-Bosscha H, Nagengast WB, Munnink THO, Kruizinga RC, Ananias HJ, et al. CXCR4 inhibition with AMD3100 sensitizes prostate cancer to docetaxel chemotherapy. *Neoplasia (New York, NY)*. 2012;14(8):709.

105. Wang J-F, Park I-W, Grooman JE. Stromal cell-derived factor-1 α stimulates tyrosine phosphorylation of multiple focal adhesion proteins and induces migration of hematopoietic progenitor cells: roles of phosphoinositide-3 kinase and protein kinase C. *Blood*. 2000;95(8):2505-13.
106. Rossi D, Zlotnik A. The biology of chemokines and their receptors. *Annual review of immunology*. 2000;18(1):217-42.
107. Yin T, Li L. The stem cell niches in bone. *Journal of Clinical Investigation*. 2006;116(5):1195-201.
108. Nagasawa T, Hirota S, Tachibana K, Takakura N, Nishikawa S, Kitamura Y, et al. Defects of B-cell lymphopoiesis and bone-marrow myelopoiesis in mice lacking the CXC chemokine PBSF/SDF-1. 1996.
109. Ara T, Tokoyoda K, Sugiyama T, Egawa T, Kawabata K, Nagasawa T. Long-term hematopoietic stem cells require stromal cell-derived factor-1 for colonizing bone marrow during ontogeny. *Immunity*. 2003;19(2):257-67.
110. Tzeng YS, Li H, Kang YL, Chen WC, Cheng WC, Lai DM. Loss of Cxcl12/Sdf-1 in adult mice decreases the quiescent state of hematopoietic stem/progenitor cells and alters the pattern of hematopoietic regeneration after myelosuppression. *Blood*. 2011;117(2):429.
111. Ponomaryov T, Peled A, Petit I, Taichman R, Habler L, Sandbank J, et al. Induction of the chemokine stromal-derived factor-1 following DNA damage improves human stem cell function. *Journal of Clinical Investigation*. 2000;106(11):1331-9.
112. Peled A, Petit I, Kollet O, Magid M, Ponomaryov T, Byk T, et al. Dependence of human stem cell engraftment and repopulation of NOD/SCID mice on CXCR4. *Science*. 1999;283(5403):845.

113. Walker L, Lynch M, Silverman S, Fraser J, Boulter J, Weinmaster G, et al. The Notch/Jagged pathway inhibits proliferation of human hematopoietic progenitors in vitro. *Stem Cells*. 1999;17(3):162-71.
114. Karanu F, Murdoch B, Gallacher L, Wu D, Koremoto M, Sakano S, et al. The notch ligand jagged-1 represents a novel growth factor of human hematopoietic stem cells. *The Journal of experimental medicine*. 2000;192(9):1365.
115. Stier S, Cheng T, Dombkowski D, Carlesso N, Scadden D. Notch1 activation increases hematopoietic stem cell self-renewal in vivo and favors lymphoid over myeloid lineage outcome. *Blood*. 2002;99(7):2369.
116. Artavanis-Tsakonas S, Rand M, Lake R. Notch signaling: cell fate control and signal integration in development. *Science*. 1999;284(5415):770.
117. Baron M, editor *An overview of the Notch signalling pathway* 2003: Elsevier.
118. Weinmaster G. The ins and outs of notch signaling. *Molecular and Cellular Neuroscience*. 1997;9(2):91-102.
119. Hadland B, Huppert S, Kanungo J, Xue Y, Jiang R, Gridley T, et al. A requirement for Notch1 distinguishes 2 phases of definitive hematopoiesis during development. *Blood*. 2004;104(10):3097.
120. Milner L, Kopan R, Martin D, Bernstein I. A human homologue of the *Drosophila* developmental gene, Notch, is expressed in CD34+ hematopoietic precursors. *Blood*. 1994;83(8):2057.
121. Swiatek P, Lindsell C, del Amo F, Weinmaster G, Gridley T. Notch1 is essential for postimplantation development in mice. *Genes & development*. 1994;8(6):707.

122. Varnum-Finney B, Purton L, Yu M, Brashem-Stein C, Flowers D, Staats S, et al. The Notch ligand, Jagged-1, influences the development of primitive hematopoietic precursor cells. *Blood*. 1998;91(11):4084.
123. Kovall RA, Blacklow SC. Chapter Two-Mechanistic Insights into Notch Receptor Signaling from Structural and Biochemical Studies. *Current topics in developmental biology*. 2010;92:31-71.
124. Burns C, Traver D, Mayhall E, Shepard J, Zon L. Hematopoietic stem cell fate is established by the Notch-Runx pathway. *Genes & development*. 2005;19(19):2331.
125. Kopan R, Ilagan MXG. The canonical Notch signaling pathway: unfolding the activation mechanism. *Cell*. 2009;137(2):216-33.
126. Radtke F, Wilson A, Stark G, Bauer M, van Meerwijk J, MacDonald H, et al. Deficient T cell fate specification in mice with an induced inactivation of Notch1. *Immunity*. 1999;10(5):547-58.
127. Uchida T, Nakashima M, Hirota Y, Miyazaki Y, Tsukazaki T, Shindo H. Immunohistochemical localisation of protein tyrosine kinase receptors Tie-1 and Tie-2 in synovial tissue of rheumatoid arthritis: correlation with angiogenesis and synovial proliferation. *Annals of the rheumatic diseases*. 2000 Aug;59(8):607-14. PubMed PMID: 10913057. Pubmed Central PMCID: PMC1753215. Epub 2000/07/27. eng.
128. Brkovic A, Pelletier M, Girard D, Sirois MG. Angiopoietin chemotactic activities on neutrophils are regulated by PI-3K activation. *J Leukoc Biol*. 2007 Apr;81(4):1093-101. PubMed PMID: 17215522. Epub 2007/01/12. eng.
129. Kosacka J, Figiel M, Engele J, Hilbig H, Majewski M, Spanel-Borowski K. Angiopoietin-1 promotes neurite outgrowth from dorsal root ganglion cells positive

for Tie-2 receptor. *Cell and tissue research*. 2005 Apr;320(1):11-9. PubMed PMID: 15714275. Epub 2005/02/17. eng.

130. Sacchetti B, Funari A, Michienzi S, Di Cesare S, Piersanti S, Saggio I, et al. Self-renewing osteoprogenitors in bone marrow sinusoids can organize a hematopoietic microenvironment. *Cell*. 2007;131(2):324-36.

131. Currie MJ, Gunningham SP, Han C, Scott PA, Robinson BA, Harris AL, et al. Angiopoietin-1 is inversely related to thymidine phosphorylase expression in human breast cancer, indicating a role in vascular remodeling. *Clinical cancer research : an official journal of the American Association for Cancer Research*. 2001 Apr;7(4):918-27. PubMed PMID: 11309342. Epub 2001/04/20. eng.

132. Schubert SY, Benarroch A, Monter-Solans J, Edelman ER. Primary monocytes regulate endothelial cell survival through secretion of angiopoietin-1 and activation of endothelial Tie2. *Arteriosclerosis, thrombosis, and vascular biology*. 2011 Apr;31(4):870-5. PubMed PMID: 21273558. Pubmed Central PMCID: PMC3104028. Epub 2011/01/29. eng.

133. Huang H, Bhat A, Woodnutt G, Lappe R. Targeting the ANGPT-TIE2 pathway in malignancy. *Nature Reviews Cancer*. 2010;10(8):575-85.

134. Shewchuk L, Hassell A, Ellis B, Holmes W, Davis R, Horne E, et al. Structure of the Tie2 RTK Domain:: Self-Inhibition by the Nucleotide Binding Loop, Activation Loop, and C-Terminal Tail. *Structure*. 2000;8(11):1105-13.

135. Kim I, Moon S-O, Kim SH, Kim HJ, Koh YS, Koh GY. VEGF stimulates expression of ICAM-1, VCAM-1 and E-selectin through nuclear factor-kappaB activation in endothelial cells. *Journal of Biological Chemistry*. 2000.

136. Kim I, Moon S-O, Park SK, Chae SW, Koh GY. Angiopoietin-1 reduces VEGF-stimulated leukocyte adhesion to endothelial cells by reducing ICAM-1, VCAM-1, and E-selectin expression. *Circulation research*. 2001;89(6):477-9.

137. Fukuhara S, Sako K, Minami T, Noda K, Kim HZ, Kodama T, et al. Differential function of Tie2 at cell–cell contacts and cell–substratum contacts regulated by angiopoietin-1. *Nature cell biology*. 2008;10(5):513-26.
138. Kim I, Kim HG, So J-N, Kim JH, Kwak HJ, Koh GY. Angiopoietin-1 regulates endothelial cell survival through the phosphatidylinositol 3'-kinase/Akt signal transduction pathway. *Circulation research*. 2000;86(1):24-9.
139. Moss A. The angiopoietin:Tie 2 interaction: a potential target for future therapies in human vascular disease. *Cytokine & growth factor reviews*. 2013 Dec;24(6):579-92. PubMed PMID: 23838360. Epub 2013/07/11. eng.
140. Puri M, Partanen J, Rossant J, Bernstein A. Interaction of the TEK and TIE receptor tyrosine kinases during cardiovascular development. *Development*. 1999;126(20):4569.
141. Suri C, Jones PF, Patan S, Bartunkova S, Maisonpierre PC, Davis S, et al. Requisite Role of Angiopoietin-1, a Ligand for the TIE2 Receptor, during Embryonic Angiogenesis. *Cell*. 1996 12/27/;87(7):1171-80.
142. Arai F, Suda T. Maintenance of Quiescent Hematopoietic Stem Cells in the Osteoblastic Niche. *New York Academy Sciences Annals*. 2007;1106:41-53.
143. Puri M, Bernstein A. Requirement for the TIE family of receptor tyrosine kinases in adult but not fetal hematopoiesis. *Proceedings of the National Academy of Sciences*. 2003;100(22):12753.
144. Steinberg M, McNutt P. Cadherins and their connections: adhesion junctions have broader functions. *Current opinion in cell biology*. 1999;11(5):554-60.
145. Koch A, Manzur K, Shan W. Structure-based models of cadherin-mediated cell adhesion: the evolution continues. *Cellular and Molecular Life Sciences*. 2004;61(15):1884-95.

146. Pettitt J. The cadherin superfamily. *WormBook*. 2005;29:1-9.
147. Angst B, Marcozzi C, Magee A. The cadherin superfamily: diversity in form and function. *Journal of cell science*. 2001;114(4):629-42.
148. Radice G, Rayburn H, Matsunami H, Knudsen K, Takeichi M, Hynes R. Developmental defects in mouse embryos lacking N-cadherin. *Developmental biology*. 1997;181(1):64-78.
149. Reiss K, Maretzky T, Ludwig A, Tousseyn T, De Strooper B, Hartmann D, et al. ADAM10 cleavage of N-cadherin and regulation of cell–cell adhesion and β -catenin nuclear signalling. *The EMBO journal*. 2005;24(4):742-52.
150. Kiel MJ, Acar M, Radice GL, Morrison SJ. Hematopoietic stem cells do not depend on N-cadherin to regulate their maintenance. *Cell stem cell*. 2009;4(2):170-9.
151. Bromberg O, Frisch BJ, Weber JM, Porter RL, Civitelli R, Calvi LM. Osteoblastic N-cadherin is not required for microenvironmental support and regulation of hematopoietic stem and progenitor cells. *Blood*. 2012;120(2):303-13.
152. Cheng S, Lecanda F, Davidson M, Warlow P, Zhang S, Zhang L, et al. Human Osteoblasts Express a Repertoire of Cadherins, Which Are Critical for BMP 2–Induced Osteogenic Differentiation. *Journal of Bone and Mineral Research*. 1998;13(4):633-44.
153. Hosokawa K, Arai F, Yoshihara H, Iwasaki H, Nakamura Y, Gomei Y, et al. Knockdown of N-cadherin suppresses the long-term engraftment of hematopoietic stem cells. *Blood*. 2010;116(4):554-63.
154. Hosokawa K, Arai F, Yoshihara H, Iwasaki H, Hembree M, Yin T, et al. Cadherin-based adhesion is a potential target for niche manipulation to protect hematopoietic stem cells in adult bone marrow. *Cell Stem Cell*. 2010;6(3):194-8.

155. Shiozawa Y, Pedersen EA, Havens AM, Jung Y, Mishra A, Joseph J, et al. Human prostate cancer metastases target the hematopoietic stem cell niche to establish footholds in mouse bone marrow. *The Journal of clinical investigation*. 2011;121(4):1298-312.
156. Wang N, Docherty FE, Brown HK, Reeves KJ, Fowles A, Ottewell PD, et al. Prostate Cancer Cells Preferentially Home to Osteoblast-Rich Areas in the Early Stages of Bone Metastasis—Evidence from In Vivo Models. *Journal of Bone and Mineral Research*. 2014.
157. Cattan AR, Douglas E. The CB 17^{scid} mouse strain as a model for human disseminated leukaemia and myeloma^{in vivo}. *Leukemia research*. 1994;18(7):513-22.
158. Bellamy WT, Mendibles P, Bontje P, Thompson F, Richter L, Weinstein RS, et al. Development of an orthotopic SCID mouse-human tumor xenograft model displaying the multidrug-resistant phenotype. *Cancer chemotherapy and pharmacology*. 1996;37(4):305-16.
159. Huang Y-W, Richardson JA, Vitetta ES. Anti-CD54 (ICAM-1) has antitumor activity in SCID mice with human myeloma cells. *Cancer research*. 1995;55(3):610-6.
160. Alsina M, Boyce B, Devlin RD, Anderson JL, Craig F, Mundy GR, et al. Development of an in vivo model of human multiple myeloma bone disease. *Blood*. 1996;87(4):1495-501.
161. Bellamy WT, Odeleye A, Finley P, Huizenga B, Dalton WS, Weinstein RS, et al. An in vivo model of human multidrug-resistant multiple myeloma in SCID mice. *The American journal of pathology*. 1993;142(3):691.
162. Suzuki H, Yasukawa K, Saito T, Goitsuka R, Hasegawa A, Ohsugi Y, et al. Anti-human interleukin-6 receptor antibody inhibits human myeloma growth in vivo. *European journal of immunology*. 1992;22(8):1989-93.

163. Namikawa R, Ueda R, Kyoizumi S. Growth of human myeloid leukemias in the human marrow environment of SCID-hu mice. *Blood*. 1993;82(8):2526-36.
164. Yaccoby S, Barlogie B, Epstein J. Primary myeloma cells growing in SCID-hu mice: a model for studying the biology and treatment of myeloma and its manifestations. *Blood*. 1998;92(8):2908-13.
165. Miyakawa Y, Ohnishi Y, Tomisawa M, Monnai M, Kohmura K, Ueyama Y, et al. Establishment of a new model of human multiple myeloma using NOD/SCID/ γ ^c_c^{null}(NOG) mice. *Biochemical and biophysical research communications*. 2004;313(2):258-62.
166. Mirandola L, Yu Y, Jenkins M, Chiaramonte R, Cobos E, John C, et al. Tracking human multiple myeloma xenografts in NOD-Rag-1/IL-2 receptor gamma chain-null mice with the novel biomarker AKAP-4. *BMC cancer*. 2011;11(1):394.
167. Radl J, Croese J, Zurcher C, Van den Enden-Vieveen M, De Leeuw A. Animal model of human disease. Multiple myeloma. *The American journal of pathology*. 1988;132(3):593.
168. Radl J, De Glopper ED, Schuit HR, Zurcher C. Idiopathic paraproteinemia. II. Transplantation of the paraprotein-producing clone from old to young C57BL/KaLwRij mice. *Journal of immunology (Baltimore, Md : 1950)*. 1979 Feb;122(2):609-13. PubMed PMID: 368243. Epub 1979/02/01. eng.
169. Buckle CH, De Leenheer E, Lawson MA, Yong K, Rabin N, Perry M, et al. Soluble rank ligand produced by myeloma cells causes generalised bone loss in multiple myeloma. *PloS one*. 2012;7(8):e41127.
170. Menu E, Asosingh K, Indraccolo S, De Raeve H, Van Riet I, Van Valckenborgh E, et al. The involvement of stromal derived factor 1alpha in homing and progression of multiple myeloma in the 5TMM model. *Haematologica*. 2006;91(5):605.

171. Vanderkerken K, De Raeve H, Goes E, Van Meirvenne S, Radl J, Van Riet I, et al. Organ involvement and phenotypic adhesion profile of 5T2 and 5T33 myeloma cells in the C57BL/KaLwRij mouse. *British journal of cancer*. 1997;76(4):451.
172. Glick AF, Song YS, Hwang B, Lillvis J, Zanzonico P, Fuchs C, et al. Age matters: Young T lymphocytes offer better protection from myeloma proliferation. *Immunity & Ageing*. 2013;10(1):5.
173. Nur H, Fostier K, Aspeslagh S, Renmans W, Bertrand E, Leleu X, et al. Preclinical Evaluation of Invariant Natural Killer T Cells in the 5T33 Multiple Myeloma Model. *PloS one*. 2013;8(5):e65075.
174. Garrett I, Dallas S, Radl J, Mundy G. A murine model of human myeloma bone disease. *Bone*. 1997;20(6):515-20.
175. Fowler JA, Mundy GR, Lwin ST, Edwards CM. Bone marrow stromal cells create a permissive microenvironment for myeloma development: a new stromal role for Wnt inhibitor Dkk1. *Cancer research*. 2012;72(9):2183-9.
176. Edwards CM, Lwin ST, Fowler JA, Oyajobi BO, Zhuang J, Bates AL, et al. Myeloma cells exhibit an increase in proteasome activity and an enhanced response to proteasome inhibition in the bone marrow microenvironment in vivo. *American journal of hematology*. 2009;84(5):268-72.
177. Dairaghi DJ, Oyajobi BO, Gupta A, McCluskey B, Miao S, Powers JP, et al. CCR1 blockade reduces tumor burden and osteolysis in vivo in a mouse model of myeloma bone disease. *Blood*. 2012;120(7):1449-57.
178. Noll JE, Williams SA, Tong CM, Wang H, Quach JM, Purton LE, et al. Myeloma plasma cells alter the bone marrow microenvironment by stimulating the proliferation of mesenchymal stromal cells. *Haematologica*. 2013:haematol.2013.090977.

179. Asosingh K, Radl J, Van Riet I, Van Camp B, Vanderkerken K. The 5TMM series: a useful in vivo mouse model of human multiple myeloma. *The Hematology Journal*. 2000;1(5):351-6.
180. Kodama H. Establishment of a clonal osteogenic cell line from newborn mouse calvaria. *Jpn J Oral Biol*. 1981;23:899-901.
181. Kitching R, Qi S, Li V, Raouf A, Vary CP, Seth A. Coordinate gene expression patterns during osteoblast maturation and retinoic acid treatment of MC3T3-E1 cells. *Journal of bone and mineral metabolism*. 2002;20(5):269-80.
182. Bakker A, Klein-Nulend J. Osteoblast isolation from murine calvariae and long bones. *Bone Research Protocols: Springer*; 2003. p. 19-28.
183. Lian JB, Stein GS. Development of the osteoblast phenotype: molecular mechanisms mediating osteoblast growth and differentiation. *The Iowa orthopaedic journal*. 1995;15:118.
184. Yang D, Atkins GJ, Turner AG, Anderson PH, Morris HA. Differential effects of 1, 25-dihydroxyvitamin D on mineralisation and differentiation in two different types of osteoblast-like cultures. *The Journal of steroid biochemistry and molecular biology*. 2013;136:166-70.
185. Brown M, Wittwer C. Flow cytometry: principles and clinical applications in hematology. *Clinical chemistry*. 2000;46(8):1221-9.
186. Sabokbar A, Millett P, Myer B, Rushton N. A rapid, quantitative assay for measuring alkaline phosphatase activity in osteoblastic cells in vitro. *Bone and mineral*. 1994;27(1):57-67.
187. Wang N, Rumney RM, Yang L, Robaye B, Boeynaems JM, Skerry TM, et al. The P2Y13 receptor regulates extracellular ATP metabolism and the osteogenic response to mechanical loading. *Journal of Bone and Mineral Research*. 2013;28(6):1446-56.

188. Singer O, Verma IM. Applications of lentiviral vectors for shRNA delivery and transgenesis. *Current gene therapy*. 2008;8(6):483.
189. Manjunath N, Wu H, Subramanya S, Shankar P. Lentiviral delivery of short hairpin RNAs. *Advanced drug delivery reviews*. 2009;61(9):732-45.
190. MacRae IJ, Zhou K, Li F, Repic A, Brooks AN, Cande WZ, et al. Structural basis for double-stranded RNA processing by Dicer. *Science*. 2006;311(5758):195-8.
191. Wang Z, Rao DD, Senzer N, Nemunaitis J. RNA interference and cancer therapy. *Pharmaceutical research*. 2011;28(12):2983-95.
192. Bouxsein ML, Boyd SK, Christiansen BA, Guldberg RE, Jepsen KJ, Müller R. Guidelines for assessment of bone microstructure in rodents using micro-computed tomography. *Journal of Bone and Mineral Research*. 2010;25(7):1468-86.
193. Nakayama T, Hieshima K, Izawa D, Tatsumi Y, Kanamaru A, Yoshie O. Cutting edge: profile of chemokine receptor expression on human plasma cells accounts for their efficient recruitment to target tissues. *The Journal of Immunology*. 2003;170(3):1136.
194. Möller C, Strömberg T, Juremalm M, Nilsson K, Nilsson G. Expression and function of chemokine receptors in human multiple myeloma. *Leukemia*. 2003;17(1):203-10.
195. Alsayed Y, Ngo H, Runnels J, Leleu X, Singha U, Pitsillides C, et al. Mechanisms of regulation of CXCR4/SDF-1 (CXCL12)-dependent migration and homing in multiple myeloma. *Blood*. 2007;109(7):2708.
196. Jung Y, Wang J, Schneider A, Sun Y-X, Koh-Paige A, Osman N, et al. Regulation of SDF-1 (CXCL12) production by osteoblasts; a possible mechanism for stem cell homing. *Bone*. 2006;38(4):497-508.

197. Nefedova Y, Cheng P, Alsina M, Dalton WS, Gabrilovich DI. Involvement of Notch-1 signaling in bone marrow stroma-mediated de novo drug resistance of myeloma and other malignant lymphoid cell lines. *Blood*. 2004;103(9):3503-10.
198. Jundt F, Probsting K, Anagnostopoulos I, Muehlinghaus G, Chatterjee M, Mathas S, et al. Jagged1-induced Notch signaling drives proliferation of multiple myeloma cells. *Blood*. 2004;103(9):3511.
199. Nefedova Y, Cheng P, Alsina M, Dalton W, Gabrilovich D. Involvement of Notch-1 signaling in bone marrow stroma-mediated de novo drug resistance of myeloma and other malignant lymphoid cell lines. *Blood*. 2004;103(9):3503.
200. Pereira RMR, Delany AM, Durant D, Canalis E. Cortisol regulates the expression of Notch in osteoblasts. *Journal of cellular biochemistry*. 2002;85(2):252-8.
201. Giuliani N, Colla S, Lazzaretti M, Sala R, Roti G, Mancini C, et al. Proangiogenic properties of human myeloma cells: production of angiopoietin-1 and its potential relationship to myeloma-induced angiogenesis. *Blood*. 2003;102(2):638.
202. Jeong B-C, Kim H-J, Bae I-H, Lee K-N, Lee K-Y, Oh W-M, et al. COMP-Ang1, a chimeric form of Angiopoietin 1, enhances BMP2-induced osteoblast differentiation and bone formation. *Bone*. 2010;46(2):479-86.
203. Tanaka H, Kono E, Tran CP, Miyazaki H, Yamashiro J, Shimomura T, et al. Monoclonal antibody targeting of N-cadherin inhibits prostate cancer growth, metastasis and castration resistance. *Nature medicine*. 2010;16(12):1414-20.
204. Nieman M, Prudoff R, Johnson K, Wheelock M. N-cadherin promotes motility in human breast cancer cells regardless of their E-cadherin expression. *The Journal of cell biology*. 1999;147(3):631.

205. Vandyke K, Chow AW, Williams SA, To LB, Zannettino AC. Circulating N-cadherin levels are a negative prognostic indicator in patients with multiple myeloma. *British Journal of Haematology*. 2013.
206. Groen RW, de Rooij MF, Kocemba KA, Reijmers RM, de Haan-Kramer A, Overdijk MB, et al. N-cadherin-mediated interaction with multiple myeloma cells inhibits osteoblast differentiation. *Haematologica*. 2011;96(11):1653-61.
207. Sadler NM, Harris BR, Metzger BA, Kirshner J. N-cadherin impedes proliferation of the multiple myeloma cancer stem cells. *American journal of blood research*. 2013;3(4):271.
208. Tsutsumimoto T, Kawasaki S, Ebara S, Takaoka K. TNF and IL 1 Suppress N Cadherin Expression in MC3T3 E1 Cells. *Journal of Bone and Mineral Research*. 1999;14(10):1751-60.
209. Vogel C, Marcotte EM. Insights into the regulation of protein abundance from proteomic and transcriptomic analyses. *Nature Reviews Genetics*. 2012;13(4):227-32.
210. Maier T, Güell M, Serrano L. Correlation of mRNA and protein in complex biological samples. *FEBS letters*. 2009;583(24):3966-73.
211. Schwanhäusser B, Busse D, Li N, Dittmar G, Schuchhardt J, Wolf J, et al. Global quantification of mammalian gene expression control. *Nature*. 2011;473(7347):337-42.
212. Greenbaum D, Colangelo C, Williams K, Gerstein M. Comparing protein abundance and mRNA expression levels on a genomic scale. *Genome Biol*. 2003;4(9):117.

213. Hatse S, Balzarini J, Liekens S. Stromal cell-derived factor 1 (CXCL12) binds to endothelial cells and signals through a receptor different from CXCR4. *Biochemical and biophysical research communications*. 2006;348(1):192-9.
214. Skrtic A, Korac P, Kristo DR, Ajdukovic Stojisavljevic R, Ivankovic D, Dominis M. Immunohistochemical analysis of NOTCH1 and JAGGED1 expression in multiple myeloma and monoclonal gammopathy of undetermined significance. *Human pathology*. 2010.
215. Zannettino AC, Farrugia AN, Kortessidis A, Manavis J, To LB, Martin SK, et al. Elevated serum levels of stromal-derived factor-1 α are associated with increased osteoclast activity and osteolytic bone disease in multiple myeloma patients. *Cancer research*. 2005;65(5):1700-9.
216. Nobta M, Tsukazaki T, Shibata Y, Xin C, Moriishi T, Sakano S, et al. Critical regulation of bone morphogenetic protein-induced osteoblastic differentiation by Delta1/Jagged1-activated Notch1 signaling. *Journal of Biological Chemistry*. 2005;280(16):15842-8.
217. Greenbaum A, Hsu Y-MS, Day RB, Schuettpelz LG, Christopher MJ, Borgerding JN, et al. CXCL12 in early mesenchymal progenitors is required for haematopoietic stem-cell maintenance. *Nature*. 2013;495(7440):227-30.
218. Kawaguchi J, Kii I, Sugiyama Y, Takeshita S, Kudo A. The Transition of Cadherin Expression in Osteoblast Differentiation from Mesenchymal Cells: Consistent Expression of Cadherin 11 in Osteoblast Lineage. *Journal of Bone and Mineral Research*. 2001;16(2):260-9.
219. Ferrari SL, Traianedes K, Thorne M, Lafage-Proust MH, Genever P, Cecchini MG, et al. A Role for N-Cadherin in the Development of the Differentiated Osteoblastic Phenotype. *Journal of Bone and Mineral Research*. 2000;15(2):198-208.

220. Van de Broek I, Leleu X, Schots R, Facon T, Vanderkerken K, Van Camp B, et al. Clinical significance of chemokine receptor (CCR1, CCR2 and CXCR4) expression in human myeloma cells: the association with disease activity and survival. *Haematologica*. 2006;91(2):200.
221. Pellegrino A, Ria R, Pietro GD, Cirulli T, Surico G, Pennisi A, et al. Bone marrow endothelial cells in multiple myeloma secrete CXC-chemokines that mediate interactions with plasma cells. *British journal of haematology*. 2005;129(2):248-56.
222. Dallas SL, Garrett IR, Oyajobi BO, Dallas MR, Boyce BF, Bauss F, et al. Ibandronate reduces osteolytic lesions but not tumor burden in a murine model of myeloma bone disease. *Blood*. 1999;93(5):1697-706.
223. Oyajobi BO, Muñoz S, Kakonen R, Williams PJ, Gupta A, Wideman CL, et al. Detection of myeloma in skeleton of mice by whole-body optical fluorescence imaging. *Molecular cancer therapeutics*. 2007;6(6):1701-8.
224. Liu Z-J, Xiao M, Balint K, Smalley KS, Brafford P, Qiu R, et al. Notch1 signaling promotes primary melanoma progression by activating mitogen-activated protein kinase/phosphatidylinositol 3-kinase-Akt pathways and up-regulating N-cadherin expression. *Cancer research*. 2006;66(8):4182-90.
225. Zhu H, Zhou X, Redfield S, Lewin J, Miele L. Elevated Jagged-1 and Notch-1 expression in high grade and metastatic prostate cancers. *American journal of translational research*. 2013;5(3):368.
226. Santagata S, Demichelis F, Riva A, Varambally S, Hofer MD, Kutok JL, et al. JAGGED1 expression is associated with prostate cancer metastasis and recurrence. *Cancer research*. 2004;64(19):6854-7.
227. Naumann U, Cameroni E, Pruenster M, Mahabaleshwar H, Raz E, Zerwes H-G, et al. CXCR7 functions as a scavenger for CXCL12 and CXCL11. *PloS one*. 2010;5(2):e9175.

228. Jennbacken K, Tešan T, Wang W, Gustavsson H, Damber J-E, Welén K. N-cadherin increases after androgen deprivation and is associated with metastasis in prostate cancer. *Endocrine-Related Cancer*. 2010;17(2):469-79.
229. Speetjens FM, Liefers GJ, Korbee CJ, Mesker WE, van de Velde CJ, van Vlierberghe RL, et al. Nuclear localization of CXCR4 determines prognosis for colorectal cancer patients. *Cancer Microenvironment*. 2009;2(1):1-7.
230. Yao X, Zhou L, Han S, Chen Y. High expression of CXCR4 and CXCR7 predicts poor survival in gallbladder cancer. *Journal of International Medical Research*. 2011;39(4):1253-64.
231. Eaton CL, Colombel M, van der Pluijm G, Cecchini M, Wetterwald A, Lippitt J, et al. Evaluation of the frequency of putative prostate cancer stem cells in primary and metastatic prostate cancer. *The Prostate*. 2010;70(8):875-82.
232. Clarke B. Normal bone anatomy and physiology. *Clinical journal of the American Society of Nephrology*. 2008;3(Supplement 3):S131-S9.
233. Friedenstein A, Chailakhyan R, Gerasimov U. Bone marrow osteogenic stem cells: in vitro cultivation and transplantation in diffusion chambers. *Cell Proliferation*. 1987;20(3):263-72.
234. Harada S-i, Rodan GA. Control of osteoblast function and regulation of bone mass. *Nature*. 2003;423(6937):349-55.
235. Caplan AI, Bruder SP. Mesenchymal stem cells: building blocks for molecular medicine in the 21st century. *Trends in molecular medicine*. 2001;7(6):259-64.
236. Otto F, Thornell AP, Crompton T, Denzel A, Gilmour KC, Rosewell IR, et al. *Cbfa1*, a Candidate Gene for Cleidocranial Dysplasia Syndrome, Is Essential for Osteoblast Differentiation and Bone Development. *Cell*. 1997;89(5):765-71.

237. Nakamura H. Morphology, function, and differentiation of bone cells. *Journal of hard tissue biology*. 2007;16(1):15-22.
238. Nakashima K, Zhou X, Kunkel G, Zhang Z, Deng JM, Behringer RR, et al. The novel zinc finger-containing transcription factor osterix is required for osteoblast differentiation and bone formation. *Cell*. 2002;108(1):17-29.
239. Hoemann C, El-Gabalawy H, McKee M. In vitro osteogenesis assays: influence of the primary cell source on alkaline phosphatase activity and mineralization. *Pathologie Biologie*. 2009;57(4):318-23.
240. Stein GS, Lian JB, Owen TA. Relationship of cell growth to the regulation of tissue-specific gene expression during osteoblast differentiation. *The FASEB journal*. 1990;4(13):3111-23.
241. Choi K-M, Seo Y-K, Yoon H-H, Song K-Y, Kwon S-Y, Lee H-S, et al. Effect of ascorbic acid on bone marrow-derived mesenchymal stem cell proliferation and differentiation. *Journal of bioscience and bioengineering*. 2008;105(6):586-94.
242. Jaiswal N, Haynesworth SE, Caplan AI, Bruder SP. Osteogenic differentiation of purified, culture-expanded human mesenchymal stem cells in vitro. *Journal of cellular biochemistry*. 1997;64(2):295-312.
243. Ecarot-Charrier B, Glorieux FH, Van Der Rest M, Pereira G. Osteoblasts isolated from mouse calvaria initiate matrix mineralization in culture. *The Journal of cell biology*. 1983;96(3):639-43.
244. Bellows C, Aubin J, Heersche J. Initiation and progression of mineralization of bone nodules formed in vitro: the role of alkaline phosphatase and organic phosphate. *Bone and mineral*. 1991;14(1):27-40.
245. Wang D, Christensen K, Chawla K, Xiao G, Krebsbach PH, Franceschi RT. Isolation and Characterization of MC3T3-E1 Preosteoblast Subclones with Distinct In

Vitro and In Vivo Differentiation/Mineralization Potential. *Journal of Bone and Mineral Research*. 1999;14(6):893-903.

246. Otsuka E, Yamaguchi A, Hirose S, Hagiwara H. Characterization of osteoblastic differentiation of stromal cell line ST2 that is induced by ascorbic acid. *American Journal of Physiology-Cell Physiology*. 1999;277(1):C132-C8.

247. Gronthos S, Graves S, Ohta S, Simmons P. The STRO-1+ fraction of adult human bone marrow contains the osteogenic precursors. *Blood*. 1994;84(12):4164-73.

248. Igarashi M, Kamiya N, Hasegawa M, Kasuya T, Takahashi T, Takagi M. Inductive effects of dexamethasone on the gene expression of Cbfa1, Osterix and bone matrix proteins during differentiation of cultured primary rat osteoblasts. *Journal of molecular histology*. 2004;35(1):3-10.

249. Peter SJ, Liang CR, Kim DJ, Widmer MS, Mikos AG. Osteoblastic phenotype of rat marrow stromal cells cultured in the presence of dexamethasone, β -glycerolphosphate, and L-ascorbic acid. *Journal of cellular biochemistry*. 1998;71(1):55-62.

250. Lynch MP, Stein JL, Stein GS, Lian JB. The influence of type I collagen on the development and maintenance of the osteoblast phenotype in primary and passaged rat calvarial osteoblasts: modification of expression of genes supporting cell growth, adhesion, and extracellular matrix mineralization. *Experimental cell research*. 1995;216(1):35-45.

251. Choi JY, Lee BH, Song KB, Park RW, Kim IS, Sohn KY, et al. Expression patterns of bone-related proteins during osteoblastic differentiation in MC3T3-E1 cells. *Journal of cellular biochemistry*. 1996;61(4):609-18.

252. Gartland A, Rumney RM, Dillon JP, Gallagher JA. Isolation and Culture of Human Osteoblasts. *Human Cell Culture Protocols*: Springer; 2012. p. 337-55.

253. Coelho M, Fernandes M. Human bone cell cultures in biocompatibility testing. Part II: effect of ascorbic acid, β -glycerophosphate and dexamethasone on osteoblastic differentiation. *Biomaterials*. 2000;21(11):1095-102.
254. Nefussi J-R, Boy-Lefevre M, Boulekbache H, Forest N. Mineralization in vitro of matrix formed by osteoblasts isolated by collagenase digestion. *Differentiation*. 1985;29(2):160-8.
255. Shui C, Spelsberg TC, Riggs BL, Khosla S. Changes in Runx2/Cbfa1 expression and activity during osteoblastic differentiation of human bone marrow stromal cells. *Journal of Bone and Mineral Research*. 2003;18(2):213-21.
256. Sudhakar S, Li Y, Katz MS, Elango N. Translational regulation is a control point in RUNX2/Cbfa1 gene expression. *Biochemical and biophysical research communications*. 2001;289(2):616-22.
257. PAUTKE C, SCHIEKER M, TISCHER T, KOLK A, NETH P, MUTSCHLER W, et al. Characterization of osteosarcoma cell lines MG-63, Saos-2 and U-2 OS in comparison to human osteoblasts. *Anticancer research*. 2004;24(6):3743-8.
258. Taichman RS, Cooper C, Keller ET, Pienta KJ, Taichman NS, McCauley LK. Use of the stromal cell-derived factor-1/CXCR4 pathway in prostate cancer metastasis to bone. *Cancer Research*. 2002;62(6):1832-7.
259. Weber JM, Forsythe SR, Christianson CA, Frisch BJ, Gigliotti BJ, Jordan CT, et al. Parathyroid hormone stimulates expression of the Notch ligand Jagged1 in osteoblastic cells. *Bone*. 2006;39(3):485-93.
260. Greenbaum AM, Revollo LD, Woloszynek JR, Civitelli R, Link DC. N-cadherin in osteolineage cells is not required for maintenance of hematopoietic stem cells. *Blood*. 2012;120(2):295-302.

261. Jung Y, Wang J, Song J, Shiozawa Y, Wang J, Havens A, et al. Annexin II expressed by osteoblasts and endothelial cells regulates stem cell adhesion, homing, and engraftment following transplantation. *Blood*. 2007;110(1):82-90.
262. Barille S, Collette M, Bataille R, Amiot M. Myeloma cells upregulate interleukin-6 secretion in osteoblastic cells through cell-to-cell contact but downregulate osteocalcin. *Blood*. 1995;86(8):3151-9.
263. Fulciniti M, Tassone P, Hideshima T, Vallet S, Nanjappa P, Ettenberg SA, et al. Anti-DKK1 mAb (BHQ880) as a potential therapeutic agent for multiple myeloma. *Blood*. 2009;114(2):371-9.
264. Singh S, Singh UP, Grizzle WE, Lillard JW. CXCL12–CXCR4 interactions modulate prostate cancer cell migration, metalloproteinase expression and invasion. *Laboratory investigation*. 2004;84(12):1666-76.
265. Chen Y, Stamatoyannopoulos G, Song C-Z. Down-regulation of CXCR4 by inducible small interfering RNA inhibits breast cancer cell invasion in vitro. *Cancer research*. 2003;63(16):4801-4.
266. Fernandis AZ, Prasad A, Band H, Klösel R, Ganju RK. Regulation of CXCR4-mediated chemotaxis and chemoinvasion of breast cancer cells. *Oncogene*. 2004;23(1):157-67.
267. Nefedova Y, Sullivan D, Bolick S, Dalton W, Gabrilovich D. Inhibition of Notch signaling induces apoptosis of myeloma cells and enhances sensitivity to chemotherapy. *Blood*. 2008;111(4):2220.
268. Hazan R, Phillips G, Qiao R, Norton L, Aaronson S. Exogenous expression of N-cadherin in breast cancer cells induces cell migration, invasion, and metastasis. *The Journal of cell biology*. 2000;148(4):779.

269. Qi J, Chen N, Wang J, Siu C-H. Transendothelial migration of melanoma cells involves N-cadherin-mediated adhesion and activation of the β -catenin signaling pathway. *Molecular biology of the cell*. 2005;16(9):4386-97.
270. Li G, Satyamoorthy K, Herlyn M. N-cadherin-mediated intercellular interactions promote survival and migration of melanoma cells. *Cancer research*. 2001;61(9):3819-25.
271. Vacca A, Ribatti D, Roncali L, Ranieri G, Serio G, Silvestris F, et al. Bone marrow angiogenesis and progression in multiple myeloma. *British journal of haematology*. 1994;87(3):503-8.
272. Tanaka Y, Morimoto I, Nakano Y, Okada Y, Hirota S, Nomura S, et al. Osteoblasts are regulated by the cellular adhesion through ICAM-1 and VCAM-1. *Journal of Bone and Mineral Research*. 1995;10(10):1462-9.
273. Kawano MM, Huang N, Tanaka H, Ishikawa H, Sakai A, Tanabe O, et al. Homotypic cell aggregations of human myeloma cells with ICAM-1 and LFA-1 molecules. *British journal of haematology*. 1991;79(4):583-8.
274. Michigami T, Shimizu N, Williams PJ, Niewolna M, Dallas SL, Mundy GR, et al. Cell-cell contact between marrow stromal cells and myeloma cells via VCAM-1 and $\alpha 4\beta 1$ -integrin enhances production of osteoclast-stimulating activity. *Blood*. 2000;96(5):1953-60.
275. Damiano JS, Cress AE, Hazlehurst LA, Shtil AA, Dalton WS. Cell adhesion mediated drug resistance (CAM-DR): role of integrins and resistance to apoptosis in human myeloma cell lines. *Blood*. 1999;93(5):1658-67.
276. Kyle R, Durie B, Rajkumar S, Landgren O, Blade J, Merlini G, et al. Monoclonal gammopathy of undetermined significance (MGUS) and smoldering (asymptomatic) multiple myeloma: IMWG consensus perspectives risk factors for progression and guidelines for monitoring and management. *Leukemia*. 2010;24(6):1121-7.

277. Abkowitz J, Robinson A, Kale S, Long M, Chen J. Mobilization of hematopoietic stem cells during homeostasis and after cytokine exposure. *Blood*. 2003;102(4):1249.
278. Augustine CK, Yoshimoto Y, Gupta M, Zipfel PA, Selim MA, Febbo P, et al. Targeting N-cadherin enhances antitumor activity of cytotoxic therapies in melanoma treatment. *Cancer research*. 2008;68(10):3777-84.
279. Gravdal K, Halvorsen OJ, Haukaas SA, Akslen LA. A switch from E-cadherin to N-cadherin expression indicates epithelial to mesenchymal transition and is of strong and independent importance for the progress of prostate cancer. *Clinical Cancer Research*. 2007;13(23):7003-11.
280. Tomita K, van Bokhoven A, van Leenders GJ, Ruijter ET, Jansen CF, Bussemakers MJ, et al. Cadherin switching in human prostate cancer progression. *Cancer research*. 2000;60(13):3650-4.
281. Vesuna F, van Diest P, Chen JH, Raman V. Twist is a transcriptional repressor of E-cadherin gene expression in breast cancer. *Biochemical and biophysical research communications*. 2008;367(2):235-41.
282. Liles WC, Broxmeyer HE, Rodger E, Wood B, Hübel K, Cooper S, et al. Mobilization of hematopoietic progenitor cells in healthy volunteers by AMD3100, a CXCR4 antagonist. *Blood*. 2003;102(8):2728-30.
283. DiPersio JF, Stadtmauer EA, Nademanee A, Micallef IN, Stiff PJ, Kaufman JL, et al. Plerixafor and G-CSF versus placebo and G-CSF to mobilize hematopoietic stem cells for autologous stem cell transplantation in patients with multiple myeloma. *Blood*. 2009;113(23):5720-6.
284. Kuhne MR, Mulvey T, Belanger B, Chen S, Pan C, Chong C, et al. BMS-936564/MDX-1338: A Fully Human Anti-CXCR4 Antibody Induces Apoptosis In Vitro and Shows Antitumor Activity In Vivo in Hematologic Malignancies. *Clinical Cancer Research*. 2013;19(2):357-66.

285. Fahham D, Weiss ID, Abraham M, Beider K, Hanna W, Shlomai Z, et al. In vitro and in vivo therapeutic efficacy of CXCR4 antagonist BKT140 against human non-small cell lung cancer. *The Journal of Thoracic and Cardiovascular Surgery*. 2012.
286. Beider K, Begin M, Abraham M, Wald H, Weiss ID, Wald O, et al. CXCR4 antagonist 4F-benzoyl-TN14003 inhibits leukemia and multiple myeloma tumor growth. *Exp Hematol*. 2011 Mar;39(3):282-92. PubMed PMID: 21138752. Epub 2010/12/09. eng.
287. Wei P, Walls M, Qiu M, Ding R, Denlinger RH, Wong A, et al. Evaluation of selective γ -secretase inhibitor PF-03084014 for its antitumor efficacy and gastrointestinal safety to guide optimal clinical trial design. *Molecular cancer therapeutics*. 2010;9(6):1618-28.
288. Samon JB, Castillo-Martin M, Hadler M, Ambesi-Impioabato A, Paietta E, Racevskis J, et al. Preclinical analysis of the γ -secretase inhibitor PF-03084014 in combination with glucocorticoids in T-cell acute lymphoblastic leukemia. *Molecular Cancer Therapeutics*. 2012;11(7):1565-75.
289. Zhang CC, Pavlicek A, Zhang Q, Lira ME, Painter CL, Yan Z, et al. Biomarker and Pharmacologic Evaluation of the γ -Secretase Inhibitor PF-03084014 in Breast Cancer Models. *Clinical Cancer Research*. 2012;18(18):5008-19.
290. Luistro L, He W, Smith M, Packman K, Vilenchik M, Carvajal D, et al. Preclinical profile of a potent γ -secretase inhibitor targeting notch signaling with in vivo efficacy and pharmacodynamic properties. *Cancer research*. 2009;69(19):7672-80.
291. Tolcher AW, Messersmith WA, Mikulski SM, Papadopoulos KP, Kwak EL, Gibbon DG, et al. Phase I study of RO4929097, a gamma secretase inhibitor of Notch signaling, in patients with refractory metastatic or locally advanced solid tumors. *Journal of Clinical Oncology*. 2012;30(19):2348-53.

292. Arcari JT, Beebe JS, Berliner MA, Bernardo V, Boehm M, Borzillo GV, et al. Discovery and synthesis of novel 4-aminopyrrolopyrimidine Tie-2 kinase inhibitors for the treatment of solid tumors. *Bioorganic & medicinal chemistry letters*. 2013.
293. Peeters M, Strickland A, Lichinitser M, Suresh A, Manikhas G, Shapiro J, et al. A randomised, double-blind, placebo-controlled phase 2 study of trebananib (AMG 386) in combination with FOLFIRI in patients with previously treated metastatic colorectal carcinoma. *British journal of cancer*. 2013.
294. Hudkins RL, Becknell NC, Zulli AL, Underiner TL, Angeles TS, Aimone LD, et al. Synthesis and Biological Profile of the pan-Vascular Endothelial Growth Factor Receptor/Tyrosine Kinase with Immunoglobulin and Epidermal Growth Factor-Like Homology Domains 2 (VEGF-R/TIE-2) Inhibitor 11-(2-Methylpropyl)-12, 13-dihydro-2-methyl-8-(pyrimidin-2-ylamino)-4 H-indazolo [5, 4-a] pyrrolo [3, 4-c] carbazol-4-one (CEP-11981): A Novel Oncology Therapeutic Agent. *Journal of medicinal chemistry*. 2012;55(2):903-13.
295. Bartee E, Chan WM, Moreb JS, Cogle CR, McFadden G. Selective purging of human multiple myeloma cells from autologous stem cell transplantation grafts using oncolytic myxoma virus. *Biology of Blood and Marrow Transplantation*. 2012;18(10):1540-51.
296. Burden-Gulley SM, Gates TJ, Craig SE, Lou SF, Oblander SA, Howell S, et al. Novel peptide mimetic small molecules of the HAV motif in N-cadherin inhibit N-cadherin-mediated neurite outgrowth and cell adhesion. *Peptides*. 2009;30(12):2380-7.